IMMUNOMODULATION FOLLOWING SEVERE MUSCULOSKELETAL TRAUMA TO IMPROVE FUNCTIONAL REGENERATION

A Dissertation
Presented to
The Academic Faculty

by

Casey Elizabeth Vantucci

In Partial Fulfillment
of the Requirements for the Degree
Doctor of Philosophy in the
Wallace H. Coulter Department of Biomedical Engineering

Georgia Institute of Technology & Emory University
December 2021

COPYRIGHT © 2021 BY CASEY VANTUCCI

IMMUNOMODULATION FOLLOWING SEVERE MUSCULOSKELETAL TRAUMA TO IMPROVE FUNCTIONAL REGENERATION

Approved by:

Dr. Krishnendu Roy, Advisor
Wallace H. Coulter Department of Biomedical Engineering
Georgia Institute of Technology

Dr. Robert E. Guldberg
Phil and Penny Knight Campus for Accelerating Scientific Impact
University of Oregon

Dr. Andrés J. García
George W. Woodruff School of Mechanical Engineering
Georgia Institute of Technology

Dr. Philipp Leucht
Departments of Orthopaedic Surgery and Cell Biology
New York University Langone Medical Center

Dr. M.G. Finn
Department of Chemistry and Biochemistry
Georgia Institute of Technology

Date Approved: December 1, 2021

To my family, John, Theresa, and Andrew, for always believing in me.

To Matt, for encouraging and supporting me through it all.

ACKNOWLEDGMENTS

I am so thankful and lucky to have an incredible number of people in my life who have supported and encouraged me throughout this entire journey. I most certainly would not have made it this far without each and every one of you.

First and foremost, I must thank my thesis advisors, Krish Roy and Bob Guldberg, for guiding me and challenging me throughout this whole process. I am thankful that Krish and Bob got together to convince me to become a co-advised student so that I did not have to pick between having one of them as my advisor. The project they proposed has taken on a whole new life and it has been so fun and challenging to watch it grow into what it is today, five and a half years later. From Krish – I have learned to not take things too seriously and to always look at all data, no matter how they might seem, with excitement and curiosity. Krish's genuine caring for all his student's personal and professional success did not go unnoticed and created a positive environment that made all the rough patches not quite as rough. From Bob – I have learned the importance of challenging one's own opinions. Bob was always the first to play devil's advocate, and this made every experiment better and more robust. Bob took the phrase "work hard, play hard" seriously, and our conference dinners and nights out with the Guldberg lab were always an adventure that I won't forget.

This thesis would not be what it is without the input of my incredible committee members. Dr. Andrés García has helped me immensely throughout this process, always challenging me to question everything, no matter how well accepted it may be in the literature. His enthusiasm for science is contagious, and his ability to remember all the

details of my project was impressive, even during our many impromptu hallway chats. Dr. M.G. Finn's chemistry expertise was invaluable, especially for my Aim 2 where I often felt like I was wandering in the dark. Despite how busy he was, Dr. Finn always made time to answer my questions, even about the smallest details of my project. Lastly, Dr. Philipp Leucht's clinical expertise enhanced this project by allowing us to focus on aspects that are most important to clinicians. This perspective is so important since the ultimate goal is not to improve healing in rodent models, but to improve healing for real patients. I also have Dr. Leucht to thank for becoming moderately ORS famous with our picture being used in promotional materials!

I was fortunate enough to have many absolutely amazing collaborators, most importantly Nick Willett and his lab. If it was possible, then Nick would be my third advisor. Without the use of his lab's infection model, I wouldn't have almost any of the data that I have. He was always willing to support my projects, and and he always had useful advice both personally and professionally. I can't thank Nick enough for all his help. Nick's lab members were also incredibly helpful, especially Hyunhee, Emily, and Travis. Hyunhee and I worked together on the first infection model project, and she was always a friendly, smiling presence. Emily assisted with blood draws from the infection animals, and she was always willing to assist me at any time of the day. Despite everything going on, Travis always made time for my experiments, and while I will miss working with him, I will not miss working in the VA animal facility procedure room with the sun beating down on us. Julia and Jarred from Nick's lab also assisted me with surgeries, and I am thankful they volunteered their time. I also owe a tremendous amount of thanks to Paramita Chatterjee in the Marcus center for all her assistance with the single cell RNA sequencing

experiments. Paramita has been beyond helpful, and I always enjoy our conversations (science and not-science related). I also have incredible collaborators in Dr. García's lab who assisted me with mouse infection model experiments, including Pranav Kalelkar. In addition, special thanks to Jinhwan Kim, Kelsey Kubelick, and Anthony Yu in the Emelianov Lab and Zhiheng Lyu in the Xia Lab for assistance with particle characterization data. Lastly, our tuberculosis work would not have been possible without collaborators in Jyothi Rengarajan's lab at Emory, especially Hedwin Kitdorlang Dhkar and Ana Enriquez. I am so excited that we received a joint grant so that we can continue working together.

To my lab members, thank you for the endless number of hours spent in and out of lab and the countless science related (and not science related) conversations. I could not have asked for a better group of people to work with, and you have made the bad days bearable. Pallab Pradhan taught me most things I know in the lab and I could always count on him to help me in lab no matter how busy he was (and he was always busy!). Jiaying Liu taught me everything I know about SNAbs and it was with her that I first became a member of the "SNAb Lab." We got to work closely together in her last two years and her genuinely kind and driven personality are admirable. Kirsten Parratt, Joscelyn Mejias, and Michael Nelson were all the oldest Roy lab members when I joined, and they were great role models and always willing to offer help. They encouraged me to propose quickly and to keep pushing through to the next experiment. I could also always count on Joscelyn for puppy pictures! Alex Atalis was my desk buddy in the Roy lab and her kindness was infectious. Alex faced many challenges throughout her time in the Roy lab, and I hope that one day I can have even half of her perseverance and dedication. Randy Toy was a steady

presence in the Roy lab and I thoroughly enjoyed our BMES trip to Philly and trying lots of new food. I'm sad we were never able to play golf in Scotland, so hopefully some day in the future that will become a reality. Hannah Song is the loveliest person you could ever meet, and her organization and talent as a scientist are unparalleled. We joined the lab around the same time and bonded over our love for Maryland and dogs (and Mr. Henry!). I'm also thankful that Hannah (and Phil and Mr. Henry) put up with Camden so I could take some much-needed vacations. Angela Jimenez, Bryan Wang, Ritika Jain, Justin Hosten, Liana Kramer, and Rachel Ringquist all joined the lab the same year and they have all been amazing additions to the lab. I can always count on Angela to help with my injections, Bryan to help with my surgeries, Ritika for her opinions on the new Taylor Swift music, Justin for conversations that always make me laugh or put a smile on my face, Liana to commiserate about the woes of running flow, and Rachel as my fellow tall friend. Drishti Maniar, Shivani Vyas, and Shaylyn Grier are the most recent lab members to join the lab. I know my project is in excellent hands with Drishti and Shivani – I could not imagine anyone better to carry on the torch of the SNAb lab. Shaylyn is also another great addition to the lab. I already enjoy her one-liners, and her attention to detail will no doubt make her very successful. Dre Devereaux has always been such a kind soul, and his openness about his personal struggles help everyone feel a little less alone in their own struggles. Alex Beach joined the lab the same year I did, and it has been a pleasure working side by side through every milestone. You can always count on Alex for a good, sarcastic joke. Bhawana Pandey joined the lab as a post-doc partway through my time in the Roy lab, and although our time together has been short, it has been very sweet. Bhawana is a chemical wizard, and I wish she had joined the lab sooner because her expertise is invaluable. Nate

Dwarshuis has been a steady presence in the lab my entire time in the Roy lab, and I suppose I will forgive him for trying to mess with my desk ultra-organization. He is a master coder and his dry humor always lightened the mood. Miguel Armenta Ochoa is just an all-around great person, and you can always count on him for some incredible homemade food and stories about his wild dog Tinto. And last but not least, Delta Ghoshal joined the lab the year after I did but she quickly became a friend. She is always down to chat (who cares about deadlines?), and I am happy I finally convinced her to get a dog because Prim snapchats make my day. I will miss her when she leaves for Philly, but I'm glad that I'll still be here when she comes back.

With two advisors comes two labs, and I also have to thank all of the Guldberg lab members for their support. I briefly met Marian Hettiaratchi for a couple of months right before she defended, but her kindness left a longer lasting impression. When I did some work on her project in later years, she made herself available to answer questions despite the fact that she was busy trying to become a professor. Giuli Salazar-Noratto was two desks away from me in the back row of the Guldberg lab, and together with Marissa Ruehle, we made up the "back row, best row." I'm thankful she took me under her wing, and I love her adventurous spirit. I could not have completed this project without Laxmi Krishnan. He is an endless fountain of knowledge, and we spent countless days working together in lab and the OR. I am so glad he decided to return to Georgia Tech so that I could continue being able to chat with him and work with him. Hazel Stevens also was a huge help in the lab, and I did my very first experiment as a graduate student under her guidance. Her sarcasm is top notch, and I'm glad she decided to stick around and work with the Marcus center. David Reece, Olivia Burnsed, and Brennan Torstrick were all older graduate

students in the Guldberg lab when I joined. Their friendliness and willingness to assist me was incredibly helpful. I got to work very closely with Albert Cheng and did my first major *in vivo* study together with him. Albert helped get me on my feet when I first started out, and it was an absolute pleasure working with him. Ramesh Subbiah's optimistic and enthusiastic spirit was contagious and the ORS quote says it best – "do you wake up and start giggling?" Angela Lin's uCT experience was incredibly useful, and I am glad I was able to work with fellow-Marylander Ryan Akman for the short time we did. Lina Mancipe Castro pushed through all challenges thrown at her, and the way she shone in the face of adversity is incredible. I am glad she continued as a post-doc so that I could continue to get to work with her scientifically (and not just on cleaning up all the leftover Guldberg lab chemicals). Kelly Leguineche helped found the Guldberg lab in Oregon and it has been an absolute pleasure working with her. I had a blast on our tour of Eugene, and I guess I understand now why Bob likes it there. Tyler Guyer recently joined the Guldberg lab at Oregon and he has been helping carry out *in vivo* studies for my Aim 3. His help has been essential. Gilad Doron joined the Guldberg lab at the same time as me, also as a co-advised student, and I'm glad there was someone else going through that experience with me. Brett Klosterhoff is an incredible scientist, and I am thankful I got to know him and become friends with him (and Kayla and obviously Malibu too). I enjoyed our sports conversations, the many surgery days in the OR, and all the laughs and adventures we had with the Guldberg lab. Marissa Ruehle was my desk buddy in the Guldberg lab, and she quickly became a close friend. I could always count on her to be my bad science day cookie eating buddy and for a good rant. I am thoroughly honored that she would reach into a trash can to retrieve some accidentally thrown away Taco Bell, and I am so immensely thankful for

all the advice she gave me and all the (many) laughs we had together. She is also an above and beyond conference roommate, and I couldn't imagine anyone better to watch some trash cable TV with.

I was fortunate enough to mentor some amazing high school and undergraduate students along the way. Ayanna Prather was my first high school student, and I am not exaggerating when I say she has changed my life. Ayanna is not only incredibly intelligent, but also incredibly caring, talented, and dedicated. I have never seen anyone work harder than her, and she deserves boundless success. I am so proud of all the work she has done, and I am thankful that she fought with the uCT analysis so that I didn't have to. Clinton Smith came to me as an experienced researcher trained up by Brett, and I have to give a special shoutout to Brett. Clinton exceeds all expectations, and he essentially functions as a graduate student. His passion for science is evident, and if his past success is any indication of his future success, well, then I hope he remembers me when he wins his Nobel prize. I have also had the pleasure of mentoring Kaya Peterson, T.K. Huynh, and David Frey. David came to me after already working with three other Roy lab members, so he probably knows more than I do at this point. I can always count on David in the lab, and his self-sufficiency and initiative make my job easy. Kaya was one of my first undergraduate students, and I'm thankful that she stuck with me through everything despite being my "guinea pig" for how to be a graduate student mentor.

Outside of my labs, I owe huge thanks to Shannon Anderson. She is my fellow soccer buddy, dog lover, game night buddy, and rowing buddy, and has been someone I have laughed with and cried and just been through it all with. I'm thankful I didn't scare you away the first day of orientation, and I just had this feeling you would become a close

friend. Your support means so much to me, and I'm thankful for you always listening to me and encouraging me, especially through these last several months. I'm also thankful that you decided to marry Leo because he makes a mean pizza, and I love the way he faces the world with a smile on his face. Meghan O'Melia and Juline Deppen have also been truly supportive classmates. I will never forget my many adventures with Meghan, because with her, it's always an adventure. Through our countless park trips and hikes, Meghan always knows how to cheer you up. While I saw Juline less when she joined a lab at Emory, she is always down to hang out and catch up, and I'm thankful for those much-needed moments away from work.

I also have to thank some tremendous other Georgia Tech staff members who I have always been able to count on. Most importantly, I need to thank all of the IBB staff for the endless things they have helped me with. Colly Mitchell, Angela Ayers, and Laura Paige always check in on me and make sure everything is going okay. Laura always makes sure I am well-fed and has adopted me as a member of her Bioengineering family. Rose Brito, Julie Langenberg, and Vivian Johnson have helped me navigate Bob and now Andrés' schedule which is no easy feat! Rose continued to take care of the remaining Guldberg lab students just because she cares, and we are all grateful. I also need to give an absolutely huge thanks to EBB and Marcus center staff Andrea Soyland, Erin Bryant, Punya Mardhanan, Carla Zachery, Adrienne Williams, and Aeryal Herrod. Andrea, Erin, and Punya were always available for me to distract them talking about random things on my way to Krish's office, and Andrea also found me my puppy, Camden! Carla took care of anything and everything you needed, and she always made sure I got paid (which was no easy task, unfortunately). Adrienne always made sure I got my reagents on time, even

when I put in ridiculous last-minute requests, and every exchange we've had has always been positive and put a smile on my face.

The animal work in this thesis would not have been possible without the PRL staff and the impeccable facilities. I especially would like to thank Andrea, Altair, Ogeda, and Rebecca for always checking in with me and helping any way they can. Dr. Richard Noel and Dr. Laura O'Farrell have been amazing resources, and I appreciate them always taking the time to assist me with procedures. This thesis would also not have been possible without the IBB and EBB core facilities and staff, and I am very grateful to each and every one of them.

Outside of Georgia Tech, I have an absolutely amazing support system. First off, I have to thank my absolute best friend, Christina Krueger. This world is a better place with you in it, and I am a better person because of you. I always know that I can turn to you when I'm feeling down or when I need some extra love and support (which was frequently throughout this PhD). I also need to thank some of my best friends who have been by my side since elementary and middle school, including Christina Kaminsky, Karen Shollenberger, and Jenn Coyne. Losing Karen in my second year of graduate school was devastating, but I know she is watching over me from somewhere and sending me love in ways only she can (as evidenced by the two kittens I now own). Christina (Bean) and Jenn know the worst of me and the best of me and love me anyways, and I am eternally grateful for that. I also need to thank my college best friends Emily Tolino, Denise McPhilmy, and Becca Moriarty. I'm not sure anyone else would've put up with my constant roller coaster of emotions about how I wouldn't even get into graduate school. Thank you for believing in me and always being ready to have a good time whatever state or city we happen to be

in. I also need to thank “Matt’s friends.” Venky Bharadwaj, Jaymin Desai, and Stanley Chen quickly became my best friends. They adopted me into their friendship and treat me as “one of the boys.” I am not exaggerating when I say I would not have made it out of the summer of 2020 without Venky and our 2-hour long walks and co-working days. Thank you for making Atlanta feel like home.

I need to take a moment to thank all of the four-legged friends who provided companionship, laughter, and snuggles for all the rough moments throughout the last five and half years, including Ellie (Eleanor), Pepper, Moose, Pico, Olive, Otis, Prim, Mr. Henry, Pablo and Lucia, Bruce, Lando, Brantley, Jefferson, Delaney, Monroe, and Ted. Most importantly, thanks to Camden, Cal, and Brooks (and Matt for letting me keep them).

I am lucky to have a soon-to-be family-in-law who has embraced me wholeheartedly. Tricia Hyer, Scott Hyer, and Meaghan Hyer- I cannot wait to officially be family. To Meaghan – your compassion for others and how hard you love every single person in your life has me in awe, and your FaceTime calls never fail to put a smile on my face. I am so excited for the adventures to come.

I am not sure I can express in words my thanks to my family, most importantly my parents, John and Theresa, and my brother Andrew. I have never and probably will never be able to believe in myself with the level of confidence and fierceness that they believe in me. The way they love and support me fills up every nook and cranny of my life without fail. To Andrew- it is most certainly him that I have to thank for my competitive and determined spirit that has undoubtedly allowed me to persevere through this degree. I would not be the way that I am if I had not constantly tried to be just as cool as my big

brother and beat him in whatever game we were playing. His unwavering and soft-spoken loyalty to those he loves is such a comfort, and I am proud to be his little sister. To my dad, I thank him for gifting me his stubbornness, but also his zest for life and his devotion his friends and family. He has always been there to remind me about the most important things in life and to maintain perspective through all the ups and downs of my project. Special thanks go to my dad for sitting at the kitchen table for hours with me just to teach me how to add and subtract (with pennies) and for always encouraging me to investigate how things work. To my mom, I thank her for gifting me with her massive, caring heart. She has guided me through this life with an enormous amount of patience and love and has always been there when I needed to talk. Having her as a female engineer role model really made me feel like I could do anything or be anything. Thank you both for giving me a life with endless opportunities and endless love. I am who I am because of you.

Lastly, I have to thank my fiancé, Matt, who has been by my side for nine and a half years. When we first met in high school, he was kind and goofy, and I always looked forward to our conversations. We never knew where life would take us, but I am thankful that we decided to always say “yes” to whatever came next and to always give it a shot. While these past five and a half years have had their ups and downs, he has stuck with me through it all, providing much needed adventures, distractions, laughs, and love. Thank you, for taking this ride with me.

TABLE OF CONTENTS

LIST OF TABLES

LIST OF FIGURES

LIST OF SYMBOLS AND ABBREVIATIONS

APCs	Antigen-presenting cells
ARDS	Acute respiratory distress syndrome
ANOVA	Analysis of variance
Au	Gold
AuNPs	Gold nanoparticles
BF	Bright field
BL	Bioluminescent
BMP-2	Bone morphogenetic protein 2
BrdU	Bromodeoxyuridine
BSA	Bovine serum albumin
CARS	Compensatory anti-inflammatory response syndrome
CCL2	CC motif chemokine ligand 2, see MCP-1
CCL5	CC motif chemokine ligand 5, see RANTES
Cd	Cadmium
CFU	Colony forming units
Co	Cobalt
CRASH	Corticosteroid randomization after significant head injury
CXCL5	CXC motif chemokine ligand 5, see LIX
CXCL10	CXC motif chemokine ligand 10, See IP-10
Cp33	Fc-mimicking ligand
Cy5	Cyanine 5
DAMPs	Damage-associated molecular patterns

DCs	Dendritic cells
DI	Deionized
DMF	N,N-Dimethylformamide
DNA	Deoxyribonucleic acid
DNase	Deoxyribonuclease
ECM	Extracellular matrix
EDC	1-ethyl-3-(-3-dimethylaminopropyl) carbodiimide
EDS	Energy dispersive spectroscopy
EGF	Epidermal growth factor
EPCs	Endothelial progenitor cells
FACS	Fluorescent activated cell sorting
FBS	Fetal bovine serum
FDA	Food and drug administration, U.S.
FMO	Fluorescent minus one
G3	MDSC-targeting ligand
GAG	Glycosaminoglycan
GM-CSF	Granulocyte macrophage colony stimulating factor
G-CSF	Granulocyte colony stimulating factor
G-MDSCs	Granulocytic myeloid-derived suppressor cells
H&E	Hematoxylin and eosin
HAADF	High-angle annular dark-field imaging
HCl	Hydrochloric acid
hCVAM	human cryopreserved viable amniotic membrane
HFP	1,1,1,3,3,3-Hexafluoro-2-propoanol
HLA-DR	Human leukocyte antigen – DR isotype

HMGB1	High mobility group box 1
HMP	Heparin microparticle
hMSCs	Human mesenchymal stromal cells
HO	Heterotopic ossification
HSC	Hematopoietic stem cell
HSP70	Heat shock protein 70
IACUC	Institutional animal care and use committee
IFNg	Interferon gamma
IgG	Immunoglobulin
IL-[number]	Interleukin [number]
IL-1a	Interleukin 1 alpha
IL-1b	Interleukin 1 beta
IL-1R	Interleukin 1 receptor
IL-17A	Interleukin 17 alpha
iNOS	Inducible nitric oxide synthase
IP-10	Interferon gamma-induced protein 10, see CXCL10
KCN	Potassium cyanide
kDa	Kilodalton
LB	Luria Burtani
LIX	Lipopolysaccharide-induced CXC chemokine, see CXCL5
LV	Latent variable
mAbs	Monoclonal antibodies
MACS	Magnetic activated cell sorting
MCP-1	Macrophage chemoattractant protein 1, see CCL2
MDSCs	Myeloid-derived suppressor cells

MEM	Minimum essential media
MIP-1	Macrophage inflammatory protein 1
Mg	Magnesium
MHC	Major histocompatibility complex
M-MDSCs	Monocytic myeloid-derived suppressor cells
MODS	Multiple organ dysregulation syndrome
MOFS	Multiple organ failure syndrome
MSC	Mesenchymal stromal cells
MVF	Microvascular fragments
MWCO	Molecular weight cut-off
NBF	Neutral buffered formalin
NF-kB	Nucelar factor kappa light chain enhancer of activated B cells
NHS	N-Hydroxysuccinimide
NK	Natural killer
NO	Nitric oxide
OPG	Osteoprotegerin
PA	Photoacoustic
PAMPs	Pathogen-associated molecular patterns
PBMCs	Peripheral blood mononuclear cells
PBS	Phosphate buffered saline
PCL	Polycaprolactone
PD-L	Programmed death ligand
PLGA	Polylactic-go-glycolic acid
PLSDA	Partial least squares discriminat analysis
PLSR	Partial least squares regression

pMOI	Polar moment of inertia
PRRs	Pattern recognition receptors
PTH	Parathyroid hormone
PMMA	Polymethyl methacrylate
QDs	Quantum dots
RANKL	Receptor activator of nuclear factor kappa-b
RANTES	Regulated on activation, normal T cell expressed and secreted, see CCL5
RBC	Red blood cell
REML	Restricted maximum likelihood estimation
RGD	Arginine glycine aspartate
ROS	Reactive oxygen species
RNA	Ribonucleic acid
RNS	Reative nitrogen species
S100A8/A9	S100 calcium binding protein A8/A9
SA-AuNP-SH	Half streptavidin coated, half thiol functionalized gold nanoparticles
SA-AuNP-SA	Streptavidin coated gold nanoparticles
scRNAseq	Single cell RNA sequencing
Se	Selenium
SEM	Standard error of the mean
Si	Silicon
SIDIS	Systemic immune dysregulation and immune suppression
SIRS	Systemi inflammatory response syndrome
SMCC	Succinimidyl 4-(N-maleimidomethyl)cyclohexane-1-carboxylate
SNAbs	Synthetic nanoparticle antibodies
SpA	Staphylococcal protein A

SR	Slow release
St	Strontium
S/TEM	Scaninning transmission electron microscopy
TBI	Traumatic brain injury
TCEP	Tris(2-carboxyethyl)phosphine
TCR	T cell receptor
TEM	Transmission electron microscopy
TEMED	Tetramethylethylenediamine
TGFb	Transforming growth factor beta
Th1	T helper type 1
Th2	T helper type 2
TLR-9	Toll-like receptor 9
TNF	Tumor necrosis factor
tSNE	t-distributed stochastic neighbor embedding
TRAIL	TNF-regulated apoptosis-inducing ligand
Tregs	Regulatory T cells
TUNEL	Terminal deoxynucleotidyl transferase dUTP nick end labeling
uCT	Micro-computed tomography
UMAP	Uniform manifold approximation and projection
US	Ultrasound
UV	Ultraviolet
VEGF	Vascular endothelial growth factor
VML	Volumetric muscle loss
VOI	Volume of interest
Zn	Zinc

SUMMARY

Severe musculoskeletal trauma is one of the most prevalent types of trauma in both combat-wounded and civilian patients. However, despite advances in trauma care, morbidity and complication rates remain high with greater than 5-10% of patients experiencing complications with healing, most commonly non-unions and infections, resulting in longer rehabilitation times and increased treatment costs. Recently, systemic immune dysregulation and immunosuppression has been implicated as a main contributor to severe trauma patients who have complications in healing and who respond poorly to treatment strategies. A notable hallmark of systemic immune dysregulation is elevated levels of immune suppressor cells, including myeloid-derived suppressor cells (MDSCs), similar to immune suppression seen in many solid tumors. Despite awareness of systemic immune dysregulation in human trauma survivors, it is still poorly understood how these systemic cellular and molecular immune responses impact regenerative intervention strategies and outcomes. Further, whether such knowledge can enable design of effective immunoengineering strategies to improve functional regeneration has not been rigorously tested. Finally, well-characterized animal models that mimic these conditions and that could allow for a better understanding of the interaction between trauma-related immunosuppression and associated impaired regeneration responses have not been established. Previous clinical attempts at systemic immunomodulation following trauma have used systemic cytokine and growth factor therapies; however, they have had very little success to restore immune homeostasis and improve patient outcomes. Borrowing from cancer immunotherapy, a treatment to address immunosuppression at the cellular

level rather than the protein level utilizes monoclonal antibodies (mAbs) to deplete MDSCs; however, they are limited by high dosage requirements and there are no mAbs that specifically target MDSCs.

Therefore, in order to better understand systemic immune dysregulation following trauma, the first aim developed and characterized systemic immune dysregulation in pre-clinical animal models of severe trauma and identified predictive markers for immune dysregulation. The next aim developed a synthetic nanoparticle strategy that mimics the function of a mAb to target and deplete MDSCs. The last aim utilized the immunomodulatory MDSC-depleting therapeutic in order to evaluate the effect of systemic immune modulation on the immune system and local bone regeneration. The overall hypothesis was that (a) immunological markers indicative of systemic immune dysregulation can be used to predict functional regenerative outcomes in a previously developed rat composite trauma model and (b) depletion of MDSCs, a hallmark of systemic immune dysregulation, will restore immune homeostasis and lead to improved bone regeneration. The overall objectives were to investigate (i) how the development of systemic immune dysregulation relates to functional bone regeneration and (ii) how systemic immunomodulation impacts the immune system and regenerative outcomes following severe trauma.

Overall, this thesis has investigated post-traumatic systemic immune dysregulation and immunosuppression in multiple different trauma models, developed and characterized a novel nanoparticle-based method to target and deplete aberrant immunosuppressive myeloid-derived suppressor cells, and increased the fundamental knowledge about the role of myeloid-derived suppressor cells on systemic immune function and healing following

trauma. These results can be leveraged to more effectively treat challenging bone injuries by identifying patients at higher risk for complications and utilizing targeted and individualized treatment strategies that not only focus on local tissue engineering strategies but also on systemic immunomodulation strategies.

CHAPTER 1. INTRODUCTION

1.1 Motivation

Musculoskeletal trauma is highly prevalent in both combat-wounded and civilian patients (1,2). Moreover, despite advances in trauma care, mortality and complication rates remain remarkably high (3). Patients who do not respond to treatment often suffer from complications, most commonly non-unions and infections, and experience poor healing, longer hospital stays, increased treatment costs, and prolonged disability (4). Recently, systemic immune dysregulation and immunosuppression has been implicated in the limited success of current intervention strategies and poor outcomes in trauma patients (5). Systemic immune dysregulation and immunosuppression results in decreased levels of circulating pro-inflammatory cytokines and a decrease in circulating immune effector cells, such as effector T cells (6). Another notable hallmark of systemic immune dysregulation is elevated levels of immune suppressor cells, including myeloid-derived suppressor cells (MDSCs), similar to immune suppression seen in cancer and tumor microenvironments (7,8). Despite awareness of systemic immune dysregulation in human trauma survivors, it is still poorly understood how these systemic cellular and molecular immune responses impact regenerative intervention strategies and outcomes. Further, whether such knowledge can enable design of effective immunoengineering strategies to improve functional regeneration has not been rigorously tested. Finally, well-characterized animal models that mimic these conditions and that could allow for a better understanding of the interaction between trauma-related immunosuppression and associated impaired regenerative responses have not been established. A better understanding of

immunosuppression following trauma in relevant animal models will aid in identifying improved immunomodulatory targets for therapeutic interventions that can guide the development of optimal clinical treatment strategies to ultimately improve outcomes for trauma survivors.

Previous attempts at immunomodulation following trauma have mostly focused on local immune modulation to improve tissue regeneration by promoting the canonical M2 pro-healing macrophage phenotype over the M1 anti-inflammatory macrophage phenotype through biomaterial-based strategies and implants at the injury site (9). There are few systemic treatments, mostly targeting molecular mediators of the immune system, such as cytokines and receptors, which have had little success in the clinic to restore systemic immune homeostasis (10). In addition, only a few studies have investigated the relationship between systemic and local immune responses. For example, one study in cancer immunotherapy demonstrated that systemic immunity is required for successful anti-tumor immune-therapy, and another study in regenerative medicine demonstrated that systemic immune homeostasis is altered by local biomaterial scaffolds for muscle wound healing (11,12). Based on the links between bone and the immune system and the relationship between the local and systemic immune environments, we posit that regenerative medicine strategies will not reach their full potential without consideration of immune homeostasis and a permissive, pro-healing immune environment at both the local *and* systemic levels.

1.2 Hypothesis and Objective

The overall hypotheses are that (a) immunological markers indicative of systemic immune dysregulation and immunosuppression can be used to predict functional

regenerative outcomes in previously developed rat trauma models of delayed non-union, implant-associated infection, and composite bone and muscle trauma and (b) depletion of MDSCs, a hallmark of systemic immune dysregulation, will restore immune homeostasis and lead to improved bone regeneration in small animal trauma models.

The overall objectives are to investigate (i) how the development of systemic immune dysregulation and immunosuppression relates to functional bone regeneration and (ii) how systemic immunomodulation impacts the immune system and regenerative outcomes following severe musculoskeletal trauma.

1.3 Specific Aims

Specific Aim 1. Characterize the development of systemic immune dysregulation and immunosuppression in pre-clinical animal models of delayed non-union, bone infection, and composite trauma and identify immunological markers predictive of poor healing. Clinically, immune dysregulation and immunosuppression has been observed to worsen with increased injury severity or with additional complications such as non-union or orthopedic infections. This is supported by clinical observations where systemic immune dysregulation has been associated with increased susceptibility to opportunistic infections and poor response to treatment (4,13,14). Therefore, it is hypothesized that a subset of animals in a delayed treatment non-union model, a bone infection model, and a delayed treatment composite trauma model will develop systemic immune dysregulation that will correlate with impaired bone regeneration and be predictive of non-responders to treatment. Longitudinal characterization of bone regeneration and circulating immune cells and cytokines will occur via micro-computed tomography (uCT), radiographic imaging,

flow cytometry, and multi-analyte profiling. Post-mortem histological evaluation and biomechanical testing will be performed to quantify functional regeneration. Finally, linear and nonlinear evolutionary multivariate analytics will be used to develop predictive models of functional regeneration based on early systemic immune response biomarkers.

Specific Aim 2. Fabricate and optimize an immunomodulatory therapeutic that targets and depletes MDSCs. Although some approaches to deplete MDSCs have been reported in cancer immunotherapy using monoclonal antibodies (mAb) and small molecules (e.g. 5-fluorouracil), they suffer from several limitations – including non-specific depletion of other immune cells, high dosage requirements, short retention time, and high costs (15–17). To improve upon this, we propose to develop synthetic nanoparticle antibodies (SNAbs), gold nanoparticles functionalized with both Fc-mimicking and MDSC-targeting ligands that can mimic mAb function and specifically deplete MDSCs via antibody-dependent killing mechanisms. These particles will be evaluated *in vitro* for their targeting specificity and their ability to deplete MDSCs in both mouse and rat animal models.

Specific Aim 3. Evaluate the effect of systemic immunomodulation on the immune system status and bone regeneration in vivo following trauma. A novel biomaterial-based systemic immune modulating therapeutic, SNAbs, will be delivered *in vivo* following severe musculoskeletal trauma. We hypothesize that this will achieve targeted depletion of MDSCs that will lead to stimulation of the immune system, and ultimately, to restoration of immune homeostasis and creation of a pro-healing immune environment that leads to enhanced healing. This will be assessed using the same longitudinal bone formation and immune response characterization analyses described for Aim 1.

1.4 Significance

Severe musculoskeletal trauma is the primary cause of death in people below the age of 34; however, despite advances in trauma care management, mortality and complication rates remain high (3,18). While musculoskeletal trauma disproportionately affects military personnel, accounting for as high as 88% of those wounded in combat, it also accounts for 58% of civilian trauma patients (1,2). These injuries are associated with high rates of complications, with bone non-union rates up to 31% in patients requiring reconstruction following limb salvage, leading to prolonged hospital stays, multiple revision procedures, increased treatment costs, and often chronic disability (4).

Recently, growing attention has been given to the role of the systemic immune response and its contributions to poor trauma patient outcomes (5). Severe trauma can result in an exaggerated systemic inflammatory response syndrome (SIRS) that if left unchecked can lead to acute respiratory distress syndrome and multiple organ failure (18). In patients with limb-threatening trauma, SIRS was noted in almost 80% of patients (18,19). On the other hand, the body's natural mechanisms to defend against tissue destruction from an excess of inflammatory mediators can lead to a compensatory anti-inflammatory response syndrome (CARS), which if not properly balanced, results in long-term post-traumatic immunosuppression and leaves patients vulnerable to infections and other complications (20). Because immunologic instability immediately following trauma often prevents early total care, underlying injuries are typically treated many days or even weeks later when patients may have already transitioned into an immunocompromised state (18). This long-term phase of systemic immune dysregulation and immunosuppression has been implicated as a major contributor to poor clinical and rehabilitative outcomes

following trauma (5,21). However, despite the wide-spread acceptance of systemic immune dysregulation and immunosuppression, there are currently no standards in place to identify and treat it in severe trauma patients and surprisingly limited work in preclinical models to study it.

This project is highly significant because successful restoration of immune homeostasis in combination with local regenerative treatment strategies may enable substantial improvement in patient outcomes following severe musculoskeletal trauma. Even just identifying biomarkers to predictive patients at risk of being non-responsive (Aim 1) to conventional treatments due to immune dysregulation would be enormously beneficial to orthopaedic trauma surgeons. In this project, we will first characterize the systemic immune status in previously established rat models of delayed non-union, bone infection, and composite bone and muscle trauma in order to identify systemic immunological markers predictive of both healing outcomes and for those at-risk to develop systemic immune dysregulation and immunosuppression. Rigorous nonlinear evolutionary multivariate analytical modeling that reduces model overfitting by minimizing variable combinations while maximizing prediction accuracy will also be used. Next, we will develop and validate a new synthetic nanotherapeutic approach (synthetic nanoparticle antibodies, SNAbs) to reduce elevated levels of immunosuppressive myeloid-derived suppressor cells (MDSCs), a hallmark of systemic immune dysregulation and immunosuppression (Aim 2). Finally, we will test the ability of a systemic immunomodulatory strategy to restore systemic immune homeostasis in combination with local treatment in order to understand how systemic immunomodulation impacts the local

environment to alter functional regeneration in our clinically-relevant composite musculoskeletal trauma model (Aim 3).

1.5 Innovation

The role of the systemic immune response in bone regeneration. Prior work in the field for improving bone regeneration has focused primarily on the *local* environment, including delivery of cells, bioactive factors, and scaffolds with osteogenic potential; local immune modulation; mechanical stimulation; and enhancement of vascularization. The proposed project is innovative because it seeks to elucidate the role of the *systemic* immune response, an under-studied area of musculoskeletal trauma, in combination with local regenerative treatment. Because of the relationship between the systemic and local immune environments, systemic immune dysregulation could be promoting an unfavorable local environment, thus hindering the success of local treatments. Current clinical strategies to address severe musculoskeletal trauma do not include immunomodulatory therapeutics. Therefore, immunoengineering strategies that modulate the systemic immune response to effectively restore immune homeostasis in combination with local treatment therefore offer a novel approach to enhance bone regeneration.

Novel approach to deplete MDSCs. A common approach currently used to deplete MDSCs for cancer immunotherapy utilizes monoclonal antibodies (mAbs) targeting MDSC cell surface markers. However, mAbs are limited by high dosage requirements, high costs, and limited retention (16,17). Further, the MDSC cell surface marker targeted by mAbs is also present on other immune cells, resulting in off-target effects (16). Our proposal to develop synthetic Janus particles with an MDSC-targeting ligand may improve

upon previous MDSC-depleting strategies by increasing specificity and decreasing off-target effects. Additionally, our biomaterial-based nanotherapeutic that mimics the antibody-dependent immune responses of natural antibodies could provide a facile, synthetic platform for recombinant or animal-derived antibodies.

Improved systemic immunotherapy by cellular targeting. Previous attempts at systemic immunotherapies to treat immune dysregulation following trauma have focused mainly on systemic cytokine or growth factor delivery. Unfortunately, while these therapies successfully altered the target of interest, they failed to restore immune homeostasis, and therefore, also failed to improve patient outcomes. The lack of success in modulating the immune system highlights the complexity of the interactions between different immune mediators as well as the synergistic and redundant effects of those mediators. Because of this complexity, we believe targeting a cell population, such as MDSCs, may have a broader range of effects that may more effectively and sustainably impact the immune status to alter regenerative outcomes. At the same time, targeting an immunosuppressive cell population will afford more specificity than broad spectrum immune-stimulants thus reducing the risk of unwanted side effects.

1.6 Outline

In CHAPTER 2, background information and previous work in the field are provided on the immune response to trauma, immunomodulatory therapies, and animal models of musculoskeletal trauma and immune dysregulation. In CHAPTER 3, characterization of systemic immune dysregulation in a pre-clinical bone non-union trauma model is presented and early systemic immune biomarkers predictive of bone regeneration are discussed (Aim

1). In CHAPTER 4, characterization of systemic immune dysregulation in a rat trauma model of biomaterial-associated infection is presented (Aim 1). In CHAPTER 5, the relationship between local treatment strategy, bone regeneration, and systemic immune responses are explored further within the context of both a nonunion and a composite defect rat trauma model utilizing various biomaterial-based delivery strategies of biological factors (Aim 1). Next, fabrication, characterization, and validation of immunomodulatory synthetic nanoparticle antibodies (SNAbs) are presented in CHAPTER 6 (Aim 2). Then, in CHAPTER 7, immunomodulation using SNAbs following musculoskeletal trauma is presented (Aim 3). Finally, in CHATPER 8, conclusions and potential future directions are discussed, including SNAb immunomodulation in other applications such as tuberculosis.

CHAPTER 2. BACKGROUND[1]

Severe trauma is the leading cause of death in people below the age of 45, and even despite advances in trauma care management, mortality and complication rates remain high (3). Severe musculoskeletal trauma of the extremities is one of the most prevalent types of trauma, accounting for as high as 88% of combat wounded patients and 58% of civilian trauma patients (1,2). Adding complexity to these injuries are high rates of complications, most commonly infections and delayed or non-unions, that result in poor outcomes, longer hospital stays, and increased treatment costs (4). Severe musculoskeletal trauma, therefore, remains a large clinical challenge.

Current clinical practices for treating musculoskeletal trauma first aim to stabilize the patient and the injury site using damage control orthopedics (10). Only after the patient's condition has stabilized will surgeons attempt to treat the underlying injuries, which can occur weeks or even months after the initial injury (22). The current gold standard for treating these injuries are autologous bone grafts; however, they are limited by donor site morbidity, lack of availability, and poor integration between graft and host tissues, which can lead to delayed or non-union of the bone defects in some patients (23). Other intervention strategies being investigated to improve upon bone grafts include delivery of cells with osteogenic potential, delivery of osteoinductive growth factors and hormones, utilization of osteoconductive scaffolds, ultrasound or shockwave therapies, and mechanical modulation (24). Despite many promising strategies to improve bone

[1] Adapted from C.E. Vantucci et al, Immunomodulatory strategies for immune dysregulation following severe musculoskeletal trauma, Journal of Immunology and Regenerative Medicine, 2018. 2: p. 21-35. Reproduced with permission from Elsevier.

regeneration, a subset of patients, termed non-responders, still experience poor healing and unsatisfactory success of these intervention strategies.

Recently, systemic immune dysregulation and immunosuppression has been implicated as a main contributor to the poor outcomes and high susceptibility to complications in non-responders (5). Upon initial injury, there is an overwhelming inflammatory response, called the systemic inflammatory response syndrome (SIRS), resulting in systemic activation of innate immune cells and release of inflammatory mediators. Concurrently, there is a systemic compensatory anti-inflammatory response syndrome (CARS), which results in suppression of immune effector cells and an increase in immunosuppressive mediators. Balanced SIRS and CARS responses result in restoration of immune homeostasis and successful healing and regeneration, whereas an imbalance between SIRS and CARS is associated with onset of systemic immune dysfunction and immunosuppression (3). Patients with immune dysfunction are more susceptible to complications, such as infections, and are also thought to be the subset of patients who respond poorly to functional restoration treatment strategies (5).

The importance of the immune system in bone regeneration suggests that for optimal success of bone regenerative strategies, underlying systemic immune dysfunction must be addressed, highlighting a strong need for immunomodulatory therapeutics. The ultimate goal of these immunomodulatory therapies is to restore immune system homeostasis to improve patient response to treatment and functional regeneration of the injury. Unfortunately, immunomodulatory strategies thus far have been largely unsuccessful in shifting the clinical paradigm and improving patient outcomes. A large part of this lack of success may be attributed to a poor understanding of the progression of non-responders

towards systemic immune dysfunction and immunosuppression. Better characterization of the immune response to trauma and the progression towards immune dysfunction may elucidate important interactions that play key roles in defining pathologic immune responses. This information can then be utilized in the design and development of improved immunomodulatory therapeutics, and ultimately, this approach may lead to improved regenerative outcomes for severe musculoskeletal trauma patients.

2.1 The Immune Response to Trauma

The discovery of the involvement of receptor activator of nuclear factor kappa-b ligand (RANKL) in both bone regeneration and the immune system, particularly concerning T cell responses, led to the advent of osteoimmunology in the early 2000s (25). This resulted in increasing interest in the interactions between bone and the immune system in the context of disease and injury, including specific mechanisms and cell types involved. The immune response to trauma highlights how changes in bone homeostasis, such as injury, impact the immune system, and subsequently how these cellular and systemic immunological changes impact bone healing and the success of regenerative intervention strategies.

2.1.1 Development of Immune Dysregulation

Immediately following injury, factors associated with tissue damage, termed damage-associated molecular patterns (DAMPs), initiate inflammatory responses. DAMPs include cellular components that would typically not be found outside of the cell, including heat shock proteins, uric acid, and nuclear proteins (10). Due to their endosymbiotic origin, mitochondrial DNA and peptide fragments mimicking pathogen-associated molecular

patterns (PAMPs) are also important inflammatory mediators that trigger inflammatory responses through toll-like receptor 9 (TLR-9) (26). A massive onslaught of inflammatory cues resulting from severe tissue damage causes both a local and systemic inflammatory response, including cell-mediated and protein-mediated changes. Neutrophils, an innate immune cell and one of the first responders at the injury site, exhibit impaired apoptosis increasing inflammation through release of granules, cytokines, and other inflammatory mediators (6,10). This overwhelming local inflammation leads to a systemic response and the development of SIRS (3).

A SIRS response left unchecked would be detrimental to the host because inflammatory mediators can eventually begin to break down host tissues, resulting in multiple organ dysregulation syndrome (MODS) and even death (3). In order to protect its own tissues, the host mounts a concurrent systemic anti-inflammatory response aimed at counter-balancing the acute inflammation caused by SIRS, termed the compensatory anti-inflammatory response syndrome (CARS) (6). For patients who resolve inflammation, the SIRS and CARS responses are able to adequately balance each other to restore homeostasis, which typically occurs between 7 and 14 days after injury (Figure 2.1). For those who are unable to resolve the initial inflammation, the genomic storm of inflammatory and anti-inflammatory genes remains elevated even at 28 days post-injury (27). A larger SIRS response with an inadequate compensatory anti-inflammatory response can lead to early deaths due to overwhelming inflammation and multiple organ failure. On the other hand, when the compensatory anti-inflammatory response overwhelms the initial inflammatory response, systemic immune dysregulation and immunosuppression develops (8). Trauma patients who develop immunosuppression are more susceptible to

opportunistic infections, and they respond poorly to healing and intervention strategies, often requiring additional surgical procedures and longer hospital stays (6).

Systemic immune dysregulation and immunosuppression impacts both the innate and adaptive immune systems. Despite systemic immunosuppression, the local site of injury suffers from chronic inflammation, creating an environment not conducive to inflammation resolution and healing. This condition has been termed persistent inflammation, immunosuppression, and catabolism syndrome (28). Maintenance of systemic immunosuppression requires significant energy, resulting in high levels of catabolism that further suppresses immune responses by preventing immune effector cells from utilizing these resources (3,5).

2.1.2 Cellular Response

Systemic immune dysregulation and immunosuppression affects cells of both the innate and adaptive immune systems, resulting in decreased function and numbers of immune effector cells, and increased function and numbers of immunosuppressive cells (Figure 2.1). One of the most historically studied changes in immune cell function after trauma is the decreased ability of antigen-presenting cells (APCs), in particular monocytes, to present antigen. This occurs due to downregulation of HLA-DR, an MHC class II molecule needed for antigen presentation (8). In patients without complications, monocyte HLA-DR levels recover around 7 to 14 days post-injury, whereas immunosuppressed patients continue to maintain low levels of HLA-DR on monocytes (29).

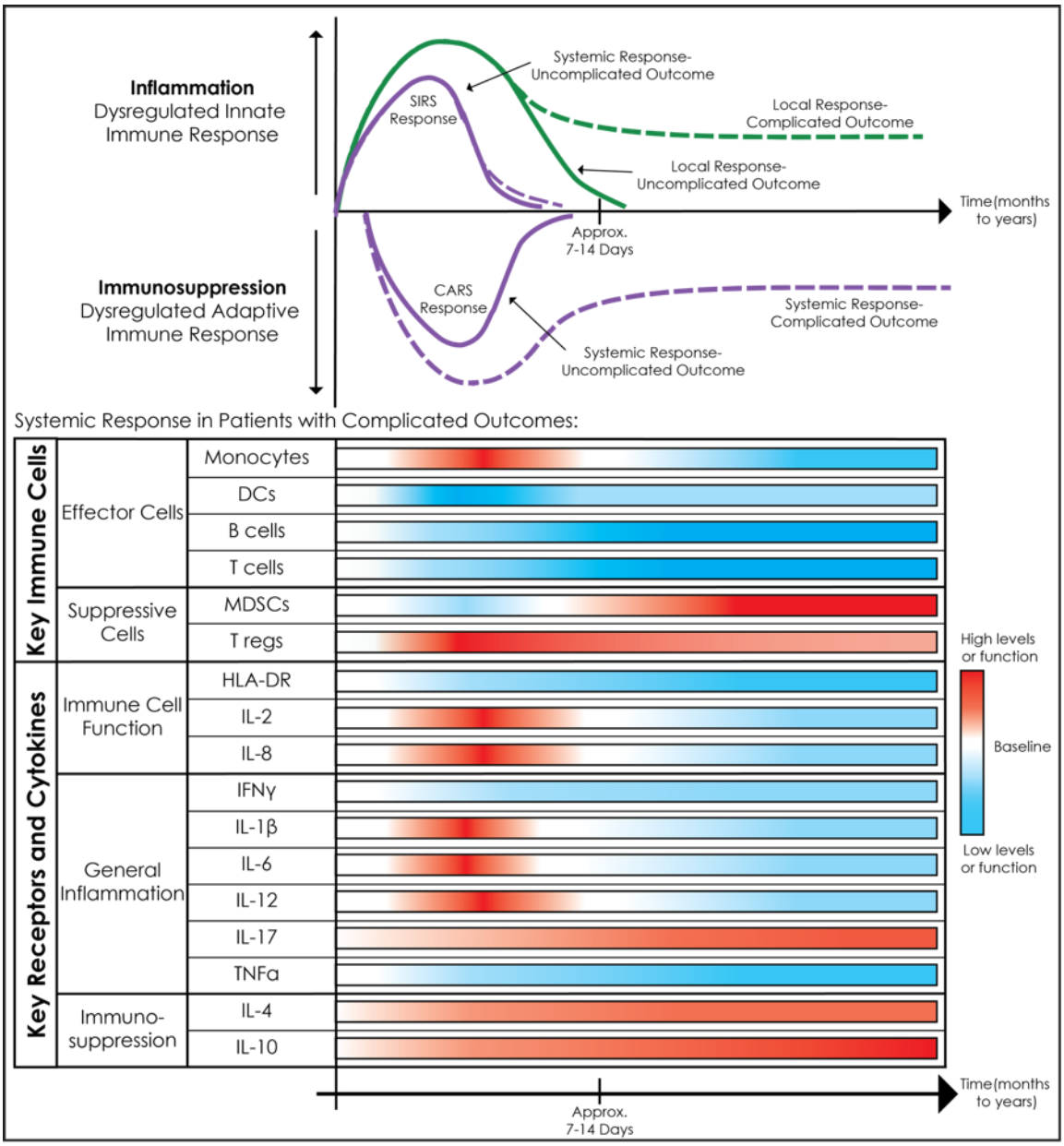

Figure 2.1. The Development of Systemic Immune Dysregulation.
Following severe injury, there is an increase in both local and systemic inflammation in response to DAMPs released from damaged tissue. Concurrently, there is a systemic anti-inflammatory response. Patients with uncomplicated outcomes will see resolution of inflammation around 7-14 days, whereas patients with complicated outcomes will maintain chronic local inflammation and systemic immunosuppression. Once in a state of systemic immunosuppression, circulating immune effector cells and inflammatory cytokines are downregulated and circulating immunosuppressive cells and cytokines are upregulated.

Along with monocytes, other APCs affected by trauma include dendritic cells (DCs) and B cells. Many immune cells suffer apoptotic losses following trauma; however, DCs are particularly susceptible to apoptosis, and this has been shown to contribute to poorer outcomes clinically (30). Along with the loss of DC numbers, their functional interactions with T cells are altered, resulting in induction of T cell anergy and T regulatory cell (Treg) expansion instead of effector T cell activation (31,32). It has also been demonstrated that under inflammatory conditions DCs can transdifferentiate into osteoclasts, further inhibiting bone regeneration (33). Although B cells have not been investigated as thoroughly as other antigen-presenting cells, there is still evidence that they play a role in the immune response to trauma. B cell-deficient mice were shown to develop osteoporosis due to a lack of B cell-derived osteoprotegerin (OPG), which is a decoy receptor for RANKL that inhibits osteoclastogenesis (34). Apoptotic losses of B cells may therefore impact bone homeostasis through B-cell derived mediators, such as OPG. B cells, along with T cells, have also been shown to impact bone quality and matrix mineralization, in particular collagen deposition, for bone healing in mice (35).

T cells, another cell of the adaptive immune response, are also altered in response to trauma. Similar to DCs, T cells undergo significant and premature apoptosis as well as changes in function following trauma (8). The initial response to injury skews CD4+ effector T cells towards differentiation into the inflammatory Th1 subtype; however, chronic inflammation at the injury site leads to T cell exhaustion, which shifts differentiation to the anti-inflammatory Th2 subtype (8). T cell apoptosis and a shift towards the anti-inflammatory Th2 subtype further contributes to systemic immune dysregulation and immunosuppression. The impact of trauma on T cells has been

investigated clinically and shown to be associated with poor outcomes (36). In a clinical study looking at patients with trauma and hemorrhage, a decrease in T cell proliferation and total lymphocyte counts was observed (37). Another clinical study looking at brain trauma patients noted similar declines in circulating T cells, declines in IL-2 (a cytokine important for T cell proliferation and expansion), and an increased susceptibility to nosocomial infections (38). Functioning T cells are generally considered anti-osteoclastogenic cells due to the cytokines and factors they release (IFNg, IL-4, and IL-10). Osteoclastogenesis increases the ratio of bone-resorbing osteoclasts to bone-forming osteoblasts, thus hindering bone regeneration. Therefore, a decline in the population of functioning T cells will decrease IFNg, IL-4, and IL-10 and reduce their ability to inhibit osteoclastogenesis (25,33).

Another contributing factor to a decline in T cells is changes in hematopoiesis that occur as a result of trauma. Inflammatory cues induce mature T cells to be released from the bone marrow and into the periphery, creating more free space within the bone marrow cavity. This empty space initiates emergency myelopoiesis and granulopoiesis at the expense of lymphopoiesis (39,40), preventing hematopoietic stem cell (HSC) differentiation into T and B cells. Further, the loss of osteoblasts, cells responsible for bone formation, along with their precursors, were shown to impact hematopoiesis because osteoblasts are an important component of the bone marrow niche and play a role in the survival and differentiation of HSCs (41). Therefore, trauma alters HSC differentiation programs as well as biological cues involved in their survival and maintenance.

In addition to deficits in functional immune cells following trauma, there are also increased numbers of suppressor cells that contribute to systemic immune dysregulation

and immunosuppression. Both myeloid-derived suppressor cells (MDSCs) and T regulatory cells (Tregs) increase in patients after trauma and are associated with worsening immune dysregulation (8,36,37,42). MDSCs are a heterogeneous population of immature myeloid cells that drastically increase during impaired hematopoiesis and emergency myelopoeisis following prolonged inflammatory genomic storm (27). While some MDSCs are thought to retain capabilities to fully differentiate into functioning immune cells, most are arrested in their immature and immunosuppressive phase (43). MDSCs primarily and potently suppress T cells, for example, by depleting arginine resources that T cells utilize for proper function (44). They also have been shown to induce immunosuppressive Treg development, creating a feedforward mechanism to rapidly increase immunosuppression (45). Tregs have a wider mechanism of action than MDSCs, suppressing both the innate and adaptive immune systems and inducing alternative activation in macrophages (6). Parallel to their contributions to the immunosuppressive environment following trauma, both MDSCs and Tregs have also been implicated as main contributors to the local immunosuppressive environments found in tumors (46,47).

2.1.3 Inflammatory Mediators

Cytokines have a significant role in directing immune responses, and thus, the cytokine milieu is also significantly altered following trauma (Figure 2.1). Initially, there is an increase in circulating pro-inflammatory and anti-inflammatory mediators, including IL-4, IL-6, IL-8, IL-10, and IL-17 (6,33). Inflammatory signals activate macrophages to release even more pro-inflammatory cytokines including IL-1b, and IL-12, which have been shown to play a role in the development of mature osteoclasts (48). Further, IL-6, IL-8, and IL-17 are also involved in osteoclastogenesis and bone resorption independent of

the RANKL pathway, indicating that these circulating mediators could be stimulating osteoclastic bone resorption and contributing to poor healing outcomes (6).

Another important early inflammatory mediator released by monocytes and macrophages is high mobility group box-1 (HMGB1), a nuclear DNA-binding protein that can bind various TLRs and promote production of reactive oxygen species (ROS) from innate immune cells (26). This creates a feedforward mechanism where activation of TLRs and release of ROS from neutrophils leads to further activation of inflammatory pathways, ultimately resulting in SIRS.

Circulating IFNg, a cytokine important for macrophage activation, is rapidly suppressed in trauma patients. Only in patients with uncomplicated outcomes do IFNg levels recover around 7 days post-injury, similarly to when HLA-DR expression recovers in these same patients (29). IL-2, a cytokine important for T cell expansion and proliferation, is also suppressed systemically in trauma patients. In combination with reduced IFNg, this results in suppression of the Th1 effector cell response. The increased circulating levels of IL-10 and IL-4 cytokines in combination with Th1 suppression by decreased levels of IFNg and IL-2 leads to enhanced differentiation into Th2 effector cells (6). These changes therefore further contribute to the development of systemic immune dysregulation and immunosuppression.

2.2 Immunomodulatory Therapies

The ultimate goal of immunomodulatory therapies following trauma is to reverse immune dysregulation to improve patient outcomes and functional tissue regeneration. Although utilization of immunomodulatory strategies dates back to the 1980s, clinically

established immunomodulatory therapies for trauma patients with immune dysregulation still do not exist.

2.2.1 Immunosuppressive Therapies

Initially, the overwhelming inflammatory response following trauma was thought to hinder successful regeneration of the injury and be detrimental to patient rehabilitation. Therefore, first attempts at immunomodulation following trauma utilized immunosuppressants, such as corticosteroids, which decrease inflammation by preventing the release of both pro-inflammatory cytokines (TNF, IL-1b) and tissue destructive factors (10). However, clinical evidence did not support the use of immunosuppressive corticosteroid treatment. The largest ever clinical trial conducted on head trauma patients, the corticosteroid randomization after significant head injury (CRASH) trial with over 10,000 enrolled, had to be stopped early due to significantly increased mortality in the corticosteroid treated group compared to the placebo control (49). Another trial aimed specifically at head trauma patients who developed acute respiratory distress syndrome (ARDS) also saw an increase in mortality compared to placebo controls when immunosuppressive steroids were used as treatment (10). Long-term steroid usage has also been associated with detrimental and irreversible damage to the patient, including osteoporosis and osteoarthritis (50).

The harmful and long-term side effects of corticosteroids for trauma patients were thought to result from their general mechanism of immunosuppression. Therefore, research continued to investigate other potential immunosuppressive therapies to modulate the immune response; however, even specific immunosuppressive therapies, including TNFa

neutralization, NO inhibition, and IL-1 inhibitors all similarly failed to improve mortality in trauma patients, and in some cases even worsened patient outcomes (3). After multiple failed attempts at using immunosuppressive therapies to improve trauma outcomes, it became generally accepted that the inflammatory response is required and even beneficial in repair and regeneration of severe injuries (26). As clinicians began to better understand systemic immune dysregulation and immunosuppression, there was a transition towards investigation of immunostimulatory therapies.

2.2.2 Immunostimulatory Therapies

Immunostimulatory therapies to treat immune dysregulation following trauma have focused mainly on systemic cytokine or growth factor delivery, in particular, IFNg, GM-CSF, and G-CSF. More recently, other targets and cell-based therapeutics have also been investigated, including IL-7 and the use of mesenchymal stromal cells (MSCs) for immunomodulation (3,32,51). While early immunostimulatory therapies successfully altered the target of interest, they failed to restore immune homeostasis, and therefore, also failed to improve patient outcomes. For example, IFNg is one of the most well-studied immunomodulatory therapeutics aimed at increasing HLA-DR expression on monocytes to restore antigen presentation and monocyte function. However, despite being studied for over 20 years, both clinical and animal studies using IFNg treatment have shown no significant changes in important metrics like mortality, hospital stay lengths, or health evaluation scores (10,52). While these studies have shown that IFNg does successfully restore HLA-DR expression, plasma levels of cytokines such as TNFa, IL-6, IL-10, and IL-8 were unaffected, as were clinically relevant endpoints (53–55). This suggests that while IFNg treatment did increase HLA-DR expression, this ultimately did not have any

major influence on other inflammatory mediators or on counteracting systemic immune dysregulation. Other studies have indicated that HLA-DR expression may not even be a relevant target due to a lack of correlation between HLA-DR expression and patient outcomes (56). Based on widely varied results and evidence that IFNg does not alter the immune system status or patient outcomes, other therapies have been investigated.

The two next most widely investigated immunostimulatory therapeutics for treatment of immune dysregulation following trauma are GM-CSF and G-CSF. GM-CSF is a growth factor that increases expression of HLA-DR and expression of pro-inflammatory cytokines while G-CSF enhances expression of both pro- and anti-inflammatory mediators (52). Similar to IFNg treatment, clinical trials showed that while HLA-DR expression was increased following GM-CSF treatment, it did not recover back to healthy patient levels and also had no impact on mortality compared to patients not receiving GM-CSF treatment (57,58). G-CSF treatment performed even worse than GM-CSF with poor recovery of HLA-DR expression on monocytes and no functional recovery of T or B cells (52). While another study demonstrated that G-CSF reduced bacteremia, hospital stays and 28 day survival were unchanged compared to untreated patients (38). Similar to IFNg, clinical results indicate that while GM-CSF and G-CSF may have some impact on HLA-DR or cytokine expression, they still failed to restore immune homeostasis and improve healing and regeneration.

More recent strategies have aimed to increase hematopoiesis or increase differentiation of MDSCs into DCs and macrophages (43,59). IL-3 and GM-CSF were shown to increase hematopoiesis *in vitro*, and retinoic acid has been used to reduce the number of MDSCs and promote differentiation into functioning immune cells in a murine

model (43,59). Parathyroid hormone (PTH) has also been used with the aim of increasing hematopoietic stem cell (HSC) number and function (60). Increasing hematopoiesis and differentiation into functional immune cells while decreasing immunosuppressive MDSC populations therefore shows promise for counteracting immune dysregulation. Other more recent therapies currently being investigated are the use of IL-7 to increase CD8+ and CD4+ T cell populations numbers as well as anti-PD-L therapy to augment T cell function. However, so far, neither have shown success in improving outcomes for trauma patients (32).

While immunostimulatory therapies have been shown to successfully modulate individual components of the immune system, such as HLA-DR expression, their main limitation is their inability to subsequently counteract systemic immune dysregulation (3). Their lack of success in modulating the immune system highlights the complexity of the interactions between different immune mediators as well as the synergistic and redundant effects of those mediators. Because of this complexity, improved immunomodulatory therapeutics are needed that address more than just one component of the immune system. For example, research in cancer immunotherapy to treat immunosuppressive environments within tumors has investigated the effect of MDSC suppression to improve immune function (61,62). Targeting an entire cell population or using cell-based therapeutics may have a more significant impact on the immune system compared to targeting individual molecules, receptors, or cytokines. In addition, patient-specific treatment strategies may be required due to the large heterogeneity in patient responses.

Recent work to treat immune dysregulation following trauma has investigated utilizing MSCs as immunomodulatory agents to target immune cell function. MSCs were

shown *in vitro* to induce IFNg synthesis in natural killer (NK) cells from severely injured patients (51). Although this study was preliminary, using MSCs for immunomodulation is currently an area of heavy investigation for a wide variety of applications and may be translatable to treat immune dysregulation following trauma (63).

2.2.3 Biomaterial-Mediated Strategies

Biomaterial-mediated strategies to improve bone regeneration and healing have largely focused on improving osteogenic capabilities of biomaterials through their biological, chemical, and physical properties (64). However, due to the significant role of the immune system in mediating osteogenesis and healing, it has become of more interest to utilize bone biomaterials that also have immunomodulatory properties (65,66). Mostly, these biomaterials have focused on decreasing local inflammation and modulating the local immune environment to improve healing (67). While this has been shown to be beneficial to address local chronic inflammation, these systems do not address systemic immune dysregulation, which may limit their usefulness translationally in treating immune dysregulation following trauma. At the same time, local immune modulation along with systemic immune modulation may be beneficial in restoring immune homeostasis both systemically and locally to improve bone healing and patient outcomes.

There are many properties of biomaterials that can be altered to impact osteogenic and immunomodulatory factors including surface topology and chemistry, pore size and porosity, inclusion of bioactive molecules, or coupling with immunomodulatory drugs (67–70). Hydrophobic surface chemistries tend to improve monocyte adhesion, while hydrophilic surfaces inhibit monocyte adhesion but also increase inflammatory cues

(71,72). Similar to hydrophilic surfaces, cationic surfaces also increase inflammatory cues, while anionic and neutral surfaces decrease inflammation (73). Microstructure and surface topography of the biomaterial can also alter responses. For example, nanoscale microstructures and topographies have been found to stimulate mineralization production in human MSCs *in vitro* without osteogenic factors (70). These surfaces can also alter the immune responses, impacting release of inflammatory mediators and angiogenic factors (68). Along with the nanoscale microstructure, pore size also impacts bone growth and inflammatory responses. Pore size should be optimized to allow ingrowth of bone tissue and to elicit the desired inflammatory responses. Larger pore sizes have been shown to increase M2 macrophage markers, typically thought of as anti-inflammatory macrophages, and to decrease M1 macrophage markers, typically thought of as inflammatory macrophages (74). Lastly, bioactive molecules tethered to bone biomaterials can induce differential inflammatory responses. Cobalt (Co) and silicon (Si) stimulate inflammation, whereas other ions like zinc (Zn), magnesium (Mg), and strontium (Sr) suppress inflammation (67). Biomaterial-mediated strategies to modulate the local immune environment may be useful in conjunction with systemic immunostimulatory therapies to more effectively counteract immune dysregulation and immunosuppression following trauma.

2.3 Considerations for Development of Immunomodulatory Strategies

Surgeons and clinicians are ill-equipped to deal with impairments in the immune system. Standard practice following trauma is to monitor systemic levels of immune mediators and wait until they reach allowable levels to proceed with intervention strategies for the patient (75). Not only do surgeons and clinicians need improved

immunomodulatory therapeutics, but essential protocols are also needed that determine when immumodulatory treatment should be administered, how it should be administered (i.e. systemically versus locally), and to whom it should be administered. Therefore, treatment timing, patient characteristics, injury severity, and delivery method must be taken into consideration during the development and optimization of immunomodulatory therapeutics to ultimately understand how these factors affect the success of subsequent regenerative interventions (Figure 2.2).

2.3.1 Treatment Timing

Treatment timing is critical for the success of immunomodulatory therapies due to significant changes in both systemic and local immune environments over time following severe trauma (Figure 2.2). Current clinical practice delays treatment of the injury until the patient has been adequately stabilized, which depending on the severity of the injury, may be a permissive amount of time for the development of immune dysregulation. For example, the Masquelet technique is commonly used to treat bone and soft tissue injuries. Patients first undergo debridement and external stabilization followed by placement of a polymethyl methacrylate (PMMA) spacer within the defect site during the first damage control surgery. Subsequent interventions aiming to treat the underlying defect do not occur for another 6 to 8 weeks after the initial stabilization surgery, potentially allowing adequate time for the development of immune dysregulation (22). Strategies are needed to both identify patients with immune dysregulation and subsequently treat them.

Clinically, there are differences in the regenerative success of early versus delayed treatment for trauma patients. A small clinical case specifically looking at craniofacial

traumas when treated immediately versus delayed (2 weeks post injury) showed 100% adequate healing in all patients treated immediately (20 out of 20 patients) and only 67% adequate healing in patients treated 2 weeks post-injury (4 out of 6 patients) (76). Another clinical study looking at early (1-22 days post injury) and delayed repair (23 days or more post injury) of fractures in 43 patients showed significantly increased rates of post-operative complications in patients receiving delayed treatment (77). Other clinical trials have shown that acutely treated patients who receive early total care have shorter hospital stays and decreased numbers of infectious complications (13,24). Although early total care is the ideal treatment course, this may not be possible in all cases due to the stability of patient. Therefore, immunomodulatory therapies are needed to target this subset of patients who are unable to receive early total care due and therefore have a higher likelihood of developing complications and immune dysregulation.

The differences in immediate versus delayed treatment are also supported in animal models of trauma. For example, a rat model of bone non-union received treatment immediately or after one week with bone morphogenetic protein 2 (BMP-2), a clinically relevant osteoinductive factor, in combination with stem cell therapy. Treatment results showed significantly better healing in the immediately treated versus delayed treatment group, where no animals had bridging of the bone defect in the delayed treatment group while 75% of the animals showed bridging in the immediate treatment group (78). Other animal models have also shown differences between delayed and immediate treatment. For example, a rat model of rotator cuff injury showed functional biomechanics and bone density were significantly reduced in the delayed treatment (3 weeks post-injury) compared to immediate treatment (79). Another example utilized a sheep model of bone fracture

combined with nerve injury to show that delayed treatment decreased functional outcomes of nerve repair (80). The delay in treatment time provides the opportunity for development of immune dysregulation that can then negatively impact healing and regenerative outcomes. However, more research is needed to better understand the relationship between the systemic immune environment and non-responders following delayed treatment.

Overall, the timing of treatment must be considered when developing and testing immunomodulatory therapeutics due to the temporal changes in the immune environment following trauma. Currently, there are not established clinical strategies to address patients who have developed systemic immune dysregulation and immunosuppression, which hinders success of therapeutic interventions. Addressing and modulating the underlying immune dysregulation that develops over time following trauma may lead to improved healing and success of treatment in patients receiving delayed treatment.

2.3.2 Patient Variability

Patient-specific factors, such as age, gender, genetic predispositions, and co-morbidities, can influence patient outcomes, and therefore must be considered in the development of immunomodulatory therapies (24). All of these factors may influence the resulting systemic and immune profiles, which may in turn alter the success of an immunomodulatory therapeutic (Figure 2.2).

2.3.2.1 Age

Age plays a critical role in patient outcomes, and this has been seen clinically and in animal models of trauma (81,82). Elderly patients have higher post-operative

complications and evidence has suggested this to be a direct consequence of ageing of the immune system. In one clinical trial, blood was collected from 20 young (<50) and 21 old patients with long bone fractures and analyzed for 6 key cytokines and growth factors. These profiles were then compared to age-matched healthy controls. Most significantly, young fracture patients showed significantly decreased levels of the inflammatory cytokines IL-6 and TNFa, but a significant increase in the growth factor GM-CSF. Old patients on the other hand showed significantly decreased IFNg and TRAIL, which is a receptor important for the induction of apoptosis. Looking at TUNEL staining to determine neutrophil activation showed a significant decrease in post-traumatic neutrophil activation in the young population (83). While only a few inflammatory outcomes were measured, it is evident that old and young patients have very different inflammatory responses to trauma.

Along with clinical evidence, the effect of age on response to trauma has also been demonstrated in animal models. An animal model of hip fracture in aged rats resulted in increased susceptibility to infection with *Pseudomonas aeruginosa.* Similar to clinical outcomes, aged rats had significantly increased levels of IL-6 and TNFa and increased mortality following a bacterial challenge (84). Animal models of tibial fracture in sheep, calvarial defect in mice, and tibial defect in mice all demonstrated that immature or juvenile animals healed significantly better than mature or aged animals (85–87).

The change in response to trauma based on age is due to underlying biological changes. Based on *in vitro* and *in vivo* experiments, older rats have significantly fewer hematopoietic and osteogenic colonies as well as increased bone resorption and osteoclast number (88,89). Further, there are changes in both mitochondrial gene expression as well

as nuclear gene expression. Some of these changes include reduction in genes involved in mitochondrial energy pathways, cell proliferation and adhesion, calcification, angiogenesis, and lipid metabolism (90–95). Along with changes in gene expression, immunoaging has been implicated in altering the response of the elderly to trauma. As people age, the ability of their stem cells to differentiate and regenerate declines, including differentiation of immune cells from hematopoietic stem cells (HSCs). Most interestingly, the subset of HSCs that are very potent for lymphocyte differentiation are lost in the aging process (96). Out of the immune cells that do differentiate successfully, many of them exhibit functional alterations. For example, in one study, younger mice had macrophages with lower resting levels of oxidative stress compared to older mice (97). In an *in vivo* test, inhibiting macrophage migration to the site of injury delays healing in younger animals, whereas in older animals, preventing macrophage recruitment to the fracture site actually stimulates repair (98). Lastly, as people get older, the average number of co-morbidities increases, which also likely plays a role in decreasing healing in elderly populations (99).

2.3.2.2 Gender

Along with age, gender also plays a role in bone healing, largely due to the female sex steroid hormones (100). Evidence has shown that estrogen impacts innate immunity, adaptive immunity, and hematopoiesis. More specifically, estrogen decreases the production of pro-inflammatory cytokines, including IL-6 and TNF, as well as alters the expression of pattern recognition receptors (PRRs) on innate immune cells (100,101). Further, dendritic cells (DCs) express the estrogen receptor, and therefore their function and numbers are altered in females versus males due to the presence of estrogen (102). On the adaptive immunity side, estrogen alters B cell activity and antibody production. The

role of estrogen in the immune response is supported by the reversal of these effects in post-menopausal females who no longer produce elevated levels of female sex steroids (103).

Clinically, these differences result in females being less susceptible to infections and sepsis, and it also significantly decrease the rates of multiple organ failure syndrome (MOFS) in females compared to age-matched males (100,103). In males, androgens are immunosuppressive, which also contributes to the higher rates of complications and the 20% higher risk of death following trauma compared to females (104,105). Results from animal models also support differences between the male and female responses to injury. In a mouse model of burn injury, decreased splenocyte proliferation was observed at 1 day post-injury for males but not until 7 to 10 days post injury for females (106) . Despite the decreased complication rates in females, males still exhibit better healing rates and biomechanical outcomes (107–109). It has been suggested that differences in mesenchymal stromal cell (MSCs) and muscle derived stem cells, such as the mobility and quality of the MSCs, between males and females alter bone formation and healing (108,110,111).

2.3.2.3 Genetic Predispositions and Co-Morbidities

Clinically, co-morbidities and pre-existing conditions are significant risk factors for trauma related mortality and increased complications following trauma (99,112–114). The type of co-morbidity also impacts the risk. Some co-morbidities have higher risks than others, while some increase risk for mortality but others can increase risk for complications (112). Co-morbidities include smoking, diabetes, arthritis, cancer, renal disease, osteoporosis, etc. (99,114). A study investigating the effect of smoking on healing showed

alterations in specific bone-related markers (115). While co-morbidities each complicate patient outcomes differently, they all consistently cause increased immunosuppression, which is important to consider when developing an immunomodulatory therapeutic.

Potentially more challenging to deal with compared to obvious co-morbidities are genetic predispositions that result in patient genome expression changes (116). These vary from patient to patient, making treatment more challenging because these predispositions may not be known a priori like co-morbidities. Systems biology approaches may help improve understanding of these patient-specific differences.

2.3.3 Injury Severity

The severity of a single trauma or the presence of multiple traumas can drastically change the immune response and cause worsening immunosuppression in patients with immune dysregulation. This has been seen both clinically and in pre-clinical animal models and leads to decreased functional outcomes and increased complications. The extent of immune dysregulation based on the severity of the injury must be considered in the design of immunomodulatory therapeutics and in determining what will be most optimal for treatment.

Clinically, polytrauma results in worsening outcomes for patients compared to single trauma. A clinical trial examining upper extremity trauma in combination with traumatic brain injury (TBI) showed significantly reduced functional outcomes leading to long term vocational restrictions in patients with combined extremity trauma and TBI compared to just extremity trauma alone (14). Further, another set of clinical trials comparing multiple trauma patients to single and minor trauma patients documented

hospital stays twice as long with twice as much resource utilization (117). While injury severity correlates with poor outcomes clinically, it also correlates with increased immunosuppression. For example, in a clinical study examining 12 patients with varying injury severity scores, the levels of the inflammatory C3 complement protein were found to be decreased in the sera of patients with higher injury severity scores compared to lower injury severity scores (118).

Animal models of trauma also reflect worsening outcomes following more severe injury. For example, rat tibial defect models with a volumetric muscle loss (VML) have shown poorer outcomes, significant functional deficits, increased inflammation, and longer lasting innate and adaptive immune responses compared to tibial defects without VML or sham animals (119,120). Rat femur defects in combination with muscle trauma also similarly show worsening immunosuppression and functional outcomes (121,122). Another rat model combining a femoral segmental defect in conjunction with nerve trauma showed significant functional deficits compared to bone only defect or nerve only defect, as assessed by gait analysis (123). In a rat model of femur fracture versus polytrauma, MDSCs were upregulated and underwent more extensive expansion in the polytrauma group, demonstrating the relationship between increased injury severity and increasing immunosuppression (124). Increased immunosuppression is important to take into consideration because it contributes to higher risks for complications and decreased regenerative outcomes in more severely injured patients.

2.3.4 Systemic versus Local Delivery

The site of delivery for any therapeutic can be critical for treatment success and therefore must be taken into consideration when designing immunomodulatory therapeutics. While systemic delivery is non-invasive and therefore easier to translate to the clinic, the downside is that the therapeutic must hone to the target of interest without causing unwanted systemic or off-target responses. While local delivery allows the therapeutic to be delivered precisely to the site of interest, this method can require more invasive delivery strategies that could make local delivery more challenging and harder to translate clinically.

In the case of systemic immune dysregulation and immunosuppression following severe trauma, the immune system is suppressed systemically, but chronically inflamed at the site of injury. While anti-inflammatory therapeutics may be beneficial when delivered locally to the site of chronic inflammation, systemic delivery of an anti-inflammatory may be detrimental, or even deadly, due to systemic immunosuppression, such as was seen during the CRASH trial. The CRASH trial which utilized a corticosteroid treatment, a systemic immunosuppressive therapeutic, actually increased mortality rates in head trauma patients (49). The surprising results from this trial highlight the importance of understanding local and systemic environments and considering how immunomodulatory therapeutics will impact those environments upon delivery to elicit a desired response.

The differences between the systemic and local immune environments following severe trauma have been documented clinically, including in patients with chest trauma, bone fractures, and surgical trauma (125–129). In a clinical trial with 16 chest trauma patients, pro-inflammatory cytokines IL-1b and IL-8 were significantly elevated locally (in the bronchoalveolar lavage fluid), but not in the plasma, compared with healthy volunteers

(125). Similarly, in a clinical trial following gastrointestinal surgical trauma, higher levels of inflammatory cytokines (TNF, IL-1, IL-6) were again found locally, but not systemically, except for IL-6 which was higher systemically (126). In an animal study using a porcine model of polytrauma (tibia fracture, lung contusion, liver laceration, and pressure-controlled hemorrhage), local and systemic levels of pro-inflammatory factors (IL-6, IL-8, HMGB1, HSP70) were all elevated; however, elevation of local levels was prolonged compared to systemic levels (128). These studies suggest temporal and spatial differences in the immune response both systemically and locally.

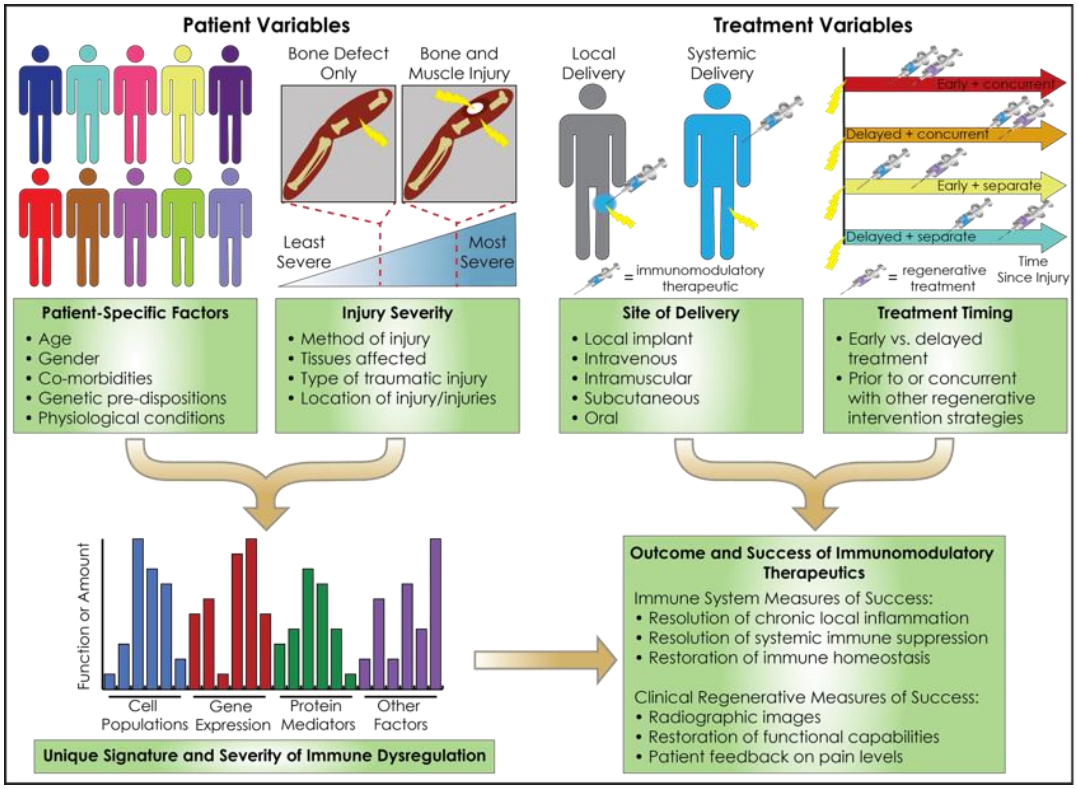

Figure 2.2. Considerations for Immunomodulatory Therapeutics.
Both patient variables and treatment variables can impact the outcomes and success of immunomodulatory therapeutics to restore immune homeostasis and improve regeneration of the injury. Patient variables include patient-specific factors and injury severity that will impact the severity of the resulting immune dysregulation, which may be unique from patient to patient. Because of the spatiotemporal changes in the immune system following

injury, treatment variables that include the site of delivery and the timing of delivery will also impact the success of the therapeutic.

Aside from changes in inflammatory mediators, there are also cellular differences systemically versus locally. A clinical trial of patients with abdominal surgical trauma noted decreased HLA-DR expression on circulating monocytes, but increased HLA-DR expression on monocytes collected from the abdominal fluids (129). Evidence of systemic immunosuppression coupled with local inflammation was further supported in another clinical trial investigating the systemic and local immune status of 56 patients following bone fracture with soft tissue trauma (127). Systemic and local environments are important when considering immunomodulatory strategies because the immune environment may alter the success of the treatment strategy.

2.4 Animal Models for Immunosuppression following Musculoskeletal Trauma

Pre-clinical animal models are essential for translating scientific discoveries to the clinic, and they can be used to either test therapeutics or to improve understanding of underlying mechanisms and biology for disease and injury. Unfortunately, although there are many trauma models, few of them, if any, have clearly established or characterized the presence of systemic immune dysregulation that is a major contributor to increased complications throughout the regeneration and rehabilitation process. Further, many of these animal models test therapeutics immediately after injury, which does not represent the clinical standard for treating musculoskeletal trauma where injuries are typically first stabilized and then later, bone grafts or other intervention strategies are used (22). Other factors affecting immune dysregulation besides timing include the presence of complicating factors, such as infection, and the extent of injury, where more severe injuries

worsen immune dysregulation. Therefore, an appropriate animal model to recapitulate immunosuppression following musculoskeletal trauma will likely require delayed treatment, increased injury severity, such as a composite critical sized bone defect combined with a volumetric muscle loss injury, or the presence of another complicating factor, such as an infection. Increased evidence of the impacts of clinical post-traumatic immune dysregulation and immunosuppression on regenerative outcomes has emphasized the need for musculoskeletal trauma research in an immune dysregulated environment. A well-characterized and standardized animal model for studying systemic immune dysregulation and immunosuppression following musculoskeletal trauma will be essential for attaining reproducible, robust, and clinically relevant results for trauma patients with immune dysregulation.

2.4.1 Selecting a Model

The goal in selecting an animal model for immunosuppression following musculoskeletal trauma is to balance clinical relevance and translational capability with a simplistic, but robust and challenging model. Considerations during selection include which species should be used, the severity of the injury (single trauma versus composite and multiple traumas), the timing of treatment (immediate versus delayed), and whether or not complicating factors, such as infection, should be included. While these components have been shown to clinically worsen immune dysregulation and immunosuppression, better characterization of these animal models will be useful in determining the extent and progression of immune dysregulation. Ultimately, a successful animal model will mimic clinical presentations and demonstrate clear immune dysregulation and immunosuppression along with poor healing and response to intervention strategies.

2.4.2 Current Animal Models of Musculoskeletal Trauma

There are a large number of animal models for trauma, reflecting not only on the prevalence of trauma seen clinically but also on the wide variety of types of traumatic injuries. Trauma models have been widely reviewed in areas of hemorrhage/shock, burn, sepsis, traumatic brain injuries, chest trauma, bone defects, soft tissue trauma, and extremity trauma (130–135). Combinatorial trauma models combining some of the above are also prevalent and are utilized to more accurately represent and study clinical scenarios of multiple trauma (135).

Rabbit and rodent models are the most commonly used species for animal models of musculoskeletal trauma, but dogs, sheep, goats, pigs, and nonhuman primates, in particular rhesus monkeys, have also been used (136,137). Rabbits have been favored in musculoskeletal trauma models because compared to larger animals, they are smaller, cheaper, and easier to maintain and house. They also have more rapid skeletal changes and bone turnover, making them useful for studying bone defects (138–140). While rabbits, dogs, sheep, goats, pigs, and nonhuman primates have more similar bone characteristics to humans, rodents are also very popular due to their low cost and ease of housing and handling (137).

Many trauma models focus on large bone defects in order to better study delayed or non-unions, two of the most clinically prevalent bone trauma complications. Segmental defects in the femur or tibia, typically critically sized, are most commonly used. A critical-sized defect will not heal spontaneously over the lifetime of the animal, thus providing a more challenging and rigorous environment to test bone-regenerating biomaterials and

other therapeutics. While critical-sized defects should progress to non-unions in animal models, the animal skeletal maturity and defect size must still be considered. In a tibial defect model in sheep, supposed critical-sized defects of 3 cm or 4.5 cm in skeletally immature animals showed bone formation (30-80%) in 50% and 25% of the animals, respectively. In the skeletally mature group with the 4.5 cm defect, no animals showed spontaneous bone formation (85).

Both rat and mouse models are commonly used for musculoskeletal trauma. One advantage of using mouse models is their widespread use in immunology research, which makes characterizing and studying the immune system in these models significantly easier due to reagent availability. However, mouse models also provide more challenges than rat models for musculoskeletal trauma research because of their much smaller size, which makes fracture fixation techniques more challenging and thus less reproducible. Bilateral femur fracture is a well-established mouse model that is commonly used for extremity trauma; however, fixation challenges hinder long term investigation. Inability to conduct long term investigations can be detrimental for looking at long term immune environments following trauma (141). Researchers have attempted to mitigate these challenges by developing a mouse pseudofracture model where an injured muscle is exposed to crushed bone fragments (141). The method of fixation typically used in mouse models has also provided added complexity. While plate fixation is more clinically relevant, external fixation or intramedullary pinning has typically been used in mice (142,143). This has led multiple researchers to develop mouse models that utilize plate fixation for femoral defects ranging from 2-3.5 mm to decrease morbidity and increase reproducibility of these models (144–146).

Despite these advances, the mouse model still lacks key components to be used successfully as a model for immunosuppression following trauma. Their small size creates a challenge for accurate local delivery of therapeutics, and their low blood volume prevents safe, repetitive blood draws, thus hindering longitudinal assessment of circulating immune biomarkers and cells (147). Further, there has been contention that the genomic responses to sepsis and trauma in particular poorly mimic the response in humans (148). While some have disputed this claim (149), most of the literature has reached a consensus that there are significant differences between the human and mouse inflammatory responses to trauma (150). This has been further emphasized and supported by a lack of clinical translation where therapeutics that have shown success in mouse models subsequently fail in the clinic (132). Because of these complications, rat rodent models may provide more robust and reproducible data as a model of immunosuppression following trauma. However, the immune responses to trauma in rat models are less well characterized to date, motivating the need for improved immune characterization to better support the use of rats for models of immunosuppression following trauma. Currently, rat trauma models commonly use critical-sized segmental defects in the femur or tibia; however, models with critical-sized calvarial or caudal vertebrae defects have also been used successfully (151,152).

2.4.3 Composite Trauma Models

Pre-clinical models of multi-tissue trauma exhibit increased immune dysregulation compared to bone trauma only, which is consistent with observations of immune dysregulation with higher levels of injury severity. Composite injuries that include a muscle defect along with a bone defect are one way to increase injury severity and thus increase immune dysregulation. In a recently developed rat model of composite trauma, a

critically-sized femoral defect is used in conjunction with a volumetric muscle loss (VML) of the adjacent quadriceps muscle (153). In this same model, it was shown that the use of a clinically-relevant BMP-2 mediated treatment strategy did not heal the composite model, whereas it did successfully heal the bone only defect (121). Similarly, a rat tibial composite injury model that contained a 5mm segmental defect combined with a VML of the adjacent muscle, showed significant functional deficits compared to sham treated animals and bone defect only animals (120). These animal models demonstrate that composite trauma models provide a much more challenging healing environment, which is hypothesized to increase the potential for non-responders and inadequate healing due to immune dysregulation.

Another option for creating muscle defects besides volumetric muscle loss is to use muscle crush injuries. For example, a mouse model and a rat model utilize muscle crush injuries in the gastrocnemius muscle and the left soleus muscle, respectively (154,155). However, muscle crush injuries may not be as effective at disrupting healing as resecting large muscle segments, such as with VML models. A rat tibial fracture stabilized with a steel pin was performed in conjunction with a muscle crush injury or a VML of the adjacent muscle. Biomechanical functional assessments and bone healing indicate significant differences in the VML group compared to fracture alone, but not in the muscle crush group (122). Therefore, to increase injury severity and potentially induce immunosuppression using composite bone and muscle injury models, a VML injury versus a muscle crush injury may be the most effective option. Aside from rodent models, some large animal models have also been used for composite trauma; including a dog model of a complex bone, tendon, and muscle injury (156). However, despite more similar characteristics to

human responses, large animals are used less frequently due to cost, size, and housing and handling challenges.

2.4.4 Delayed Treatment Models

Another potential method to induce immune dysregulation based on clinical evidence is to delay treatment of defects and injuries to allow enough time for systemic immune dysregulation and immunosuppression to develop. Delayed treatment models may be more clinically relevant because patients typically undergo initial defect stabilization followed by treatment that can be weeks later (22). The current animal trauma models investigating delayed treatment have waited 1-3 weeks before treating the defects; however, these animal models have not been immunologically characterized so their immune status at the time of treatment is uncertain. The uncertainty in the immune status in these animal models likely explains the varied results of different delayed treatment models. For example, a rat femoral segmental defect of 8 mm was treated immediately or at 7 days post-injury with adipose and bone-marrow derived stem cells in combination with bone-morphogenetic protein 2 (BMP-2), an osteoinductive factor that has been used clinically to treat bone defects. In this study, the delayed treatment group showed no bridging of defects, whereas the immediate treatment group showed bridging in 75% of the animals (78). On the other hand, another study looking at immediate and delayed transplantation (7 days post injury) of mesenchymal stromal cells (MSCs) in a rat model with muscle crush trauma to the left soleus muscle showed similar functional muscle regeneration between the immediate and delayed treatment groups (157). Further, another group delivering endothelial progenitor cells (EPCs) to a 5mm critically-sized femoral defect in a rat model at 3 weeks post-injury showed no significant differences in bone

healing between acute and delayed treatment (158). These varied results suggest that understanding the progression of immunosuppression over time is critical as well as better understanding how different injury severities impact this progression.

2.4.5 Infection Models

The presence of a complicating factor, such as infection, may also be another way to enhance immune dysregulation and immunosuppression in animal models. Some models have combined infection with a traumatic insult to better study mechanisms to counteract infection following trauma, but these models may also be useful for studying the development and progression towards immune dysregulation. There are many different infection models used that vary in the animal species (i.e. rabbit, rat, pig, or sheep), the location of the injury (i.e. tibia, femur, or radius), the type of inoculation (i.e. local injection or systemic injection), and the type of bacteria used (159). Rats are commonly utilized in infection trauma models because of their lower cost and ease of handling. However, rabbits are also used because they are the most prone to developing robust infection after inoculation. Pigs are also sometimes used because of their larger size and ability to accommodate human-sized implants. *Staphylococcus aureus* and *Pseudomonas aeruginosa* are the most commonly used bacterial species in infection models (159). *S aureus* in particular is commonly used because of the need to address the development of partially or totally antibiotic resistant strains (160).

Infections can be combined with different types of musculoskeletal trauma including crush injury, bone fracture, and muscle injuries. Crush injuries or soft tissue trauma combined with infection are often used to represent battlefield trauma and blast

injuries in military personnel that have a high incidence of infection (1,161). A model in rats combines a femur fracture with a muscle crush injury followed by stabilization and then inoculation with *S. aureus* (162). Another model in rabbits targets the flexor carpi ulnaris muscle and combines that with a *S. aureus* infection (163). Similar models exist in large animals, including a sheep model of a *S. aureus* infected tibia fracture with intramedullary nailing (164) and a porcine model of soft tissue blast injury (165). A rat model solely looking at infected bone defects combined a 6 mm rat femoral defect with infection by soaking collagen in *S. aureus* and then placing that into the bone defect site (166). All of these animal models that combine bone and muscle trauma with infection provide a more challenging and rigorous model for bone regeneration and clearance of pathogens by the immune system. In addition, animal models combining infection with trauma are particularly relevant because wound infection is the leading clinical complication following musculoskeletal trauma (4). Further, models that combine trauma and infection may be an efficient way to induce systemic immune dysregulation and immunosuppression.

2.5 Future Directions

Severe musculoskeletal trauma is prevalent in both military and civilian patients, but current strategies are inadequate in regenerating lost or damaged tissues. Significant numbers of severe trauma survivors enter into a state of systemic immune dysregulation and are resistant to recovery treatments, resulting in decreased healing and regenerative capacity, thus highlighting a need for improved therapeutic strategies. Therefore, it is critical to better understand (a) how severe trauma leads to systemic immune dysregulation, (b) how this affects regenerative outcomes in appropriate models, and (c) how to develop

improved, targeted systemic immunomodulatory therapies with the goal of restoring immune homeostasis and ultimately improving healing and regenerative outcomes in these patients.

The immune response to trauma is complex, with spatial and temporal changes in cellular and molecular mediators of inflammation. A better understanding of these changes and the factors that can influence them will be essential in the development of effective immunomodulatory therapeutics for systemic immune dysregulation and immunosuppression following trauma. Important considerations should include: (a) how injury severity and patient-specific factors alter the immune response over time, both systemically and locally, (b) the timing of treatment (acute or delayed, as well as concurrent or prior to regenerative interventions), (c) the target cell(s) or the target molecules/pathways, and (d) the vehicle and route of delivery for the most effective and safe interventions.

The ultimate goal is to restore immune homeostasis and improve healing and regenerative outcomes for patients. However, in order to develop successful immunomodulatory therapeutics that would improve outcomes of regenerative interventions, robust pre-clinical models are needed. This requires generating and characterizing animal models of immune dysregulation that mimic clinical scenarios. Further, better methods are needed to identify at risk patients and patients who could potentially benefit from immunomodulatory therapies. This will require gathering large sets of human data from current trauma conditions for predictive modeling to help clinicians decide which patients are likely to respond poorly to conventional treatment. Systems biology approaches may be essential to identifying signatures of immune

dysregulation or specific biomarkers of interest. The development of well-characterized pre-clinical models that correlate to clinical presentations of immune dysregulation will enable experiments involving a priori or concurrent immune modulation with regenerative interventions. Understanding how immunomodulatory therapeutics and other interventions interact systemically to improve healing will be important for translation and ultimately improving patient outcomes. The complex interactions of the musculoskeletal system and the immune system and the importance of systemic and local immune function for healing highlight the necessity for further research into the role of systemic immune dysregulation and immunosuppression in severe trauma patients.

CHAPTER 3. CHARACTERIZATION OF SYSTEMIC IMMUNE DYSREGULATION IN A PRE-CLINICAL TRAUMA MODEL OF BONE NON-UNION[2]

3.1 Introduction

Musculoskeletal trauma involving extremities is quite common, occurring in up to 71% of battlefield (1) and 59% of civilian injuries (2). Despite advances in treatment, failure of bone healing continues to be a significant clinical concern. A large population study found a 4.9% overall risk of nonunion for fractures, and reported even higher nonunion rates depending on anatomical location and patient comorbidities (114). Recent studies have also identified a dysregulated immune response, including chronic immunosuppression and immune paralysis, as an important cause of morbidity following severe trauma (6,8,167). It has been hypothesized that trauma-induced immune dysregulation occurs in multiple stages. The first stage encompasses a systemic inflammatory response syndrome (SIRS), characterized by acute hyper-inflammation with overproduction of pro-inflammatory cytokines (IL-1, IL-6, TNFα), countered by a compensatory anti-inflammatory response syndrome (CARS) with increased expression of anti-inflammatory cytokines (IL-1RA, IL-10, TGFβ)(168). CARS follows almost immediately after SIRS is initiated, as prolonged exposure to the high levels of inflammatory factors and reactive oxygen species generated during SIRS is damaging to

[2] Adapted from A. Cheng and C.E. Vantucci, et al. Early systemic immune biomarkers predict bone regeneration after trauma, Proceedings of the National Academy of Sciences, 2021. 118(9): e2017889118. Reprinted with permission. This work was completed equally in collaboration with Albert Cheng (co-first authors).

the surrounding tissues and can lead to multiple organ failure if left unchecked (3,169). In most cases of uncomplicated healing, the SIRS and CARS responses resolve, and systemic immune homeostasis is restored within a couple weeks. Failure to achieve this balance can lead to a storm of elevated pro- and anti-inflammatory signals that persists for several weeks (27), and can eventually result in a destructive catabolic phase. This phase is characterized by the onset of systemic immune dysregulation and immune suppression (SIDIS) (21). Patients exhibiting symptoms of SIDIS are more prone to opportunistic infections, sepsis, organ dysfunction, and often require multiple surgical interventions and hospitalizations, which incur greater long-term healthcare costs for the patient (5,169).

Some of the primary cellular mediators of long-term immune dysregulation observed in SIDIS are the immune suppressor cell types, including T regulatory cells and myeloid-derived suppressor cells (MDSCs) (5,6,8). These cells suppress immune function by secreting anti- inflammatory factors such as IL-1RA, IL-10, and TGFβ, which can subsequently inhibit activation of other immune cells, such as in T cell anergy, or even reduce immune populations over time by promoting premature apoptosis of these cells (5,42). MDSCs in particular are immature myeloid lineage cells, distinct from other myeloid immune cells such as macrophages, granulocytes, and dendritic cells (170). Additionally, MDSCs are heterogeneous in nature and most commonly identified in rats as expressing both neutrophil (His48) and monocyte (CD11b) markers (171,172). These cells can directly suppress T cell function through depletion of the amino acid L-arginine (36,173), which is a critical mediator of T cell metabolism and activity (174), as well as through promotion of nitric-oxide-mediated T cell apoptosis (171). MDSCs are also involved in TGFβ1-mediated suppression of natural killer cells and can enhance T

regulatory cell survival (45,175). In human patients, circulating MDSCs have been observed to persist at high levels up to 28 days in severely septic patients, and were linked to adverse outcomes and prolonged ICU stays (42). However, the influence of MDSCs following traumatic musculoskeletal injuries, particularly in cases of poor healing such as bone fracture nonunion, remains unclear.

Herein, we utilized a previously established femoral bone defect model of chronic nonunion in rats (176) to investigate systemic immune dysregulation and how it relates to functional bone regeneration. In this model, treatment with BMP-2 is delivered 8 weeks after initial creation of the bone defect (delayed treatment), which is the time needed to establish nonunion, as defined by radiographic mineralized capping of bone ends. This delayed treatment group mirrors the clinical standard of care given that nonunions are not diagnosed and reintervened on until several months after the initial injury (177). Acute treatment (i.e. treatment delivered immediately following defect creation) was also investigated and represented an example of a relatively uncomplicated bone healing scenario. We hypothesized that delayed treatment would result in poor bone healing compared to acute treatment and furthermore, that this impairment could be linked to systemic immune dysregulation involving an increase in immunosuppressive cell types and cytokines and a simultaneous decrease in immune effector cells and cytokines. Systemic immune characterization was performed on blood samples collected longitudinally over multiple weeks (Figure 3.1) to investigate immune profile changes during healing. Blood collected at each time point was analyzed for immune cell populations by flow cytometry as well as for serum cytokines and chemokines through a multiplexed array. These results were evaluated concurrently with bone healing, which was quantified by *in vivo* micro-

computed tomography (μCT) and *ex vivo* biomechanical testing of the regenerated femurs. Finally, univariate and multivariate analyses were performed to develop computational predictive models of bone healing based on the blood immune cell and cytokine data.

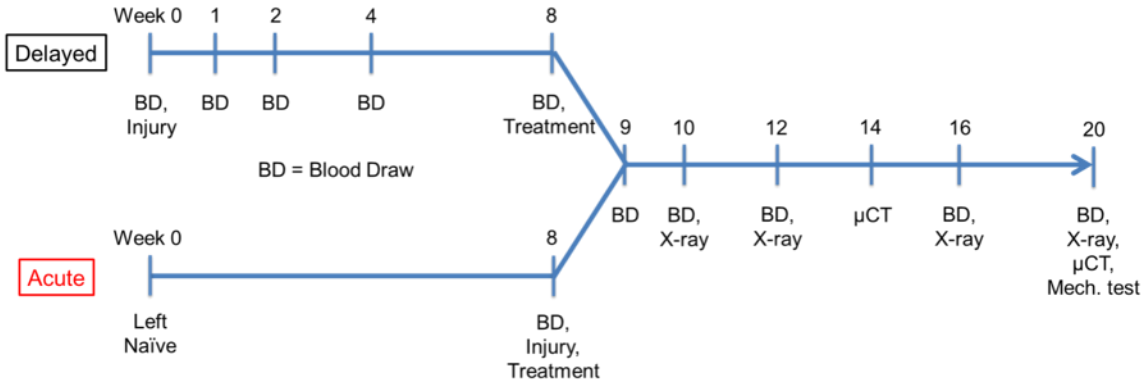

Figure 3.1 Overview of experimental design showing timeline of experimental assays for delayed and acute treatment groups.

3.2 Materials and Methods

3.2.1 Experimental Design

The objective of this study was to investigate whether the early systemic immune response following traumatic injury in a recently established animal model of nonunion (176) could be predictive of long-term bone regeneration. We set up the in vivo study as described below and collected blood samples at multiple time points to perform *ex vivo* cell and proteomic analyses. Concurrently, non-invasive imaging techniques (radiographs/ micro-computed tomography) were used to evaluate bone formation over time. At the final time point, terminal mechanical testing was performed to functionally assess the regenerated bones. Sample numbers for each experiment were determined using power analyses based on inputs from previous studies and are noted in the figure legends. All

animals and treatment groups were randomly assigned, and investigators were blinded for all *in vivo* and *ex vivo* analyses.

3.2.2 Alginate BMP-2 Preparation

RGD-functionalized alginate (FMC BioPolymer) was reconstituted in MEM alpha (Thermo Fisher Scientific) to create a 2% w/v solution, as described previously (178). Recombinant human bone morphogenetic protein 2 (BMP-2, Pfizer Inc.) was reconstituted in a solution of 0.1% rat serum albumin (Sigma Aldrich) in 4 mM hydrochloric acid and mixed with the alginate solution to yield 2 μg BMP-2 per 150 μl of final solution. This alginate/BMP-2 solution was gelled with the addition of calcium sulfate (Sigma Aldrich) at a 1:25 volume ratio. Hydrogels were prepared under sterile conditions inside a laminar flow hood and stored overnight at 4°C before use in surgery the next day.

3.2.3 Animal Model

For these studies, 13-week-old female SASCO Sprague Dawley rats (Charles River Laboratories, Inc.) were used. Rats were pair housed in individually ventilated caging (Tecniplast) with a tunnel and gnawing blocks (Bio-Serv) for enrichment. Bedding was a mixture of corn cob and processed paper. Purina Mills International #5001 was fed ad libitum. Filtered tap water treated with ultraviolet light was provided ad libitum in bottles. Sentinel results from Charles River Laboratories International Rat Prevalent PRIA testing were negative for all pathogens in the housing room. All animals were allowed to acclimate for at least 2 weeks before any procedures were performed. Following each procedure, a divider was temporarily placed in the cage for better monitoring of post-operative recovery. Animals were randomly allocated to treatment groups.

3.2.4 Surgical Procedures

All surgical procedures were approved by the Georgia Institute of Technology Institutional Animal Care and Use Committee. Anesthesia was induced and maintained using isoflurane (Henry Schein Animal Health) inhalation. Prior to each procedure, all animals were given a subcutaneous injection of sustained-release buprenorphine (ZooPharm) for analgesia. Briefly, an anterolateral skin incision was made in the thigh followed by blunt dissection to separate the overlaying muscles to reach the femur. Limited extension of this muscle window allowed for placement of a radiolucent polysulfone fixation plate for internal stabilization. Critically-sized 8 mm defects were created in the mid-diaphysis of the femur using an oscillating saw. For the acutely-treated animals, a 6 mm diameter poly-caprolactone (PCL, Sigma Aldrich) nanofiber mesh was carefully placed around the newly exposed bone ends and alginate loaded with BMP-2 was delivered via syringe injection through the mesh perforations. Subsequently the muscle and skin were closed using 4-0 vicryl suture and wound clips, respectively. In contrast, for the animals receiving delayed treatment, the bone defects were initially left empty (no treatment), and the muscle and skin were closed. At 8 weeks, a second procedure was performed on these animals where the original incision was re-opened to expose the fixation plate and femur. An oscillating saw was used to remove any mineralized end capping of the defects and any soft tissue ingrowth within the defect space was cleared to allow for placement of the PCL nanofiber mesh. Finally, alginate/BMP-2 was delivered, and the muscle and skin were closed as before.

3.2.5 Radiograpy and Micro-Computed Tomography

To qualitatively assess longitudinal bone regeneration, 2D in vivo digital radiographs were acquired with an MX-20 digital machine (Faxitron X-ray Corp) at 2, 4, 8, and 12 weeks post-treatment. Longitudinal bone formation was quantitatively evaluated using 3D micro-computed tomography (μCT) at 4, 8, and 12 weeks post-treatment. In vivo scans of the harvested femora were performed before mechanical testing using the vivaCT40 (Scanco Medical) at a 38 μm voxel size, 55 kVp voltage, and a 145 μA current. A threshold corresponding to 50% of native cortical bone density was applied to segment bone mineral and identify newly regenerated bone, as established previously. The volume of interest (VOI) consisted of the central 6.46 mm (170 slices) of the 8 mm defect.

3.2.6 Biomechanical Testing

Torsional testing to failure was performed as previously described (178). Femurs were excised at week 20 (12 weeks post-treatment), wrapped in PBS-soaked gauze, and stored at -20°C until testing could be performed. On the day of testing, samples were thawed, the surrounding soft tissues were excised, and the femora were first μCT-scanned, as described above. Subsequently, the fixation plate was removed so that the native bone ends could be potted in Wood's metal (Alfa Aesar). The potted femurs were tested to failure in torsion at a rotation rate of 3° per second using the EnduraTEC ELF3200 axial/torsion testing system (Bose). Failure strength was determined by locating the peak torque within the first 60° of rotation. Torsional stiffness was calculated by finding the slope of the linear region before failure in the torque-rotation plot.

3.2.7 Tissue Collection and Processing

Blood was collected longitudinally via the rat tail vein at 0 (baseline), 1, 2, 4, 8, 9, 10, 12, 16, and 20 weeks into two fractions: one for whole blood and the other for serum in the appropriate microvette collection tubes (Kent Scientific). For serum isolation, tubes were allowed to clot at room temperature for 30 minutes before storage at 4°C overnight. The following day, all serum tubes were centrifuged at 10,000g for 5 min and the yellow (straw) serum was collected and stored at -20°C.

The spleen, bone marrow from the left tibia, and muscle adjacent to the defect were all harvested at the endpoint (week 20). Red blood cells were lysed in all samples using 1X RBC Lysis Buffer (eBioscience) according to the manufacturer's instructions. Following lysis, cells were fixed using Cytofix fixation buffer (BD), resuspended in FACS buffer containing 2% fetal bovine serum (FBS) in 1X PBS, and stored at 4˚C until staining for flow cytometry.

3.2.8 Luminex Multiplex Array and Flow Cytometry

Serum isolates collected at all time points were analyzed for cytokines via Milliplex MAP Rat Cytokine/Chemokine Magentic kit (Millipore Sigma). The assays were read using a MAGPIX Luminex instrument (Luminex), and the median fluorescent intensity values read by the machine (with background subtracted) were recorded.

Processed whole blood samples were stained for flow cytometry analysis. Prior to staining, cells with Fc receptors were blocked with purified mouse anti-rat CD32 (BD) for 10 minutes at 4˚C to prevent non-specific binding. Cells were then stained for various immune cell populations, including T cells ($CD3^+$), T helper cells ($CD3^+CD4^+$), cytotoxic T cells ($CD3^+CD8^+$), T regulatory cells ($CD3^+CD4^+FoxP3^+$), myeloid-derived suppressor

cells ($His48^+CD11b^+$), B cells ($B220^+$), and monocytes ($CD68^+$, Bio-Rad) with specific anti-rat antibodies (eBioscience, unless otherwise noted). Sample data was collected using a BD Accuri C6 flow cytometer and analyzed using FlowJo software. Gates were positioned based on fluorescent minus one (FMO) controls with less than 1% noise allowed.

3.2.9 Linear Multivariate Analyses

Cytokine and immune cell data for each time point were compiled. Partial least squares regressions (PLSR) were conducted in MATLAB (Mathworks) using the partial least squares algorithm by Cleiton Nunes (available on the Mathworks File Exchange). The data were z-scored (mean subtracted and normalized to standard deviation for each cytokine) before being passed into the algorithm. This multivariate method requires scale-free data so that the analysis would not be biased towards variables with extremely high values. An orthogonal rotation in the LV1-LV2 plane was used to define the axis that best matched the continuum of healing responses (Week 20 bone volume). A Monte Carlo sub-sampling using 1,000 iterations was used to characterize standard deviation on the individual signals involved in LV1 of the PLSR model. For each iteration, 85% (17/20) of the samples used to construct the total PLSR model were randomly sampled, and a new PLSR model was constructed. To correct for sign reversals, each sub-sampled LV1 was multiplied by the sign of the scalar product of the new LV1 and the corresponding LV1 from the total model. The same orthogonal rotation used for the total model was applied to the LV1s from each iteration, and the mean and standard deviation were computed for each signal across all iterations.

3.2.10 Non-Linear Multivariate Analyses

Nonlinear regression was performed using the Evolved Analytics DataModeler software to further investigate cytokine and immune cell correlations with bone volume. Nonlinear algebraic models from 20 independent evolutions were generated using DataModeler's SymbolicRegression function, which utilizes evolutionary symbolic algorithms. These models were then plotted as a function of fit ($1\text{-}R^2$) and complexity. Next, 191 models with complexity less than 80 and a $1\text{-}R^2$ value less than 0.175 were selected as the "fittest" models, which represent the models with the optimal balance of fit (R^2) and complexity observed at the knee of the Pareto front. These selected models were then analyzed using the VariablePresence and VariableCombinations functions to identify the dominant variables and variable combinations. Finally, the models involving the top variable combination were identified and aggregated into a model ensemble using the VariablePresence and CreateModelEnsemble functions, respectively. The resulting model ensemble is composed of all the generated models for the chosen variable combination, and defines a predictive model that best fits the imported dataset. This model ensemble was further evaluated using the ResponsePlotExplorer function to visualize the response of bone volume as a function of each individual variable within the ensemble.

3.2.11 Single-cell RNA-sequencing (scRNAseq)

For cell isolation, whole blood was collected via the rat tail vein from trauma rats, as previously described (179), and myeloid-derived suppressor cells (MDSCs) were sorted via magnetic-activated cell sorting (Miltenyi Biotec) using His48 according to

manufacturer's instructions. FACS analysis following cell sorting confirmed greater than 85% CD11b+His48+ MDSCs.

Next, the cells were spun down and washed immediately after diluting the samples in 10mL PBS+0.1% BSA. The samples were then processed through a cell strainer to filter out any debris and cell clumps. The cells were counted for each sample using Cellometer (Nexcelom) and Nucleocounter (Cemometec) automated cell counter to check the targeted cell number and viability. The volume was optimized to achieve the target 5000 barcoded cells. scRNAseq was performed using 10X Genomics Single Cell 3′ Solution, version 3.1, according to the manufacturer's instructions (protocol rev C). Libraries were sequenced on Nextseq500 (Illumina).

The data was de-multiplexed, aligned, and counted using Cell Ranger version 3.1.0 (10X Genomics). Samples were analyzed using Seurat (https://satijalab.org/seurat/) using CCA with Louvain clustering and visualized by tSNE projections. Quality control metrics were used to select cells with mitochondrial gene percentage less than 10% and filter cells that have unique feature counts over 2,500 or less than 200. These include the selection and filtration of cells based on QC metrics, data normalization and scaling, and the detection of highly variable features.

3.2.12 T Cell Immunosuppression Assay

Whole blood was collected via the rat tail vein from 4 trauma rats and 3 healthy rats as previously described (179). 1X RBC lysis buffer (eBioscience) was used to remove red blood cells. Cells were rinsed twice with 1X PBS and then MDSCs were sorted out of the trauma rat cells via magnetic-activated cell sorting (Miltenyi Biotec) using His48

according to manufacturer's instructions. The MDSC fraction and the remaining PBMC fraction were saved. The PBMC fraction from the trauma rats (Trauma - MDSCs) and the PBMCs from the healthy rats (Naïve) were plated in tissue culture plates treated with 5ug/mL of immobilized anti-rat CD3 and 0.5ug/mL of soluble CD28 (BioLegend). A third and fourth group were also plated which contained the MDSC and PBMC fractions from the trauma rats in a 1:1 ratio (Trauma with MDSCs) or MDSCs from the trauma rats and PBMCs from the healthy rats in a 1:1 ratio (Naïve + Trauma MDSCs). Cells were incubated for 16 hours and then 10uM of BrdU was added to each well. After 24 hours, cells were collected and stained for CD3, CD3, CD8, and BrdU. Surface antigens were stained as previously described prior to BrdU staining. After surface antigen staining, cells were permeabilized with BD Cytoperm Permeabilization Buffer Plus (BD) according to manufacturer's instructions. Cells were then treated with 300ug/mL of DNAse for 1 hour at 37C and then washed in 1X BD Perm/Wash Buffer (BD). Next, cells were stained with anti-BrdU APC (BioLegend) and analyzed via flow cytometry.

3.2.13 Statistical Analyses

All data are reported as mean ± standard error of the mean. Significance was determined by t-test or analysis of variance (ANOVA) as appropriate, with multiple comparisons made by Tukey's post-hoc test. Significance was determined by a p-value < 0.05. All statistical calculations were performed using GraphPad Prism 7 software. Sample sizes were determined by performing a power analysis in G*Power software based on bone volume and maximum torque results obtained from previous studies. These power calculations, along with historical data using this segmental bone defect rat model, suggest a sample size of 7-8 is sufficient to give statistical differences between groups.

3.3 Results

3.3.1 Functional Regeneration is Impaired Following Delayed Treatment of Bone Defects

Bone regeneration and mechanics were significantly decreased with delayed treatment. Longitudinal radiographs showed progression of bone healing following delayed and acute treatment with BMP-2 (Figure 3.2A). While both groups exhibited increased bone formation over time, the defects that received delayed treatment had qualitatively less bone than the acutely-treated defects, particularly in the center of the newly regenerated defect. This observation was supported by the μCT reconstructions of the new bone at 20 weeks (Figure 3.2B), which demonstrated more void space within the bone defect in the delayed treatment group. Quantification of new bone formation by μCT revealed that the acutely-treated defects had significantly higher bone volumes at both Weeks 14 and 20 (Figure 3.2C). No differences were observed in local bone mineral density (Figure 3.2D). Furthermore, biomechanical testing demonstrated that delayed treatment resulted in regenerated bones with lower mechanical strength and stiffness (Figure 3.2E and F) compared to acute treatment. Additionally, acute treatment resulted in complete restoration of intact bone stiffness, whereas defects receiving delayed treatment recovered on average only 32% of the intact bone stiffness. In terms of bone strength, acutely treated defects were over twice as strong as delayed treated defects, demonstrating a significant detrimental effect of delayed treatment on functional regeneration.

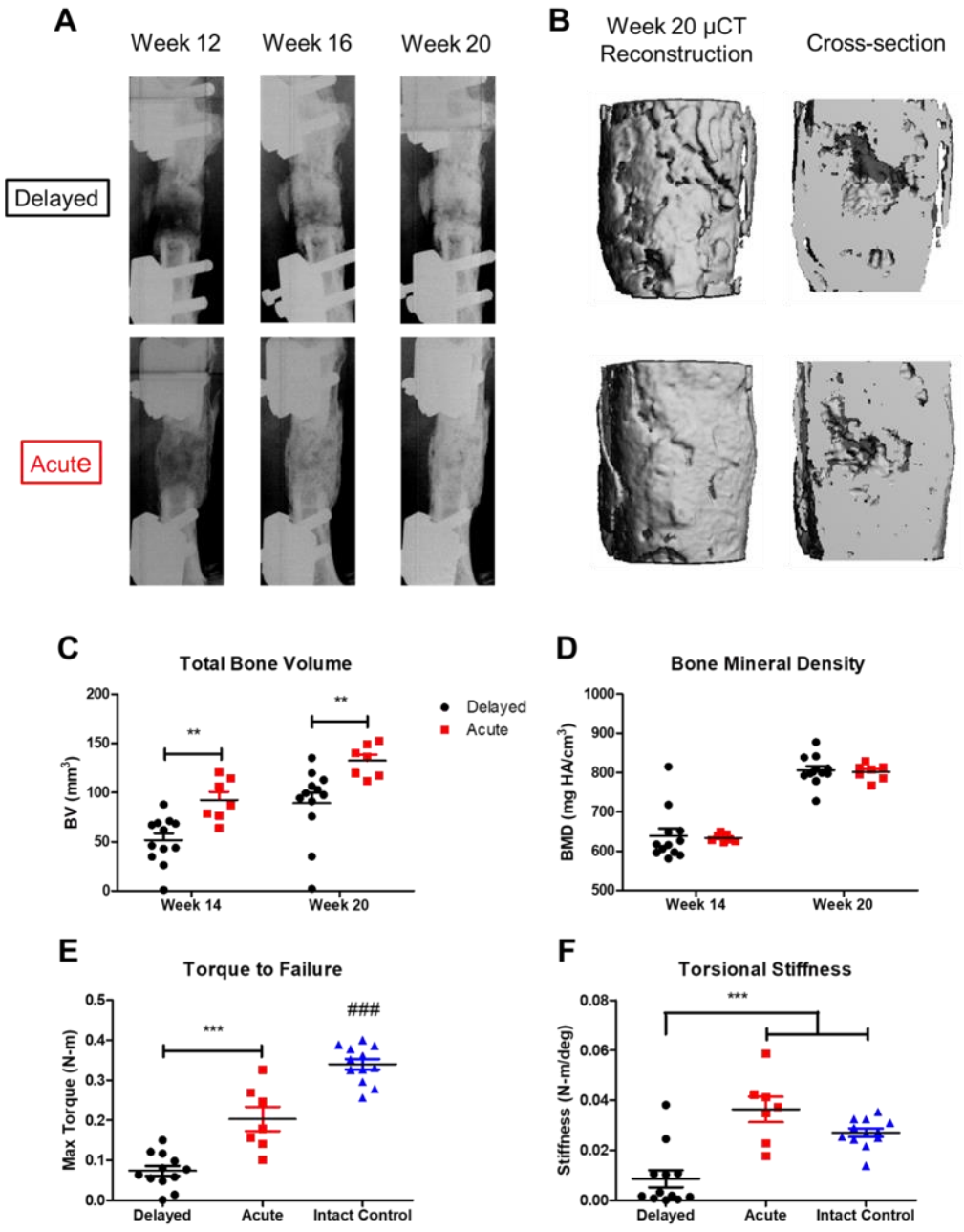

Figure 3.2. Functional regeneration is impaired following delayed treatment of bone defects.

(A) Representative radiographs (median healing sample for each treatment group) demonstrating bone formation at weeks 12, 16, and 20 (corresponding to 4, 8, and 12 weeks post-treatment). (B) Week 20 µCT reconstructions of the same representative sample and the associated cross-sectional view. (C) Total bone volume and (D) bone mineral density for the newly formed bone, as quantified by in vivo micro-computed tomography (µCT). (E) Mechanical strength and (F) stiffness of the regenerated femurs were determined by ex

vivo torsional testing to failure at Week 20. Mean ± SEM, n = 8-12/group. **p<0.01, ***p<0.001 as indicated, ###p<0.001 vs all other groups.

3.3.2 Circulating and Local Immune Cells Correlate with Bone Regeneration

Immune cell characterization from blood was performed at multiple time points (

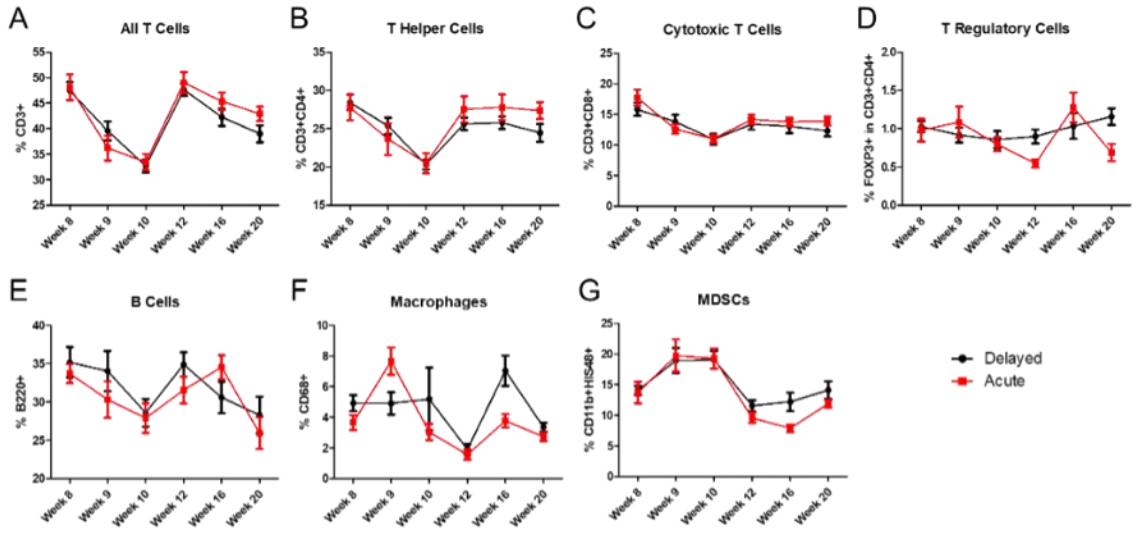

Figure 3.3A to G). No significant differences were observed between acute and delayed treatment for all cell types evaluated. However, multivariate linear regression analysis revealed several significant correlations with respect to Week 20 bone volumes (Figure 3.4A to E). A table of the linear regression statistics can be found in Table 3.1. Immunosuppressive MDSCs and monocytes in blood were negatively correlated with bone healing at multiple timepoints post-treatment (Figure 3.4A and B). Of note, blood MDSC levels were significantly negatively correlated as early as Week 9, or 1 week post-treatment. In contrast, the immune effector T cells, including the T helper cell subset, and B cells in blood were positively correlated with bone healing (Figure 3.4C to E). Interestingly, blood B cells were significantly correlated at Weeks 1 and 4 following trauma, several weeks before the delayed BMP-2 treatment was administered at Week 8.

Independent analyses of local tissues harvested at Week 20 demonstrated consistent correlations to the blood immune response profiles; MDSCs in the bone marrow were negatively correlated with healing, while B cells in the muscle tissue adjacent to the defect were positively correlated (Figure 3.5).

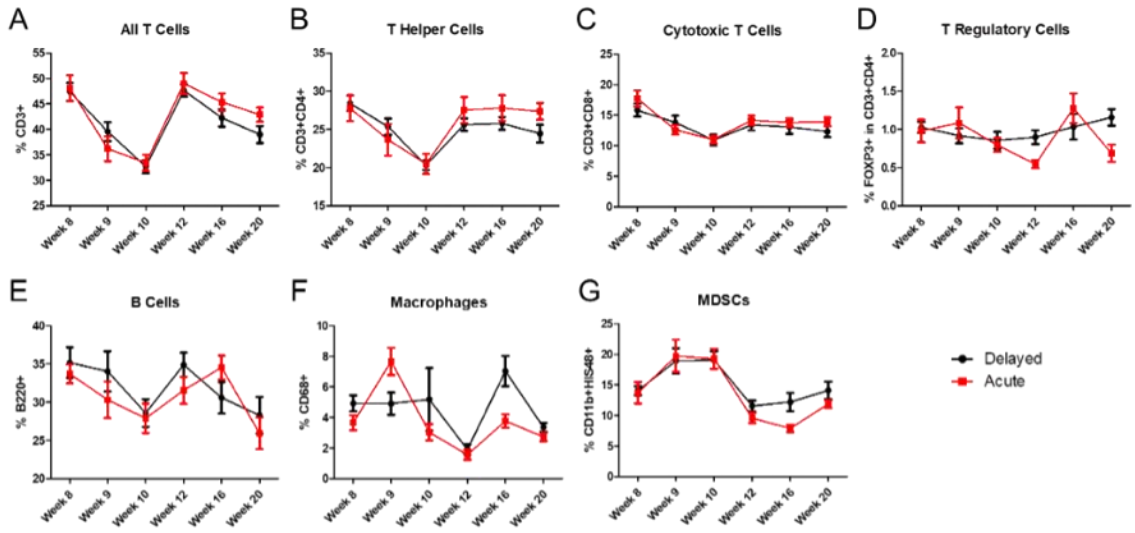

Figure 3.3 Longitudinal characterization of circulating immune cells.
(A to G) No significant differences between delayed and acute groups were observed in circulating immune cell populations from Week 8 (baseline immediately before treatment) through Week 20 (12 weeks post-treatment). Mean ± SEM, n = 8-12/group. Figure 3.3

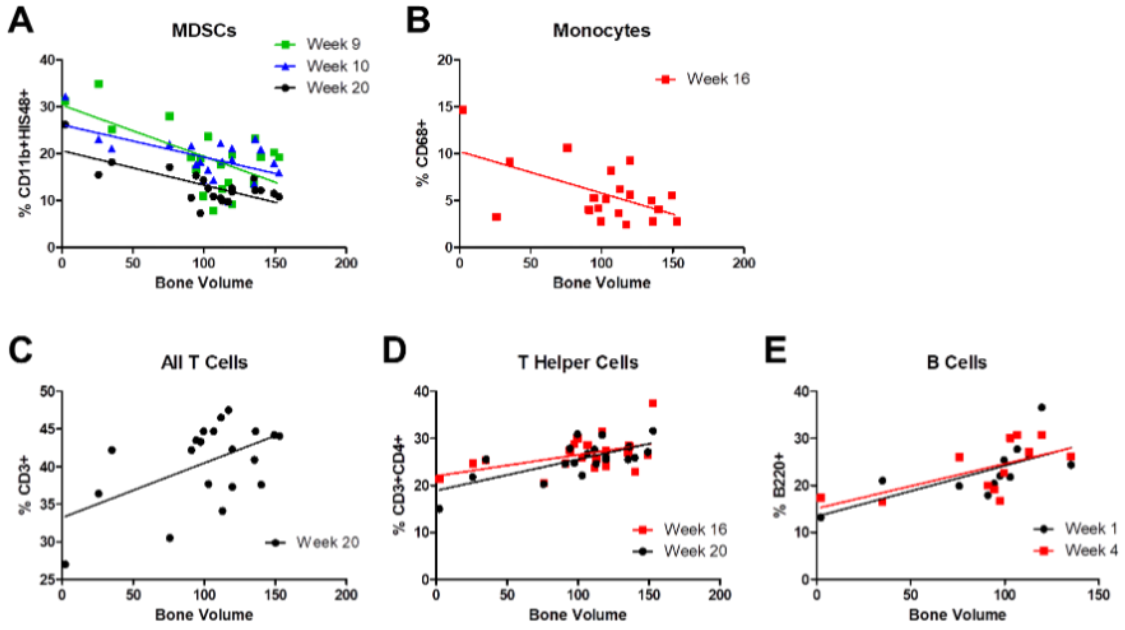

Figure 3.4. Circulating immune cells correlate with bone regeneration.
(A to E) Select cell populations from peripheral blood demonstrated a significant correlation to Week 20 bone volumes. MDSCs and monocytes were negatively correlated with bone healing (A and B) while T cells, T helper cells, and B cells were positively correlated (C to E). The positive B cell correlations observed at Weeks 1 and 4 are notable given they occur several weeks before BMP-2 treatment is administered at Week 8. n = 12-20/time point, slope of linear regression significantly non-zero for all data shown $p<0.05$.
Table 3.1 Linear regression table describing the significant correlations shown in Figure 3.4.

Linear Regression	Blood MDSCs Week 9	Blood MDSCs Week 10	Blood MDSCs Week 20	Blood Monocyte Week 16	Blood All T cells Week 16	Blood T helper Week 16	Blood T helper Week 20	Blood B cells Week 1	Blood B cells Week 4
Slope	-0.1095	-0.06899	-0.07326	-0.04439	0.07269	0.04528	0.06644	0.1082	0.09514
Y-intercept	30.35	26.15	20.64	10.23	33.21	22.00	18.89	13.38	15.09
Pearson r	-0.6227	-0.5885	-0.7268	-0.5632	0.5400	0.4858	0.6950	0.6874	0.6322
p-value	0.0034	0.0063	0.0003	0.0097	0.0140	0.0299	0.0007	0.0135	0.0274

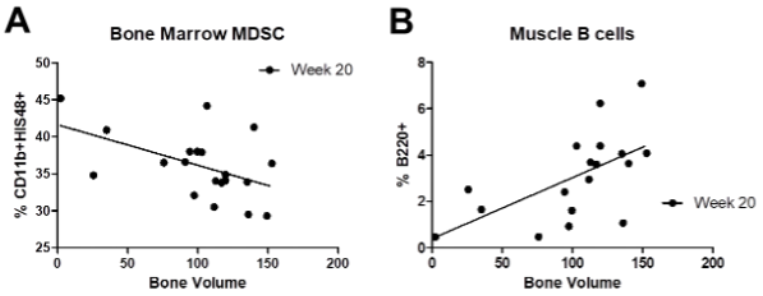

Linear Regression	Bone marrow MDSC Week 20	Muscle B cells Week 20
Slope	-0.05477	0.02630
Y-intercept	41.64	0.3920
Pearson r	-0.5003	0.5958
p-value	0.0247	0.0091

Figure 3.5. Significant immune cell correlations from harvested tissues at Week 20. MDSCs in bone marrow from the ipsilateral tibia were negatively correlated with healing (A) while B cells in the muscle adjacent to the injured femur were positively correlated with healing (B).

3.3.3 Multivariate Analysis Identifies Immune Cells and Cytokines Associated with Healing

Using the blood immune cell and cytokine data for all time points pooled together (Weeks 0 through 20), partial least squares regression (PLSR) was performed to identify the most influential factors during the entire course of the study. This analysis revealed an axis, called latent variable 1 (LV1), that successfully describes the gradient of observed healing responses as defined by bone volume (Figure 3.6A). The LV1 profile shows factors that are elevated (positive bars) and diminished (negative bars) with respect to bone healing (Figure 3.6B). In agreement with the conventional linear regression results, MDSCs and monocytes were most negatively correlated with bone healing, while B cells were most positively correlated. Furthermore, IL-6 and IL-13 were the top cytokine correlates with successful healing.

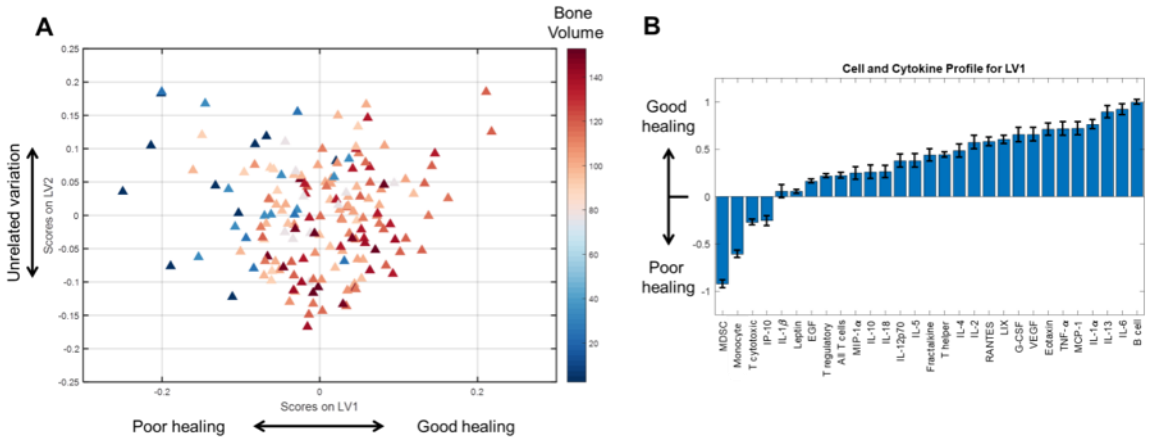

Figure 3.6. Partial least squares regression (PLSR) of cell and cytokine data for all time points identifies immune profile associated with healing.
(A) The regression analysis established latent variable 1 (LV1) that describes samples along the continuum of healing responses. (B) LV1 defines the profile of immune cells and cytokines correlated with healing and shows that MDSCs, monocytes, cytotoxic T cells, and IP-10 were negatively correlated with healing while B cells, IL-6, IL-13, and IL-1α were positively correlated with healing.

3.3.4 Myeloid-Derived Suppressor Cells are an Early Indicator of Poor Healing

Pooled analyses of all time points provided broad insight into factors that are most influential during the entire timespan of healing; however, early markers post-treatment are most useful for clinical prediction of treatment success and bone healing outcomes, so we next performed univariate and multivariate analyses of the immune cells and cytokines at Week 9, just 1 week post-treatment. Across the Week 9 samples, we observed a spectrum of different immune cell and cytokine responses, as visualized in the heatmap (Figure 3.7A).

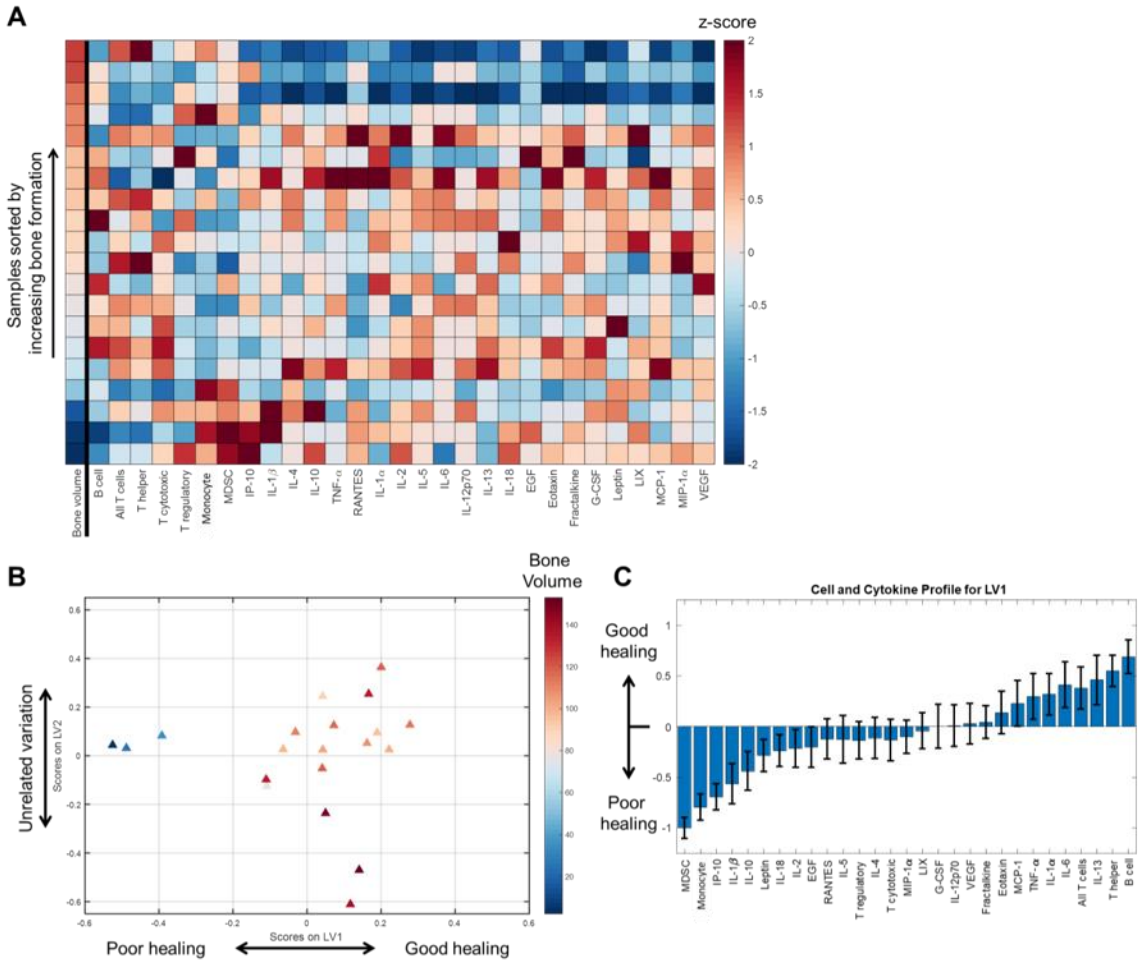

Figure 3.7. PLSR of Week 9 samples identifies early factors that are positively correlated and inversely correlated with healing.
(A) Heatmap of z-scored Week 9 immune cell and cytokine levels, sorted by Week 20 bone volumes. (B) PLSR analysis established a new latent variable 1 (LV1) that describes samples along the continuum of healing responses. (C) This LV1 defines the profile of Week 9 immune cells and cytokines correlated with healing and shows that MDSCs, monocytes, IP-10, and IL-1β were most negatively correlated with healing while B cells, T helper cells, and IL-13 were most positively correlated with healing.

The univariate analyses revealed that only the cytokines IP-10, IL-1β, and IL-10 exhibited significant correlations with bone volume, with all being negative correlations (Figure 3.8). The multivariate PLSR was able to segregate the Week 9 samples by bone volume using a new LV1 (Figure 3.7B). This LV1 profile shows the Week 9 factors that are positively or negatively correlated with long-term bone healing (Figure 3.7C), several of which overlap

with those identified by the pooled time points PLSR. In support of the previous results, MDSCs and monocytes were most negatively correlated with bone healing while B cells, T helper cells, and all T cells were most positively correlated. Furthermore, cytokines IP-10, IL-1β, and IL-10 were negatively correlated with healing while IL-13 and IL-6 were positively correlated with healing.

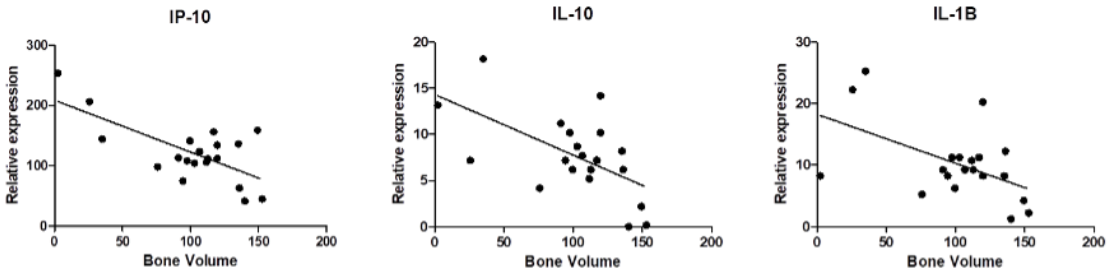

Linear Regression	IP-10	IL-10	IL-1β
Slope	-0.8577	-0.06570	-0.07944
Y-intercept	208.6	14.33	18.27
Pearson r	-0.6886	-0.5906	-0.5200
p-value	0.0008	0.0061	0.0188

Figure 3.8. Significant serum cytokine correlations for Week 9.

3.3.5 Nonlinear Multivariate Regression Further Supports MDSCs and IL-10 as Early Negative Predictors of Bone Healing

Lastly, nonlinear regression was independently performed using Evolved Analytics DataModeler software to further evaluate the Week 9 immune cells and cytokines. This approach has an advantage over linear regression methods by making fewer *a priori* assumptions about model form. Over 1800 unique models were generated using this computational approach, and of these only 242 were selected as the fittest models (Figure 3.9A). The variable distribution of the selected models was subsequently analyzed (Figure

3.9B), which revealed MDSCs and IL-10 were present in over 90% of these models. Furthermore, models involving the top variable combination of MDSCs, IL-10, and RANTES were chosen and aggregated into a predictive model ensemble. This model ensemble represents the collection of models that best maximize diversity of the error residuals for the Week 9 data, and further analysis of the ensemble variable response plots (Figure 3.9C) showed that MDSCs and IL-10 were negatively correlated with bone volume while RANTES was positively correlated with bone volume. Interestingly, the MDSC response plot demonstrated a distinct nonlinear behavior with respect to bone volume, whereas IL-10 and RANTES both exhibited a more linear response. Finally, the model ensemble bone volume predictions were compared to the observed bone volumes for all samples (Figure 3.9D) and demonstrated high predictive power based on just the 3 variable inputs of MDSC, IL-10, and RANTES ($R^2 = 0.9255$).

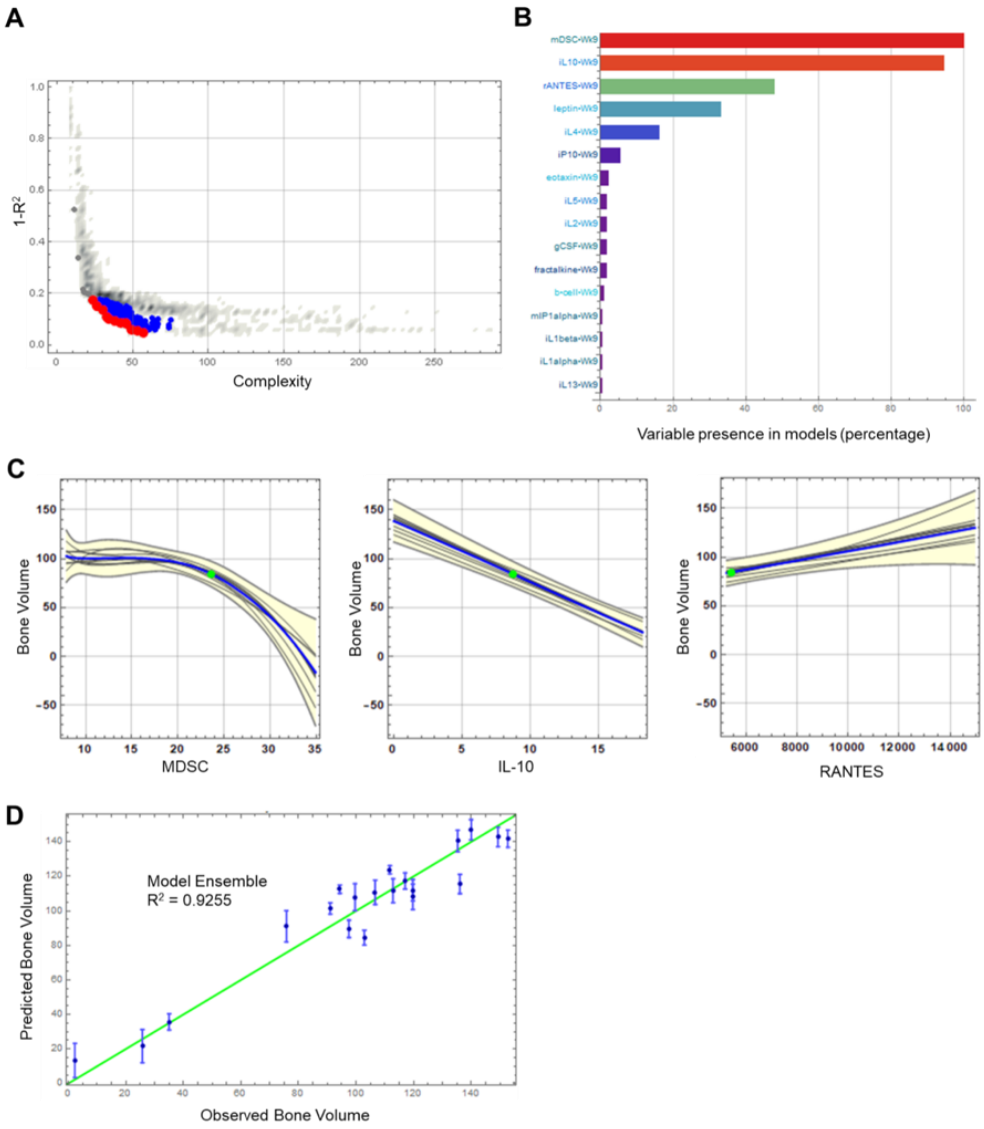

Figure 3.9. Nonlinear multivariate analyses using Evolved Analytics DataModeler software supports MDSC and IL-10 as early negative predictors of bone healing.
Over 1800 unique models were generated using evolutionary symbolic regression algorithms, and (A) the top 242 models were selected at the "knee" of the Pareto front, which represent the highest accuracy models with the lowest degree of complexity. (B) Variable presence chart shows MDSC, IL-10, and RANTES were the top 3 most common variables in the selected models. (C) Response profile plots of the model ensemble for the top variable combination. The gray lines represent individual models while the blue line represents the predictive model ensemble (aggregate of the top 9 individual models). The yellow envelopes demonstrate the variance in the ensemble as a function of each variable. (D) Model ensemble prediction plot demonstrates high predictive power of the model ensemble for the observed data. This can be seen visually by how closely the data points lie to the green line (a representation of 100% model ensemble prediction accuracy). The error bars around each data point illustrate the spread of the ensemble predictions.

3.4 Discussion

Systemic immune dysregulation has recently emerged as an important clinical consideration following severe trauma, even in the absence of sepsis or multiple organ failure. Efforts towards identifying predictive biomarkers and better diagnostics for disorders like SIDIS are still in the nascent stages (5). Furthermore, the influence of systemic immune dysregulation on bone repair has yet to be directly investigated, particularly in poor healing outcomes such as nonunion. Herein, we sought to address these substantial clinical and scientific gaps.

To the best of our knowledge, this work represents the first of its kind to demonstrate long-term immune dysregulation in a preclinical model of chronic nonunion – a serious orthopedic complication that remains challenging to treat. In support of our hypothesis, we observed that acute treatment with BMP-2 resulted in improved healing compared to equivalent delayed treatment after nonunion has already been established. We did not observe outright differences in the individual immune cell populations or cytokine levels at any time point between the acute and delayed treatment groups. However, differences may have been hard to discern by simple comparative analyses due to the redundant and pleiotropic effects of these factors. Instead, correlative analyses utilizing univariate and multivariate methods are perhaps more appropriate and insightful. Univariate analyses of immune cells in blood at multiple time points revealed a significant negative correlation between MDSCs and long-term bone regeneration, as early as Weeks 9 and 10 (1 and 2 weeks post-treatment, respectively). In contrast, B cells, T cells, and T helper cells were positively correlated with bone repair. These results suggest that impaired bone healing in this model involves a systemic rise in MDSCs that coincides with a reduction in effector B

and T cell populations, which is consistent with previously reported profiles of chronic systemic immune dysregulation associated with infection and cancer (170,173,180).

Linear multivariate regression of all time points implicated IL-6 and IL-13 as the cytokines most positively correlated with bone formation, whereas IP-10 was the cytokine most negatively correlated with bone formation. These findings are consistent with previous reports that IL-6 stimulates angiogenesis and promotes callus mineralization (181,182), while IL-13 inhibits bone resorption and enhances the ALP activity of osteoblasts (183,184). In addition, IP-10 (also called CXCL10) has been associated with bone destruction by inducing osteoclast differentiation (185) and inhibiting angiogenesis (186). Interestingly, it has been shown that IP-10 is expressed by MDSCs in a murine cancer model (187) and furthermore, that plasma levels of IP-10 are correlated with MDSC frequency in a nonhuman primate model of viral infection (188), which corroborates our findings that both IP-10 and MDSCs were highly negatively correlated with bone healing. Taken together with the immune cell data, these observations support our initial hypothesis that poor bone healing is associated with systemic immune dysregulation.

Next, we performed more in-depth analyses for the Week 9 immune cell and cytokine data as an effort to identify early markers that could potentially be predictive of the long-term bone healing outcomes. Conventional univariate regression as well as both linear and nonlinear multivariate analyses all demonstrated that MDSCs and IL-10 were unmistakable negative correlates of bone formation at this early time point. Using stochastic subsets of the Week 9 data to generate nonlinear evolutionary models, we found that MDSCs and IL-10 were indeed the most influential biomarkers and could successfully be leveraged in a model ensemble to predict functional bone regeneration for the entire dataset. It is well

established that MDSCs are one of the major producers of immunosuppressive IL-10 (189–191), and that both factors are critical for the induction of T regulatory cells (175). Recent work has also shown that IL-10 has a reciprocal effect on MDSCs by promoting MDSC expansion during late-stage sepsis, which leads to enhanced and more detrimental immunosuppression (192). Our results suggest that elevated MDSC and IL-10 levels soon after trauma may be indicative of an aberrant early immunosuppressive response that can cascade into more severe long-term immune suppression and derail the normal bone healing response.

Overall, these results identified MDSCs and B cells as the most negative and positive immune cell correlates with respect to bone healing, respectively. Work from other groups have shown that B cells massively infiltrate the fracture callus soon after injury and differentiate into plasma cells that secrete large quantities of factors including osteoprotegerin, which inhibits osteoclastogenesis and promotes fracture healing (193). Furthermore, B cells are critical for the production of high quality bone as the absence of mature B and T cells alters the matrix composition and results in stiffer, more brittle bones (35). In addition, there is evidence that MDSCs can directly suppress B cell differentiation, proliferation, and cytokine secretion (194–196). Therefore, the findings from our study serve as further evidence that B cells play an important role in bone repair and that the dynamic between MDSCs and B cells may be indicative of an overall pro- or anti-regenerative response.

Regarding further characterization of MDSCs, we did confirm the presence of both granulocytic and monocytic populations by performing single-cell RNA-sequencing (scRNAseq) (Figure 3.10A to C). scRNAseq also demonstrated that isolated MDSCs

(CD11b+His48+ cells) expressed functional markers including the genes encoding iNOS, Arginase, and IL-1β (Figure 3.10D). Additional *in vitro* functional assessment of T cell suppression was performed by harvesting peripheral blood mononuclear cells (PBMCs) from naïve and trauma rats and culturing with or without CD11b+His48+ MDSCs isolated from the trauma rats. In this experiment, we found that T cell proliferation following CD3 and CD28 stimulation, including proliferation of CD4+ and CD8+ subsets, significantly decreased when MDSCs were added to the culture for both naïve and trauma PBMCs (Figure 3.11). These results demonstrate that MDSCs generated following traumatic injury remain functionally active and can directly suppress T cell proliferation.

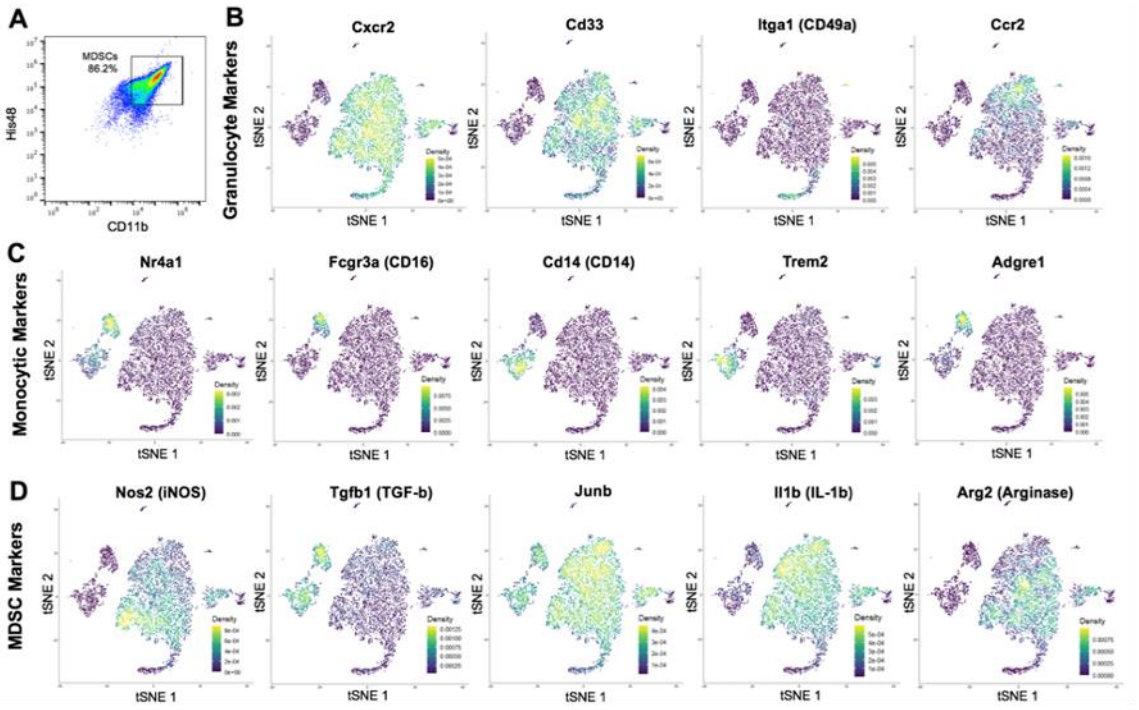

Figure 3.10. Single Cell RNA Sequencing of Rat CD11b+His48+ MDSCs.
(A) Flow cytometry dot plot showing cell population used for scRNAseq and the percentage of CD11b+His48+ cells. tSNE projection plots showing density of (B) granulocyte markers, (C) monocytic markers, and (D) MDSC markers.

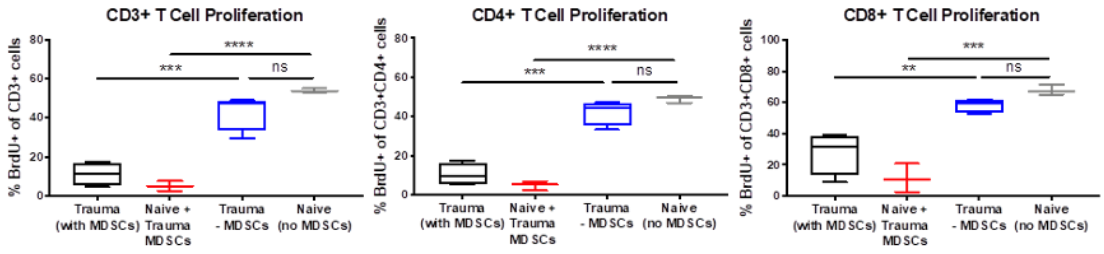

Figure 3.11. MDSC Depletion Restores T cell Function.
BrdU incorporation as a percentage of the CD3+, CD4+, and CD8+ cell populations after culture with or without MDSCs and compared to naïve control group. One-way ANOVA with $p<0.0005$(***) and $p<0.0001$(****), n=3-4 animals.

It is important to acknowledge that correlation does not imply causation, and mechanistic experiments are still needed to validate the factors identified here as the predominant drivers of systemic immune dysregulation. Nonetheless, these results motivate future work to investigate how modulation of these cell populations and/or cytokines would influence bone healing. Other groups have begun exploring immunomodulatory strategies for enhancing bone repair by targeting macrophages (197) and T cells (198,199) through the delivery of factors locally. However, there do not appear to be many examples in literature that target B cells or MDSCs, particularly at the systemic level.

A potential limitation of this work is that the alterations observed in immune cell populations over time may have been affected by normal changes due to animal aging rather than just the response to trauma and subsequent treatment. In fact, immunosenescence with aging has been well-documented (200,201). One of the hallmarks is an overall reduction in T and B lymphocytes as hematopoietic progenitors gradually favor a shift towards myeloid lineage cells, particularly pro-inflammatory monocytes and macrophages (202,203). However, many of these studies focus on age-related immune

changes from childhood to geriatric age. In this study, all rats were 13 weeks-old at the start and 33 weeks-old at the terminal time point, which falls well within early adulthood for rats, which typically live around 2.5-3 years in captivity (204,205). Consequently, we would expect age-related immune changes over the time course of this study to be minimal.

Despite these limitations, the results shown here provide significant insight into long-term immune profile changes following treatment of nonunion and demonstrate a link between systemic immune health and bone healing. Furthermore, this work establishes a viable framework for assessing multiple variable inputs (cells and cytokines measured from blood) to identify the most influential factors that may be predictive of a complex biological process such as bone repair. Additional work is needed to validate the predictive power of these computational models, and reproducibility in experiments with human clinical samples remains to be determined. Of note, recent clinical studies have taken a similar approach by analyzing serum/plasma from trauma patients and finding that levels of certain cytokines were associated with greater immune dysregulation and multiple organ dysfunction (206,207). In that same vein, the results from this study motivate further investigation into systemic immune profiles as a potentially powerful tool for early prediction of trauma healing outcomes.

3.5 Conclusions

In conclusion, this study explored the role of systemic immune dysregulation on healing in a rat model of chronic nonunion. Our results showed that delayed treatment of an established nonunion resulted in impaired bone healing compared to acute treatment. Although average levels of circulating immune cells and cytokines were not different

between acute and delayed treatment groups overall, univariate and multivariate regression modeling revealed significant correlations between early cell and cytokine biomarkers and functional bone regeneration. Elevated circulating levels of MDSCs, IP-10, and IL-10 were all inversely correlated with healing whereas B cells, T helper cells, IL-6, and IL-13 were positively correlated. Some of these correlations, MDSCs and IL-10, were significant as early as 1 week post-treatment as determined through univariate and multivariate analyses. Taken together, these results suggest that MDSCs and long-term immune dysregulation play a key role in impaired healing after nonunion and could potentially serve as novel therapeutic targets to enhance bone repair.

CHAPTER 4. DEVELOPMENT OF SYSTEMIC IMMUNE DYSREGULATION IN A RAT TRAUMA MODEL OF BIOMATERIAL-ASSOCIATED INFECTION[3]

4.1 Introduction

Orthopedic implant-associated infections, such as those following joint replacement or trauma surgery, represent a significant clinical challenge, costing up to an additional $150,000 per patient in the United States (208). For most orthopedic patients, implant-associated infections occur at a rate of about 1-5%; however, for certain higher-risk groups, including patients with open fractures or those requiring revision surgery of failed prosthetic joints, infection rates are drastically increased, affecting around 20% of patients (209–212). Orthopedic infections are the most common complication with procedures involving orthopedic implants and hardware (213). In addition, these infections are challenging to treat and can result in impaired bone healing and hardware or implant failure, requiring subsequent interventions, extended rehabilitation times, long-term antibiotics, and overall increased total health and societal costs (214).

Orthopedic hardware and biomaterial implants can provide necessary fracture stability, support tissue regeneration, and replace damaged or diseased joints; however, these materials also provide an ideal environment for bacteria to colonize and grow. *Staphylococcus aureus* is the most frequent orthopedic-implant associated organism, found

[3] Adapted from C.E. Vantucci and H. Ahn et al., Development of systemic immune dysregulation in a rat trauma model of biomaterial-associated infection, Biomaterials, 2021. 264: 120405. Reproduced with permission from Elsevier.

in 34% of orthopedic infections (215). *S. aureus* can adhere to biomaterial implant surfaces within hours and form a complex structure surrounded by self-generated extracellular polymeric substance matrix, called a biofilm, which is comprised of proteins, polysaccharides, lipids, and nucleic acids (216). These biofilms have an extensive secretome, releasing proteins that include hemolysins, leukocidins, nucleases, and endotoxins which lyse or inactivate innate and adaptive immune cells, alter immune cell signaling pathways and cytokine expression, and prevent complement activation, all ultimately inhibiting and depressing host immunity (217). The specialized microenvironment created by the biofilm also results in decreased metabolism and growth rate, altered nutrient requirements, and mutability, all contributing to extreme antibiotic resistance where biofilms can survive antibiotic exposures up to 1000 times greater than planktonic *S. aureus* (217). Additionally, biofilm impairment of host immunity and resistance to antimicrobial factors can enable *S. aureus* invasion and colonization of the canalicular network within the bone, making the infection even more challenging to treat as bacterial cells become inaccessible deep within these networks (217,218). Successful survival of the bacteria in the host and the subsequent release of bacterial factors in combination with host immune responses can result in eventual bone lysis with decreased osteoblast viability and increased bone resorption (219,220).

The ability of biomaterial-associated infections to form biofilms that can evade the immune response and that can colonize within the canalicular networks may result in a local, indolent and chronic infection, meaning that the infection is slow-growing and does not pose an immediate threat to the patient or initially result in outward systemic symptoms, such as a fever or pain and swelling of the joint (221). However, although the patient is not

in any immediate danger, these types of chronic indolent infections can persist for months or even years without symptoms and are often only discovered after catastrophic joint or hardware failure, non-union of the bone in the case of traumatic injuries, or even bacteremia and sepsis (222). Current treatment for chronic orthopedic infections requires surgical removal and debridement of the biofilm and infected tissue, removal of the implant or hardware, and eventual replacement and re-implantation of a new implant or prosthesis (223). Additionally, patients are put on an intense antibiotic regimen that can last weeks or even months in an attempt to eliminate any residual colonies or bacteria that may have detached from the biofilm during surgery and debridement (220). However, despite these aggressive measures, the rate of joint re-infections is still around 10%, with some studies observing re-infection rates above 50% (220). Because of this, current research is focused on addressing orthopedic infections through various methods including polymeric carriers for targeted delivery of antibiotics or antimicrobial peptides, implant materials with anti-infection and antimicrobial properties, and local immune modulation (209,224).

Strategies aiming to modulate the local immune environment to treat orthopedic implant-associated infections are thought to have some parallels to local immune modulation strategies of the immunosuppressive tumor environment. In particular, an ineffective T cell response and an increase in immunosuppressive cell types. such as myeloid-derived suppressor cells (MDSCs) and T regulatory cells (Tregs), are hallmarks of the immune-compromised local environment of implant-related bone infections, similar to the tumor microenvironment (225,226). Immune therapies targeting various immune cells, including T cells and MDSCs, have shown promise in cancer immunotherapy for reducing tumor burden and increasing patient survival, and have the potential to be

repurposed for other diseases involving immunosuppression, such as chronic infections (220). However, despite extensive work understanding the local infection immune microenvironment and the mechanisms of immune evasion by *S. aureus*, very little focus has been placed on understanding the systemic immune response and its role in host immunity, infection clearance, and bone regeneration in the case of traumatic injury. Recent biomaterials work has highlighted the relationship between the systemic and local immune environments and the importance of systemic immunity. In particular, systemic immune homeostasis is shown to be altered by local biomaterial scaffolds for tissue regeneration (11), and more interestingly, systemic immunity is required for successful anti-tumor immune therapy, suggesting that local immune modulation alone without systemic modulation may not be sufficient for successful intervention (12). Based on the links between bone, orthopedic infections, and the immune system, as well as the relationship between the local and systemic immune environments, the systemic immune environment may be crucial for successful immune modulation to treat chronic infections.

Host immunity is essential for bacterial clearance and appropriate and regulated healing; however, the role of the systemic immune response in particular is not well understood and has not been a major focus for addressing orthopedic implant-associated infections thus far. Therefore, in this study, the objective was to characterize the systemic immune response to an orthopedic biomaterial-associated infection following severe trauma. We hypothesized that a local, indolent infection combined with trauma would not only lead to local changes in the immune environment, but also to systemic immune dysregulation and immunosuppression. A better understanding of the systemic immune response to an orthopedic biomaterial-associated infection could provide biomarkers for

early identification of chronic infection patients prior to catastrophic events such as hardware failure, bone non-union, and sepsis and could identify potential immunomodulatory targets, optimizing therapeutic interventions and improving outcomes for these patients.

4.2 Materials and Methods

4.2.1 Micro-organism Preparation

A bio-luminescent strain of *Staphylococcus aureus* (Xen29, PerkinElmer, Waltham, MA) was cultured in Luria Bertani (LB) medium containing 200 μg/ml kanamycin at 37ºC, under aerobic conditions while agitated at 200 rpm for ~2-3 hours.

4.2.2 Surgical Procedures

All animal care and experimental procedures were approved by the Veterans Affairs Institutional Animal Care and Use Committee (IACUC) and carried out according to the guidelines. Unilateral 2.5mm femoral segmental defects were created in 21-week old female Sprague-Dawley rats (Charles River Labs) in a similar manner to previous segmental defects (227). Briefly, an anterolateral incision was made along the length of the femur and the vastus lateralis was split with blunt dissection. A modular fixation plate was affixed to the femur using miniature screws (JI Morris Co., Southbridge, MA, USA). The 2.5mm segmental defect was then created in the diaphysis using a Gigli wire saw (RISystem, Davos, Switzerland). A collagen sponge with bacteria inoculum, *S. aureus* at 10^7 CFU (infection, n=6 due to one rat euthanized on Day 2) or without bacteria inoculum (control, n=7) was placed in the defect (Figure 4.2A). The fascia was then sutured closed

with absorbable 4-0 sutures, and the skin was closed with wound clips. Buprenorphine SR (0.03 mg/kg; 1 ml/kg) was used as an analgesic and applied via subcutaneous injection. Antibiotics were not administered based on current clinical standard of care that exclude long-term antibiotic treatment for closed fractures (228). Body temperature and weight were recorded prior to surgery and monitored longitudinally after surgery at days 1, 3, 7, 14, 28, and 56.

4.2.3 Microbiological Analysis

Bacterial metabolic activity was monitored *in vivo* using serial bioluminescent (BL) scanning (In-Vivo Xtreme, Bruker Corp., Billerica, MA, USA) at days 3, 7, 14, and 56. X-rays were taken together with BL scanning as reference images. Bacterial contamination was also confirmed at 8 weeks post-surgery via wound swab culture. Presence of Xen29 can be distinguished from background levels around ~1.80e10 CFU *in* vitro in optimal growth conditions (LB media, 37C). (Figure 4.1).

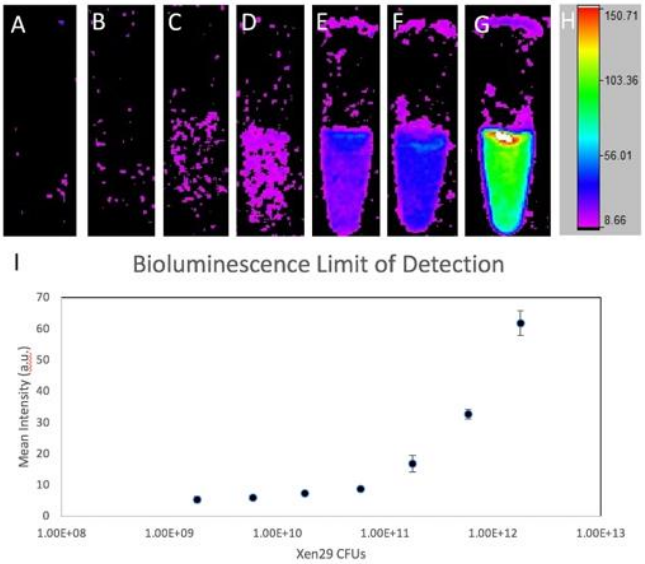

Figure 4.1. Limits of detection of in vitro bioluminescent signal.

Luminescent images of serial dilutions of Xen29 starting at $1.8x10^9$ CFU (A) and increasing by one half order of magnitude to $1.8x10^{12}$ CFU (B-G) with scalebar of luminescent intensity (H). Presence of Xen29 can be distinguished from background luminescent at around ~$1.8x10^{10}$ CFU (C). Mean intensities of the serial dilutions from A-G (n=3) are shown (I).

4.2.4 Immune Characterization

4.2.4.1 Circulating Cellular Analysis

Whole blood was collected via the rat tail vein longitudinally at days 0 (baseline), 1, 3, 7, 14, 28, and 56 for flow cytometry analysis. Red blood cells were lysed using 1X RBC lysis buffer (eBioscience) according to the manufacturer's instructions. Cells were then fixed using Cytofix fixation buffer (BD) and resuspended in buffer containing 2% fetal bovine serum (FBS) in 1X PBS and stored at 4˚C until stained. Prior to staining, cells were blocked with purified anti-rat CD32 (BD) to prevent nonspecific binding. Cells were then stained for various immune cell populations, including T cells (CD3+) and T cell subsets (CD4+, CD8+, and FoxP3+), B cells (B220+), and MDSCs (His48+CD11b+) with specific anti-rat antibodies (eBioscience). Sample data were collected using a BD Accuri C6 flow cytometer and analyzed with FlowJo. Gates were positioned with less than 1% noise allowed based on fluorescent minus one (FMO) controls.

4.2.4.2 Tissue Cellular Analysis

At the week 8 endpoint, tissues were harvested for immune cell population analyses including: local soft tissue adjacent to the defect site, the spleen, and bone marrow from both the contralateral leg and the tibia from the injured leg. Cells were stained for various immune cell populations, including B cells (B220+), MDSCs (His48+CD11b+), tissue macrophages (His36+), and hematopoietic stem cells (HSCs, CD45+CD90-) in the bone

marrow only with specific anti-rat antibodies (eBioscience). Staining and analysis procedures were the same as for the circulating cellular analyses.

4.2.4.3 Cytokine and Chemokine Analysis

Serum was isolated from whole blood at the same timepoints as the circulating cellular analysis by allowing the blood to clot overnight at 4˚C. Samples were then centrifuged at 1500g for 10 min and the supernatant was collected and stored at -80˚C until analysis. Multiplexed chemokine and cytokine analysis was performed using Milliplex MAP Rat Cytokine/Chemokine Magnetic kit (Millipore Sigma) and analyzed using a MAGPIX Luminex instrument (Luminex). Median fluorescent intensity values with the background subtracted were used for multivariate analyses.

4.2.5 Micro-Computed Tomography

Bone formation from the injured site was quantitatively assessed using micro-computed tomography (uCT) scans (Micro-CT40, Scanco Medical, Bruttisellen, Switzerland) at 8 weeks. Samples were scanned with a 20 μm voxel size at a voltage of 55 kVp and a current of 145 μA. The bone volume was quantified only from the defect region, and new bone formation was evaluated by application of a global threshold corresponding to 50% of the cortical bone density (386 mg hydroxyapatite/cm^3).

4.2.6 Histological Analysis

After euthanasia at 8 weeks post-surgery, upper hindlimb explants were harvested and fixed with 10% neutral buffered formalin (10% NBF) for 3 days and then stored in 70% ethanol until processing. To observe bone structure, decalcified bone samples were

embedded in paraffin and cut using a microtome (Leica Microsystems, Wetzlar, Germany) to an average thickness of 10 µm. Deparaffinized slides were then stained with Hematoxylin &Eosin (H&E) staining to demonstrate new bone formation. Images were obtained with an Axio Observer Z1 microscope (Carl Zeiss, Oberkochen, Germany) and captured using the AxioVision software (Carl Zeiss, Oberkochen, Germany).

4.2.7 Statistical Analysis

Statistical significance for quantitative results was assessed using appropriate parametric or non-parametric tests. For data that met the assumptions, an unpaired Student's t-test, one-way analysis of variance (ANOVA), or two-way ANOVA with repeated measures were used. Multiple comparisons were made using Sidak's multiple comparisons test, and significance was determined by p values less than 0.05. For data that did not meet the assumptions for parametric tests, the Mann-Whitney test was used. Additionally, restricted maximum likelihood estimation (REML), a method for mixed effects modeling, was used for repeated measures analysis of the circulating immune cell data. This test is recommended for multiple comparisons of repeated measures data when some values are missing. Numeric values are presented as the mean ± SEM. All statistical analysis was performed using GraphPad Prism 8.0 software (GraphPad, La Jolla, CA, USA).

Luminex data was further analyzed by partial least square discriminate analysis (PLSDA) in MATLAB (Mathworks) using the partial least squares algorithm by Cleiton Nunes (Mathworks File Exchange) following z-scoring to normalize the data. PLSDA analysis reduces the dimensionality of the input variables into a set of latent variables (LVs)

that maximally separate discrete groups (i.e. infection versus control). Latent variables are composed of profiles of the input variables that represent their relative contributions to the latent variables, and thus the separation between the groups. Monte Carlo sub-sampling with 1,000 iterations was done to determine the standard deviation for each of the individual signals in the LV loading plot. For each iteration, all but one of the samples were randomly sampled and a new PLSDA model was determined. Sign reversals were corrected by multiplying each sub-sampled LV by the sign of the scalar product of the new LV and the corresponding LV from the total model. The mean and standard deviation were then computed for each signal across all iterations. Lastly, heat maps of the z-scored data for all cytokine values were generated.

4.3 Results

4.3.1 Establishment of a Local Infection Associated with a Biomaterial Implant

4.3.1.1 Temperature and Weight

Body temperature and weight change were measured longitudinally after surgery. Neither body temperature nor weight were significantly different between the infection animals and the non-infected, control animals at any time point or overall (Figure 4.2B). Throughout the 56-day time period, infection animals showed normal weight gain and did not have elevated body temperatures compared to the control animals, indicating that the infection remained local and did not spread systemically.

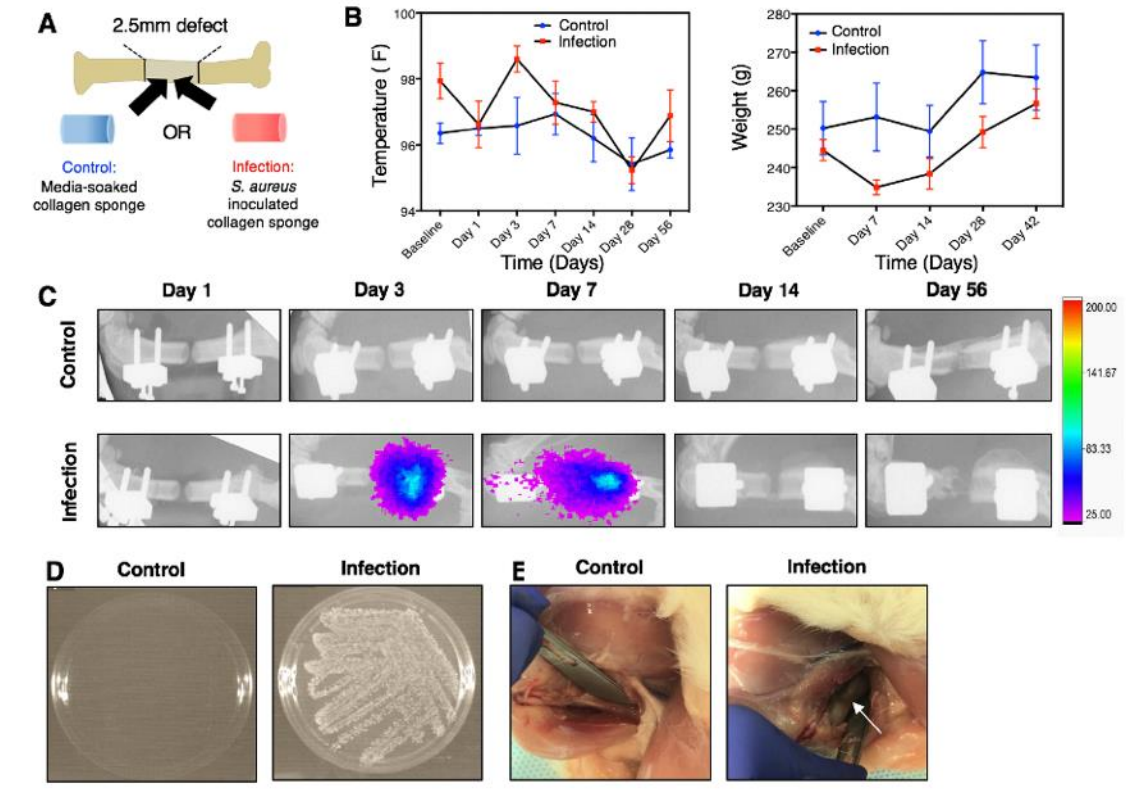

Figure 4.2. Establishment of a local infection associated with a biomaterial implant.
A) Each animal will receive a 2.5mm segmental bone defect supported by an internal fixation plate. An untreated, media-soaked collagen sponge (control) or a collagen sponge inoculated with *S. aureus* (infection) will be placed into the defect site prior to closure of the surgical site. B) Temperature (left) and weight (right) of the non-infected, control animals and the infection animals. No significant differences between groups overall or at any time point for temperature and weight were observed according to repeated measures 2-way ANOVA. C) Serial bioluminescent and radiograph images taken at Days 1, 3, 7, 14, and 56. Bioluminescent signal appeared in infection animals at Day 3 post-surgery and was present up to Day 7. D) Bacterial culture following wound swab of control and infection animals at the Day 56 endpoint. Bacterial growth is present in the infection group, but not in the control group. E) Representative images of the thighs of euthanized control and infection animals. The white arrow points to gray necrotic soft tissue and purulence around the hardware.

4.3.1.2 Bioluminescent Scans and Endpoint Evaluation of Infection

Bioluminescent scans indicating metabolic activity of the bacteria were assessed following inoculation (Figure 4.2C). Bioluminescent signal was present in infection animals as early as Day 3 post-surgery and up until Day 7; however, it should be noted that

bioluminescence is indicative of metabolic activity of the cells, not necessarily cell presence. No signal was observed in the control animals at any time point. Despite the absence of bioluminescent signal beyond Day 7 *in vivo*, wound swab culture conducted at the Day 56 endpoint confirmed the presence of bacteria in the infection animals (Figure 4.2D, Figure 4.3). Additionally, in another animal cohort, wound swab cultures at both 8 and 10 weeks exhibited bioluminescent signal, demonstrating long-term persistence of the infection (Figure 4.4). No bacterial growth was observed in culture following wound swab of the non-infected, control animals (Figure 4.2D, Figure 4.3). Further, inspection of the thighs of euthanized infection animals showed gray, necrotic soft tissue and purulence around the implant hardware, which was not present in the control animals (Figure 4.2E).

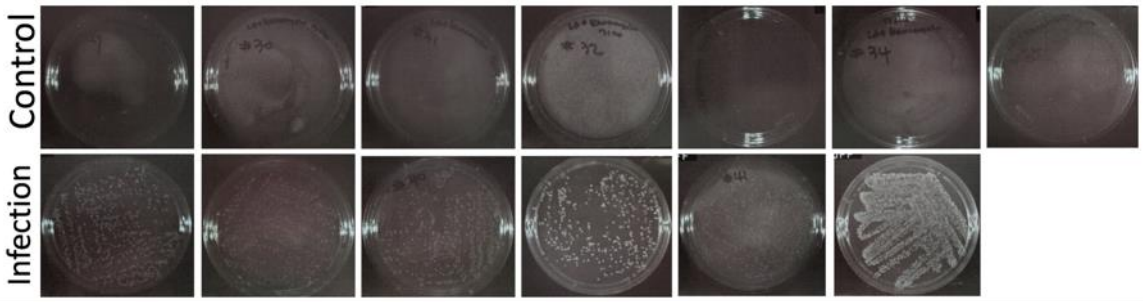

Figure 4.3. Bacterial growth only observed in infection group defects.
Images showing bacterial growth from muscle swabs applied to the surgery site after overnight incubation at 37C. Swabs from the control group show bacterial growth in 0/7 of the animals. Swabs from the infection group show bacterial growth in 6/6 of the animals.

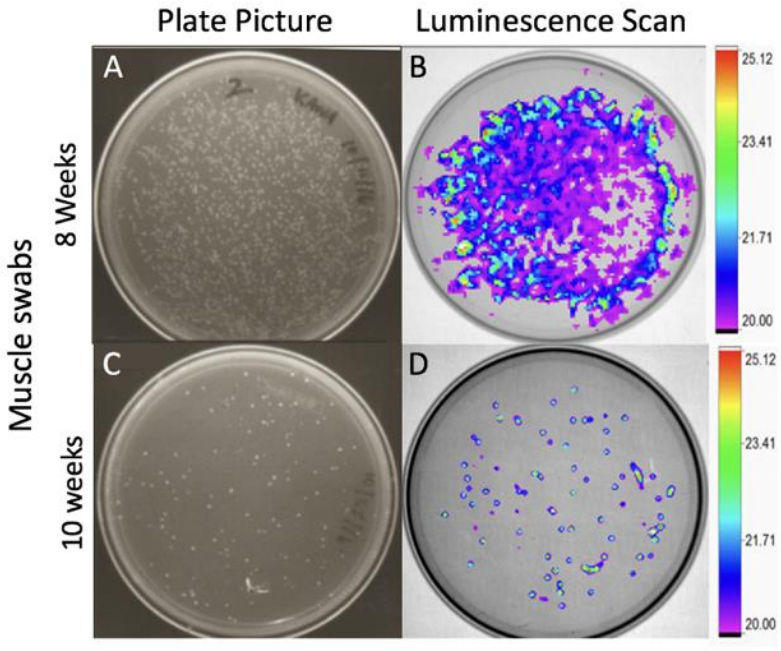

Figure 4.4. Bioluminescence of wound swab cultures.
Bacterial growth from muscle swabs of infection rats euthanized at 8 weeks (A,B) and 10 weeks (C,D). Plate pictures show the total number of bacterial colonies (A,C) and luminescence scans show the associated Xen29-dependent luminescence (B,D).

4.3.2 Local Infection Alters Local and Systemic Immune Profiles

4.3.2.1 Systemic Immune Cell Populations

Circulating immune cell populations of both immune effector cells and immunosuppressive cells were evaluated using flow cytometry and revealed differences in the systemic immune response in the infection versus control animals (Figure 4.5). Immune effector cells evaluated included both T and B cells (Figure 4.5A), as well as the helper T cell and cytotoxic T cell subsets (Figure 4.5B). Immunosuppressive cells evaluated (Figure 4.5B,C) included MDSCs and Tregs, an immunoregulatory T cell subset. At Day 1 post-injury, there was a significant decrease in circulating T cells, helper T cells, and cytotoxic T cells in both the infection and control groups compared to the baseline. Over time, T cell

populations, including helper T cell and cytotoxic T cell subsets, gradually increased in both groups until Day 28. However, while the T cell populations in the control group increased back to baseline levels, the T cell populations in the infection group remained significantly lower overall compared to baseline and the control group.

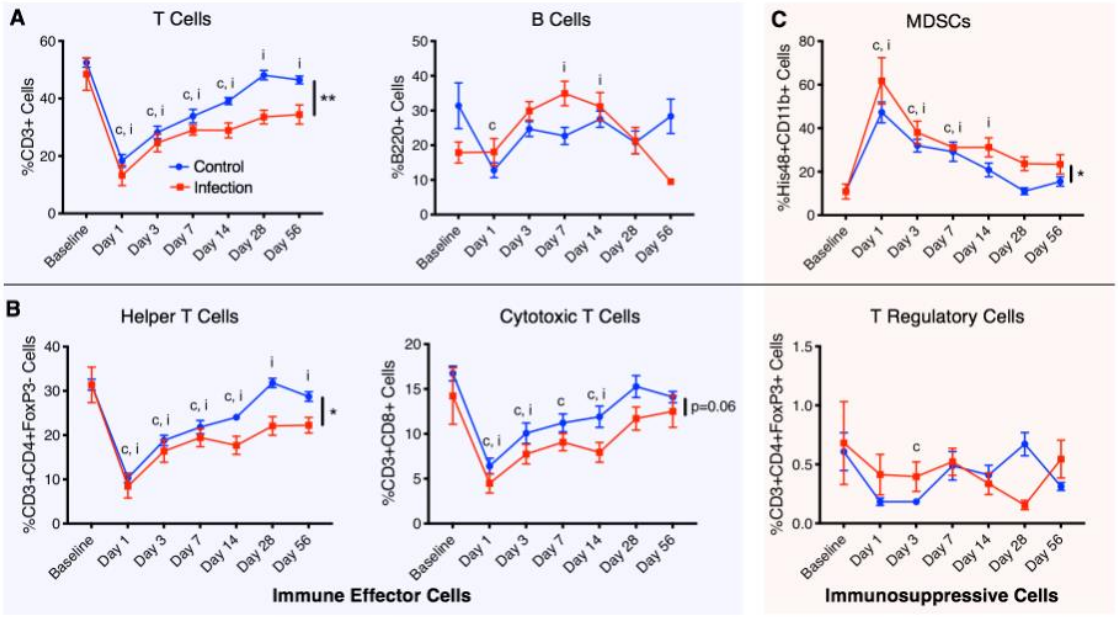

Figure 4.5. Local infection alters systemic immune cell populations.
Longitudinal analysis of immune cells circulating in the blood including A) lymphocytes (T cells and B cells), B) T cell subsets that include helper T cells, cytotoxic T cells, and T regulatory cells, and C) immunosuppressive MDSCs. These cell types are divided into immune effector cells (T cells, B cells, helper T cells, and cytotoxic T cells) and immunosuppressive cells (MDSCs and T regulatory cells). Overall differences between groups are indicated with a line and the p value or by a ** ($p<0.01$) or * ($p<0.05$). Significant differences ($p<0.05$) from the baseline in the control group and the infection group at specific timepoints are indicated with a "c" and an "i," respectively. P values were determined by fitting a mixed-effects model (REML) with Sidak's multiple comparisons test, an analysis similar to repeated measures 2-way ANOVA that can handle missing data points.

For B cells, there was a similar decrease in cell numbers in the control group, whereas there was an increase in B cells in the infection group, which peaked at Day 7.

Following Day 7, B cells in the infection group continue to decline, whereas B cells in the control group remained relatively constant. For the immunosuppressive cell types, at Day 1 post-injury, there was a significant systemic increase in MDSCs in both the infection and control groups compared to baseline with the highest peak level of MDSCs in the infection group. MDSCs in both groups gradually decreased until Day 28; however, MDSCs in the infection group were overall elevated compared to the control group. Tregs showed no significant differences between the groups. Overall, there were decreases in T cells, helper T cells, and cytotoxic T cells ($p=0.06$) and increases in immunosuppressive MDSCs in the infection group compared to the control group.

4.3.2.2 Tissue Immune Cell Populations

At the Day 56 endpoint, tissue was collected from the spleen, the soft tissue adjacent to the defect, and the bone marrow in the injured and contralateral legs. Similar to systemic cellular analysis, immunosuppressive MDSCs were elevated in infection animals compared to control animals in both local soft tissue and the bone marrow, but not in the spleen (Figure 4.6). Macrophages, another immune effector cell type, were found to be decreased in the infection group in the local soft tissue (adjacent to the bone defect), the spleen, and the bone marrow compared to the control group. Additionally, B cells in the local soft tissue and the spleen were found to be lower in the infection group compared to the control group, consistent with Day 56 circulating B cell levels which were also lower in the infection group. Analysis of hematopoietic stem cells in the bone marrow revealed a slight decrease in the infection animals compared to the control animals but were not significantly different (Figure 4.6C,D). Despite a decrease in circulating T cells in infection

animals compared to the control animals, there were no significant differences in T cell populations in any of the tissues.

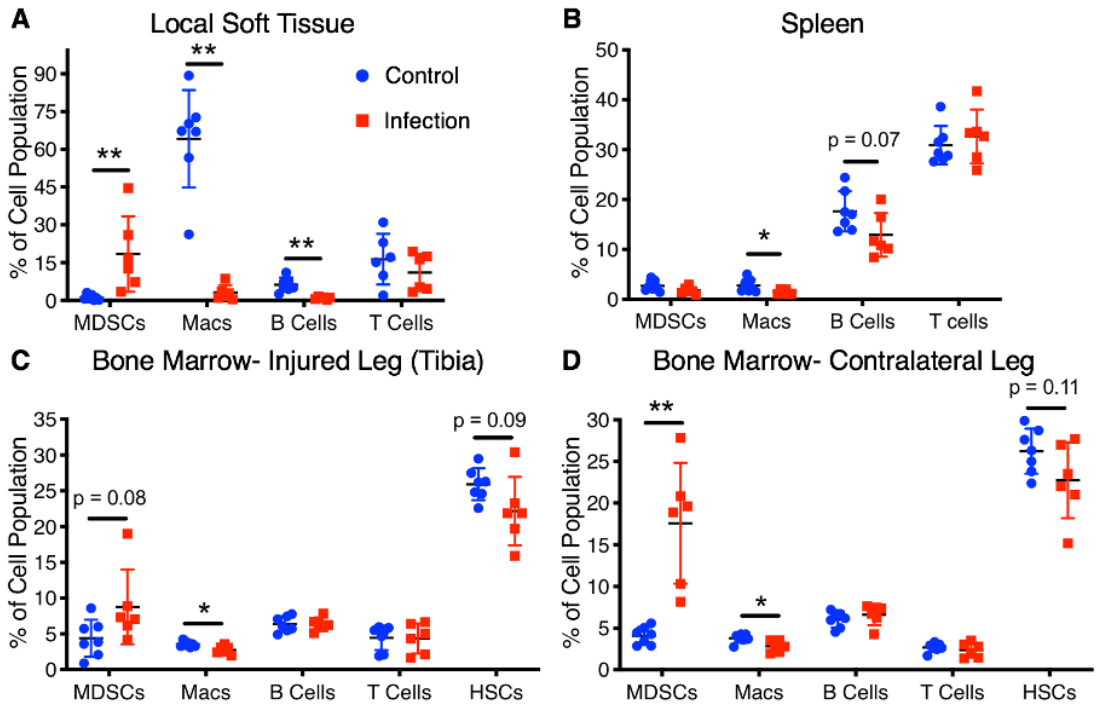

Figure 4.6. Local infection alters tissue immune cell populations.
Endpoint cellular analyses (Day 56) of tissues including the local soft tissue adjacent to the defect, the spleen, the bone marrow from the contralateral leg, and the bone marrow from the tibia of the injured leg. Differences between groups are indicated by a p value or by * ($p<0.05$) or ** ($p<0.01$). P values obtained using Student's t test or non-parametric Mann-Whitney test when variances are significantly different between groups.

4.3.2.3 Cytokine and Chemokine Profiles

Serum was analyzed for changes in systemic cytokine and chemokine levels over time. The cytokine and chemokine data were z-scored (mean subtracted and normalized to standard deviation for each cytokine) and plotted on a heat map (Figure 4.7A). The control group revealed coordinated up-regulation of specific cytokines at Day 1, Day 7, and Day 14, which appeared to resolve by Day 28. Qualitatively, the coordinated regulation of

cytokine and chemokine levels was not observed in the infection group. Quantitatively, there were no significant differences in baseline levels between the groups for any of the cytokines. At Day 1, epidermal growth factor (EGF), macrophage chemoattractant protein-1 (MCP-1), and LIX were significantly upregulated in the control group compared to the infection group (Figure 4.7B). All of these factors are involved in cell migration and recruitment, cell survival, and differentiation. Additionally, IL-2, a cytokine important for T cell function, was upregulated in the infection group compared to the control group at Day 1 (Figure 4.7B). No other cytokines were significantly different between groups at Day 1. On Day 3, RANTES, a chemokine important for leukocyte recruitment, was significantly upregulated in the control group compared to the infection group, and IL-10, a general immunosuppressive cytokine, was significantly elevated in the infection group compared to the control group (Figure 4.7C). No other cytokines were significantly different between groups at Day 3. By Day 7 and 14, a large number of both pro- and anti-inflammatory cytokines were all significantly upregulated in the control group compared to the infection group (Figure 4.8 and Figure 4.9). The inflammation in the control group resolved between Day 14 and Day 28, with cytokine and chemokine levels returning to baseline levels. At Day 28, there were no significant differences between groups for any of the cytokines; however, by Day 56, several cytokines including IL-4, IL-12p70, IL-17A, and TNFa were all upregulated in the infection group compared to the control group (Figure 4.10).

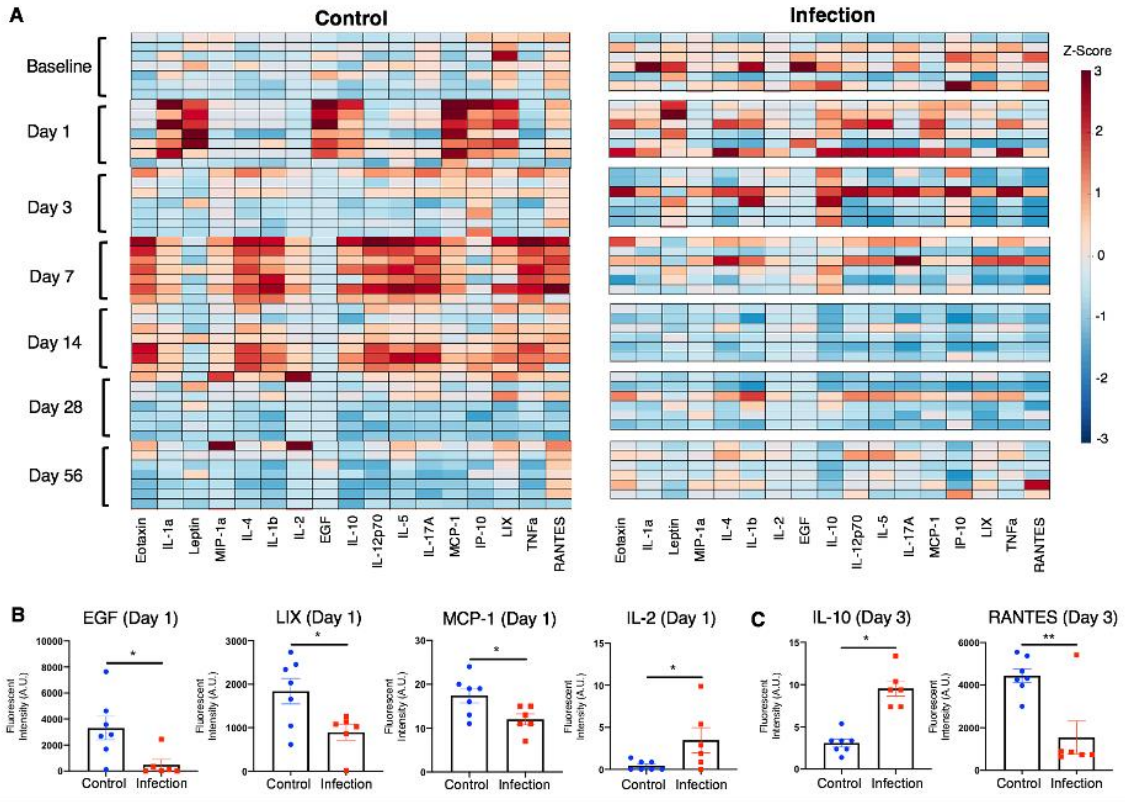

Figure 4.7. Local infection alters cytokine and chemokine profiles.
A) Heat map of z-scored cytokine levels (each column represents a different cytokine) in the control group (n=7, one n per row) and the infection group (n=6, one n per row) prior to surgery (Baseline) and at Days 1, 3, 7, 14, 28, and 56 post-surgery. Cytokine levels at the two earliest time points that exhibited significant differences between groups are shown for B) Day 1 and C) Day 3. Significance was determined using Student's t-test or with Mann-Whitney test for non-parametric data with $p<0.05$ (*) and $p<0.01$ (**).

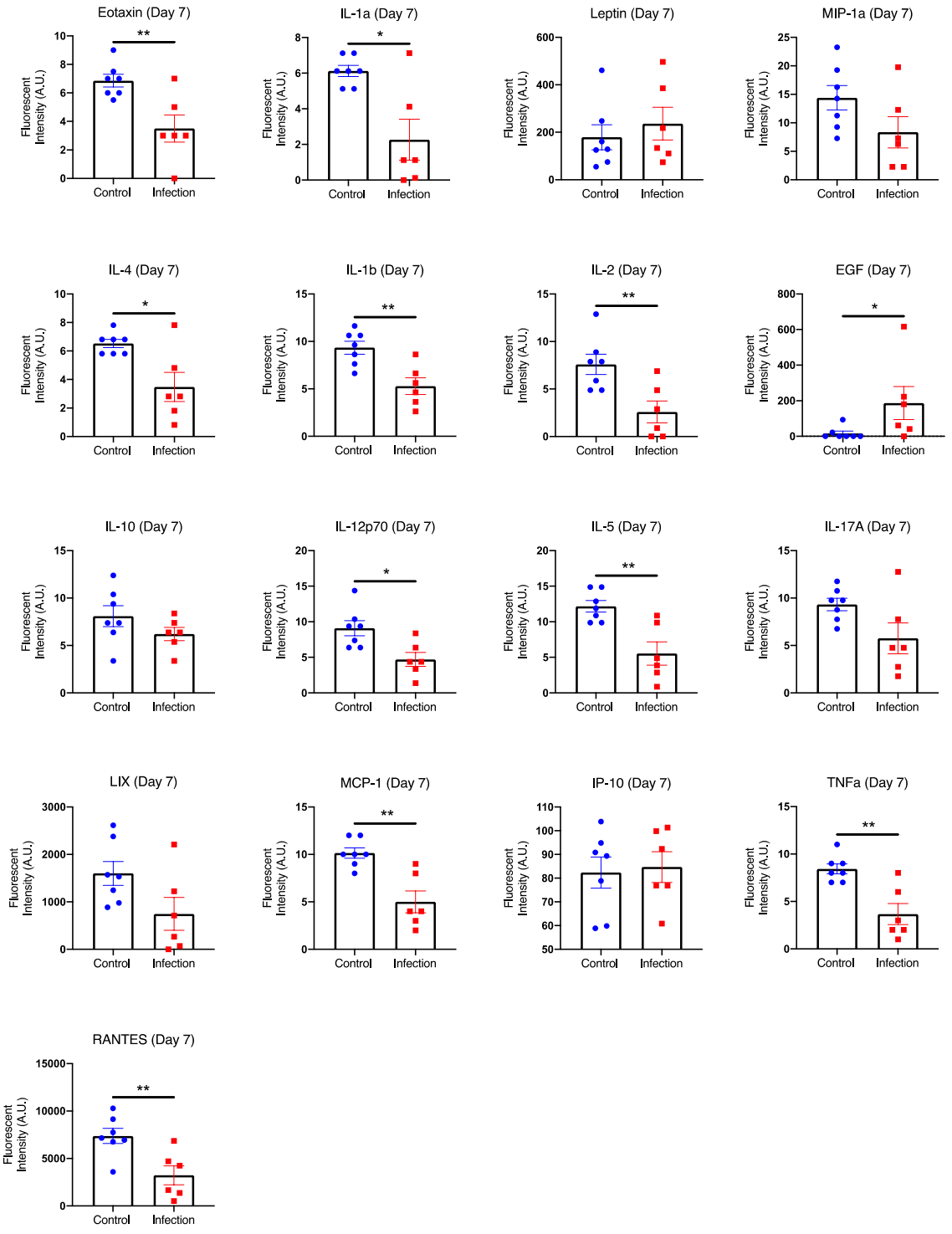

Figure 4.8. Cytokine evaluation at Day 7.
Cytokine levels in the control group and infection group at Day 7. Significance was determined using Student's t-test or with Mann-Whitney test for non-parametric data with $p<0.05$ (*) and $p<0.01$ (**).

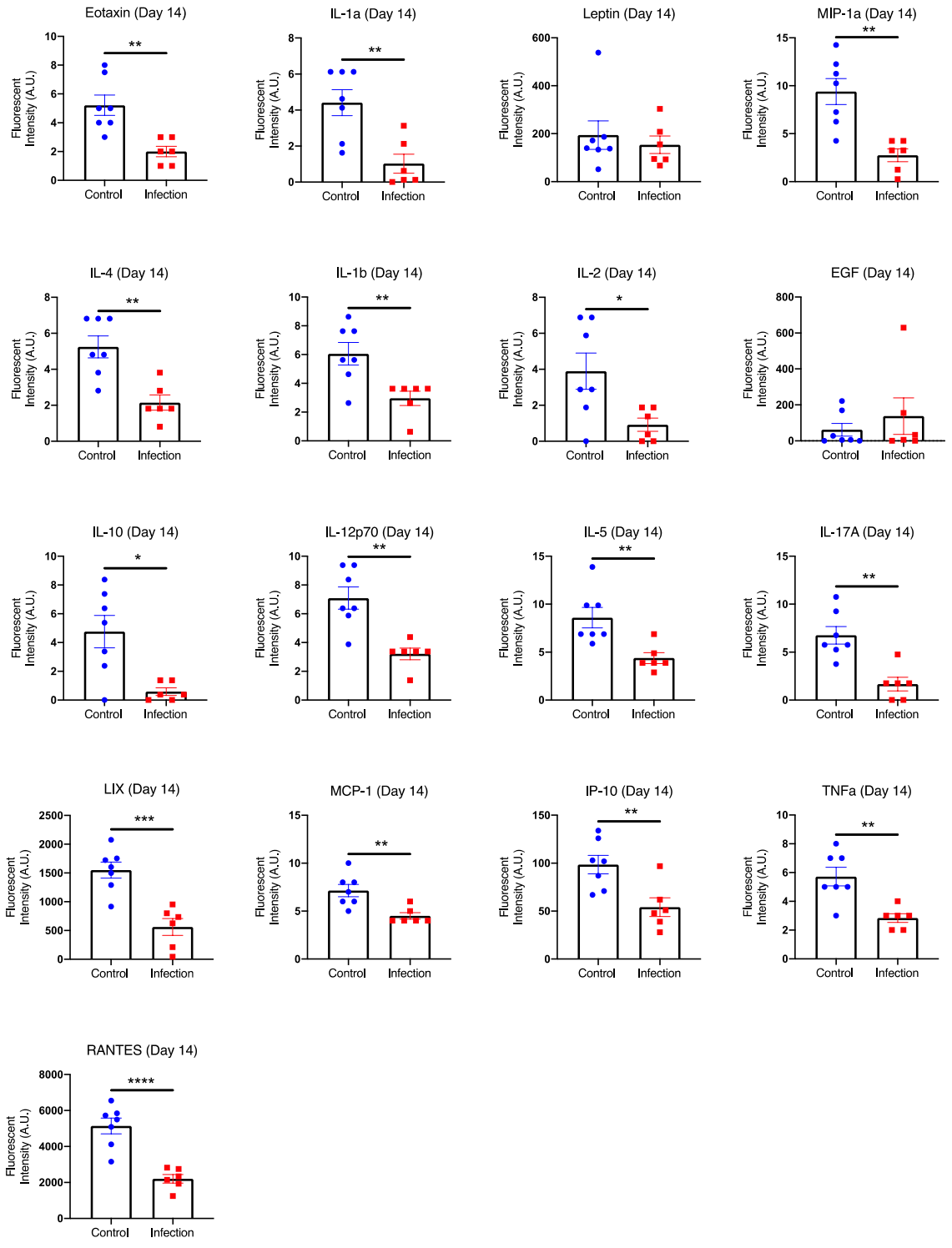

Figure 4.9. Cytokine evaluation at Day 14.
Cytokine levels in the control group and infection group at Day 14. Significance was determined using Student's t-test or with Mann-Whitney test for non-parametric data with $p<0.05$ (*), $p<0.01$ (**), $p<0.005$ (***), and $p<0.001$ (***).

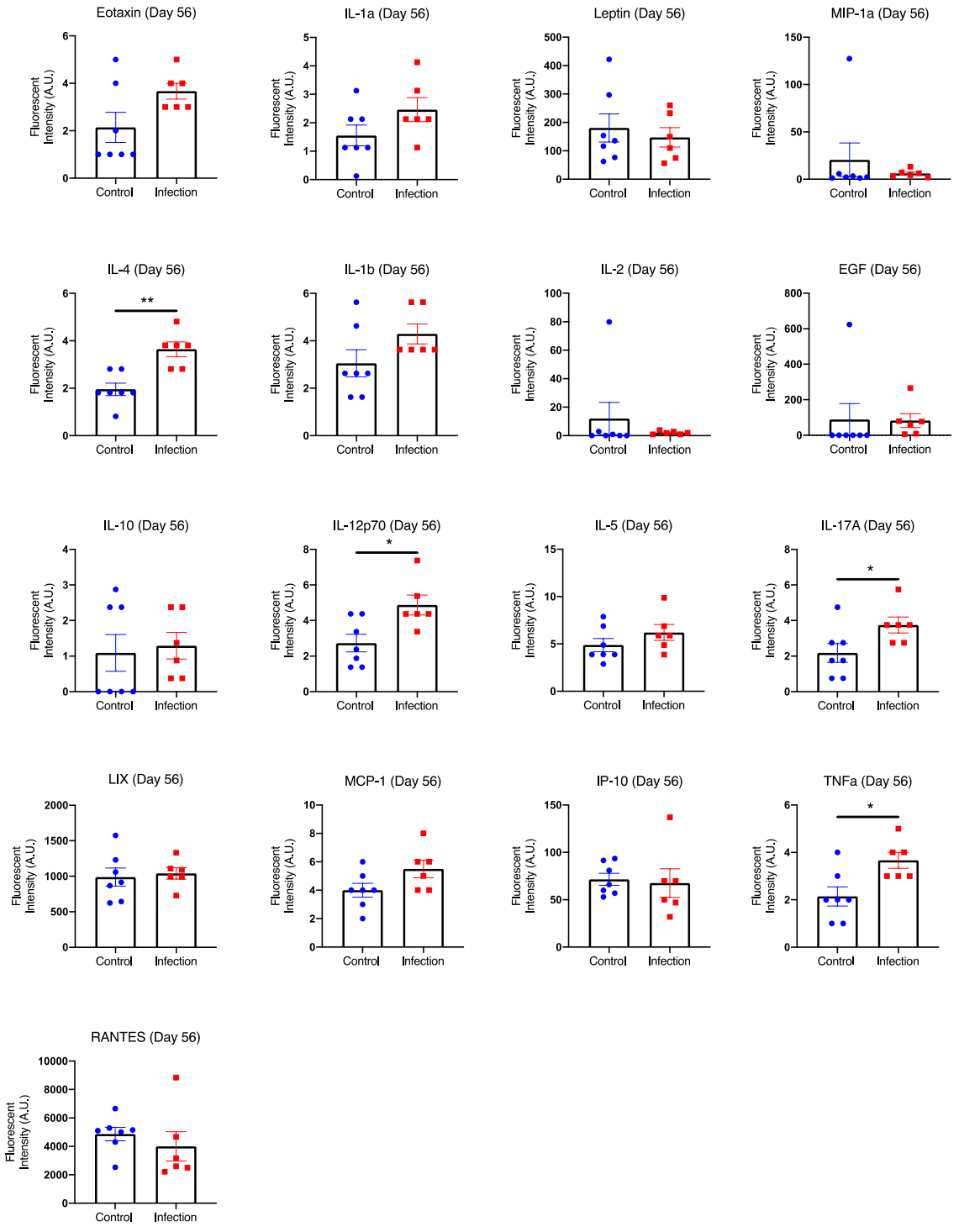

Figure 4.10. Cytokine evaluation at Day 56.
Cytokine levels in the control group and infection group at Day 56. Significance was determined using Student's t-test or with Mann-Whitney test for non-parametric data with $p<0.05$ (*) and $p<0.01$ (**).

4.3.2.4 Overall Systemic Immune Characterization

To investigate the overall contributors that distinguished the infection group from the non-infected, control group, partial least squares discriminant analysis (PLSDA) was conducted on data aggregated from all timepoints post-injury, including cellular and chemokine data (Figure 4.11A). This analysis revealed a significant separation of the two groups according to latent variable 1 (LV1) (Figure 4.11B). The LV1 loading plot shows the major contributors to positive LV1 values (control group) and negative LV1 values (infection group) (Figure 4.11C). The main contributors to the control group were T cells and the T cell effector subsets, including helper T cells and cytotoxic T cells. Contributing most to the infection group were the immunosuppressive MDSCs, B cells, and the cytokine IL-10, which has typically been considered immunosuppressive in the context of trauma and sepsis (229,230). Plotting the same datapoints from the PLSDA plot in Figure 4.11A with only the infection group data points (Figure 4.11D) or only the control group data points (Figure 4.11E) highlights that there is a separation based on response time regardless of infection. The early response (Day 1 and Day 3), the intermediate response (Day 7 and Day 14), and the late response (Day 28 and Day 56) of the cells and cytokines all cluster separately on the PLSDA plot for the infection group and the control group. The infection group clusters are significantly separated only on the LV1 axis (Figure 4.12A,B), where the top factors correlated with separation are cells, including T cells, MDSCs, and B cells, but not cytokines (Figure 4.12E). On the other hand, the control group clusters are significantly separated based on both the LV1 and LV2 axes (Figure 4.12C,D). The intermediate response (Day 7 and Day 14) for the control group shows significant separation from the early and late responses along the LV2 axis, where the top factors

correlated with separation are cytokines (Figure 4.12F), consistent with the large upregulation of cytokines observed in the heat map for the control group at Days 7 and 14. The late response (Day 28 and Day 56) for the control group shows significant separation from the early and intermediate responses along the LV1 axis, where the top factors correlated with separation are again cells, but not cytokines. These data highlight whether cells or cytokines are the major drivers of the systemic immune response at different timepoints in the control and infection groups.

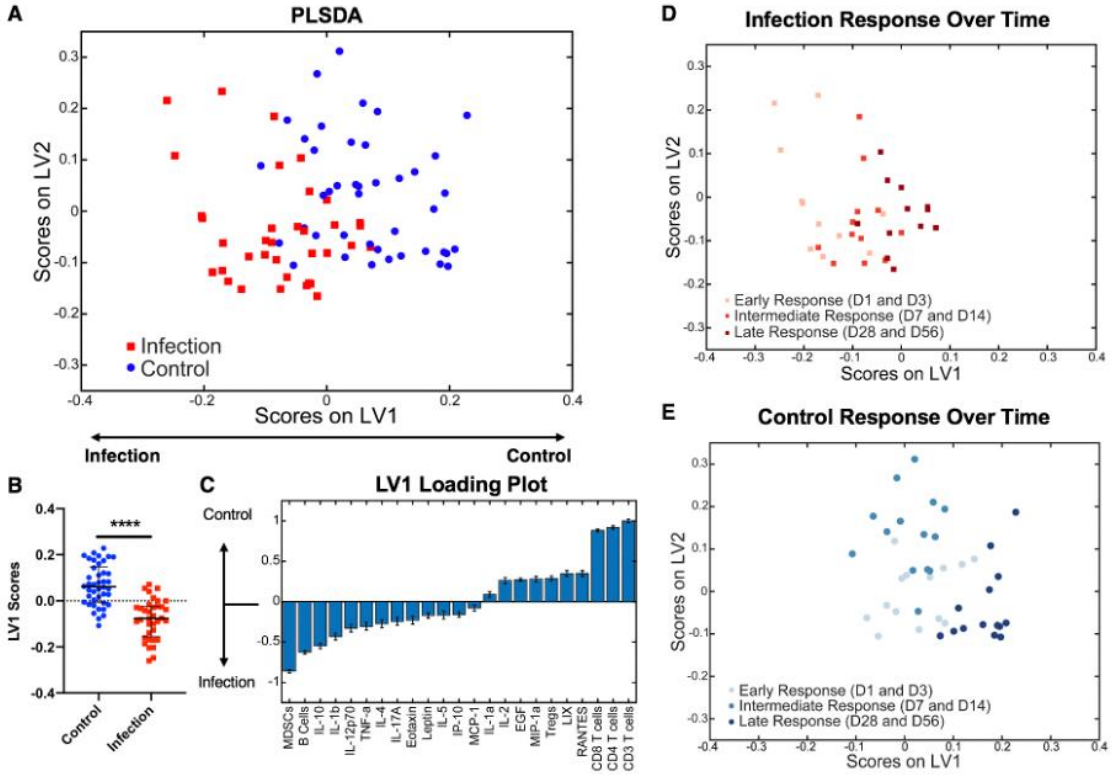

Figure 4.11. Overall systemic immune characterization.
A) PLSDA plot shows all cytokine levels and cell population values post-surgery for the control group (blue squares) and the infection group (red circles) plotted on latent variable 1 (LV1) and latent variable 2 (LV2) axes. B) Plotting only LV1 scores shows a significant difference ($p<0.001$ (****) according to Student's t-test) between the control and infection groups based on LV1 values. C) The LV1 loading plot shows the top factors that most contributed to positive LV1 scores (right) and the top factors that most contributed to negative LV1 scores (left). Plotting the same datapoints from (A) with only infection data

points (D) or only control data points (E) highlights that there is a separation based on response time regardless of infection, including the early response (Day 1 and Day 3), the intermediate response (Day 7 and Day 14), and the late response (Day 28 and Day 56).

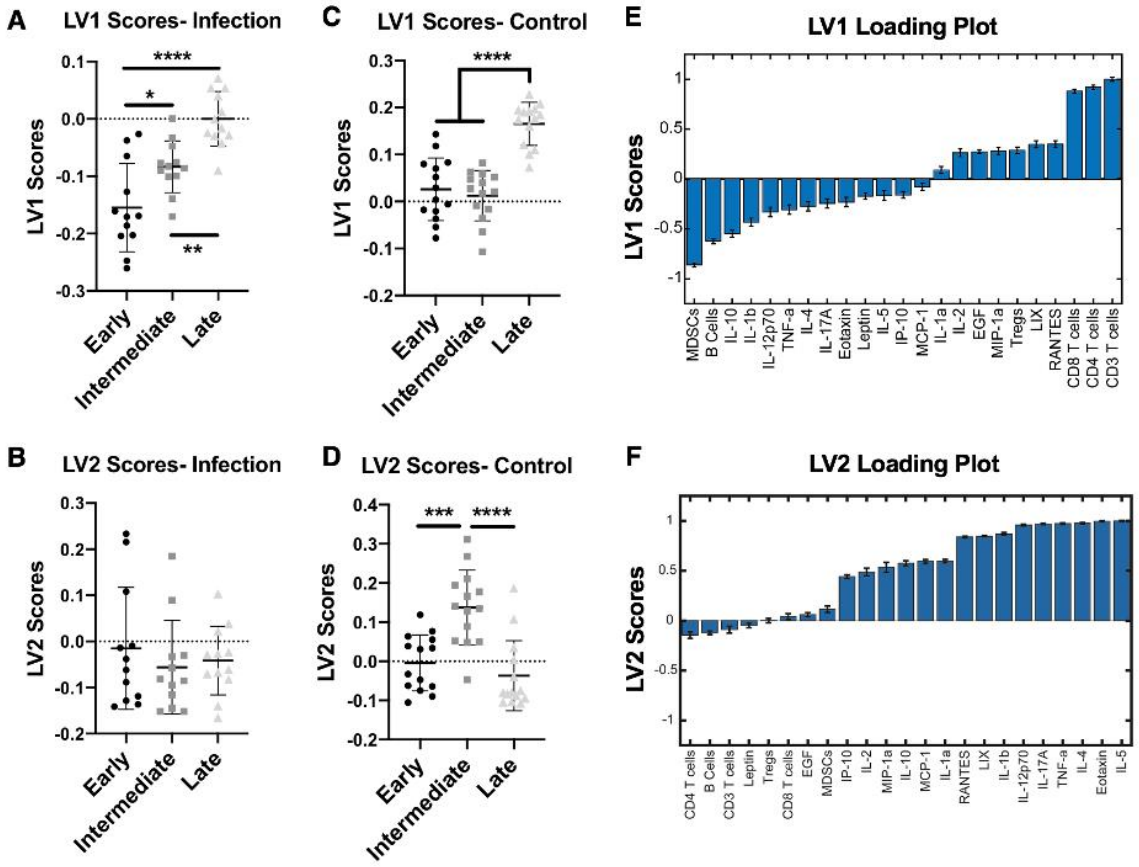

Figure 4.12. Infection and control responses over time.
The early (Day 1 and Day 3), intermediate (Day 7 and Day 14), and late (Day 28 and Day 56) immune responses for the infection group show significant separation on the LV1 axis based on LV1 scores (A), but show no significant sepration on the LV2 axis based on LV2 scores (B). The early, intermediate, and late immune responses for the control group show groups with significant separation on both the LV1 and LV2 axes based on the LV1 scores (C) and the LV2 scores (D). The LV1 loading plot (E) and the LV2 loading plot (F) show which cytokines and cell types are highly correlated with both high and low LV1 and LV2 scores, respectively. Significance was determined using a one-way ANOVA with Tukey's multiple comparisons test where $p<0.05$ (*), $p<0.005$ (***), and $p<0.001$ (****).

4.3.3 Bone Regeneration and Histological Analysis

At the Day 56 endpoint, bone explants were harvested for micro-computed tomography (uCT) and histological evaluation. There were no significant differences in

new bone formation between the control and infection animals, although the control group did have higher peak bone formation (Figure 4.13A). Further, histological analysis revealed an abnormal ectopic periosteal response in the bone from the infection animals, with aberrant and scattered periosteal bone formation (Figure 4.13B). Bone in the non-infected, control group showed new bone formation at the defect region according to hematoxylin and eosin staining.

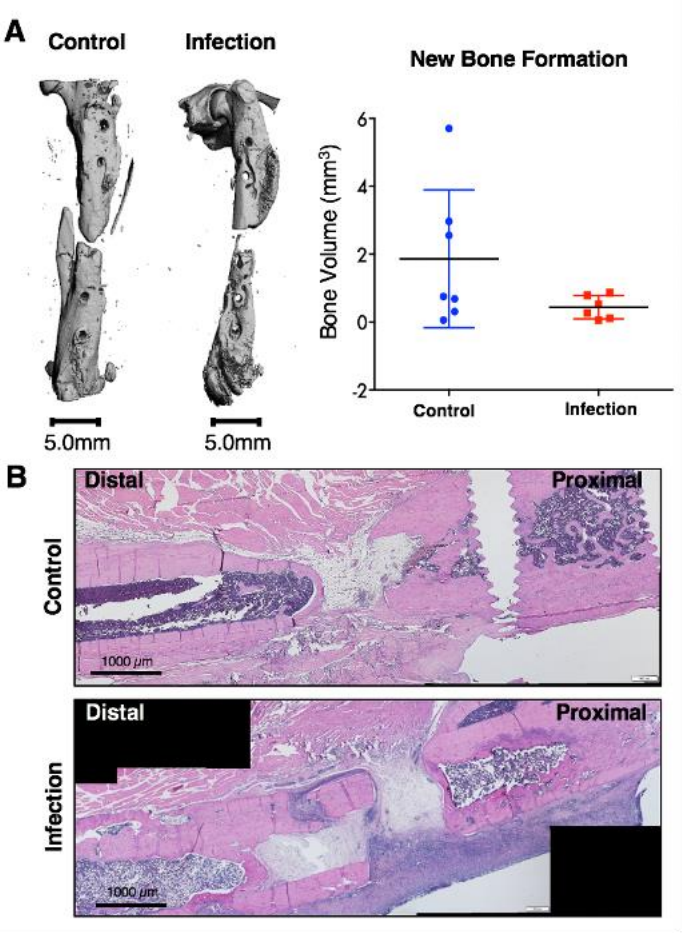

Figure 4.13. Bone regeneration and histological analysis.
A) Representative endpoint (Day 56) uCT reconstructions (left). Quantification of uCT scans showed no significant differences between the control and infection groups via Mann-Whitney test ($p=0.2343$). B) Representative Hematoxylin &Eosin (H&E) stains of the defect depicting bone formation (pink) and cell presence (nuclei stained purple) within the defect region.

4.4 Discussion

Despite advancements in surgical procedures and antimicrobial regimens, orthopedic biomaterial-associated infections remain a challenging clinical problem; failure rates remain high and there has been little to no improvement in infection-related patient outcomes over the past several decades (231). Complicating the matter for fracture-associated infections, there is currently no consensus on diagnostic criteria and therefore very few protocols for diagnosis and treatment (232). Characterization of the systemic immune response to an orthopedic biomaterial-associated infection could allow for better identification of biomarkers to identify at-risk patients and for immunotherapeutic targets that could improve local therapeutic interventions and overall outcomes for these patients. In this manuscript we utilized a rat trauma model with a biomaterial-associated infection to analyze the long-term immune response to a local, indolent orthopedic infection. While this model does not investigate the complexities of bacteria-scaffold interactions, this model still mimics clinical aspects of a chronic implant-associated bone infection, including no systemic symptoms (weight loss, fever, etc.) and eventual detection of the infection by hardware failure and/or nonunion of the defect. Pilot studies exhibited hardware failure at higher CFU; however, the dose was reduced for this study to prevent hardware failure during the time course of the experiment. One limitation of this study is the lack of longitudinal local immune analysis and evaluation of specific antibody responses against *S. aureus*. However, both of these aspects of the immune response to infection have been extensively studied (220,231), whereas this study focuses on the under-investigated systemic immune response to a local infection.

In the presence of orthopedic infection in a rat trauma model, depressed systemic immunity was observed compared to trauma without infection. This change was most notable with increased immunosuppressive MDSCs and decreased T cells, including the helper T cell and cytotoxic T cell subsets. MDSCs are a heterogeneous and immature myeloid-derived cell population characterized by their immunosuppressive function, and they expand during conditions of acute and chronic inflammation, including trauma, sepsis, infection, and cancer (7,43,47,233). MDSCs utilize various mechanistic pathways to suppress the activity of immune effector cells, including the production of immunosuppressive cytokines such as IL-10 and TGF-b, release of reactive oxygen and reactive nitrogen species (ROS/RNS), and stimulation of immunosuppressive Tregs. Additionally, MDSCs can suppress T cell function through arginase-1 activity that depletes L-arginine, an essential amino acid required for T-cell receptor (TCR) signaling (44,234). Prevention of T cell activation inhibits one of the major adaptive immune response mechanisms to pathogen-associated molecular patterns (PAMPs) and danger-associated molecular patterns (DAMPs), which are molecular motifs associated with infection and damaged or stressed tissue (220). Additionally, in the context of infection and cancer, MDSCs are known for suppressing cytotoxic T cell and Natural Killer (NK) cell function, preventing immune responses to bacteria and tumors (233,235). The resulting immunosuppression allows bacteria to evade recognition and clearance by the immune system, contributing to bacterial persistence and chronicity of local, indolent infections (220).

In this study, B cells in the blood of the infection group initially increased to levels higher than the non-infected, control group, peaking around Day 7. Following Day 7, B

cell levels in the infection group notably decline, whereas B cell levels in the control group remain relatively constant and are not significantly different from baseline levels from Day 3 onward. *S. aureus* is known to modulate the B cell response by triggering B cell-mediated immune tolerance through the virulence factor Staphylococcal Protein A (SpA)(236). SpA stimulates B cell expansion and subsequently activation-induced B cell death due to the absence of co-stimulation (237). Additionally, SpA is known to manipulate B cell affinity maturation, inhibit long-lived plasma cells, and induce immune tolerogenic IL-10 producing B cells, thus limiting the host response, preventing memory formation, and increasing the risk for chronic and recurring infection (238,239). This mechanism is consistent with our observation of the cellular immune data showing a continual decline in B cells in the infection group after a peak at Day 7 and with the cytokine data showing a significant increase in IL-10 in the infection group compared to the control group.

While there were overall differences in systemic cellular immunity between the infection and control groups and between each group and their baseline levels, there were few significant differences between groups at individual timepoints. The lack of individual differences in cell populations may in part be due to the complexity of the interactions between the different mediators. Additionally, as a limitation of this study, we did not conduct functional analyses of the various immune cell populations or investigate heterogeneity within subsets of cell types, which may highlight further and more significant differences in these populations.

Cellular analyses of local tissues showed similar results as the systemic analysis with upregulation of immunosuppressive MDSCs in the local soft tissue surrounding the defect, as well as in the bone marrow, compared to the control group. Conversely, macrophages

were elevated in the non-infected, control group in the bone marrow and the spleen as well as dramatically in the local soft tissue when compared to the infection group. This is consistent with *S. aureus* biofilm formation which is known to alter the local environment in order to impair immune effector cell function, such as macrophages, while enhancing the expansion of immunosuppressive MDSCs (220). Therefore, in the presence of infection, the immunosuppressive immune environment can prevent infiltration of macrophages, whereas, the lack of infection in the control group can permit extensive macrophage infiltration into the defect site. Due to an emphasis on the systemic immune response, one limitation of this study was a lack of characterization of macrophage phenotype infiltrating into the defect region. Future work to better understand the interactions between both the local and systemic environments could be essential for identifying appropriate immunomodulatory targets to enhance bacterial clearance and improve tissue regeneration.

Overall analysis of circulating cytokine levels revealed a regulated and coordinated immune response with resolution of inflammation sometime between Day 14 and Day 28 in the non-infected, control group. In contrast, the infection group lacked a similar coordinated response at any timepoint or with any set of cytokines compared to the control group. Looking at significant cytokine differences between groups prior to Day 7, there was early upregulation of cytokines involved in cell recruitment, proliferation, and survival in the control group compared to the infection group, including EGF, MCP-1 (also known as CCL2), and LIX (also known as CXCL5) at Day 1, and RANTES (also known as CCL5) at Day 3. Under inflammatory conditions, EGF is a potent inducer of angiogenesis and bone growth, significantly upregulating secretion of vascular endothelial growth factor

(VEGF) and bone morphogenetic protein-2 (BMP-2), an osteoinductive growth factor (240). MCP-1 has also been shown to be a key cytokine involved in both inflammation and bone remodeling, in part by promoting neutrophil migration, macrophage infiltration, and angiogenesis (241). Similarly, LIX and RANTES are known for their chemotactic and pro-inflammatory properties that have both been associated with the necessary early inflammatory phase during the fracture repair process (242,243). In the infection group however, immunosuppressive IL-10 was upregulated as early as Day 3 compared to the control animals, which may have subsequently inhibited a coordinated and regulated inflammatory response. This increase in IL-10 is supported by a sharp increase in MDSCs, which are known to release IL-10, as early as Day 1 in the infection group. At Days 7 and 14, multiple inflammatory cytokines were upregulated in the control group compared to the infection group, which all resolved back to baseline levels by Day 28. The inflammatory response after fracture repair is a highly coordinated process that is required for successful repair and regeneration of severe injuries in order to recruit appropriate cells and clear necrotic tissue (10). However, a similar inflammatory response was not seen in the infection group. Many of the cytokines that were elevated in a coordinated, temporal process in the control animals remained at low levels in the infection animals, particularly in the first two weeks. At Day 56, several cytokines, including IL-4, IL12p70, IL-17A, and TNFa, were upregulated in the infection group compared to the control group, highlighting that the dysregulated cytokine response continues long-term in the infection group.

In addition to looking individually at cell populations and cytokine levels, we also conducted multivariate analyses that can account for interaction effects to allow us to better understand the role of systemic factors in response to an orthopedic biomaterial-associated

infection. The PLSDA loading plot showed mainly cell types, not cytokines, as the top factors associated with each group. The non-infected, control group was most positively associated with T cells (CD3 T cells), including the helper T cell (CD4 T cells) and cytotoxic T cell (CD8 T cells) subsets. Functioning immune effector cells are necessary for a coordinated and regulated immune response to trauma. In particular, an absence of T cells following fracture has been shown to result in disrupted bone mineralization and decreased bone regeneration. This effect has been associated with the role of T cells in normal collagen deposition during the early stages of callus formation (35). In addition, systemic dysregulation of helper T cells has been associated with increased risk for multiple organ failure and death in trauma and burn patients (244), again highlighting the importance of T cells and their subsets for appropriate healing. In contrast, the top factors most associated with the infection group included MDSCs, B cells, and IL-10. Immunosuppressive MDSCs, which are known to release the cytokine IL-10 and expand following bacterial infection, can be a sign of a dysregulated immune response (233). In addition, *S. aureus* is also known to modulate the B cell response by enhancing the population of immune tolerogenic IL-10 producing B cells (236,238).

Interestingly, the systemic immune dysregulation and immunosuppression evidenced in the infection group has been reported before in other diseases and conditions, including sepsis and severe musculoskeletal trauma (21). In both trauma and sepsis, there is a massive early innate immune response, resulting in over-production of pro-inflammatory mediators (e.g. Type I Interferons, IL-1, IL-6, IL-8, TNFa) and systemic activation of innate immune cells (10,245). Concurrently, the body's defense mechanisms trigger a compensatory anti-inflammatory response through systemic up-regulation of

immunosuppressive mediators (e.g. IL-10, TGF-b) and cells, such as MDSCs and Tregs (6,7,28,32,246). A balance between the two responses leads to restoration of systemic immune homeostasis typically within the first week or two and is associated with successful healing and regeneration, similar to what we see in the control group in our rat infection model. However, when the anti-inflammatory response overwhelms the initial inflammatory response, systemic immune dysregulation develops, marked by increases in immunosuppressive mediators, decreases in immune effector cell numbers and function, and an overall decrease in host immunity (28,247). In all of the cases discussed – implant-associated orthopedic infection, sepsis, and severe musculoskeletal trauma – widespread systemic immunosuppression results after overactivation of the immune system either from bacterial infection or from damaged host tissue. Therefore, in any situation resulting in similar immune overactivation, systemic immune dysregulation could arise and may impact patient outcomes.

Creation of a local, indolent infection with *S.* aureus-soaked collagen sponges implanted in the defect site was confirmed by normal weight gain and temperature, bacterial presence after endpoint wound swab culture, and longitudinal bioluminescent imaging, although bioluminescent signaling dropped below the threshold of detection past Day 7. Following biofilm formation, *S. aureus* is known to undergo significant metabolic changes, including down-regulation of transcription, translation, and aerobic processes, resulting in an overall decrease in metabolic activity of the active infection. For example, physiologically dormant "persister" cells are protected by the biofilm matrix and thought to grow at significantly slower rates than metabolically active planktonic cultures (248–250). Reductions in bioluminescent signal despite no significant decrease in bacterial load

has also been observed in several other related mouse osteomyelitis models (251–253). Therefore, the absence of bioluminescent signal past Day 7 is not indicative of infection clearance but likely indicative of biofilm formation and decreased metabolic activity, resulting in bioluminescent signal that falls below the limits of detection of our instrumentation (Figure 4.1).

In addition to the unexpected lack of bioluminescent signal past Day 7 in the infection group, we also observed no significant differences in bone regeneration volumes between groups, despite the sub-critical size of the bone defect. The non-infected, control group bone defects contained a collagen sponge, which is clinically approved for use in patients in conjunction with BMP-2, an osteoinductive growth factor. While this study did not utilize BMP-2, collagen based-materials are attractive options for bone substitutes because collagen is the main organic polymer in bone matrix. Additionally, collagen scaffolds have had success in tissue engineering and wound healing applications to facilitate cell growth and differentiation, promote intrinsic vascularization, and provide an infrastructure for osteogenesis and chondrogenesis by supporting cell invasion (254). There are multiple collagen-based composite bone substitutes used clinically for bone applications, including Cerasorb Ortho Foam, a collagen-tricalcium phosphate composite, and OssiMend, a collagen-carbonate apatite composite (255). Despite the widespread use of collagen-based materials for bone tissue engineering, the effects of collagen sponge alone on bone healing without exogeneous factors, such as BMP-2, still remain largely unknown. However, in a recent study, *in vivo* testing of collagen sponge unexpectedly showed a negative impact on bone healing, with significantly decreased bone formation in a mouse osteotomy model compared to an empty defect (256). These results are consistent

with the lack of healing observed in our study for the non-infected, control group; however, further mechanistic studies are needed to understand the potential inhibitory effects of empty collagen sponge in sub critical-size bone defects.

The systemic immune characterization from this study identified multiple differences in immune factors as early as 3 days post-surgery that could be used to identify patients exhibiting systemic immune dysregulation following implant-associated orthopedic infection. Currently, chronic infections are often not diagnosed until weeks or months later following a catastrophic event such as hardware failure, bone non-union, or sepsis. The immune markers evaluated in this study could be used for early identification of patients exhibiting systemic immune dysregulation, which could then allow clinicians to investigate and treat patients for potential infections significantly earlier, improving outcomes and reducing healthcare costs. In addition to using early systemic immune markers to diagnose at-risk patients, this study also identified the significant driving factor of immune dysregulation to be the immunosuppressive MDSC population, offering a promising immunomodulatory target that could synergistically improve current treatment strategies, similar to cancer immunotherapy. However, further studies are still needed to better understand the role of systemic immune dysregulation and systemic immunomodulation on the local environment, including bacterial clearance and bone regeneration.

4.5 Conclusions

To our knowledge, this is one of the first studies investigating the systemic immune response and immune dysregulation resulting from trauma-associated orthopedic biomaterial infections. The presence of a local, indolent *S. aureus* bacterial infection

resulted in widespread systemic effects, including an uncoordinated and dysregulated systemic immune response with systemic increases in immunosuppressive MDSCs and decreases in immune effector cells, including T cells. This systemic immune dysregulation and immunosuppression in combination with the local *S. aureus* infection could contribute significantly to the clinical challenges associated with infected trauma, in particular, chronic and recurring infections and poor bone regeneration. An improved understanding of the systemic immune response and its relationship with the local environment, including bacterial clearance and bone healing, could provide promising early diagnostic markers and systemic immunomodulatory targets to improve the ability to fight orthopedic biomaterial-associated infections and improve patient outcomes.

CHAPTER 5. BMP-2 DELIVERY STRATEGY MODULATES LOCAL BONE REGENERATION AND SYSTEMIC IMMUNE RESPONSES TO COMPLEX EXTREMITY TRAUMA[4]

5.1 Introduction

Five to ten percent of the more than twelve million fractures a year experience complications with healing, most commonly nonunions and infections (4,98,257). Nonunions can be considered as any fracture that persists without any healing progression for at least 3 months. In rodent models, this can be accomplished by creation of a critical size segmental bone defect which will always lead to non-union (258). For composite injuries, which contain volumetric tissue defects in both the bone and the adjacent soft tissue and muscle, the risk for nonunion is twice as high (4,259). Revision surgery to address nonunions is typically successful in upwards of 90% of patients; however, chronic nonunions that result after one or more failed interventions still pose a significant clinical challenge. Chronic nonunions are defined as a fracture that has failed to heal for more than 12 months, and they can result in multiple revision surgeries, prolonged hospital stays, increased treatment costs, and even limb loss, with one prospective study reporting around 2% of patients undergoing amputations following nonunion of a severe lower limb extremity trauma (3,5). Despite advancements in surgical procedures and regenerative

[4]Reproduced from C.E. Vantucci and L. Krishnan et al., BMP-2 delivery strategy modulates local bone regeneration and systemic immune responses to complex extremity trauma, Biomaterials Science, 2021. 9: p. 1668-1682 with permission from the Royal Society of Chemistry.

strategies, there is still an urgent need for improved treatment strategies for chronic nonunions (261).

Currently, the exact underlying biological and physiological mechanisms leading to the development of nonunion are poorly understood, and further, how these biological changes impact treatment outcomes for patients is also poorly understood (262). It is generally accepted that there are various risk factors, such as age, gender, smoking, and medical comorbidities, that can increase the likelihood of nonunion and decrease treatment success; however, recent work has also identified other factors that can impact treatment outcomes for trauma patients, including systemic immune function (263). Long-term poor clinical outcomes, such as chronic nonunions, have been associated with systemic immune dysregulation and immunosuppression, marked by functional decreases in immune effector cells and cytokines and increases in immunosuppressive cells and cytokines (21). Systemic immune dysregulation is hypothesized to occur when the immune system overcompensates for high levels of inflammation, and this has been observed clinically and in pre-clinical models following severe injury, sepsis, and orthopedic infection (32,167,264). Additionally, observation of systemic immune dysregulation in a pre-clinical model of chronic nonunion revealed correlations between impaired bone healing and systemic cytokine expression (265). The immune system is essential for appropriate and regulated healing, and the field of osteoimmunology has highlighted the complex relationship between bone and the immune system (266). It is unknown if improper functioning of the systemic immune system contributes to nonunion progression or results from nonunion progression; however, treatment strategies that are not only osteogenic but also capable of

overcoming systemic immune dysregulation could be essential to improving patient outcomes following treatment of chronic nonunions.

One treatment approach for complex bone injuries employs bone morphogenetic protein 2 (BMP-2) delivered on an absorbable collagen sponge (267–269). BMP-2 is a potent osteoinductive growth factor with FDA approval for use in select applications like spinal fusions and some tibial fractures; however, pre-clinical and clinical studies over the past 10 years have shown significant promise for BMP-2 treatment in long bone fractures (270,271). In addition, BMP-2 has exhibited a positive immunomodulatory effect through macrophage stimulation and upregulation of cytokines important for MSC recruitment and angiogenesis, resulting in enhanced osteogenesis of bone marrow stromal cells (272). Despite clinical use of collagen sponges for BMP-2 delivery, they have been shown to retain only 10% or less of the BMP-2 at the implant site 1 to 2 weeks after delivery, minimizing treatment efficacy and increasing risk for adverse side effects such as inflammation, heterotopic ossification (HO), and irregular bone organization (273–278). Delivery vehicles with improved spatiotemporal release profiles may be essential for decreasing unwanted side effects and improving efficacy by maintaining BMP-2 locally and preventing systemic spread of BMP-2. In addition, by maintaining BMP-2 locally, these improved delivery vehicles could also allow for safe and controlled delivery of higher BMP-2 doses, which may be beneficial since bone healing has previously exhibited a dose response to BMP-2 (265,273,279). For example, in a rat chronic nonunion bone defect model, treatment with 2.5ug BMP-2 resulted in only a 50% bridging rate of the defect, whereas 5ug BMP-2 resulted in a 75% bridging rate (265). Similarly, in a rat composite bone-muscle defect model, acute treatment with 10ug BMP-2 showed increased bone

regeneration compared to a 2.5ug BMP-2 dose (279). Additionally, both studies showed enhanced mechanical properties, including strength and stiffness, at the higher BMP-2 doses. Interestingly, these dosages in the rat correspond to human dosages around 5-10 times below the typical clinical dosage of 0.1-0.5mg/kg. Higher dosages of BMP-2 need to be evaluated to better correspond to clinical practices. In addition, the ability to spatiotemporally deliver even higher doses of BMP-2 may be essential for minimizing side effects and for sustaining endogenous repair mechanisms that could improve outcomes, especially in more challenging bone defect scenarios, such as chronic nonunions.

Many alternatives to collagen sponges have been investigated in pre-clinical models to improve BMP-2 retention and prevent rapid release, including polylactic-co-glycolic acid (PLGA) and alginate (178,280,281), and these, along with other strategies, have been extensively reviewed (282–284). One particularly promising approach to appropriately deliver high doses of BMP-2 utilizes heparin, a naturally occurring biomolecule, that can retain large amounts of bioactive BMP-2 through reversible, non-covalent electrostatic interactions (285,286). Our laboratory has previously fabricated heparin methacrylamide microparticles (HMPs) loaded with BMP-2 that can easily be incorporated within an alginate hydrogel which is then spatially constrained to the injury site by a polycaprolactone nanofiber mesh (279). This HMP delivery system enhances the spatiotemporal release profile of moderately high doses of BMP-2, increases long-term retention of BMP-2 at the defect site, and decreases heterotopic bone formation in a pre-clinical bone defect model when treated immediately after injury (287–289), all highlighting the potential of this strategy for successful and controlled delivery of high doses of BMP-2. The ability to safely deliver higher doses of BMP-2 through the HMP

system may allow BMP-2 to act as both an osteoinductive and immunomodulatory agent to overcome additional immunological challenges associated with chronic nonunions, ultimately enhancing bone regeneration. At the same time, excessive doses of BMP-2 could harmful, so appropriate dosing for the type and severity of trauma is essential.

In this study, a moderately high dose of BMP-2 (30ug or 0.12mg/kg) delivered from clinical standard collagen sponge is compared to the same dose of BMP-2 delivered from our previously established HMP delivery system in two clinically-relevant chronic nonunion models: a bone defect chronic nonunion model and a more severe composite injury chronic nonunion model with concomitant volumetric muscle loss. While this strategy showed promise in an acutely treated segmental defect model, this is the first time that this delivery strategy has been investigated in more complex and challenging chronic nonunion models exhibiting systemic immune dysregulation, which has previously been associated with poor patient outcomes. Specifically, two main hypotheses are investigated: first, that the high dose BMP-2 delivered through the HMP system will promote spatially controlled functional bone regeneration in chronic nonunion models, even under challenging conditions exemplified by the composite bone-muscle injury model; and second, that spatially controlled BMP-2 release from the HMP system will support immunomodulatory functions of BMP-2 that result in positive modulation of the systemic immune response. A better understanding of the regenerative response to therapeutic strategies and the immunological changes and biological mechanisms associated with nonunion progression are both critical to improving patient outcomes and reducing the morbidity associated with challenging bone nonunions.

5.2 Materials and Methods

5.2.1 Delivery Vehicle Preparation

5.2.1.1 Heparin Microparticle Fabrication

Heparin microparticles were fabricated as previously described (287,288). Briefly, EDC/Sulfo-NHS chemistry was used to substitute methacrylamide groups on heparin. Heparin methacrylamide was then dissolved in phosphate-buffered saline (PBS) and mixed with equimolar amounts of the free radical initiators, ammonium persulfate (Sigma Aldrich) and tetramethylethylenediamine (TEMED, Sigma Aldrich). A water-in-oil emulsion was then formed by adding the heparin solution dropwise into 60mL of corn oil and 1mL of polysorbate 20 (Promega) and then homogenized on ice for 5 min at 3000rpm (Polytron PT3100 Homogenizer, Kinematica). Free radical polymerization and thermal cross-linking of the methacrylamide groups was carried out by immersing the emulsion in a 55˚C water bath under constant stirring and nitrogen purging for 30 minutes. The HMPs were collected following centrifugation for 10 minutes at 3000rpm and subsequently washed in acetone, deionized water several times, and 70% ethanol for sterilization. HMPs were lyophilized and stored at 4˚C until ready for incorporation into the alginate constructs. HMPs were characterized following fabrication and confirmed to retain their functionality with evaluation of growth factor binding and release kinetics(287).

5.2.1.2 Alginate and Nanofiber Mesh Construct Fabrication

Alginate hydrogels were fabricated as previously described (178). Briefly, a 3% alginate solution was made by slowly dissolving irradiated, RGD-functionalized alginate (FMC Biopolymer) into sterile alpha-MEM (Corning). The solution was then mixed with 0.1% rat serum albumin (RSA) in 4mM HCl containing 30ug of BMP-2 and 0.1mg of

HMPs to make a 2% alginate solution. The final alginate solution containing BMP-2 and HMPs was then cross-linked in an excess of calcium sulfate (8.4mg/mL; Sigma Aldrich) by thorough mixing and stored in 4˚C. Polycaprolactone (PCL) nanofiber meshes were fabricated as previously described (178). Briefly, a 12% (w/v) PCL solution is formed by dissolving PCL overnight in a 90:10 solution of 1,1,1,3,3,3-Hexafluoro-2-propanol, 99+% (HFP; Sigma Aldrich) and *N,N*-Dimethylformamide, anhydrous, 99.8% (DMF; Sigma Aldrich). The PCL solution is then electrospun onto aluminum foil until an approximate thickness of 500um. Rectangular perforated meshes (12mm by 19mm with 0.7mm diameter holes) were then cut from the electrospun PCL nanofiber meshes and rolled to have an inner diameter of 4.5mm and a length of 12mm. The meshes were glued with UV cure adhesive (DYMAX), sterilized in 70% ethanol, and then stored in alpha-MEM at 4˚C until use. For *in vivo* studies, the PCL nanofiber mesh tube was placed within the defect site and subsequently 150uL of the alginate hydrogel was syringe injected with a blunt-tip needle into the center of the mesh so each defect received 0.1mg HMPs and 30ug BMP-2.

5.2.2 Surgical Procedures

All animal procedures were performed in accordance with the Guidelines for Care and Use of Laboratory Animals of the Georgia Institute of Technology and approved by the Animal Ethics Committee of the Georgia Institute of Technology. Thirteen-week old female Sprague Dawley rats (Charles River Laboratories) received a unilateral segmental defect in the left femora, as previously described (290). Briefly, a polysulfone internal fixation plate provided stabilization while an oscillating saw was used to remove 8mm from the mid-diaphysis of the femur. The polysulfone plate sits outside the defect region on metal risers that are about 2-3mm thick. In the composite defect animals, an additional

8mm diameter, full-thickness defect was created in the overlying quadriceps, as previously described (121). All defects were left untreated until 8 weeks post-surgery. At 8 weeks, animals underwent an additional procedure where the defect site was cleared, and treatment was administered (Figure 5.1A). Animals received a clinically-equivalent dose of 30ug BMP-2 (0.12kg/mg) loaded in a collagen sponge, n=10 or in the HMP delivery system (HMPs in alginate gel + PCL nanofiber mesh), n=11 (Figure 5.1B). Additionally, all composite defect animals received 30ug BMP-2 delivered in the HMP system, n=6, and the muscle defects were left untreated. In order to minimize animal number used, there was no collagen sponge treated composite defect group since previous work in our lab has consistently shown that composite defects heal worse compared to bone only defects with the same treatment (121). Therefore, comparisons between the HMP treated composite defect group and the collagen sponge treated bone defect only group exhibit treatment outcomes despite the additional challenge of a muscle defect. Following surgical procedures, animals were given ad libitum access to food and water and showed no signs of pain or distress. Animals were euthanized by carbon dioxide inhalation at twenty weeks from the first surgical procedure.

5.2.3 Bone Regeneration

5.2.3.1 Radiography and Micro-Computed Tomography

Longitudinal bone regeneration was qualitatively assessed with radiographs taken at 4, 8, and 12 weeks post-treatment (12, 16, and 20 weeks post-injury) (Faxitron MX-20 Digital, Faxitron X-ray Corp.). At the same time points, micro-computed tomography (Viva-CT 40, Scanco Medical) was used for quantitative assessment of newly regenerated

bone, determined using a threshold corresponding to ≥ 50% of the density of native cortical bone. Along the long axis of the femur, the central 166 slices (~6.5mm of the 8mm defect) were evaluated with a 38um voxel size, 55kVp voltage, and 145uA current. To differentiate between bone formed within the defect (defect bone volume) and bone formed outside of the defect (heterotopic bone volume), 2 volumes of interest (VOI) were evaluated, as previously described (268). The first VOI encompassed a large diameter to characterize all bone formation within the thigh, while the second VOI encompassed only a 6mm-diameter to characterize bone formation within and immediately bordering the PCL nanofiber mesh. Heterotopic bone volume was determined by subtracting the bone volume of the second VOI (defect bone volume) from the bone volume of the first VOI (total bone volume) (Figure 5.4A). Trabecular thickness, trabecular number, and connectivity were determined using a Scanco evaluation script according to previously set guidelines for assessing bone microstructure in rodents (291). Polar moment of inertia (pMOI) was also determined using a Scanco evaluation script that measures and calculates the bone distribution along the central longitudinal axis for each individual slice. These values are then averaged to determine a global pMOI value for each sample (268,292).

5.2.3.2 Biomechanical Testing

Following euthanasia at the week 20 endpoint, femora were harvested for biomechanical testing. The soft tissue was cleared, and the fixation plates were carefully removed. Each femur end was then potted in Wood's metal (Alfa Aesar) and tested to failure in torsion at a rotation rate of 3˚ per second (ELF 3200, TA ElectroForce), as previously described (290). Torque-rotation curves were used to calculate failure strength

(maximum torque) and torsional stiffness for each sample. Contralateral femora were used to determine biomechanics of intact bone.

5.2.3.3 Histological Analysis

After mechanical testing, one representative sample from each group was selected for histology. The samples were fixed in 10% neutral buffered formalin (NBF) for 24 hours and then decalcified in a formic citrate solution (Newcomer Supply, Inc). The bone tissue was embedded in paraffin and sectioned at a thickness of 5 um and then stained with hematoxylin & eosin (H&E) and safranin-O/fast green (Histotox Labs; Boulder, CO).

5.2.4 Immune Characterization

Approximately 500uL of blood was collected longitudinally via the rat tail vein at weeks 0 (baseline), 2, 8 (prior to treatment), 10, and 20. Half of the blood collected was allowed to clot overnight at 4˚C. The next day, the samples were centrifuged down at 1500g for 10 minutes and the serum was collected and stored at -20˚C for cytokine and chemokine analysis. The other half of the blood collected was stored in heparin coated tubes to prevent clotting. Following red blood cell lysis (1X RBC Lysis Buffer, eBioscience,), cells were fixed (BD Cytofix, BD), resuspended in FACS buffer (2% fetal bovine serum in 1X PBS), and then stored at 4˚C until staining for cellular analysis via flow cytometry.

5.2.4.1 Cellular Analysis

Flow cytometry was used to evaluate circulating immune cell populations. Prior to staining, cells were blocked with anti-rat CD32 (BD) for 10 minutes at 4˚C to prevent non-specific binding. Samples were then stained for the following immune effector cell

populations: T cells (CD3+), helper T cells (CD3+CD4+FoxP3-), cytotoxic T cells (CD3+CD8+), and B cells (B220+). Samples were also stained for the following immunosuppressive cell populations: myeloid-derived suppressor cells (MDSCs, His48+CD11b+) and T regulatory cells (Tregs, CD3+CD4+FoxP3+). All antibodies were purchased from eBioscience. Data were collected using a BD Accuri C6 flow cytometer, and FlowJo was used for data analysis. All gates were set based on fluorescent minus one (FMO) and unstained controls with less than 1% noise allowed.

5.2.4.2 Cytokine and Chemokine Analysis

Serum cytokines and chemokines were evaluated via a multiplexed immunoassay (Milliplex MAP Rat Cytokine/Chemokine Magnetic Kit, Millipore Sigma), and data were collected using a MAGPIX Luminex reader (Luminex). Median fluorescent intensity values with the background subtracted were used for multivariate analyses.

5.2.5 Statistical Analysis and Partial Least Squares Discriminant Analysis

Cytokine, chemokine, and cellular data were compiled at each time point for multivariate analysis using partial least squares discriminant analysis (PLS-DA). PLS-DA analysis reduces the dimensionality of the input variables into a set of latent variables (LVs) that maximally separate discrete groups (i.e. collagen sponge treatment group vs. HMP treatment groups). Latent variables are composed of profiles of the input variables that represent their relative contributions to the latent variables, and thus the separation between the groups. PLS-DA was conducted in MATLAB (Mathworks) using Cleiton Nunes' partial least squares algorithm (Mathworks File Exchange) following z-scoring to normalize the data. All data are represented as the mean ± standard deviation, and analyses

were conducted using GraphPad Prism 7. Parametric and non-parametric statistical tests were used as indicated based on if assumptions were met or not.

5.3 Results

5.3.1 Clinically-Relevant Bone Nonunion Models

Two previously established and challenging animal models of chronic nonunion were used in this study: one consisting of a segmental bone defect (Bone Only) and the other consisting of a segmental bone defect with concomitant volumetric muscle loss (Composite), representing a more challenging case of nonunion. In both models, treatment was delayed until 8 weeks after creation of the defect at which point capping of the bone ends was seen, indicating little or no further mineralization and establishment of nonunion. Following treatment with 30ug BMP-2 delivered in either the HMP construct or the clinical standard collagen sponge (Figure 5.1B), animals underwent longitudinal evaluation of bone regeneration and the systemic immune response for an additional 12 weeks (week 20 after the initial defect surgery; Figure 5.1C). At Week 0 prior to treatment (8 weeks post-injury), circulating immune cell populations were evaluated and compared to baseline levels that had been assessed immediately prior to injury. T cells were significantly decreased compared to baseline levels, whereas immunosuppressive MDSCs and macrophages were significantly elevated in both the Bone Only and Composite injury groups (Figure 5.2). Although there was no significant difference in B cell populations, B cells did show a decreased peak in cell counts compared to baseline (Figure 5.2).

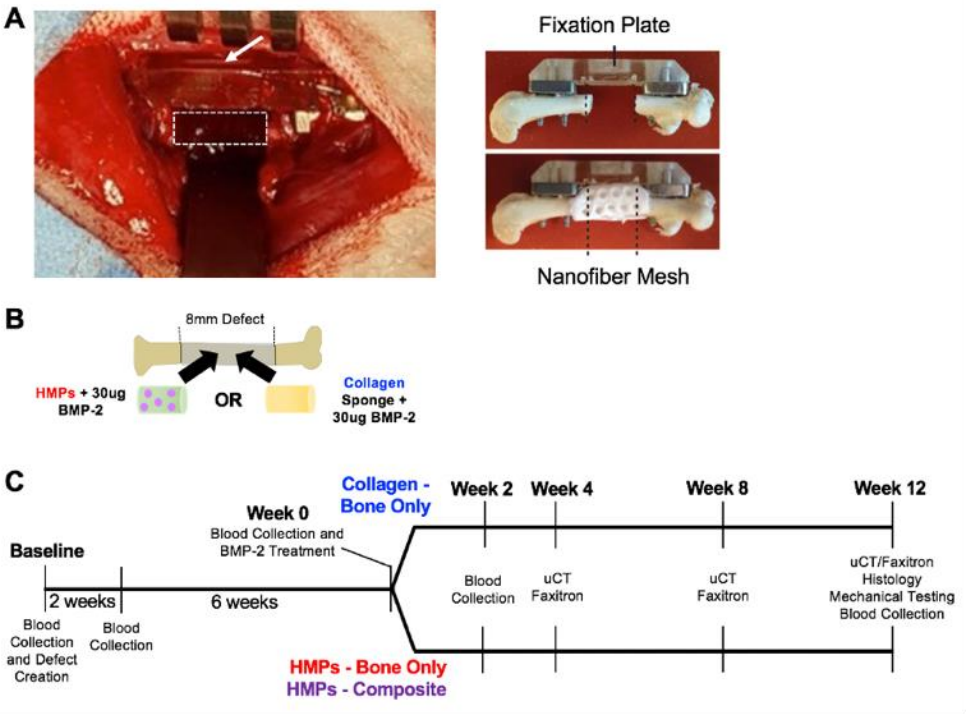

Figure 5.1. Clinically-relevant bone nonunion models.
A) Each animal received an 8mm femoral segmental defect, stabilized by a polysulfone internal fixation plate. The white, dotted rectangle indicates the location of the defect and the white arrow indicates the fixation plate. Additionally, one group of animals will also receive an 8mm volumetric muscle loss in the adjacent quadricep muscle (not shown). Ex vivo imaging shows the fixation plate stabilizing the femur and the nanofiber mesh construct within the defect site, which is used for the HMP hybrid delivery system. Ex vivo images are reproduced with permission from Krishnan et al (269). B) The defects will be treated with 30ug BMP-2 delivered in HMPs within an alginate/nanofiber mesh construct or 30ug BMP-2 delivered on an adsorbable collagen sponge. C) The timeline of the study indicates the timepoints for defect creation, BMP-2 treatment, blood collections, uCT scans, radiographic images (Faxitron), histology, and mechanical testing.

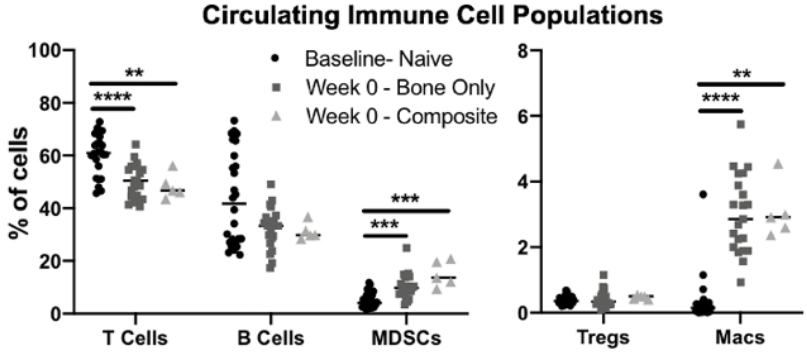

Figure 5.2. Circulating Immune Cell Populations.

Circulating immune cell populations at baseline prior to defect creation, and at Week 0 prior to BMP-2 treatment (8 weeks post-defect creation) for the bone only defect group and the composite defect group. Significance was determined using one-way ANOVA with $p<0.01$ (**), $p<0.005$ (***), and $p<0.001$ (****).

5.3.2 Radiography and Micro-Computed Tomography

Radiographs demonstrated qualitative bridging in all samples regardless of group; however, they also revealed larger variability in healing responses in the collagen sponge group compared to the HMP treated groups (Figure 5.3A). In order to minimize animal number used, a collagen sponge treated composite defect group was not included since previous work in our lab has consistently shown that composite defects heal worse compared to bone only defects with the same treatment (121). Therefore, comparisons between the HMP treated composite defect group and the collagen sponge treated bone defect only group exhibit treatment outcomes despite the additional challenge of a muscle defect. Representative samples with low and high amounts of heterotopic ossification (HO) in each group showed that the collagen sponge group had increased HO compared to the HMP groups. Additionally, the collagen sponge group also had a lower valley of HO compared to the HMP groups, although this appears to be due to decreased overall bone volume. In contrast, samples in the HMP groups with the highest and lowest levels of HO appeared much more consistent and similar with robust defect bone formation and minimal heterotopic bone formation, although the more challenging composite nonunion model appeared to have slightly more HO than the bone only nonunion model. The radiographs are supported by uCT reconstructions, again showing increased variability and higher peak HO in the collagen sponge group compared to the HMP groups (Figure 5.3B).

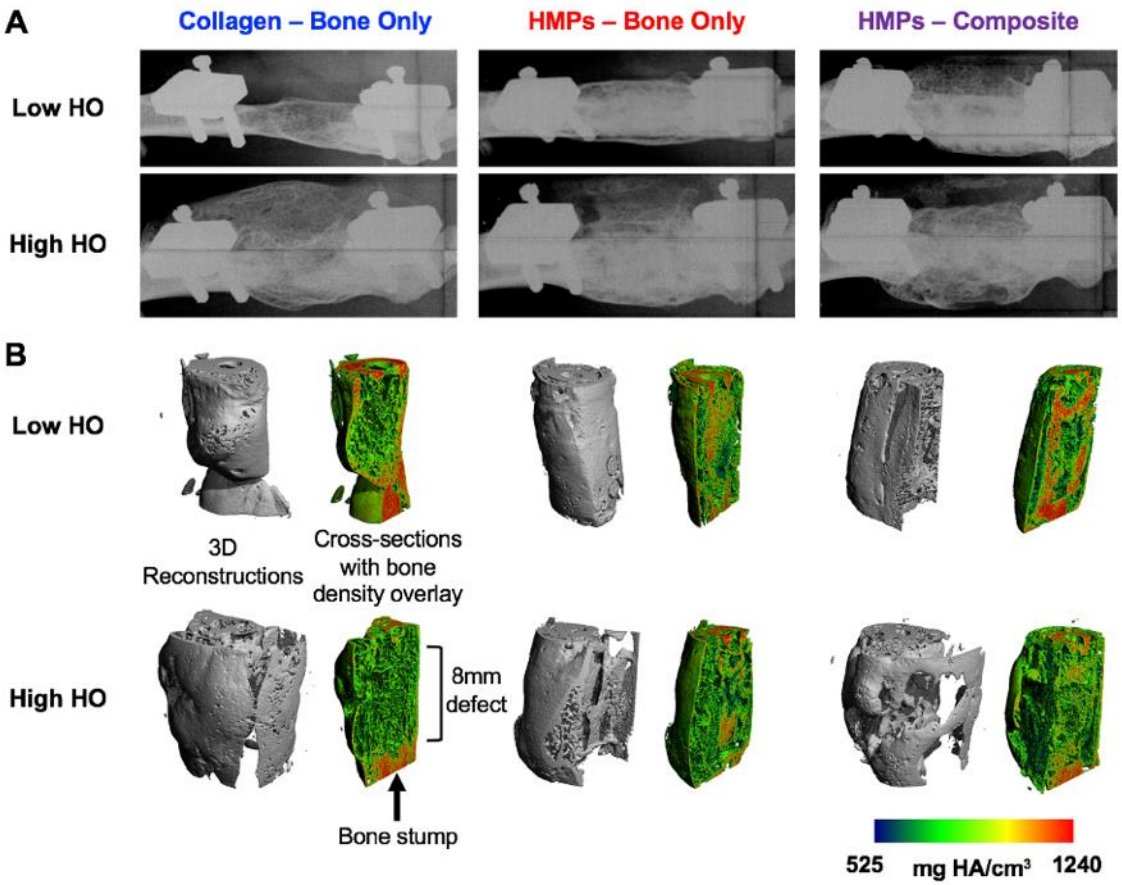

Figure 5.3. Endpoint radiographs and uCT reconstructions of regenerating bone defects. A) Week 12 endpoint (20 weeks post-injury) representative radiograph images of both low heterotopic ossification (HO) and high HO for each group are shown. B) uCT reconstructions with both the 3D reconstruction and the cross section with the bone density overlay are shown.

Quantitation of uCT reconstructions additionally supports radiographic observations. The HMP delivery strategy resulted in significantly increased new total bone volume at both 4 and 8 weeks post-treatment in both nonunion models (Figure 5.4B). Looking more specifically at bone formed within the defect site, there were clear differences between the BMP-2 delivery strategies. Similar to total bone volume, the HMP groups had significantly increased defect bone volume at both 4- and 8-weeks post-treatment (Figure 5.4C). Although there were no significant differences in heterotopic bone

volume, at 12 weeks post-treatment, the HMP groups exhibited decreased variability of HO at week 8 (Brown-Forsythe test, p=0.07) and at week 12 (Brown-Forsythe test, p=0.09) and a lower level of peak HO at week 12 compared to the collagen sponge group (Figure 5.4D). The percentage of heterotopic bone observed in each group also shows lower peak HO in the HMP groups compared to the collagen group. Further, at week 12, 40% of the collagen group exhibited higher HO compared to any sample in either of the HMP groups, and 70% of the collagen group exhibited higher HO than the average HO in both of the HMP groups (Figure 5.4E). Because irregular bone formation can be an adverse side effect of BMP-2 administration, we also investigated the trabecular number, trabecular thickness, and connectivity of the newly formed bone. Here, the HMP group for the bone only nonunion model had significantly increased trabecular number at all weeks post-treatment compared to the collagen sponge group (Figure 5.4F). Both HMP groups exhibited significantly increased trabecular thickness and connectivity at weeks 8 and 12 post-treatment compared to the collagen sponge group (Figure 5.4G,H). There were no significant differences in the polar moment of inertia between groups (Figure 5.4I).

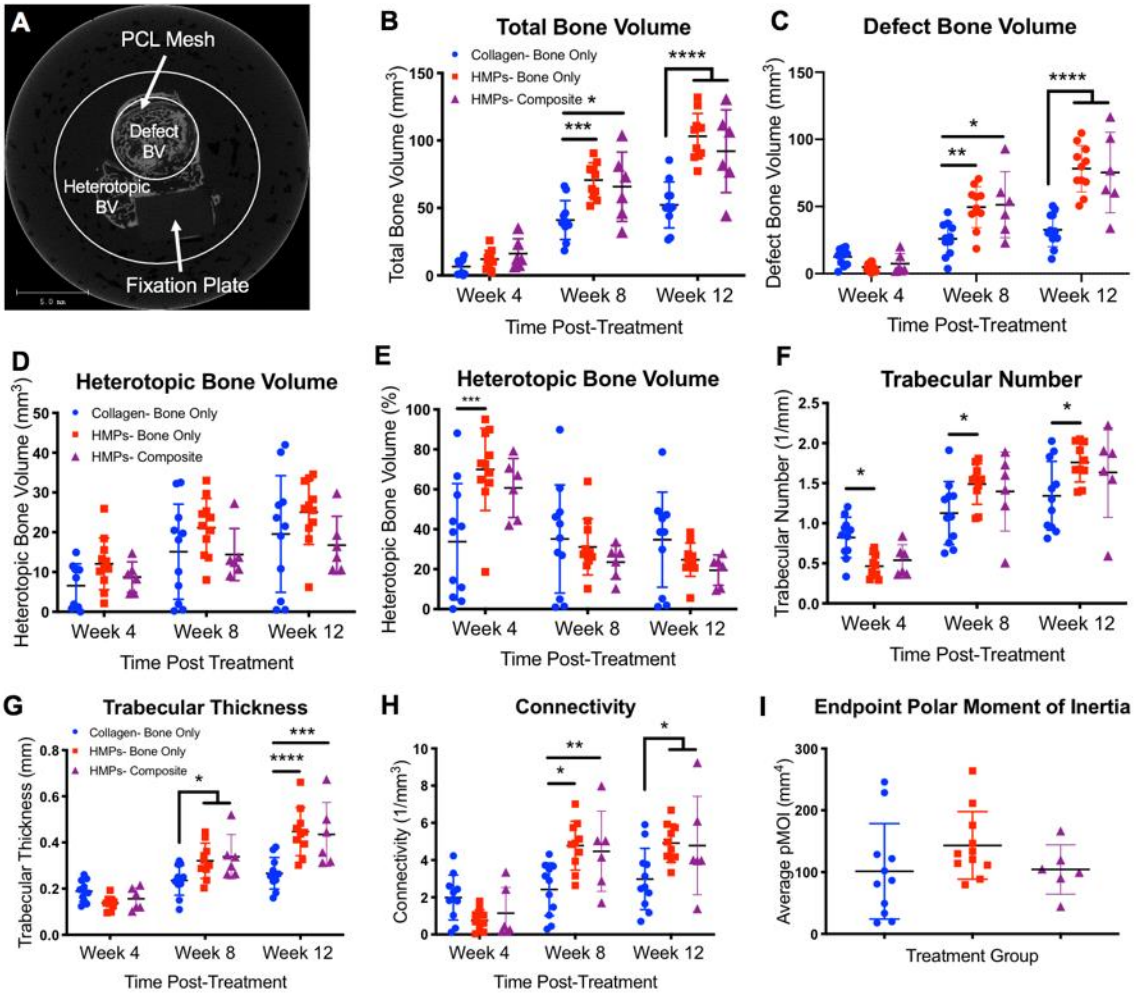

Figure 5.4. Longitudinal evaluation of bone regeneration and morphological bone characteristics.

A) A representative image of one slice taken from uCT imaging shows the defect bone volume region and the heterotopic bone volume region. In addition, the shadow of the fixation plate can be seen, and the PCL mesh can be seen just inside the defect bone volume region. Total bone volume includes both defect bone volume and heterotopic bone volume. Longitudinal quantification of total bone volume (B), defect bone volume (C), absolute heterotopic bone volume (D), and percent of heterotopic bone (E) reveals differences in bone regeneration over time between the collagen and HMP groups. Morphological bone characteristics, including trabecular number (F), trabecular thickness (G), and connectivity (H), were also evaluated and reveal differences in bone structure over time between the collagen and HMP groups. There were no differences in the polar moment of inertia between groups (I). Significance was determined using two-way ANOVA with Sidak's multiple comparisons test where $p<0.05$ (*), $p<0.01$ (**), $p<0.005$ (***), and $p<0.001$ (****).

5.3.3 Biomechanical Testing and Histological Analysis

Endpoint evaluations of bone regeneration included both biomechanical testing and histological analysis. There were no significant differences between groups in the torque to failure; however, all groups exhibited lower failure strengths compared to intact bone (Figure 5.5A). Further, there were no differences in torsional stiffness between groups, and all were slightly higher than the stiffness of intact bone (Figure 5.5B). Prior finite element modeling at sub-failure rotation demonstrates that the largest strains are present in the outermost connected regions and there is minimal strain along the central access (268). Therefore, the central bone actually contributes relatively little to the mechanical properties measured by torsion testing.

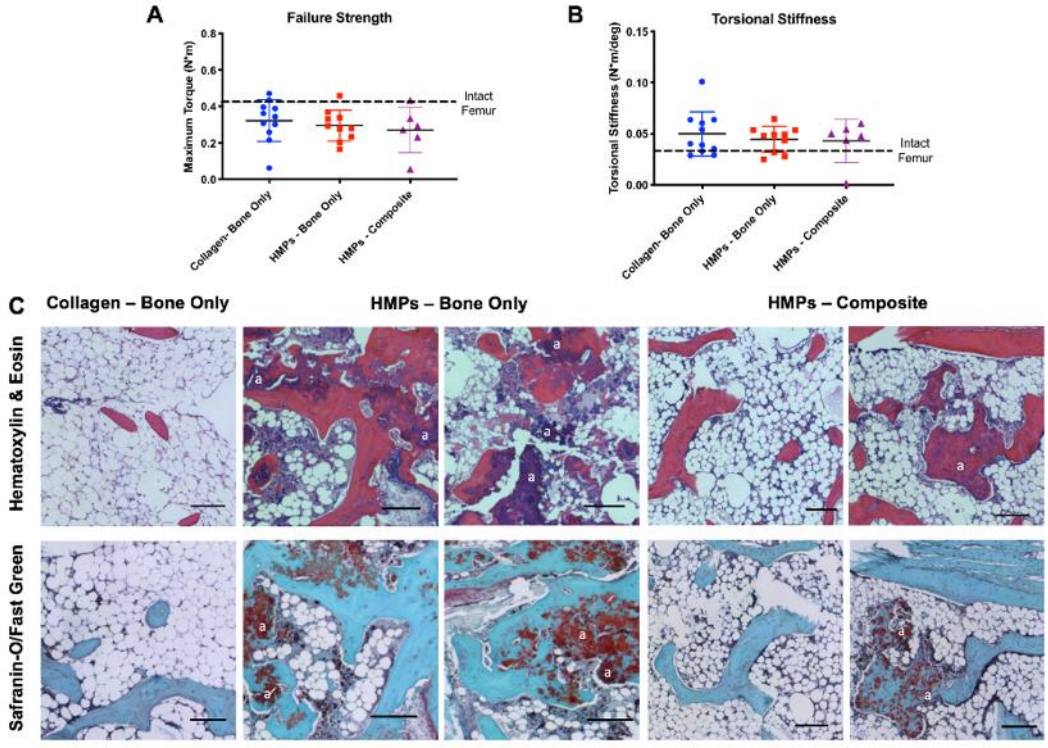

Figure 5.5. Biomechanical testing and histological analysis.

Mechanical testing of A) failure strength and B) torsional stiffness shows no difference between groups. The dotted black line indicates the average failure strength and torsional stiffness of the contralateral intact femurs, respectively. C) Staining with Hematoxylin & Eosin and Safranin-O/Fast Green at the 12 week endpoint (20 weeks post-injury) shows mineralized tissue in the HMP groups and non-mineralized, marrow-like tissue in the collagen group. Residual alginate can also be seen in the HMP groups and examples are marked with an "a". Scale – 150um.

Qualitative histological analysis of bone regeneration (Figure 5.5C) supports both the radiographs and the quantitative uCT data. Hematoxylin & Eosin and Safranin-O/Fast Green staining both reveal larger sections of mineralized tissue in the HMP groups. In the collagen sponge group, there are larger areas of non-mineralized, marrow-like tissue compared to the HMP groups; although, the composite nonunion HMP-treated group did have larger areas of marrow-like tissue compared to the bone only nonunion HMP-treated group. Residual alginate can also be seen in the HMP groups, indicating that the tissue engineered construct remained within the defect site. More fatty infiltrate into the marrow cavity can be seen within the composite defect group compared to the segmental defect only groups.

5.3.4 Systemic Immune Characterization

Blood was collected at the baseline (prior to injury) and at various timepoints following injury and treatment in order to assess the systemic immune response. While there were changes in circulating immune cell populations over time, there were no differences in immune cell populations between treatment groups at any time point (Figure 5.6). Additionally, there were no differences in cytokine levels across treatment groups at any time point (Figure 5.7).

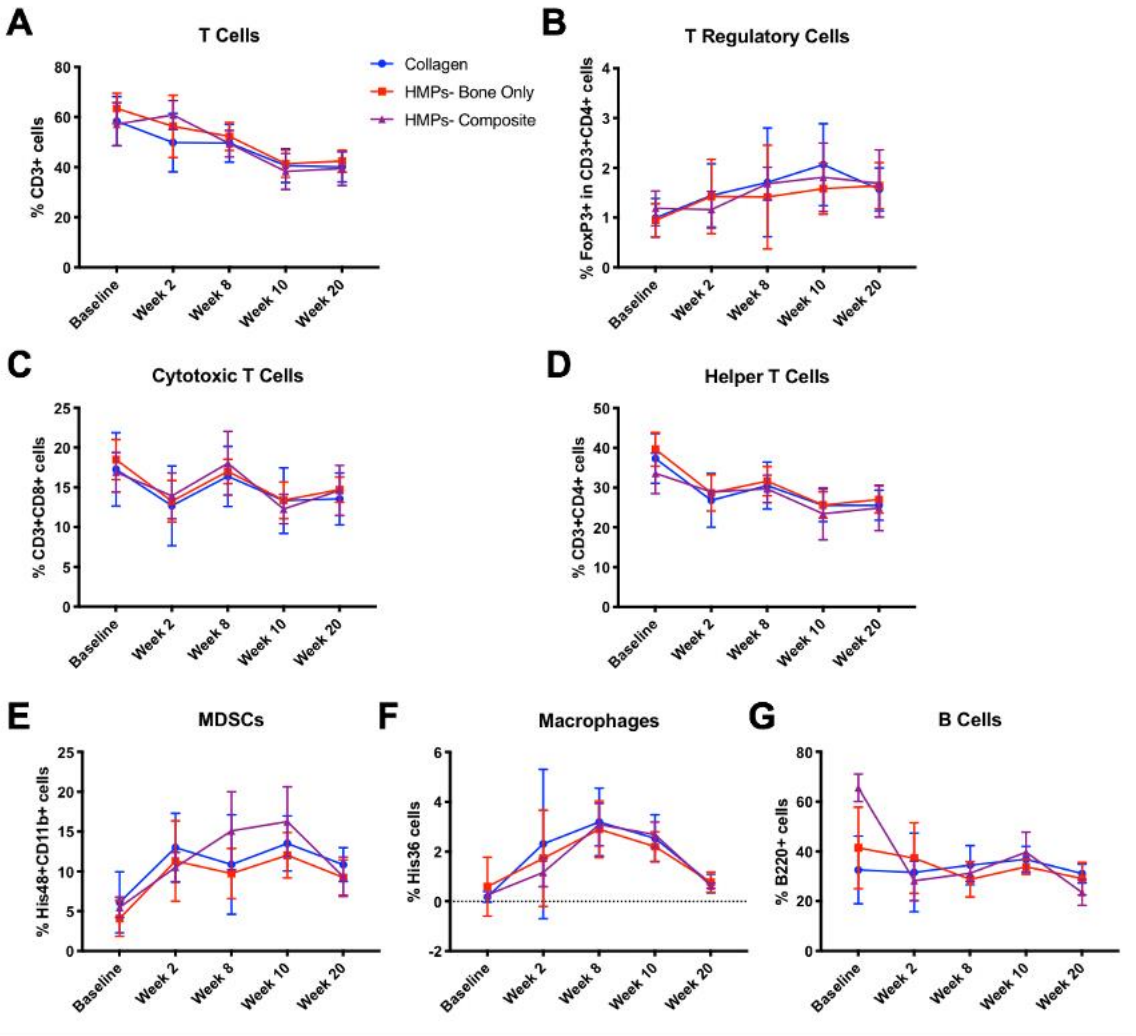

Figure 5.6. Longitudinal evaluation of circulating immune cell populations.
No significant differences between groups were observed at any time point for A) T cells and T cell subsets, including B) T regulatory cells (Tregs), C) cytotoxic T cells, and D) helper T cells. Additionally, no differences in cell populations levels were observed for E) myeloid-derived suppressor cells (MDSCS), F) macrophages, and G) B cells.

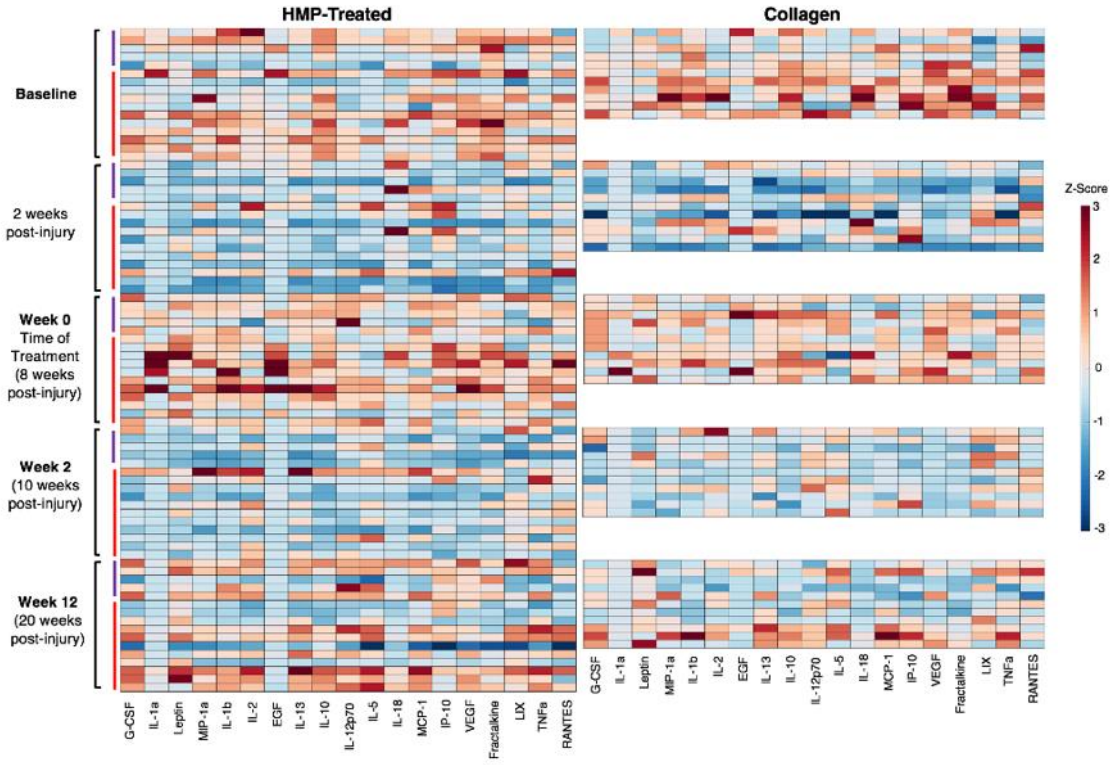

Figure 5.7. Longitudinal evaluation of circulating cytokine levels.
Heat map of z-scored cytokine levels (each column represents a different cytokine) in the HMP-treated and collagen treated groups prior to injury (Baseline) and at 2 weeks post-treatment, Week 0 (time of treatment, 8 weeks post-injury), Week 2 (10 weeks post-injury), and Week 12 (20 weeks post-injury). Purple and red vertical bars represent the HMP-treated composite injury group (n = 5) and the HMP-treated bone only injury group (n = 11), respectively.

We hypothesized that the lack of differences for markers of the systemic immune response between the HMP-treated and collagen sponge groups could be due to the wide variability of responses in the collagen sponge group. Therefore, to better understand the relationship between the systemic immune response and healing, linear regression of immune cell populations at the Week 12 endpoint for all samples together was performed against defect bone volume (as a percent of the total bone volume). Defect bone volume was selected as a metric for good healing because it encompassed animals with high defect bone volume in addition to low heterotopic bone formation. Linear regression of week 12

MDSCs versus defect bone volume percent showed a significant negative correlation (Figure 5.8A, $r^2 = 0.24$, $p = 0.012$), whereas linear regression of week 12 CD3+ T cells and week 12 effector T cells (CD3+CD4+ cells and CD3+CD8+ cells) versus defect bone volume percent both showed positive correlations (Figure 5.8B and Figure 5.8C). In an effort to better understand the best and worst responders, we compared the top and bottom quartiles of defect bone volume data and compared differences in immune cell populations. The top quartile of responders (best responders) consisted of 4 out of 7 from the HMP-treated groups, and the bottom quartile of responders (worst responders) consisted of 6 out of 7 from the collage sponge group. Comparisons between the best and worst responders revealed more pronounced differences in immune cell populations with the top quartile of responders exhibiting lower numbers of MDSCs ($p = 0.011$, Figure 5.8D), higher numbers of CD3+ cells ($p = 0.13$, Figure 5.8E), and higher numbers of effector T cells ($p = 0.098$, Figure 5.8F) compared with the bottom quartile of responders.

These analyses highlight that the complexities of the immune response, especially for average responders, which may mask differences between individual cells and cytokines. Hence, multivariate partial least squares discriminant analysis (PLS-DA) was performed to better determine further differences in the overall systemic immune response between groups. Immune cell and cytokine levels at all timepoints were compiled for PLS-DA. Results show no separation of data between the HMP and collagen sponge groups based on the latent variable 1 (LV1) axis (Figure 5.9A). However, there is separation along the latent variable 2 (LV2) axis with the HMP groups having significantly lower LV2 scores compared to the collagen sponge group (Figure 5.9B). The LV2 loading plot reveals the immune factors that most contribute to the higher and lower LV2 scores, showing

which cells and cytokines are most correlated with the collagen sponge treated group versus the HMP treated groups (Figure 5.9C). The top factors most associated with the HMP groups were T cells, including the helper (CD4+) and cytotoxic (CD8+) T cell subsets, and the hormone leptin. On the other hand, the top factors most associated with the collagen sponge group include the immunosuppressive MDSCs and Tregs as well as the chemotactic factors LIX and RANTES, also known as CXCL5 and CCL5, respectively.

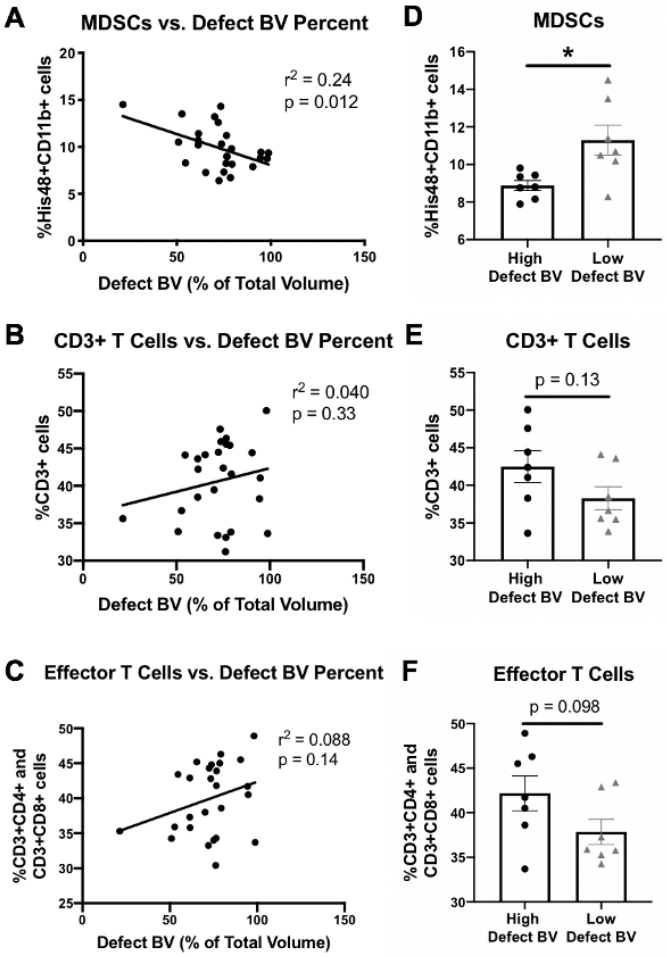

Figure 5.8. Linear regression analyses comparing systemic immune cell populations with defect bone volume percent.
Linear regressions comparing defect bone volume as a percent of total bone volume versus week 12 (endpoint) circulating immune cell populations for A) MDSCs, B) CD3+ T cells, and C) effector T cells which includes both helper (CD3+CD4+) and cytotoxic (CD3+CD8+) T cells with r^2 and p values as indicated. Removal of the middle 50% of the

data set according to defect bone volume percent left 25% of the lowest defect bone volume percent samples and 25% of the highest defect bone volume percent samples. The high defect bone volume percent samples and the low defect bone volume percent samples were then compared for their levels of D) MDSCs, E) CD3+ T cells, and F) effector T cells. Mann-Whitney or Student's t-test were performed with p values as indicated or a * (p = 0.011).

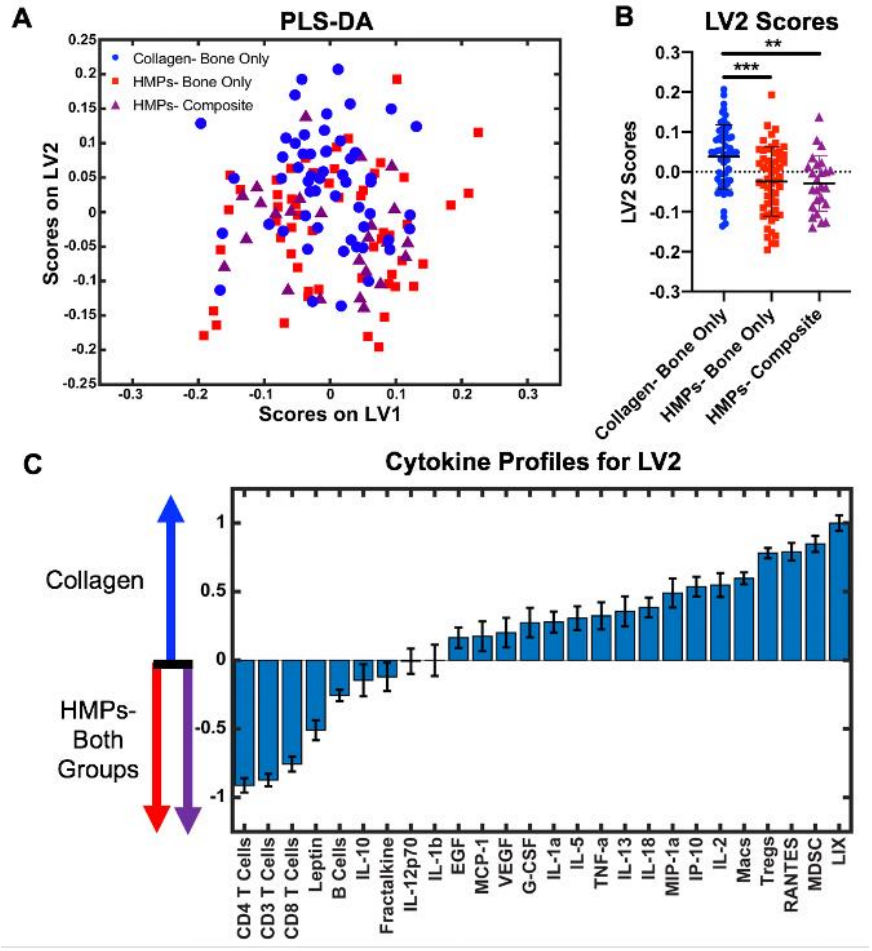

Figure 5.9. Multivariate analysis of the systemic immune response.
A) PLS-DA plot shows all cytokine levels and cell populations for the collagen treated group (blue circles), the HMP treated bone only nonunion model (red squares), and the HMP treated composite defect nonunion model (purple triangles) plotted on the latent variable 1 (LV1) axis and the latent variable 2 (LV2) axis. Cytokine levels and cell populations were pooled across all time points. Significance was determined using one-way ANOVA with Tukey's post hoc test where $p<0.01$(**) and $p<0.005$(***). B) Plotting only LV2 scores reveals a significant separation between the collagen group and the HMP groups. C) The LV2 loading plot shows the top factors most correlated with positive LV2 scores on the right (collagen group) and the top factors most correlated with negative LV2 scores on the left (HMP groups). There was no significant separation between the two HMP treated groups.

5.4 Discussion

Despite advances in trauma care management, orthopedic surgeons still need better strategies to improve outcomes for patients with chronic nonunions, especially for more challenging cases with concomitant volumetric muscle loss. While there are many factors that influence nonunions and bone healing, one promising strategy has focused on the delivery of BMP-2 in an absorbable collagen sponge. However, if not contained to the injury site, BMP-2 has been shown to have adverse side effects, highlighting the need for improved delivery vehicles that can maintain BMP-2 bioavailability and minimize side effects. Previously, our lab evaluated an HMP hybrid delivery system in an acutely treated segmental defect model, which resulted in increased long-term retention of BMP-2 at the defect site and decreased heterotopic bone formation (287–289). The current study evaluates delivery of a moderately high dose (30ug) of BMP-2 from this same HMP delivery system in two more complex and challenging chronic nonunion models, and additionally, this study attempts to preliminarily evaluate the systemic immunological changes associated with each delivery system.

Evaluation of circulating immune cell populations show changes in the immune response over time prior to treatment of the defect when compared to pre-injury baseline levels, with significant decreases in T cells and increases in immunosuppressive MDSCs and macrophages (Figure 5.2). These changes are characteristics of systemic immune dysregulation observed clinically in trauma patients and have been associated with increased susceptibility to infection and decreased treatment success (6,8,247,293). Following severe trauma, damaged tissue and high levels of inflammation lead to a systemic inflammatory response, marked by increases in pro-inflammatory mediators and

activation of innate immune cells (10,116,245). To prevent against harmful levels of systemic inflammation, a compensatory anti-inflammatory immune response develops to counteract the initial inflammation and restore immune homeostasis, marked by increases in anti-inflammatory cytokines and increases in immunosuppressive cells, such as MDSCs and Tregs (288,289). However, in some patients, especially those with complications and more challenging injuries, the compensatory anti-inflammatory response overcompensates for the initial inflammation and immune homeostasis is not restored, resulting in systemic immune dysregulation and immunosuppression (5). Systemic immune dysregulation has been associated with decreased success of treatment; and therefore, effective treatment strategies may need to be able to overcome any adverse immunological changes that could hinder successful healing. Our chronic nonunion model exhibits characteristics of systemic immune dysregulation and could therefore allow for new regenerative strategies to be evaluated in a more clinically-relevant model by more accurately representing the immune environment at the time of treatment. This more recent interest in the systemic immune response differs from historical data that has typically associated local immune responses with interventional outcomes. However, systemic immune markers may offer more promise than local immune data because systemic immune markers can be used clinically to identify patients at-risk for poor healing. This information would be easy to obtain non-invasively and longitudinally in a clinical setting through routine blood draws. In comparison, local immune data is not easy to obtain in a clinical setting. For these reasons, we chose to more heavily investigate the systemic immune response in this study. Further work will aim to evaluate not just the population levels of circulating immune cells, but also their function. Additionally, while our model did not include a naïve group to confirm

that the immunological changes observed are not simply due to aging, the 8-week delayed treatment time period is still well within what is considered a young adult rat (294). Typically, immunoaging and immunosenescence begin past adulthood, so there should not be significant immunological changes occurring in our model due to aging over the time course of this study (295,296).

We observed differences in bone regeneration between the two delivery vehicles for high-doses of BMP-2, with the HMP delivery system resulting in more consistent and robust bone regeneration compared to the collagen sponge delivery vehicle, even despite the additional challenges historically associated with chronic nonunions and concomitant muscle injury. The most significant challenge BMP-2 usage faces clinically is the adverse side effects, including excessive inflammation, heterotopic ossification and irregular bone formation, which can lead to pain and less desirable patient outcomes (275–278). The HMP delivery system showed increased bone formation within the defect, lower peak heterotopic ossification, lower percentage of heterotopic bone, and more regular bone formation compared to the collagen sponge delivery group. Decreased side effects can be attributed to increased bioavailability and retention of the BMP-2 at the injury site. Bone formation can be attributed to the system's ability to appropriately retain and slowly release BMP-2, even though the biomaterials themselves likely have minimal impact on bone formation. The nanofiber mesh and alginate hydrogel alone have been shown to result in minimal bone formation in previous studies (178,268). In addition, we have also previously investigated delivery of BMP-2 in the alginate/mesh system alone or on HMPs within the alginate/mesh system and have seen significant differences in bone formation, highlighting the specific role of HMPs on bone formation (297). BMP-2 alone would not be expected to enhance

bone formation because BMP-2 would diffuse out of the defect region rapidly, resulting in more heterotopic bone formation and negative systemic side effects. Although the biomaterial itself may have minimal direct impact on bone formation, it enables specific spatiotemporal delivery of BMP-2 that directly results in the bone formation patterns observed.

Heparin is one of the key components to the hybrid delivery system and is a glycosaminoglycan (GAG). GAGs are molecules that make up components of the extracellular matrix (ECM) and are naturally involved in binding and sequestering growth factors in the cellular microenvironment (298,299). The strong negative charge allows for a high affinity and reversible electrostatic interaction with BMP-2 which increases retention within the alginate gel and at the injury site, stimulating progenitor cells and endogenous repair mechanisms (287,300,301). Although heparin is a known anti-coagulant and has been shown to inhibit angiogenesis (302), delivery of a potent angiogenic factor (BMP-2) likely outweighs any potential effects of heparin on angiogenesis, which is essential during the bone regeneration process. In vitro evaluation of BMP-2 release from HMPs showed sustained release over a 4 week period, with low burst release (<10% in the first 6 hours). The cumulative percentage of BMP-2 released over the 4 week period was independent of loading mass and was <20% of the loaded BMP-2, demonstrating the capability of the HMPs to retain BMP-2. The presence of the alginate tissue engineered construct can be observed in histological stain 12 weeks after treatment within the defect site, although it is unknown how much BMP-2 remains in the construct. The uncontrolled burst release of BMP-2 from the collagen sponge delivery system decreases bioavailability (274), leading to decreased bone formation within the defect and increased side effects,

including higher percentage of heterotopic ossification, higher peak HO and irregular bone formation. Additionally, the inconsistent and uncontrolled release of BMP-2 from collagen sponge leads to similarly inconsistent bone healing results with wide variability in response to treatment, which is undesirable for clinical applications. Differences in bone formation can also be observed in the histology images with increased bone formation in the HMP groups. Interestingly, there is more lipid and fatty infiltration in the composite defect group, which has been observed previously in skeletal muscle trauma especially for larger volumetric defects (303). Bone marrow adipose tissue has previously been shown to decrease bone regeneration (304), which could be a contributing mechanistic factor to differences in bone regeneration in the composite group versus the bone only group. Despite clear differences between the two delivery groups from radiographs, uCT, and histology, there were no significant differences in the biomechanics of the newly formed bone between the two groups. However, the method of mechanical testing evaluates the strength and stiffness is biased towards the outermost regions of bone, not defect bone formation, meaning the higher percentages of heterotopic ossification observed in the collagen sponge delivery group likely inflated the observed mechanical properties. This lack of difference in mechanical properties aligns with the uCT polar moment of inertia data (Figure 5.4I) which shows no significant differences in the spatial extent of bone formation. However, despite the lack of biomechanical differences, the HMP delivery system still had improved spatial localization of bone regeneration compared to the collagen sponge for two challenging cases of nonunion with adverse systemic immune environments.

Along with optimizing spatiotemporal BMP-2 delivery with appropriate scaffolds, the immunological host response to severe injury presents additional challenges for successful treatment. Although there were no differences between the groups for individual cell populations or cytokines by routine univariate comparisons between groups, this may be due to the complexities of the immune system and extensive interactions between immune mediators (305). The pleiotropic and redundant interactions between various cytokines and cells make it difficult to identify clear differences between immune responses without the help of multivariate analyses that can minimize effects of confounding factors and reduce noise. Following multivariate analyses, the cell populations most associated with the collagen sponge group include the immunosuppressive MDSC and Treg populations. Notably, these are the cell populations that most contribute to systemic immune dysregulation, with MDSCs increased prior to treatment. The continued association with these cell types suggests that the collagen sponge group may not have been successful at overcoming the additional challenge associated with immune dysregulation. On the other hand, the cell types most associated with the HMP groups include all CD3+ T cells, including the CD4+ helper and CD8+ cytotoxic T cell subsets. Increased numbers and function of immune effector cells are essential for restoration of immune homeostasis and re-establishment of a pro-healing and pro-regenerative immune environment, suggesting that the HMP groups were more successful at addressing the systemic immune dysregulation present at the time of treatment based on multivariate discriminant analyses. The cytokines most associated with the collagen sponge group included LIX and RANTES, also known as CXCL5 and CCL5. LIX is released from inflammatory and endothelial cells and is known for its chemotactic and

activation properties, functioning during both acute and chronic inflammatory responses (306). Similarly, RANTES is also a chemotactic and pro-inflammatory cytokine with a wide variety of functions (307). Preliminary studies have also shown that RANTES may modulate the activity of MDSCs from the bone marrow and suppress cytotoxic T cell function (308). While chemotactic and pro-inflammatory cytokines may seem contrasting to elevated levels of immunosuppressive cells, heterotopic ossification and BMP-2 are known to result in increased inflammation (179,267). Chronic local inflammation may result in increased levels of pro-inflammatory cytokines while elevated levels of anti-inflammatory cells maintain a systemic immunosuppressive environment that together adversely alter bone healing progression. This is further supported by work in the same bone nonunion model that shows elevated levels of inflammatory cytokines in non-healing rats versus healing rats (265).

In a related composite trauma model receiving acute treatment, a similar pattern was observed where serum levels of both pro- and anti- inflammatory cytokines were elevated in the groups that received 2.5ug BMP-2 and had lower endpoint bone volumes compared to the groups that received 10ug of BMP-2 and had higher endpoint bone volumes (Figure 5.10). The 2.5ug dose group's failure to completely heal may have prolonged the inflammatory stage of the wound healing process and the persistent local inflammation may then have resulted in altered systemic immune cytokine profiles. In contrast, rather than a high BMP dose inducing inflammation, the successful bridging and restoration of

function may have resolved the local inflammation and led to lower cytokine levels by the 12-week endpoint.[5]

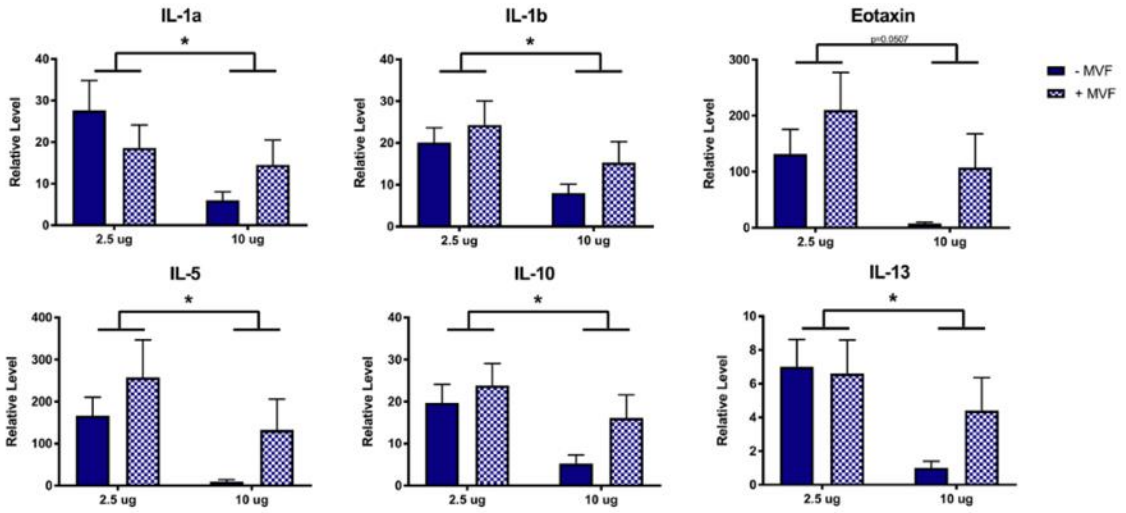

Figure 5.10. Relative serum levels of pro- and anti-inflammatory cytokines by treatment group.[5]
Pro-inflammatory cytokines on top and anti-inflammatory cytokines on bottom as measured by multiplexed analyte analysis. Groups received either 2.5ug or 10ug BMP-2 with or without microvascular fragments (MVF). Post-hoc differences are due to BMP dose, $p<0.5$(*); 2-wy ANOVA; n=5/group.

On the other hand, leptin was the cytokine most associated with the HMP groups. While leptin is largely known for its role in maintaining energy homeostasis, it has also been found to play a role in bone metabolism through a hypothalamic relay (309,310). Leptin-deficient mice exhibit decreased bone growth and bone formation rate as well as a decrease in osteoblasts (310). The association of leptin with the HMP groups could be a result of neuroendocrine function that is essential for the increased levels of bone formation observed. This is supported by work in the same bone nonunion model showing leptin to

[5] Adapted from M.A. Ruehle, L. Krishnan, C.E. Vantucci et al., Effects of BMP-2 dose and delivery of microvascular fragments on healing of bone defects with concomitant volumetric muscle loss, Journal of Orthopaedic Research, 2019. 37(3): p. 553-561. Reproduced with permission from Wiley.

be the cytokine most associated with healing rats versus non-healing rats (265). Further studies investigating the role of the systemic immune response throughout the bone regeneration process are needed to more definitively understand the relationship between systemic immune mediators and local bone healing and to understand the role of immune dysregulation in nonunion progression.

Composite tissue polytrauma injuries present additional challenges for orthopedic surgeons with high rates of complications, such as nonunions, and long-term disability. Strategies that successfully heal injuries to bone alone may not adequately compensate for the additional loss of endogenous stem and progenitor cells from damaged vascularized muscle tissue, resulting in deficient healing and tissue regeneration. For example, in a pre-clinical composite bone-muscle defect model, five times the BMP-2 dosage (10ug) is required to achieve robust bone bridging compared to a bone only defect model (2ug) (265,279). Here, we found that despite addition of a volumetric muscle loss, 30ug BMP-2 delivered in the HMP system resulted in similar levels of bone regeneration and mechanical strength between the composite defect and bone defect only chronic nonunion models. Based on this study, sustained delivery of moderately high doses of BMP-2 may be able to overcome more challenging bone healing scenarios, including chronic nonunions with concomitant muscle injury, and adverse immunological environments.

5.5 Conclusions

The results obtained in this study indicate that if appropriately delivered spatiotemporally, a high dose of BMP-2 may be able to overcome the additional challenges associated with chronic nonunions, including concomitant muscle injury and systemic

immune dysregulation. Evaluation of the HMP delivery system showed improved bone regeneration and decreased side effects compared to the collagen sponge in clinically-relevant chronic nonunion models. Utilization of BMP-2 is an attractive option to address challenging musculoskeletal injuries because it has already received FDA approval and has shown success clinically. Further work will be essential to better understand biological mechanisms of nonunions, in particular how systemic and local immunological changes affect treatment outcomes.

CHAPTER 6. FABRICATION AND CHARACTERIZATION OF BIFUNCTIONAL JANUS NANOPARTICLES FOR SELECTIVE DEPLETION OF IMMUNONOSUPPRESSIVE MDSCS[6]

6.1 Introduction

A well-regulated and coordinated immune response on both the systemic and local level are essential to successful healing and disease clearance in a wide variety of indications. Chronic immunosuppressive environments prevent proper immune surveillance, appropriate healing of damaged tissue, clearance of infection, and targeting of malignant cells or tissues. In particular, immunosuppressive cells of myeloid origin, termed myeloid-derived suppressor cells (MDSCs), have been shown to be upregulated in tuberculosis and staphylococcal infections; systemically following severe trauma, burn, or sepsis; and during cancer within the immunosuppressive tumor microenvironment. These immunological challenges make treatment more difficult and frequently result in poor treatment response, extended hospital stays, increased treatment costs, and susceptibility to opportunistic infections (7,311–316).

MDSCs have been a particular target of interest as they are a common culprit within immunosuppressive environments. In particular, MDSCs are a heterogeneous population of immature myeloid cells that expand rapidly during impaired hematopoiesis and

[6] Marked sections from this chapter are reprinted with permission from J. Liu, R. Toy*, C.E. Vantucci*, P. Pradhan*, et al. Bifunctional Janus Particles as Multivalent Synthetic Nanoparticle Antibodies (SNAbs) for Selective Depletion of Target Cells, Nano Letters, 2021. 21(1): p. 875-886. Copyright 2021 American Chemical Society. *indicates equal contributions. Marked sections indicate experiments conducted independently by C. Vantucci or in collaboration with J. Liu. Link to article

emergency myelopoeisis, and they potently suppress T cells and other immune effector functions (27,43). In addition, they also have been shown to induce immunosuppressive regulatory T cell (Treg) development, creating a feedforward mechanism to rapidly increase immunosuppression (45). MDSCs utilize various mechanisms to suppress immune function, including the production of reactive oxygen and reactive nitrogen species (ROS/RNS) and secretion of immunosuppressive cytokines and molecules, such as IL-10, TGF-b, and arginase. These mediators are known for suppressing cytotoxic T cell and Natural Killer (NK) cell function, and arginase in particular is known to deplete L-arginine, an essential amino acid required for T-cell receptor (TCR) signaling, which then hinders appropriate T cell activation (43,44).

MDSC-targeted immunotherapies have been used previously, mostly in the context of cancer. Previous therapeutics include small molecule chemotherapeutics (doxorubicin, 5-fluorouracil), inhibitors (cyclooxygenase-2 inhibitor, Silibinin), and broadly-targeted monoclonal antibodies (mAbs; anti-mouse Gr-1). Despite the promise of these therapeutics, they have been limited by high systemic toxicity, off-target effects, or have only shown success in mouse models (15,191,317–323). For mAbs specifically, there are still significant challenges that hinder their full and widespread use, including a complex and expensive production process requiring animals and cell culture, short retention time, high dosage requirements, and non-specific depletion of other immune cells due to a narrow range of available targets (16,17). Existing alternatives to mAbs, such as diabodies, minibodies, and peptibodies contain synthetic components to try and improve targeting specificity, but as a result of their smaller size, all have rapid clearance from the body (324).

Lastly, the lack of known exclusive surface antigens on MDSCs impedes the development of specific mAbs to overcome immune suppression.

Here, we describe the fabrication and characterization of synthetic nanoparticle antibodies (SNAbs), which are bifunctional Janus gold nanoparticles that mimic the structure and function of antibodies to specifically target and deplete MDSCs. Gold nanoparticles are an attractive option as a biomaterial scaffold for a synthetic antibody because they are well-studied, easy to modify, relatively inert, and can be made small enough that their size is on the same order of magnitude as antibodies (325–327). These fully synthetic and multivalent SNAbs have the advantages of a cell-free, animal-free, purely chemical synthesis method in addition to tailorable properties, such as size, valency, and surface chemistry, allowing targeting of a wide variety of cell types. These advantages allow for optimization of particles and can potentially reduce costs and improve potency through better targeting specificity compared to mAbs, ultimately providing a novel method for immunomodulation across many diseases and conditions.

6.2 Materials and Methods

6.2.1 Preparation of MDSC-Targeting SNAbs[6]

The process to generate SNAbs is divided into two parts: production of Janus streptavidin-coated Au nanoparticles (SA-AuNP-SH) and surface modification of the Janus Au nanoparticles with MDSC-targeting ligands (G3) and Fc-mimicking ligands (cp33). To generate Janus Au nanoparticles, aminomethyl ChemMatrix resins were functionalized with biotin groups by reacting with bifunctional, thiolytic cleavable crosslinkers, sulfo-NHS-S-S-biotin, in a 10 mL reaction vessel for 4 hours at 37°C with

gentle rotation. As a quality control step to verify the success of the functionalization, absorbance at 260 nm of the solution in liquid phase inside the reaction vessel, which reflects the reactivity of sulfo-NHS group, was measured and compared to that of the unreacted crosslinker solution. Subsequently, streptavidin-coated Au nanoparticles (SA-AuNP-SA) (Streptavidin-coated Au nanospheres from Nanohybrid Inc., USA), 30nm in diameter, were added to the reaction vessels and bound onto the resin beads by reacting with the biotins overnight at 37°C with gentle rotation. Then, the addition of tris(2-carboxyethyl)phosphine (TCEP) released the bound Au nanoparticles into the liquid phase again by reduction of the disulfide bonds in the crosslinkers after 24 hours at room temperature. To concentrate the collected Janus nanoparticles, solutions were centrifuged at 4500 g for 2 hours and the supernatant was discarded. To remove the remaining TCEP, the concentrated Janus nanoparticle solution were dialyzed against PBS in gamma-irradiated, MWCO 10KDa slide-A-lyzer (ThermoFisher Scientific, USA) and then stored at 4°C until use.

To modify the Janus nanoparticles, 200-fold (to the molar concentration of streptavidin) excess of the SMCC-terminated version of the desired ligands (cp33-SMCC were conjugated onto the thiol hemisphere of the nanoparticles through thiol-maleimide reaction at pH 7.4 in PBS with 0.001% Tween-20 with gentle rotating at room temperature overnight at 4°C. 50-fold excess of biotinylated G3 ligand (Genemed Synthesis Inc., San Antonio, TX, USA, see Supplementary Table 1) of the molar concentration of total streptavidin molecules on the nanoparticles were coated onto the streptavidin hemisphere through streptavidin-biotin interaction in PBS with 0.01% Tween-20 with gentle rotating at room temperature overnight at 4°C. Excess ligands were washed out by centrifugation

at 6500g for 15min. Modified nanoparticles were resuspended in PBS with 0.001% Tween-20 and stored in 4°C until use. For *in vitro* and *in vivo* assays, tween-20 was removed from the nanoparticle formulation by centrifugal washes of nanoparticles with PBS.

6.2.2 Verification of Asymmetric Surface Chemistry of the Janus Au Nanoparticles[6]

To study the surface topology of the Janus nanoparticles (SA-AuNP-SH) or non-Janus nanoparticles (SA-AuNP-SA), we tagged available biotin-binding pockets or thiol groups with 10-12 nm biotinylated quantum dots (QDs) containing cadmium (Cd) or 1.8nm maleimide-Au nanoprobes and then acquired transmission electron microscopy (TEM) images with Hitachi HT7700 TEM at 120 kV (for biotinylated QD-conjugated samples) and FEI Tecnai F30 TEM at 300 kV (for 1.8 nm maleimide-Au nanoprobe-conjugated samples). The asymmetric surface chemistry of the Janus Au nanoparticles with QDs before and after modification were further investigated using advanced TEM techniques such as scanning/transmission electron microscopy (S/TEM) bright-field imaging, high-angle annular dark-field imaging (HAADF), X-ray energy dispersive spectroscopy (EDS) mapping with a ThermoFisher Scientific Talos F200X S/TEM at 200 kV. STEM-BF images are very similar to TEM images, which can reveal light elements of the streptavidin layer showing a weak dark layer surrounding Au nanoparticles. STEM-HAADF imaging has Z-contrast (approximately proportional to Z^2) function, showing the distribution of heavy elements such as Au, Cd, Se in the imaging field, while EDS mapping helps illustrate the distribution of both the light and heavy elements in x and y directions. For sample preparation, five times excess of QDs were incubated with Janus or non-Janus Au nanoparticles under vortex for 2 hours at room temperature. After incubation, nanoparticles were washed 3 times with DI water by centrifugation at 7500 g for 15 mins. Nanoparticles

were then resuspended in DI water and loaded onto the 400-mesh ultrathin carbon film on Lacey Carbon support film TEM grids for imaging. Similarly, five hundred times excess of maleimide Au nanoprobes were incubated with Janus nanoparticles and washed with DI water. The samples were then loaded onto the 200-mesh formvar carbon-coated copper grids for imaging.

6.2.3 Quantification of Modification Level Using Fluorophores[6]

Differing amounts of excess of sulfo-maleimide Cy5 or biotin Cy5, or SMCC cp33 Cy5 or biotin G3 Cy5, were reacted with Janus nanoparticles (0.2 nM-0.4 nM) on vortex for 2 hours at room temperature. After reaction, nanoparticles were washed 3 times with DI water by centrifugation at 7500 g for 15 min. According to the previous report (328), the amount of fluorophores immobilized on each Janus nanoparticle was quantified with a slight modification. Briefly, the concentration of Janus nanoparticles was first quantified by measuring the absorbance at 522-525 nm. Janus nanoparticles were then incubated at room temperature with 50 mM potassium cyanide (KCN) solution until the reddish solution became transparent to confirm the complete dissolution of gold nanoparticles (30 min). The fluorescence intensity of the sample solution was measured with a SynergyHT Biotek plate-reader with a filter set of 590/20 (excitation), 645/40 (emission). A standard curve was obtained by measuring the fluorescence intensity of free Cy5 ranging from 0.5 to 20 nM. The average number of fluorophores per Janus gold nanoparticle was calculated by dividing the concentration of the fluorophore by the concentration of the Janus nanoparticles. For the 30 minute incubation period, KCN was shown to induce ~20% quenching of the Cy5 signal, and this signal reduction was accounted for when quantifying peptide modification.

6.2.4 Generation of Rat Infection Trauma Model[6]

Unilateral 2.5mm femoral segmental defects were created in 21-week old female Sprague-Dawley rats as previously described. Briefly, an anterolateral incision was made along the length of the femur and the vastus lateralis was split with blunt dissection. A modular fixation plate was affixed to the femur using miniature screws (JI Morris Co., Southbridge, MA, USA). The 2.5mm segmental defect was then created in the diaphysis using a Gigli wire saw (RISystem, Davos, Switzerland). A collagen sponge with bacteria inoculum (*S. aureus* at 10^7 CFU) was placed in the defect (Figure 6.1. Rat bone trauma model for MDSC isolation.Figure 6.1). The fascia was then sutured closed with absorbable 4-0 sutures, and the skin was closed with wound clips. Buprenorphine SR (0.03 mg/kg; 1 ml/kg) was used as an analgesic and applied via subcutaneous injection.

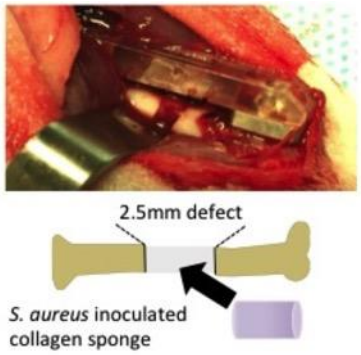

Figure 6.1. Rat bone trauma model for MDSC isolation.
Unilateral 2.5mm femoral segmental defects were created in 21-week old female Sprague-Dawley rats. A collagen sponge with bacteria inoculum (S. aureus at 10^7 CFU) was placed in the defect to induce infection.

6.2.5 Isolation of Rat MDSCs and Rat Macrophages

For Rat MDSCS, PBMCs were isolated from the infected trauma rats following arterial blood collection, and myeloid-derived suppressor cells (MDSCs) were sorted via

magnetic-activated cell sorting (MACS) using biotin-conjugated mouse anti-rat His48 antibody. FACS analysis confirmed that 88.7% of the cells in the post-sort MDSC enhanced fraction was $His48^{+}CD11b^{+}$ MDSCs (Figure 6.2).

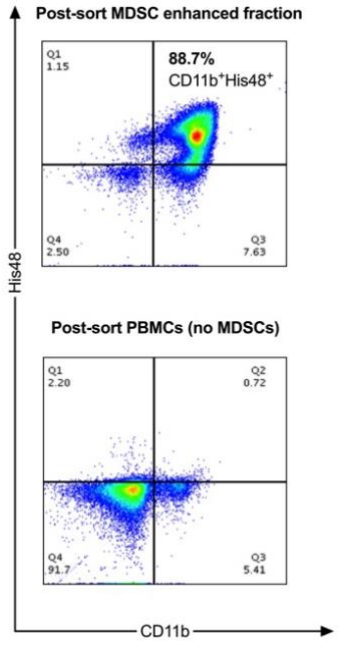

Figure 6.2. MDSC isolation from PBMCs of rat trauma model.
MDSC were sorted via magnetic-activated cell sorting (MACS) using biotin mouse anti-rat His48 antibody from blood of the rats. The purity of $CD11b^{+}His48^{+}$ cells was 88.7% in the post-sort MDSC enhanced fraction.

For rat macrophages, bone marrow-derived cells were isolated from the femur of naïve rats and cultured with 20ng/mL of recombinant rat M-CSF for 7 days. After 7 days, cells were collected from culture and immediately used for experiments.

6.2.6 Photoacoustic Imaging of Peptide-Modified Particles Binding on Cells[6]

The isolated MDSCs or macrophages from rat were conditioned to 4 °C to prevent endocytosis of particles. Cells were then incubated with nanoparticles at a ratio of 5×10^{10}/million cells or 2×10^{11}/million cells in 1mL of PBS for 1 hr at 4 °C. After

incubation, cells were washed three times with PBS by centrifugation at 500 g for 5 mins and then fixed with BD fixation buffer. The cell-nanoparticle samples were resuspended into 20 μL per 0.5 million cells in PBS and kept at 4 °C until use.

The tissue-mimicking gelatin phantom was prepared for US/PA imaging. The phantom base layer was composed of 8% gelatin and 0.2% silica. The solution was heated to around 50 °C under stirring to dissolve the gelatin. Next, the solution was degassed to remove bubbles, poured into a container and solidified at 4 °C to form the base layer. Each cell-NP sample was mixed with an equal volume of 16% gelatin solution (heated and degassed) to prepare the cell inclusions. Once the base layer was solidified, the cell solution was pipetted onto the surface to form the cell-containing dome-shaped inclusions. The phantom was refrigerated again at 4 °C fridge to set the dome inclusions. After roughly 30 minutes, the phantom container was filled with ultrapure water.

The inclusions were imaged using the Vevo LAZR (Fujifilm VisualSonics Inc, Toronto, Canada) combined ultrasound and photoacoustic (US/PA) imaging system. US/PA images were acquired at a frame rate of 5 Hz with an OPO, Q-switched Nd:YAG pumped laser (λ = 532 nm or 680 - 970 nm) with a 20 MHz US/PA linear array transducer (LZ250). Three cross-sections of each sample were randomly acquired. The data was exported and post-processed in MATLAB (Natick, MA).(329) The average PA signal was calculated for the single wavelength datasets acquired at 532 nm wavelength. PA signals from the inclusions were normalized to the PA background signal, i.e. a region containing no cells, to adjust for uncontrollable system differences between imaging frames. PA signals from the inclusions were also normalized to the corresponding average ultrasound signal. Ultrasound normalization was used to adjust for small variations in cell

concentration. However, note that normalization had little impact on the imaging results, indicating similar imaging conditions and inclusion preparation were maintained, as expected.

6.2.7 Rat MDSC-Macrophage Co-Culture Assay[6]

Infection trauma-derived MDSCs and bone marrow-derived macrophages were co-cultured at a 1:10 ratio and incubated for 24 hours with or without treatment of nanoparticles. Treatment groups included Janus nanoparticles functionalized with G3 and cp33 (G3-SNAbs or SNAbs), non-Janus SA-AuNP-SA (AuNP), and no treatment. Following treatment, cells were stained with FITC-anti-rat His48 and PE-anti-rat CD11b antibodies and analyzed for the percentage of MDSCs ($His48^+CD11b^+$ cells) remaining using a BD Accuri C6 flow cytometer. Data was analyzed using FlowJo based on fluorescent minus one (FMO) controls with <1% noise allowed.

6.2.8 PBMC Killing of MDSCs Triggered by SNAbs[6]

RBC-lysed PBMC suspensions were seeded into 96 well plates at 1×10^6 cells/well in 200 μL of RPMI 1640 complete medium. Equal amount ($2\text{-}5\times10^{11}$/mL) of SNAbs or buffer in 50 μL sterile PBS was added into the corresponding wells respectively. After 20 hours of incubation at 37°C, cells were harvested, washed and stained with antibodies for MDSCs (CD11b+His48+), macrophages (CD11b+CD68+), T cells and subsets (CD3+, CD3+CD4+, CD3+CD8+), and B cells (B220+). FMO (fluorescence-minus-one) control samples were prepared with corresponding staining reagents. Samples were analyzed on a BD Accuri C6 flow cytometer.

6.2.9 Isolation of MDSCs from the Spleens of Tumor-Bearing Mice[6]

Balb/c mice were inoculated with 0.5×10^6 4T1 breast cancer cells on day 0. Spleens were harvested after 16-18 days from the tumor-bearing animals, minced into thin pieces, and dissociated in collagenase (2 mg/mL) in OptiMEM for 30-60 mins at room temperature. Dissociated spleen tissue was passed through a 40 μm nylon cell strainer to obtain a single cell suspension. Red blood cells in the single cell suspension were lysed in 1X RBC lysis buffer. After removing the lysed RBCs by centrifugation, the splenocytes were resuspended in RPMI 1640 complete medium and directly used for scRNAseq experiments.

6.2.10 Single Cell RNA Sequencing (scRNAseq) of In Vitro *MDSC Depletion Assay*

Rat MDSCs and rat macrophages were isolated following the same procedures for the rat MDSC-macrophage co-culture assay. Mouse MDSCs were isolated from the spleens of tumor-bearing mice according to the procedures above. Mouse macrophages were isolated from bone marrow by culturing bone-marrow derived cells with 20ng/mL of recombinant murine M-CSF for 7 days. Rat MDSCs and macrophages were then co-cultured at a 1:10 ratio and incubated for 24 hours with or without treatment of SNAbs. Mouse MDSCs and macrophages were similarly co-cultured at a 1:10 ratio and incubated for 24 hours with or without treatment of SNAbs. Following 24 hours, cells from both the mouse and rat assays were collected and enhanced for MDSCs with MACS sorting with anti-Gr-1 for mice and anti-His48 for rats. The four samples collected included cells enhanced for rat MDSCs with and without 24 hour SNAb treatment and cells enhanced for mouse MDSCs with and without 24 hour SNAb treatment. These samples were then used

for single cell RNA sequencing (scRNAseq). First cells were processed by diluting the samples in PBS+0.1% BSA and filtering through a cell strainer. Cells were then counted to check cell number and viability to achieve the target 5000 barcoded cells. scRNAseq was performed using 10X Genomics Single Cell 3' Solution, version 3.1, according to the manufacturer's instructions (protocol rev C). Libraries were sequenced on Nextseq500 (Illumina). Data were then de-multiplexed, aligned, and counted using Cell Ranger version 3.1.0 (10X Genomics) and analyzed using Seurat (https://satijalab.org/seurat/) which utilizes Louvain clustering. Cells with mitochondrial gene percentage greater than 10% or with highly variable features were excluded from analyses and only cells that had unique feature counts between 200 and 2,500 were used in the analyses.

6.2.11 Statistical Analysis[6]

Statistical analysis was performed using GraphPad Prism software. Shalpiro-Wilk test was used to determine the normality of data in each experiment. ROUT method with Q=1% was used to identify outliers. To determine statistical differences between two groups with normal Gaussian distributions, a Student's t-test (two-tailed, unpaired, unequal variance, $p<0.05$) was performed. To determine if statistical differences were significant between three or more groups, with normal Gaussian distributions, one-way ANOVA was performed followed by a post-hoc Tukey's test. To determine if statistical differences were significant between three or more groups, with non-normal distributions, Kruskal-Wallis test was performed followed by a post-hoc Dunn's multiple comparison test.

6.3 Results

6.3.1 Synthetic Nanoparticle Antibody (SNAb) Mechanism of Action[6]

Synthetic nanoparticle antibodies (SNAbs) consist of multivalent, bifunctional, Janus gold (Au) nanoparticles modified with cell-targeting ligands on one "face" and antibody-Fc-mimicking ligands on the other "face" (Figure 6.3A). Janus particles are particles that have anisotropic surface chemistry and have previously been reported for *ex vivo* activation of T-cell receptors (330,331), drug delivery (332,333), cell tracking (334) and bio-imaging (335–339). Leveraging the bifunctionality of the Janus structure, SNAbs have the capability, like mAbs, to pair specific target cells with effector cells (*e.g.*, macrophages or Natural Killer (NK) cells), thereby triggering target cell killing (Figure 6.3B).

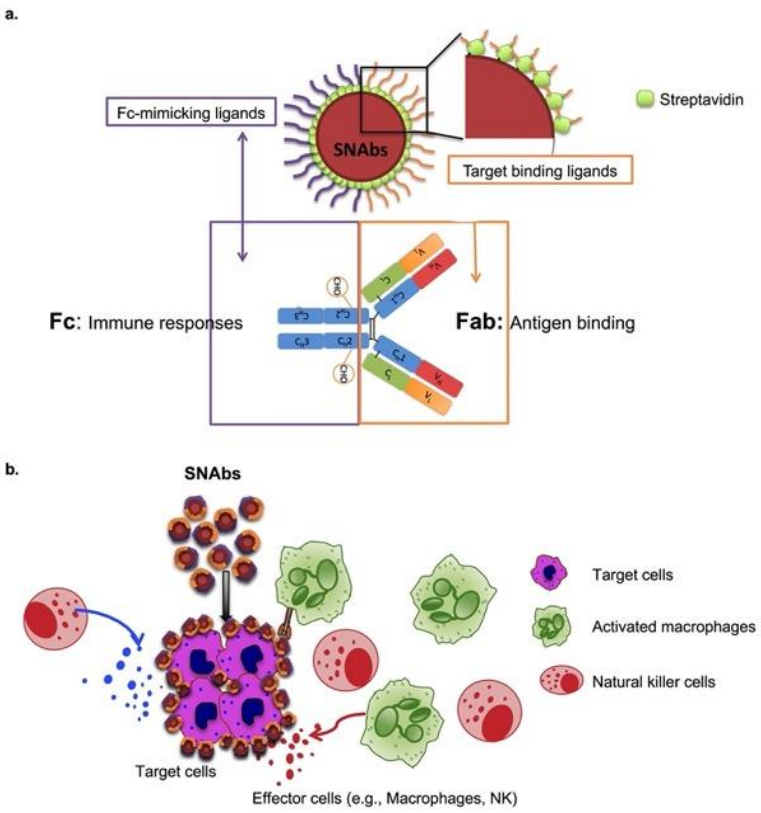

Figure 6.3. Schematic illustration of SNAbs and their hypothetical mechanism of action. (a) SNAbs are Janus nanoparticles bearing two distinct chemically modified faces. One of the two faces presents targeting ligands to perform the function of Fab domains in mAbs,

and the other displays Fc-mimicking ligands to crosslink Fc receptors on the effector cells as Fc fragments in mAbs. (b) Once administered into patients or animals with diseases, the SNAbs circulate and recognize target cells in blood or organs of interest by binding onto their surface proteins and engaging with effector cells (e.g. macrophages, NK cells) to induce antibody-like cellular cytotoxicity or phagocytosis.

6.3.2 SNAb Synthesis and Characterization of Janus Structure[6]

To generate SNAbs, first, Janus Au nanoparticles were synthesized using solid-phase chemistry (Figure 6.4) (340). Briefly, streptavidin (SA)-coated Au nanoparticles (SA-AuNP-SAs, 30 nm spheres, with an average hydrodynamic diameter of 70 nm) were bound onto aminomethyl resin (200-300 μm) via a reducible crosslinker, sulfo-NHS-S-S-Biotin. After washing off the unbound SA-AuNP-SAs, the crosslinkers' disulfide bonds were cleaved with tris(2-carboxyethyl)phosphine (TCEP), resulting in the release of Janus nanoparticles (SA-AuNP-SH) with asymmetric surface chemistry. One face of the Janus nanoparticles contained free-streptavidin (SA) for binding to biotin, and the other face provided biotin-NH-$(CH_2)_2$-SH, for reaction with maleimide group, which allowed spatially separated conjugation and presentation of two different ligands. Scanning transmission electron microscopy (S/TEM) bright-field (BF) imaging, high-angle annular dark-field (HAADF) imaging, and X-ray Energy Dispersive Spectroscopy (EDS) mapping of the SA-AuNP-SHs and SA-AuNP-SAs with biotinylated quantum dots (QDs) (Figure 6.5, Figure 6.6A,B), or maleimide-Au nanoprobes (Figure 6.6C) confirmed the asymmetric distribution of available biotin binding sites or free SH groups on the Janus nanoparticles, respectively.

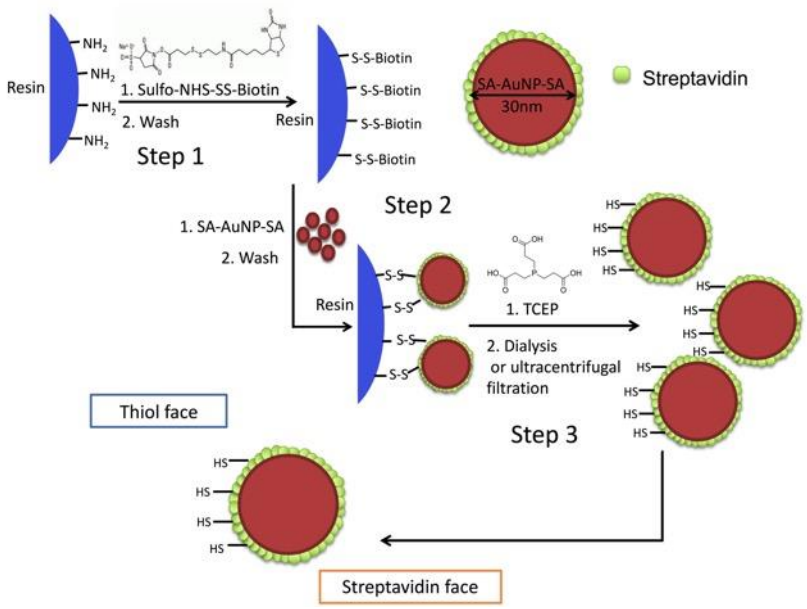

Figure 6.4. Fabrication of the Janus Au nanoparticles.
Aminomethyl resins were functionalized with sulfo-NHS-S-S-biotin crosslinker (step 1) and then bound with streptavidin-coated, 30nm Au nanoparticles (step 2). The cleavage of the disulfide bonds in the crosslinker by TCEP releases the Janus Au nanoparticles (step 3), which has a streptavidin face with open biotin-binding pockets and a thiol face with available free thiols.

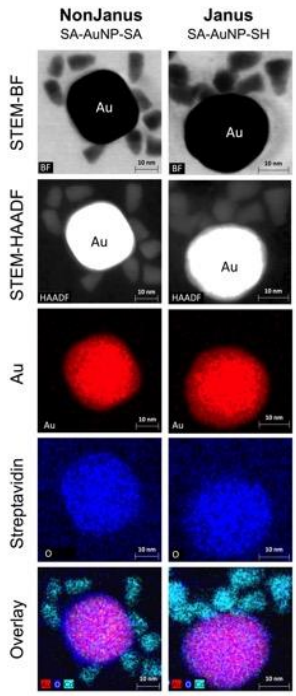

Figure 6.5. Characterization of Janus Au nanoparticles.

STEM-BF, STEM-HAADF, and EDS mapping images of 10-12 nm biotinylated quantum dot (QD)-conjugated nonJanus (SA-AuNP-SA, left column) and Janus (SA-AuNP-SH, right column) gold nanoparticles demonstrates the asymmetric distribution of open biotin-binding sites on the Janus nanoparticles. Colors: red-gold (nanoparticles), blue-oxygen (streptavidin), cyan blue-Cadmium (biotinylated QDs).

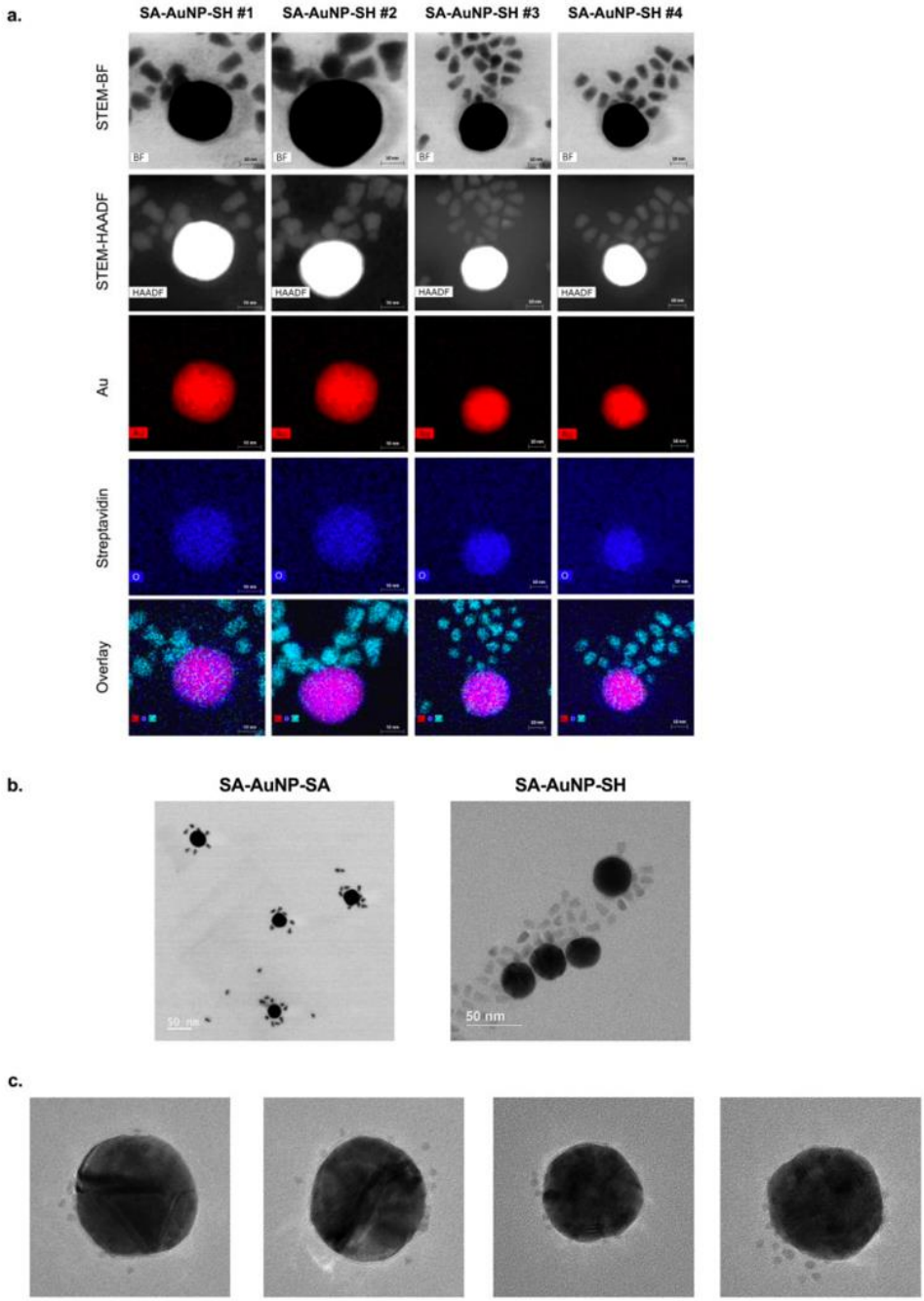

Figure 6.6. Validation of asymmetric surface chemistry of the Janus nanoparticles (SA-AuNP-SHs).

(a) S/TEM-BF images, STEM-HAADF images, and EDS mapping images of biotinylated quantum dot (QD)-conjugated Janus gold nanoparticles. Colors: red-gold (nanoparticles), blue-oxygen (streptavidin), cyan blue-Cadmium (biotinylated QDs). SA-AuNP-SH #2 is also used in Figure 2 in the main paper. (b) Bright field TEM/STEM image of multiple nonJanus (left, taken by ThermoFisher Scientific Talos F200X S/TEM at 200 kV) or Janus nanoparticles conjugated with biotinylated QD (right, taken by Hitachi HT7700 TEM at 120 kV). Only part of the surface of the Janus nanoparticles was coated with QDs while nonJanus nanoparticles were coated with QDs all over the surfaces. (c) TEM images of Janus nanoparticles conjugated with 1.8 nm maleimide-Au nanoprobes. Only part of the surface of the Janus nanoparticles was coated with maleimide nanoprobes.

6.3.3 Ligand Modification and Evaluation of Binding to Target Cells

6.3.3.1 Ligand Modification[6]

To target MDSCs, we first selected the G3 peptide (WGWSLSHGYQVK), a 12-mer peptide previously identified through phage-display against murine MDSCs with specific binding affinity to S100A8/A9 proteins (341). S100A8/A9 are pro-inflammatory proteins that participate in local intracellular communications and regulate MDSC recruitment in the tumors (342). MDSCs have high levels of surface-receptors that bind soluble S100A8/A9 proteins, and also express 10-fold higher cell-surface S100A8/A9 proteins compared to other cell types in tumor and inflammation (313,343–345). To make MDSC-targeting SNAbs, we proceeded to functionalize the streptavidin "face" of the Janus SA-AuNP-SH with C-terminal-biotinylated G3 peptides (Figure 6.7). On the opposite thiol (SH) "face," we conjugated the cp33 peptide, a human IgG1 Fc-mimicking ligand for binding to Fc gamma receptors (FcγRs) on immune effector cells, through the succinimidyl-4-(N-maleimidomethyl) cyclohexane-1-carboxylate (SMCC) group on the C-terminus of cp33 (Figure 6.7) (346,347).

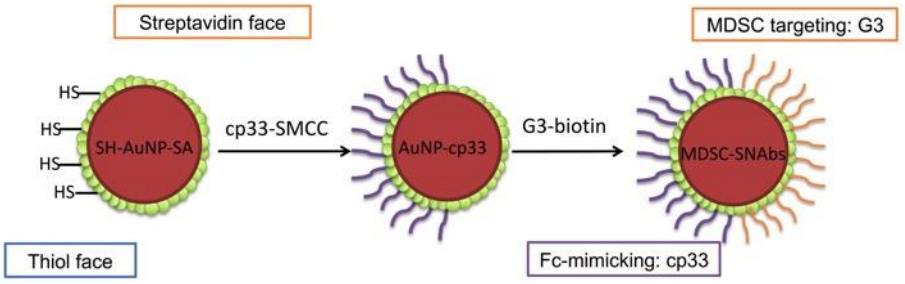

Figure 6.7. Ligand modification on Janus Au nanoparticles.
Following fabrication of Janus nanoparticles, the Fc-mimicking ligands, cp33, was conjugated onto the thiol face of the Janus nanoparticles via thiol-maleimide reaction, and the targeting ligands, G3, was modified onto the streptavidin face via biotin-streptavidin interaction.

6.3.3.2 Quantification of Modification Level

To quantify the modification level of the Janus nanoparticles, we first used sulfo-maleimide Cy5 and biotin Cy5 to confirm the number of available binding spots. An average of 18.79 Cy5 maleimide molecules bound to each particle and an average of 15.73 Cy5 biotin molecules bound to each particle. Next, we used 50x excess, 100x excess, and 200x excess of fluorophore-labeled G3 and cp33 peptides to confirm successful surface functionalization of the ligands onto the Janus nanoparticles (Table 6.1). An average of 17.59 Cy5 G3 biotin peptides bound to each particle when an excess of 200x was added to the particle solution. This average number of G3 peptides per particle is similar to the average number of Cy5 biotin that bound to each particle. Lower excess G3 peptide amounts showed fewer average peptides per particle with only 5.39 G3 peptides per particle at 50x excess. For the cp33 peptide, a more similar average number of peptides bound at all excess amounts, with 12.37 peptides bound at 200x excess compared to an average of 10.18 peptides per particle at 50x excess peptide added to solution. The average number of cp33 peptides per particle is again similar to, although slightly lower than, the

average number of Cy5 maleimide that bound to each particle. This is likely due to the cyclical nature of the cp33 peptide and the increased steric hindrance when bound to the nanoparticle scaffold compared to Cy5 maleimide alone.

Table 6.1. Quantification of Peptide Binding and Modification Level of Janus Nanoparticles.

	50x Excess Peptide	**100x Excess Peptide**	**200x Excess Peptide**
Cy5 G3-Biotin	5.39	11.89	17.59
Cy5 cp33-SMCC	10.18	10.54	10.31

6.3.3.3 Evaluation of Binding to Target Cells[6]

Traditional methods, like FACS, could not detect the AuNPs due to small particle size and lack of fluorescence without particle modification. However, gold nanoparticles are a well-established contrast agent in photoacoustic (PA) imaging due to strong optical absorption and surface plasmon resonance. Because PA signal is directly proportional to nanoparticle concentration and absorption coefficient, gold nanoparticles have been used for PA cell tracking applications (329,348,349). For these reasons, we used PA imaging to evaluate the binding of ligand modified nanoparticles to the target and effector cells *in vitro*. The PA images of cell samples treated with G3 modified AuNPs (NonJanus AuNP-G3) showed specific binding to rat PBMCs enhanced for MDSCs, whereas particles with only the cp33 ligand (NonJanus AuNP-cp33) and unmodified particles (NonJanus SA-AuNP-SA, or AuNP for short) showed minimal binding to MDSCs (Figure 6.8A,B).

Binding of ligand modified particles to rat bone-marrow derived macrophages showed successful binding of both G3 and cp33 modified particles compared to minimal binding of unmodified nanoparticles (Figure 6.8C), indicating that SNAbs can recognize both target cells (MDSCs) and effector cells (macrophages).

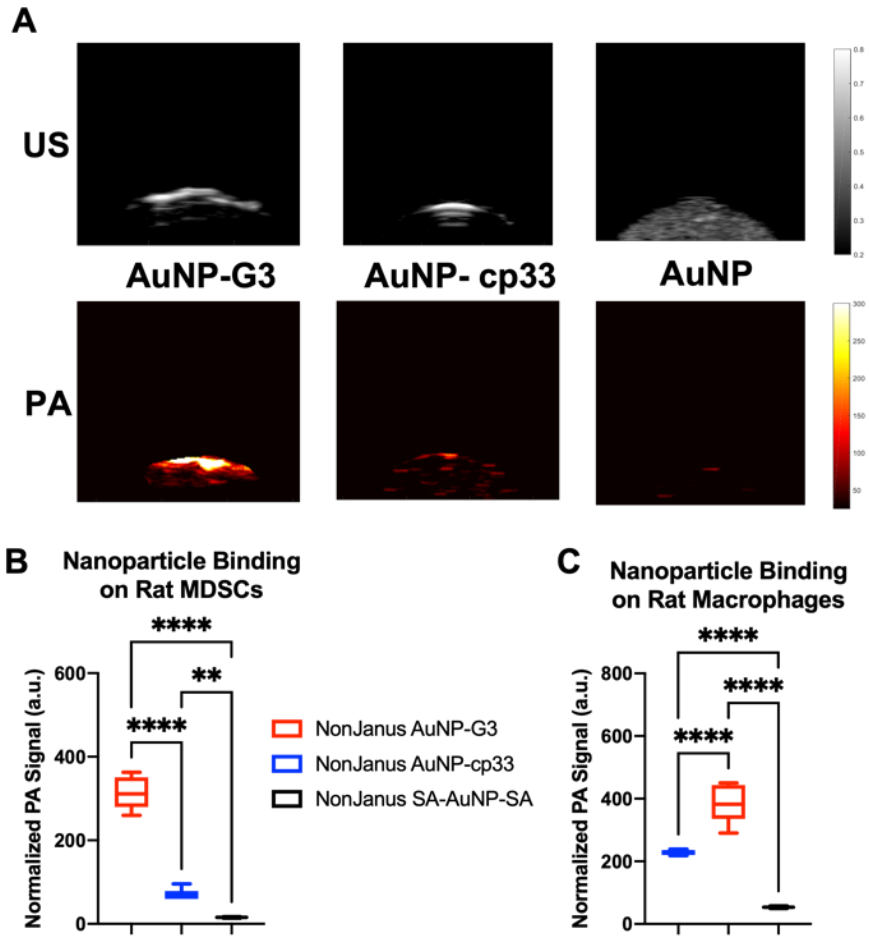

Figure 6.8. Binding of nanoparticles onto rat MDSCs and macrophages by photoacoustic (PA) imaging.
(A) The photoacoustic (PA) and ultrasound (US) images of nanoparticle-treated samples of rat MDSCs. Top: US images of the cell inclusions of modified or unmodified nanoparticles. Bottom: PA images of the cell inclusions of modified or unmodified nanoparticles at a wavelength of 532 nm. (B,C) The relative amount of nanoparticles bound to rat MDSCs (B) or rat bone marrow-derived macrophages (C) based on the average PA signals of each cell inclusion (0.5 million cells/40μL). PA signals shown in the graphs were normalized against the laser energy and backscattered ultrasound signals. Data are presented as mean ± s.d. of at least six cross-section images of two or more technical

replicates of corresponding independent samples. ANOVA with post-hoc Tukey's test show $p<0.0001$(****) and $p<0.01$ (**).

6.3.4 SNAb In Vitro *Depletion of Target Cells*[6]

Ex-vivo experiments were performed to test the mAb-like cell killing capability of the SNAbs. In an effector-target co-culture assay (trauma-associated MDSCs:macrophage = 1:10 ratio), 24 hours of SNAb treatment significantly reduced the percentage of MDSCs compared to control treatments, including unmodified AuNPs, PBS, and no treatment (Figure 6.9). Interestingly, despite the presence of peptides binding to both target and effector cells, the non-Janus modified particles (Non-Janus G3 cp33 AuNPs) did not significantly reduce MDSC percentage compared to the controls, suggesting that the polarized presentation of both G3 and cp33 peptides in a Janus structure is essential to induce efficient killing of MDSCs.

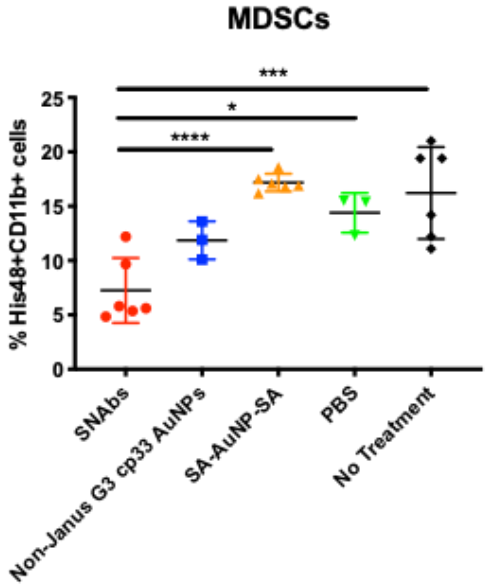

Figure 6.9. SNAbs induce antibody-like killing of rat MDSCs in the presence of effector cells.
Rat MDSC enhanced from peripheral blood mononuclear cells (PBMCs) from the infected trauma model and rat bone marrow-derived macrophages sorted from peripheral blood

mononuclear cells (PBMC) were cultured ex vivo at 1:10 ratio and treated with SNAbs or control treatments for 24 hours. The percentages of MDSCs ($CD11b^{+}His48^{+}$) in the co-culture after treatment were measured by flow cytometry. Data are presented by individual values with mean and standard deviation (n=6). Significance was determined using one-way ANOVA with Tukey post-hoc test (**** $p<0.0001$, *** $p<0.0002$). SA-AuNP-SA are unmodified non-Janus streptavidin coated Au nanoparticles. Non-Janus G3 cp33 AuNPs are modified with both ligands but without the Janus orientation. SNAbs are Janus G3-AuNP-cp33 nanoparticles targeting MDSCs.

To test SNAb-mediated MDSC-specific killing, we conducted a PBMC suspension assay, in which a mixture of PBMCs (containing MDSCs, macrophages, neutrophils, T and B cells, etc.) isolated from the rat infected trauma model were treated with SNAbs or left untreated. The percentage of the major cell populations in the culture were measured using flow cytometry after 24 hours (Figure 6.10). This assay reflects the *in vivo* microenvironment with a mixture of various types of immune cells and varied effector cell-to-target cell ratios dictated by disease progression. SNAbs reduced the total MDSCs compared to the untreated group. In addition, there is also some reduction in the macrophage and neutrophil populations due to SNAbs, which is expected due to the presence of S100A8/A9 (the target of the G3 peptide) on the surface of both macrophages and neutrophils (350). While S100A8/A9 is present in much higher quantities on MDSCs, we still expect some macrophage and neutrophil cell death. This SNAb-specific reduction is remarkable, considering that the macrophage to MDSC ratio in the PBMC assay was very low. Apart from MDSCs, treatment with the SNAbs resulted in higher average percentages of B220+ B cells, CD3+ T Cells, CD4+ T cells, and CD8+ T cells, likely due to the reduction of MDSCs. Of note, only B cells were significantly increased in the SNAb treated group.

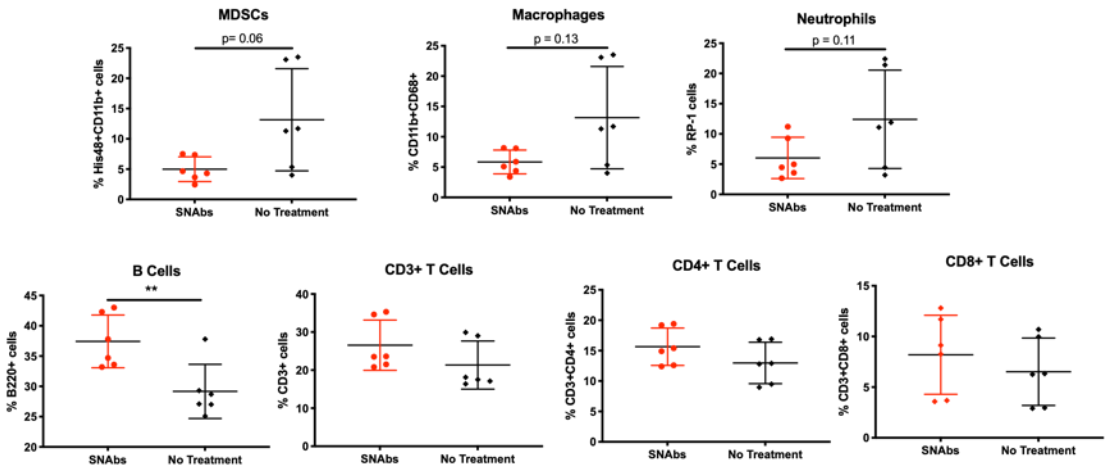

Figure 6.10. SNAb depletion of MDSCs in a rat PBMC culture.
In a rat PBMC assay, the PBMCs from the rat infected trauma model were treated with SNAbs or left untreated for 24 hours. The cells were then stained with fluorescent antibodies and analyzed by flow cytometry for the total percentage of MDSCs, macrophages, neutrophils, B cells, and T cells out of total cells. Significance was determined using Student's t-test with $p<0.01$ (**) or as indicated.

6.3.5 Single Cell RNA Sequencing of SNAb In Vitro *Depletion of Target Cells*

To further investigate SNAb specificity for both mouse and rat MDSCs, single cell RNA sequencing (scRNAseq) was conducted on cells enhanced for MDSCs both before and after SNAb treatment in an MDSC and macrophage *in vitro* co-culture assay. For the rat cells where MDSCs were enhanced from infected trauma PBMCs, clustering shows the presence of MDSC, macrophage, and neutrophil populations, and an overlay of plots from pre-SNAb and post-SNAb treatment shows depletion of the MDSC clusters (Figure 6.11). Expression of macrophage gene markers (Cd68 and Adgre1) confirms that the population appearing in the post-SNAb treatment group are macrophages from the co-culture assay (Figure 6.12A). Expression of immunosuppressive gene markers known to be highly expressed on MDSCs (S100a9, Il1b, Arg1, and Junb) are significantly decreased post-SNAb treatment (Figure 6.12B). This demonstrates that SNAbs can not only decrease the

MDSC population (as confirmed previously by flow cytometry in *in vitro* assays), but that SNAbs can functionally decrease immunosuppressive gene expression.

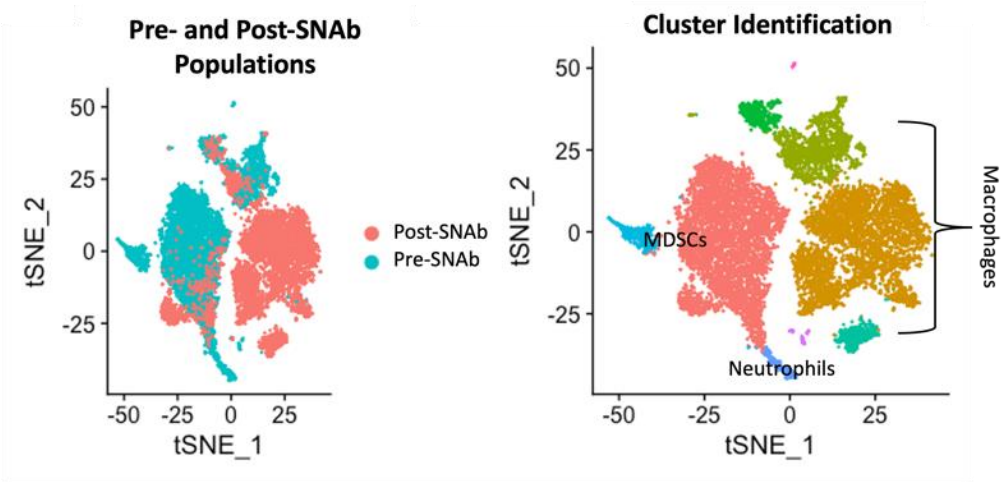

Figure 6.11. scRNAseq tSNE plots of cells enhanced for rat MDSCs pre- and post-SNAb treatment.
Left: Overlay of tSNE pre-SNAb treatment (blue) and post-SNAb treatment (red). Right: Identification of clusters in the tSNE showing multiple MDSC clusters, multiple macrophage clusters, and neutrophil clusters.

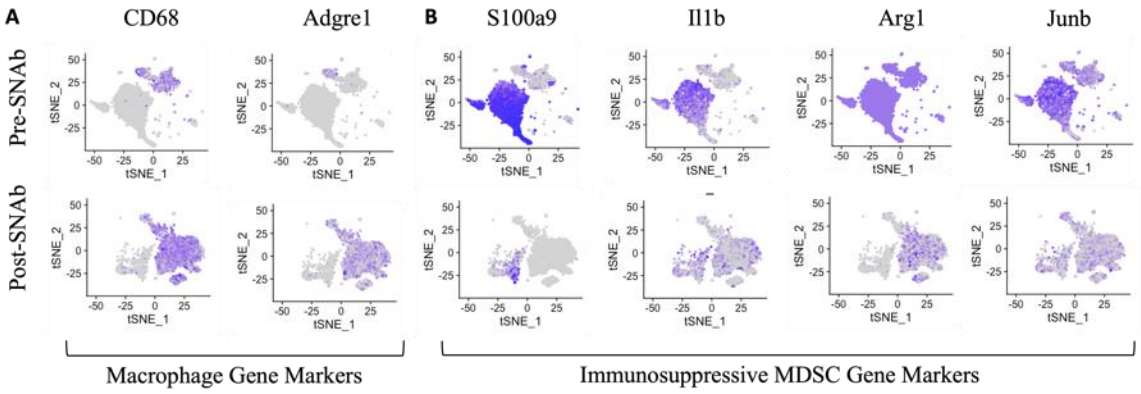

Figure 6.12. Gene expression from scRNAseq pre-SNAb and post-SNAb treatment.
A) Gene expression for macrophage gene markers (CD68, Adgre1) pre- and post-SNAb treatment. B) Gene expression for immunosuppressive MDSC gene markers (S100a9, Il1b, Arg1, Junb) pre- and post-SNAb treatment.

For the mouse cells where MDSCs were enhanced from spleen of 4T1 tumor-bearing mice, clustering shows the presence of MDSC, monocyte/macrophage, neutrophil, and B cell populations, and an overlay of plots from pre-SNAb and post-SNAb treatment shows depletion of the MDSC cluster (Figure 6.13). Expression of monocyte/macrophage gene markers (Il4ra, Cd74, and Cd36) confirms that the population appearing in the post-SNAb treatment group are macrophages from the co-culture assay (Figure 6.14A). The macrophage clusters are more apparent in the post-SNAb treatment groups for both mouse and rat since the co-culture assay requires the presence of effector cells (macrophages), and the amount of MDSCs has decreased, leaving the macrophage populations remaining. Expression of immunosuppressive gene markers known to be highly expressed on MDSCs (S100a9, Il1b, and Tgfbi) are significantly decreased post-SNAb treatment (Figure 6.14B), again showing the ability of SNAbs to functionally alter the immune environment through depletion of MDSCs. These data also suggest that SNAbs can work in multiple species and different disease scenarios.

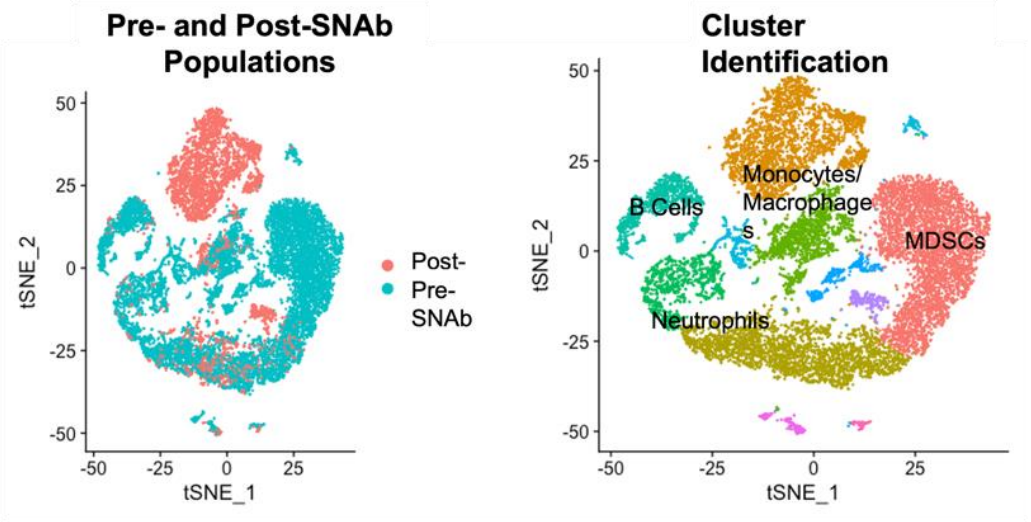

Figure 6.13. scRNAseq tSNE plots of cells enhanced for mouse MDSCs pre- and post-SNAb treatment.

Left: Overlay of tSNE pre-SNAb treatment (blue) and post-SNAb treatment (red). Right: Identification of clusters in the tSNE showing MDSC, neutrophil, monocyte/macrophage, and B cell clusters.

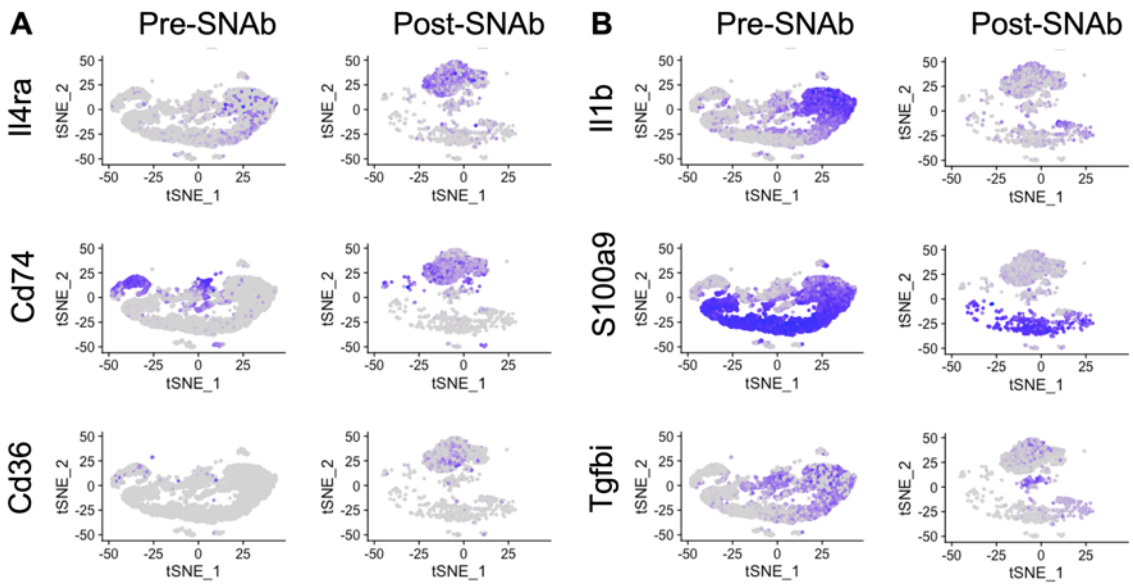

Figure 6.14. Gene expression from scRNAseq pre-SNAb and post-SNAb treatment.
A) Gene expression for macrophage gene markers (Il4ra, Cd74, and Cd36) pre- and post-SNAb treatment. B) Gene expression for immunosuppressive MDSC gene markers (S100a9, Il1b, and Tgfbi) pre- and post-SNAb treatment.

6.4 Discussion

Monoclonal antibodies (mAbs) as an immunotherapy have emerged as one of the leading forms of immunotherapy, in particular for treatment of cancers, with almost 80 different mAbs approved for clinical-use by the FDA (351). Unlike radiation or chemotherapy, mAbs offer a more specific and targeted approach that can be tailored to each individual with fewer side effects and less toxicity (352). However, the manufacturing process for mAbs is challenging as the most common methods require immunization of mice or the use of transgenic mice for the generation of hybridomas, the use of bacteriophages and cell culture for the phage display technique, or human donors who have

already been infected or immunized (351). In addition, mAbs have a short retention time, require high dosages, and offer low specificity for certain immune cell populations due to the use of surface markers that are present on multiple immune cell subsets (353). This work focuses on the development of synthetic nanoparticle antibodies (SNAbs) that improve upon the limitations of mAbs by utilizing a completely synthetic fabrication process. In addition, SNAbs offer a plug-and play-platform for targeting peptides to potentially improve specificity, and the multivalent design can potentially improve efficacy, thus decreasing dosage requirements compared to mAbs.

First, we show that we are able to synthesize Janus gold nanoparticles that display Fc-mimicking peptides on one hemisphere and MDSC targeting peptides on the other hemisphere, creating a bifunctional structure mimicking that of an mAb. TEM and EDS/STEM imaging allow visualization of the Janus structure, and fluorescent-based assays determined that around 15 peptides per hemisphere are bound to the particles. This improved valency compared to mAbs could offer improved efficacy. Multivalent interactions are required in many biological processes, including antibody-dependent Fc signaling activation which relies on the clustering of multiple Fc-receptor molecules following pathogen opsonization with immunoglobulin (IgG) antibodies (354). This is further supported by multiple previous studies demonstrating that multivalent display of antibodies or peptides on the surface of nanoparticle constructs will increase the binding affinity to its target as well as the biological functions of the constructs (355–357). In addition, multivalent constructs, such as the SNAbs, can distinguish cell targets based on receptor density profiles, which can result in higher targeting specificity (358,359). This is essential for SNAbs to target the high density of S100A8/A9 complexes on the surface of

MDSCs since these molecules are also present in lower quantities on neutrophils, myeloid-derived dendritic cells, and monocytes (350). Overall, the multivalency of the SNAbs could improve efficacy by increased binding affinity to target cells and could improve targeting specificity of MDSCs by distinguishing cell targets based on increased S100A8/A9 density.

Next, we showed through *in vitro* assays that SNAbs could successfully bind to both target and effector cells, induce killing of MDSCs, and decrease immunosuppressive markers. The bifunctional structure of the SNAbs resulted in a significant decrease in MDSCs compared to controls, whereas the non-Janus modified particles did not result in a significant decrease in MDSCs compared to controls. The orientation, localization, and multivalency of the targeting and Fc-mimicking ligands on the Janus nanoparticles may bind to and activate receptors more effectively on effector cells (339,360–362). Along with a decrease in MDSCs, SNAbs also resulted in a decrease in immunosuppressive gene expression determined by single cell RNA sequencing. In particular, S100A9, IL-1b, Arginase, TGFb, and Junb expression were all downregulated following *in vitro* SNAb treatment. S100A9 is both upregulated on the surface of MDSCs and secreted by MDSCs, which results in premature death of hematopoietic stem and progenitor cells and induces upregulation of PD-1/PD-L1, leading to T cell exhaustion and apoptosis (345,363). SNAbs target S100A9 via the G3 peptide conjugated to the surface of the nanoparticles. Il-1b is another important MDSC-associated cytokine which recruits and activates MDSCs through the IL-1R/NF-kB pathway, resulting in further accumulation of MDSCs (364,365). TGFBI is a secreted protein found in the extracellular matrix (ECM) that has been shown to inhibit the proliferation and activation of both helper and cytotoxic T cells by reducing

production of inflammatory cytokine IFNg and protease granzyme B (366). Arginase (Arg1) is a well-known method for MDSCs to suppress T cell functions by depleting L-arginine, an essential amino acid for T cell receptor (TCR) signalling (173). Lastly, Junb, a transcription factor in the activating protein (AP-1) family, is another marker of aberrant immune cell responses and is involved in the immune cell activation program in MDSCs (367). Significant reduction in expression of all of these immunosuppressive and MDSC-associated genes shows promise that SNAbs can be utilized to successfully alter an immunosuppressive environment by targeted killing of MDSCs.

Lastly, the evidence that SNAbs work successfully in both tumor-derived MDSC killing and rat infected trauma MDSC killing exhibits their usefulness to alter aberrant immune environments across multiple disease models and species. This capability demonstrates that SNAbs could be a highly effective tool for individualized and targeted immunotherapies that could improve upon the current standard of care.

6.5 Conclusions[6]

In summary, we have designed, fabricated, and characterized fully-synthetic Janus nanoparticle antibodies (SNAbs) that can target and kill specific cells, like mAbs. The G3 and cp33 ligands were identified through peptide-phage display techniques, one of the many high-throughput molecular evolution tools. The targeting and activation ligands of SNAbs can also be identified and developed through other high-throughput screening tools, like aptamer screening. These techniques can identify ligands with comparable affinity as conventional mAbs to relevant antigens through iterative screening of a library of peptide (or aptamer, etc.) sequences against a selected protein, cell, or tissue of interest without the

need to know cell-specific surface markers (368). The identified peptides (or aptamer, etc.) have the advantages of small physical size, flexible structure, and low immunogenicity compared to mAbs and can be easily chemically synthesized at lower cost. They can be readily used to functionalize onto the surface of Janus nanoparticles to generate a multitude of SNAbs targeting a wide range of cell types (368,369). Unlike mAbs or peptibodies, SNAbs use nanoparticles as scaffolds which have a high surface-area-to-volume ratio for the presentation of a high density of ligands, leading to high binding efficiency and increased targeting specificity (359,370). As shown by the PA images and ex vivo killing experiments, SNAbs possess strong binding capability on both target cells (MDSCs) and effector cells. Besides targeting capability, we also showed that SNAbs were able to induce specific killing of MDSCs *ex vivo* in two disease-relevant animal models, *i.e.*, the murine 4T1 breast cancer model and the rat infected-trauma model. These results demonstrated that the synthetic Janus nanoparticles modified with both targeting and Fc-mimicking ligands can trigger effective antibody-like innate immune responses in the presence of effector cells.

As a synthetic, functional alternative to mAbs, the potential of SNAbs is not limited to MDSC depletion. As a platform nanotechnology, its flexibility lies in the tailorability of physical and chemical properties, e.g., particle material, size, and shape; ligand valency; ligand types (aptamer, peptides, protein domain, complementary RNA or DNA sequence). Such design flexibility could allow for improved biodistribution and targeting efficiency, and the plug-and-play facile conjugation of ligands would allow rapid development of a wide variety of specific cell-depleting nanotherapeutics (369). In conclusion, our results demonstrated the synthesis and characterization of a novel class of nanotherapeutics,

SNAbs, that functions as multivalent mAbs, and offer a promising platform tool for treating malignancies, infectious diseases, and other immune disorders.

CHAPTER 7. EVALUATION OF SNABS TO DEPLETE MDSCS IN VIVO AND THE EFFECTS ON THE SYSTEMIC IMMUNE SYSTEM AND REGENERATION

7.1 Introduction

Severe musculoskeletal trauma remains a significant clinical challenge with around 5-10% of fracture patients experiencing complications with healing, most commonly infections and nonunions (4,98,257). Infections can be challenging to treat and can result in impaired bone healing, requiring revision surgeries, extended rehabilitation time, long-term antibiotics, and increased treatment costs (214). For open fractures, such as composite injuries with concomitant muscle damage, the complication rate is twice as high, with significantly increased risk for infectious complications. Despite extensive treatment regimens that often include multiple interventions, nearly two-thirds of patients with composite tissue injuries remain significantly disabled long-term (261). Improved treatment strategies are needed to improve patient outcomes for these challenging bone healing scenarios.

In both infected trauma and composite injuries, systemic immune dysregulation and immunosuppression has recently been highlighted as a contributing factor to poor healing and increased susceptibility to complications, such as opportunistic infections (5,169). Following severe trauma, overwhelming local inflammation results in systemic inflammation, termed the systemic inflammatory response syndrome (SIRS) where there is an increase in pro-inflammatory cells and cytokines. Concurrently, the compensatory

anti-inflammatory response syndrome (CARS) occurs to counteract high levels of systemic inflammation, and this phase includes increases in anti-inflammatory cells and cytokines (3,6). In patients with uncomplicated outcomes, these two phases balance each other out around 7 to 14 days post-injury; however, in patients with complicated outcomes, systemic immune dysregulation and immunosuppression can result, characterized by a dysregulated cytokine response and high levels of immunosuppressive mediators, most notably myeloid-derived suppressor cells (MDSCs) (21,27). Clinically, worsening immune dysregulation has been associated with observed increases in MDSCs in patients following trauma (8,36,37,42).

MDSCs are a heterogeneous population of immature myeloid cells that expand rapidly during impaired hematopoiesis and emergency myelopoeisis, and they potently suppress T cells and other immune effector functions (27,43). In addition, they have also been shown to induce immunosuppressive regulatory T cell (Treg) development, creating a feedforward mechanism to rapidly increase immunosuppression (45). MDSCs utilize various mechanisms to suppress immune function, including the production of reactive oxygen and reactive nitrogen species (ROS/RNS) and secretion of immunosuppressive cytokines and molecules, such as IL-10, TGF-b, and arginase. These mediators are known for suppressing cytotoxic T cell and Natural Killer (NK) cell function, and arginase in particular is known to deplete L-arginine, an essential amino acid required for T-cell receptor (TCR) signaling, which then hinders appropriate T cell activation (43,44). Recent work in a pre-clinical trauma model has further supported the immunosuppressive role of MDSCs with their observations of direct negative correlations between systemic MDSC populations and bone regeneration. These correlations were present at multiple weeks post-

treatment suggesting that high levels of systemic MDSCs result in decreased bone regeneration (371). Because of this, MDSCs could be an optimal target for immunomodulation to restore immune homeostasis and support a permissive, pro-healing immune environment.

Previous work in our lab has developed synthetic nanoparticle antibodies (SNAbs) to target and deplete MDSCs. SNAbs are bifunctional Janus gold nanoparticles that contain both MDSC targeting ligands and Fc-mimicking ligands, and they deplete MDSCs through antibody-mediated cell killing. So far, SNAbs have been used to deplete MDSCs in a murine breast cancer tumor model, reducing disease burden and increasing immune effector infiltration at the tumor site (372). SNAbs have also had success at depleting MDSCs from an infected rat trauma model *in vitro* and therefore show promise to deplete MDSCs following challenging cases of severe trauma, ultimately restoring immune homeostasis and improving local bone regeneration.

In this study, we investigate the use of SNAbs to deplete MDSCs *in vivo* in an infected trauma model. Subsequently, we investigate if SNAb treatment in a composite trauma model can restore immune homeostasis and improve local bone regeneration synergistically with a local treatment strategy. Here, we use bone morphogenetic protein 2 (BMP-2) delivered in an alginate nanofiber mesh delivery system as the local treatment strategy. Previous work has shown that this system results in improved spatiotemporal BMP-2 delivery and improved bone regeneration compared to clinical standard adsorbable collagen sponge (267). This work will provide a better understanding of the relationship between the systemic immune response and the local injury environment, ideally providing

clinicians another strategy to improve patient outcomes in complicated bone healing scenarios.

7.2 Materials and Methods

7.2.1 Preparation of MDSC-Depleting SNAbs

Synthetic nanoparticle antibodies (SNAbs) were prepared as previously described (372). Briefly, aminomethyl ChemMatrix resin (SigmaAldrich) was reacted with a biotin crosslinker containing a disulfide (sulfo-NHS-SS-biotin, ThermoFisher Scientific) for 4 hours at 37C. Next, the resin-crosslinker was reacted with streptavidin-coated 30nm gold nanoparticles (Nanohybrids) overnight at 37C. Reaction vessels were washed with 0.01% Tween 20 in 1X PBS to remove unbound particles. Tris(2-carboxyethyl)phosphine (TCEP, ThermoFisher Scientific) was then added overnight at room temperature to cleave the particles from the resin at the disulfide bond present in the crosslinker. Janus particles were then collected and dialyzed against PBS to remove the TCEP. Following dialysis, G3-biotin and cp33-SMCC peptides were added sequentially at 4C overnight with washing via centrifugation in between peptides. Final particles were collected via centrifugation and resuspended in 1X sterile PBS and stored at 4C until injection.

7.2.2 Nanofiber Mesh and Alginate BMP-2 Preparation

Nanofiber mesh and alginate hydrogels were prepared as previously described (178). Alginate hydrogels were made by dissolving RGD-functionalized alginate (FMC Biopolymer) into sterile alpha-MEM (Corning) to make a 3% w/v alginate solution. The solution was then mixed with 0.1% rat serum albumim (RSA) in 4mM HCl containing

2.5ug of BMP-2 and cross-linked in an excess of calcium sulfate by thorough mixing. Hydrogels were stored at 4C until use. Polycaprolactone (PCL) nanofiber meshes were fabricated by forming a 12% w/v PCL solution in a 90:10 solution of 1,1,1,3,3,3-Hexafluoro-2-propanol, 99+% (HFP; Sigma Aldrich) and *N*,*N*-Dimethylformamide, anhydrous, 99.8% (DMF; Sigma Aldrich) overnight. Meshes were electrosupun to an approximate thickness of 500um and perforations were formed using a laser cutter (0.7mm diameter holes). The meshes were then rolled to an inner diameter of 4.5mm and a length of 12mm and glued with UV cure adhesive (DYMAX), sterilized in 70% ethanol, and then stored in alpha-MEM at 4˚C until use.

7.2.3 Surgical Procedures

7.2.3.1 Infection Model

All animal care and experimental procedures were approved by the Veterans Affairs Institutional Animal Care and Use Committee (IACUC) and carried out according to the guidelines. Surgical procedures were carried out as previously described (179). Briefly, unilateral 2.5mm femoral segmental defects were created in 12-week old female Sprague-Dawley rats (Charles River Labs) in the mid-diaphysis using a Gigli wire saw (RISystem, Davos, Switzerland) and stabilized with a modular fixation plate. A collagen sponge inoculated with 10^7 CFU of *Staphylococcal aureus* was placed in the defect site. The incision site was then sutured shut with absorbable 4-0 sutures and the skin was closed with wound clips. Slow release buprenorphine (0.03 mg/kg; 1 ml/kg) was administered subcutaneously and used as an analgesic.

7.2.3.2 Composite Trauma Model

All animal care and experimental procedures were approved by the University of Oregon IACUC and carried out according to the guidelines. Surgical procedures were carried out as previously described (373). Briefly, 13-week-old female Sprague Dawley rats (Charles River Laboratories) received unilateral 8mm femoral segmental defects in the mid-diaphysis using an oscillating saw. Defects were stabilized with a polysulfone internal fixation plate. In the adjacent quadriceps, an additional 8mm diameter, full-thickness defect was created using a biopsy punch. All defects were left untreated until 8 weeks post-surgery. At 8 weeks, the animals underwent an additional surgery where the bone defect site was cleared and 2.5ug BMP-2 treatment was added via the nanofiber mesh alginate hybrid delivery system. The muscle defects were left untreated. At 9 weeks, a subset of animals received arterial injections of synthetic nanoparticle antibodies (SNAbs).

7.2.4 Immune Characterization

Blood was drawn via a vacuette catheter system (Greiner Bio-One) from the tail artery of rats at 24 hours post-SNAb treatment to monitor changes in MDSCs. Following red blood cell lysis (1X RBC Lysis Buffer, eBioscience,), cells were fixed (BD Cytofix, BD), resuspended in FACS buffer (2% fetal bovine serum in 1X PBS), and then stored at 4˚C until staining for cellular analysis via flow cytometry. Cells were stained using standard staining protocols for MDSCs (CD11b+His48+), run on a BD Accuri C6 flow cytometer, and analyzed using FlowJo software. Gates were set with <1% noise allowed based on fluorescent minus one (FMO) controls.

7.2.5 Bone Regeneration

Longitudinal bone regeneration was qualitatively assessed with radiographs (Faxitron MX-20 Digital, Faxitron X-ray Corp.) and quantitatively assessed via micro-computed tomography (Viva-CT 40, Scanco Medical). The middle region of the defect was analyzed (~6.5mm) with a 38um voxel size, 55kVp voltage, and 145uA current and newly regenerated bone was determined using a threshold corresponding to ≥ 50% of the density of native cortical bone.

7.2.6 Single Cell RNA Sequencing

Rat PBMCs were isolated from both the infection model and the composite trauma model. Cells were processed by diluting the samples in PBS+0.1% BSA and filtering through a cell strainer. Cells were then counted with Cellometer (Nexcelom) and Nucleocounter (Cemometec) automated cell counters to check cell number and viability to achieve the target 5000 barcoded cells. scRNA-seq was performed using 10X Genomics Single Cell 3' Solution, version 3.1, according to the manufacturer's instructions (protocol rev C). Libraries were sequenced on Nextseq500 (Illumina). Data were then de-multiplexed, aligned, and counted using Cell Ranger version 3.1.0 (10X Genomics) and analyzed using Seurat (https://satijalab.org/seurat/) which utilizes Louvain clustering and tSNE or UMAP projections. Cells with mitochondrial gene percentage greater than 10% or with highly variable features were excluded from analyses and only cells that had unique feature counts between 200 and 2,500 were used in the analyses.

7.2.7 Statistical Analysis

Statistical significance for quantitative results was assessed using appropriate parametric or non-parametric tests. For data that met the assumptions, an unpaired

Student's t-test, one-way analysis of variance (ANOVA), or two-way ANOVA with repeated measures were used. Multiple comparisons were made using Sidak's multiple comparisons test, and significance was determined by p values less than 0.05. For data that did not meet the assumptions for parametric tests, the Mann-Whitney or Kruskal-Wallis test was used. Numeric values are presented as the mean ± SEM. All statistical analysis was performed using GraphPad Prism 9.0 software (GraphPad, La Jolla, CA, USA).

7.3 Results

7.3.1 SNAbs Deplete Rat MDSCs in the Infection Model

To investigate the capability of SNAbs to deplete rat MDSCs *in vivo,* a pilot study was conducted in the rat infected trauma model. At 5 days post-injury and infection, animals were injected with SNAbs or left untreated, and uninjured naïve rats were used as a control. Blood was collected immediately prior to treatment, at 24 hours, and at 48 hours post-treatment to assess for circulating immune cell populations. At 24 and 48 hours, MDSCs were significantly decreased in the SNAb treated group compared to the untreated group, although MDSCs were still significantly elevated compared to the naïve group (Figure 7.1). Despite a decrease in MDSCs, there was no observed increase in CD3+ T cell populations at 24 hours or 48 hours in the SNAb treated group.

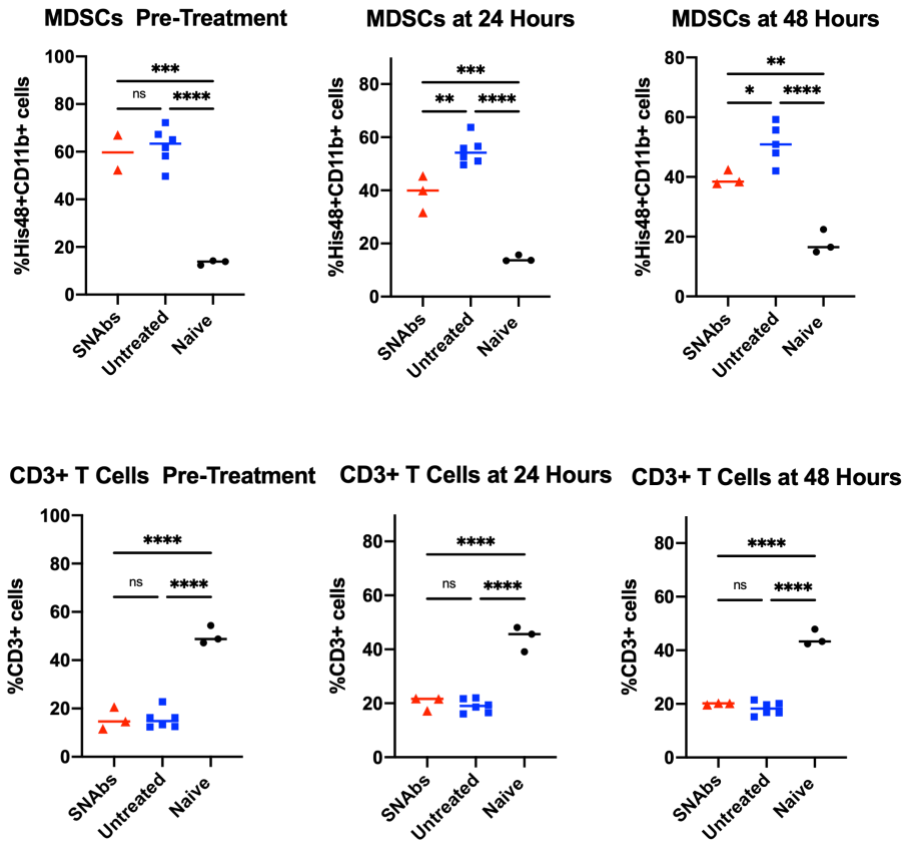

Figure 7.1. MDSC and T Cell Levels Following SNAb Treatment *In Vivo.*
SNAbs were delivered intraarterially to infected trauma rats at 5 days post-injury and infection. MDSCs (top) and CD3+ T Cell (bottom) populations were assessed at 24 and 48 hours post-treatment as well as immediately prior to treatment.

7.3.2 SNAb Treatment in the Composite Trauma Model

At 8 weeks post-injury, composite trauma animals were treated with 2.5ug of BMP-2 delivered in an alginate nanofiber mesh delivery system. Previous work revealed a significant negative correlation at one-week post-treatment (week 9) between systemic MDSC levels and endpoint bone regeneration. Therefore, we chose immunomodulatory SNAb treatment to be one-week post BMP-2 treatment at the same week 9 timepoint. One dose or a double dose of SNAbs were delivered intraarterially, and MDSC levels were assessed 24 hours later. Unexpectedly, overall MDSC levels drastically increased

following SNAb treatment (Figure 7.2). However, looking at MDSC subsets based on side scatter revealed that high side scatter MDSCs were significantly reduced at 24 hours post-treatment. However, low side scatter MDSCs were significantly increased at 24 hours post-treatment.

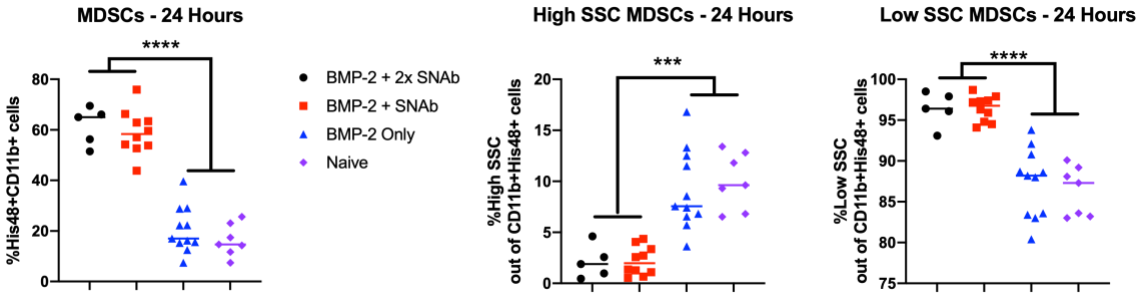

Figure 7.2. MDSCs at 24 hours Post-SNAb Treatment in the Composite Trauma Model. Systemic levels of MDSCs and the MDSC subsets at 24 hours post-SNAb treatment in the composite trauma model. Significance was determined using a one-way ANOVA where $p<0.005$ (***) and $p<0.0001$(****); n=5-11 depending on the group.

7.3.3 Bone Regeneration following SNAb Treatment in the Composite Trauma Model

Radiographs show qualitative bone regeneration at 6 weeks post-BMP-2 treatment (5 weeks post-SNAb treatment). Radiographs were assigned a qualitative bridging score from 0 to 3 where 0 indicates no bridging, 1 indicates just bridged, 2 indicates bridging with some additional defect bone regeneration, and 3 indicates robust bridging with significant defect bone regeneration. The SNAb treated group had an average bridging score of 1.33 whereas the BMP-2 only treated group had an average bridging score of 1.8. Next, each group was split by high and low Week 7 pre-treatment levels of MDSCs. In the BMP-2 + SNAb treated group, the high MDSC SNAb treated group had an average bridging score of 0.25 with 3 out of 4 rats showing no bridging at all, whereas the low MDSC SNAb treated group had an average bridging score of 2.2 with only 1 out of 5 rats

not bridged (p=0.06 between groups, Figure 7.3). In the BMP-2 only treatment group, the bridging scores were more consistent with the high MDSC group having an average bridging score of 2.

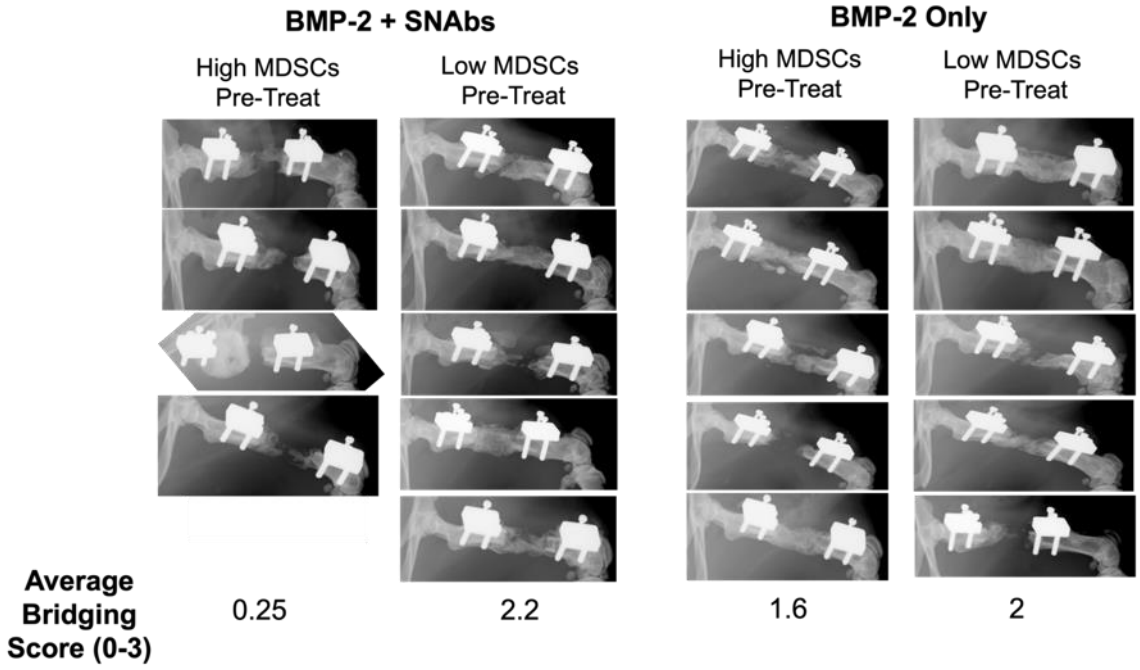

Figure 7.3. Week 6 Post-Treatment Radiographs of Defect Bone Regeneration.
Radiographs from the BMP-2 and SNAb treated group and the BMP-2 only treated group separated by animals with high and low levels of MDSCs at 1 week pre-treatment. Qualitative average bridging score on a range of 0-3 are shown below each group. These data were collected in collaboration with Kelly Leguineche and Tyler Guyer at the University of Oregon.

Quantitation of micro-computed tomography (uCT) reconstructions also shows bone volumes at 6 weeks post-treatment for each treatment group when split by high and low Week 7 pre-treatment MDSC levels (Figure 7.4A). Although there are no significant differences ($p<0.05$) between groups, the differences in bone volumes between samples with high MDSCs pre-treatment and low MDSCs pre-treatment warrants further investigation, in particular, for the SNAb treated group which had more notable separation

between populations. In addition, bone volumes in the BMP-2 only treated group had higher peak bone volumes but also lower overall bone volumes compared to the BMP-2 + SNAb treatment group. Looking at bone volumes across all treatment groups without separation based on pre-treatment level of MDSCs show no significant separation between groups although the BMP-2 only treated group did have a higher peak bone volume than either of the SNAb treated groups. (Figure 7.4B).

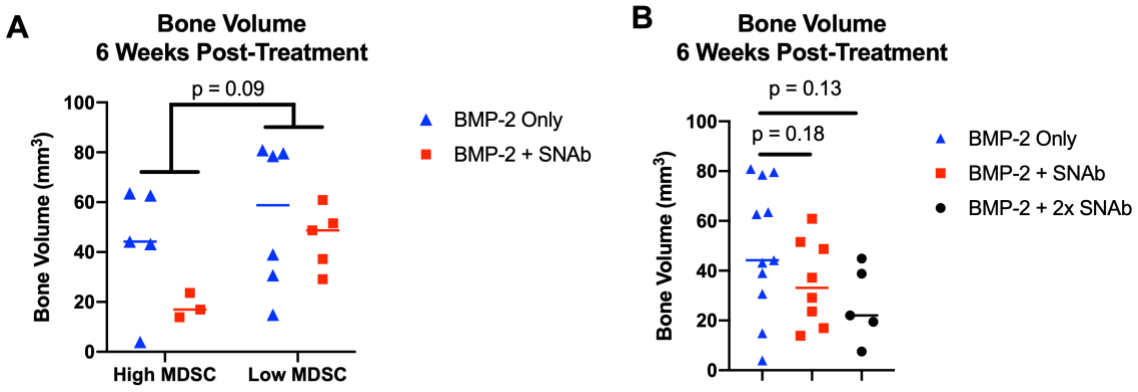

Figure 7.4. Micro-Computed Tomography of Defect Bone Regeneration.
A) Bone volumes from uCT analysis in the BMP-2 only treatment group and the BMP-2 + SNAb treatment group split up by high and low levels of 1 week pre-treatment MDSCs. B) Bone volumes from uCT analysis for groups treated with BMP-2 only, BMP-2 + SNAbs, and BMP-2 + a double (high) dosage of SNAbs (BMP-2 + 2x SNAb). These data were collected in collaboration with Kelly Leguineche and Tyler Guyer at the University of Oregon.

7.3.4 Single Cell RNA Sequencing Shows Differing MDSC Gene Expression Patterns in the Infection Model versus the Composite Trauma Model

Based on differences in MDSC depletion in the infection versus the composite trauma models, we further investigated MDSCs in these two models using single cell RNA sequencing (scRNAseq). PBMCs derived from both models were analyzed via scRNAseq and clustered together following integration (Figure 7.5). S100A8/A9 expression, the

target of the MDSC-targeting G3 peptide, is highest in clusters 2, 3, and 11 (Figure 7.6). Differential gene expression analysis between these three clusters reveals differences in expression of MDSC and neutrophil gene markers. In particular, clusters 2 and 11 have higher expression of neutrophil gene markers (Figure 7.7A), whereas cluster 3 has higher expression of MDSC gene markers (Figure 7.7B). Despite all three clusters exhibiting higher expression of S100A8/A9 compared to all other clusters, the neutrophil and MDSC differentially expressed genes highlight cluster 3 as the primary target for MDSC depletion. However, cluster 3 alone exhibits lower S100A8/A9 expression in the composite trauma model compared to expression in the infected trauma model (Figure 7.8). Therefore, SNAbs are likely preferentially targeting neutrophil clusters 2 and 11 in the composite trauma model compared to the MDSC cluster, whereas all three clusters are targeted in the infected trauma model.

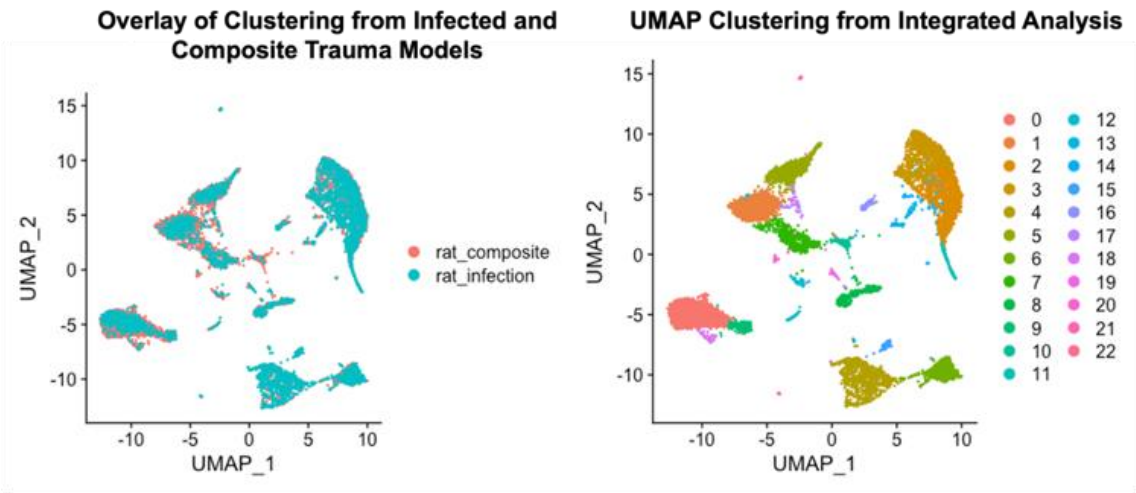

Figure 7.5. UMAP Clustering of Infected and Composite Trauma Models.
PBMCs were isolated from both the infected and composite trauma models and analyzed via integrated scRNAseq analysis. Left: UMAPs from the rat composite trauma model and rat infection trauma model are overlayed. Right: Integrated UMAP shows 22 distinct clusters. Data collected in collaboration with Paramita Chatterjee.

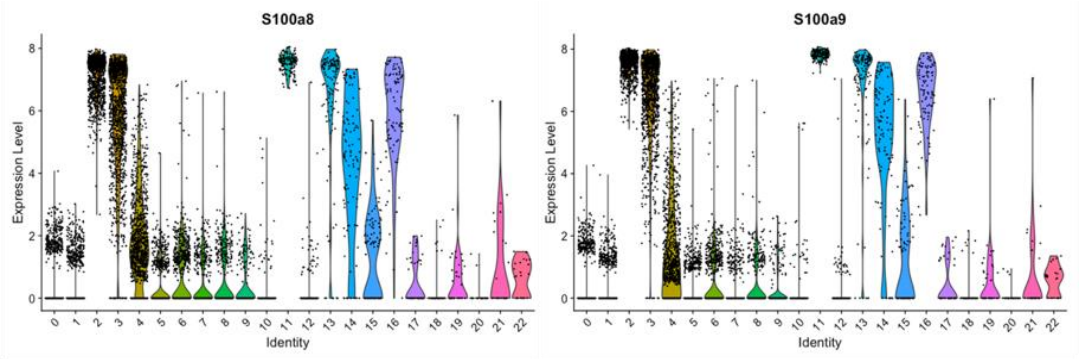

Figure 7.6. S100A8 and S100A9 Expression.
Violin plots of integrated clustering of PBMCs from the infected and composite trauma models shows S100A8 expression (left) and S100A9 expression (right) is highest in clusters 2, 3, and 11. Data collected in collaboration with Paramita Chatterjee.

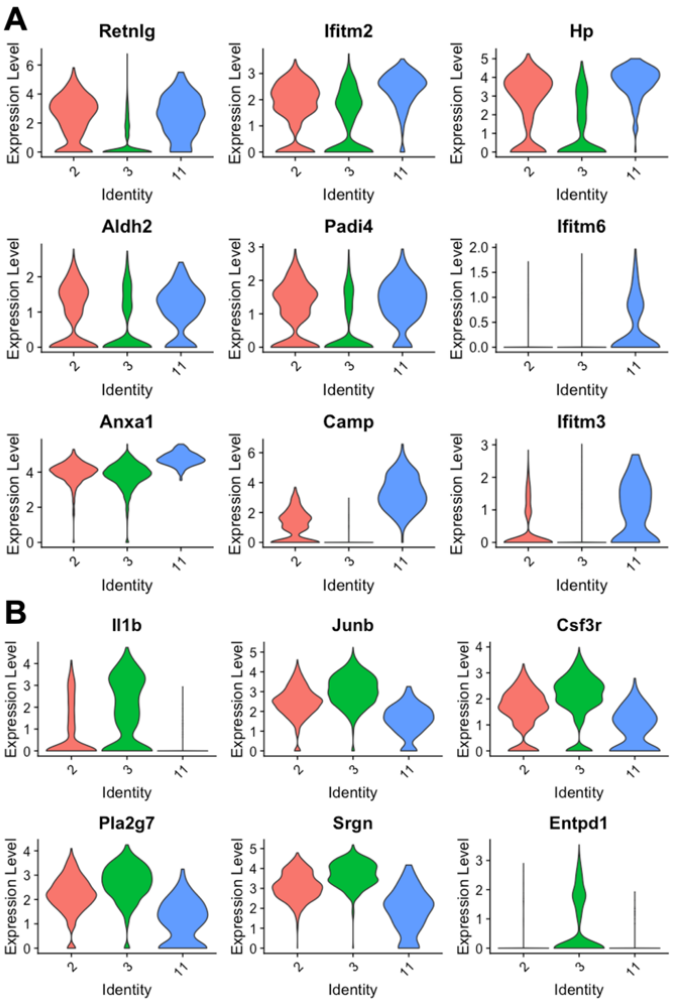

Figure 7.7. Expression of Neutrophil and MDSC Gene Markers in Clusters 2, 3, and 11.

A) Gene expression in clusters 2, 3, and 11 of neutrophil gene markers. B) Gene expression in clusters 2, 3, and 11 of MDSC gene markers. Data collected in collaboration with Paramita Chatterjee.

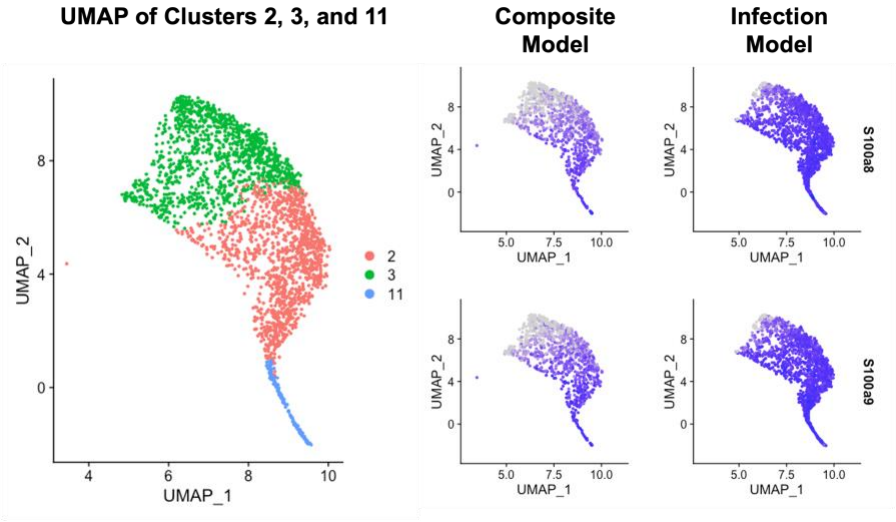

Figure 7.8. UMAP of MDSC and Neutrophil Clusters.
Integrated single cell RNA sequencing data from the MDSC and neutrophil clusters identified through differentially expressed genes. Left: UMAP of MDSC and neutrophil clusters. Right: differential S100A8/A9 expression in the composite trauma model versus the infection trauma model in the MDSC and neutrophil clusters. Data collected in collaboration with Paramita Chatterjee.

7.4 Discussion

Despite advances in trauma care and management, orthopedic surgeons still need better strategies to improve outcomes for patients with complicated musculoskeletal trauma, especially for more challenging cases with concomitant volumetric muscle loss or bone infections. Recent work in our lab has highlighted the role of MDSCs on systemic immune dysregulation and immunosuppression following trauma and the impact of a systemic immunosuppressive environment on local healing. Most notably, there was an inverse correlation at 1-week post-treatment between circulating MDSC levels and endpoint bone volume, suggesting that immunomodulatory therapeutics that target and deplete MDSCs could potentially improve healing outcomes (371). This study seeks to

address this question by evaluating the ability of MDSC-targeting synthetic nanoparticle antibodies (SNAbs) to deplete MDSCs, subsequently restore immune homeostasis, and ultimately, improve local bone regeneration. Recently, more work has been done to show the relationship between the systemic immune system and the local environment. For example, one study in cancer immunotherapy demonstrated that systemic immunity is required for successful anti-tumor immune-therapy and another study showed that systemic immune homeostasis is altered by local biomaterial scaffolds for tissue regeneration (11,12). Based on the links between bone and the immune system and the relationship between the local and systemic immune environments, we posit that regenerative medicine strategies will not reach their full potential without consideration of immune homeostasis and a permissive, pro-healing immune environment at both the local *and* systemic levels.

Preliminary depletion studies in the pre-clinical infected trauma model resulted in successful depletion of MDSCs; however, depletion in the related pre-clinical composite trauma model resulted in depletion of only high side scatter MDSCs and a large increase in the low side scatter MDSCs. Single cell RNA sequencing analyses revealed differences in MDSC and neutrophil gene expression, especially S100A8/A9 expression, which is the target molecule of SNAbs. S100A8/A9 are calcium-binding proteins that participate in cytoskeleton rearrangement and are released during inflammation to stimulate leukocyte recruitment and induce cytokine secretion (350,374). Despite its role in inflammation, S100A8/A9 also has a significant anti-inflammatory role. In certain cases, S100A8 has been shown to impair neutrophil infiltration, reduce cytokine secretion, inhibit antigen presentation on antigen presenting cells, and suppress leukocyte adhesion and migration (192,344,345,363,375). S100A8/A9 is known to be highly expressed in myeloid-lineage

cells following inflammation, such as myeloid-derived suppressor cells, and they are also highly expressed in neutrophils, with S100A8/A9 making up approximately 45% of cytoplasmic proteins (350). Expression and secretion of S100A8/A9 change drastically during inflammation, including inflammation resulting from trauma and infection. An improved understanding of S100A8/A9 expression and secretion patterns and also how the inflammatory/anti-inflammatory duality of the S100A8/A9 proteins impact the systemic immune response over time in different cases of inflammation will be important for robust and consistent SNAb targeting of MDSCs.

SNAb targeting of only high side scatter MDSCs in the composite trauma model did not improve local healing. In contrast, SNAb treatment may have even had the opposite effect, although further investigation is needed to confirm this. However, due to aberrant SNAb targeting and a large increase in low side scatter MDSCs following SNAb treatment, it would not be a surprising result to see negative impacts on bone regeneration. Previous work has shown that MDSCs at one-week post-treatment negatively correlate with endpoint bone healing (371). SNAb delivery occurred at one-week post-BMP-2 treatment, thus stimulating high levels of MDSCs at a time where MDSC levels have previously been predictive of healing outcomes. High levels of MDSCs in a clinical setting have also been associated with poor healing outcomes and increased susceptibility to complications (5). It was unexpected for SNAb treatment to have such different results between the two trauma models, and data suggests that the low side scatter MDSCs may play a more important role in the composite trauma model since depletion of the high side scatter MDSCs had no effect on bone regeneration. These data also suggest that robust depletion of both subsets

of MDSCs may be necessary to restore immune homeostasis and positively impact regeneration.

This study has some limitations that should be addressed. First, no unmodified particles or scrambled peptide modified particles were used as controls. Unfortunately, there is no known scrambled peptide for the G3 peptide. However, prior work with SNAbs in a murine cancer model utilized irrelevant peptide and unmodified particles as controls, and these did not elicit responses similar to fully functionalized G3 and cp33 modified SNAbs (372). While these controls would have also strengthened the current work, reagent scale-up and animal limitations precluded the use of multiple control groups. Because we expect both non-responders and responders within each treatment group, this requires a higher number of animals per group and therefore, including multiple control groups would not be physically feasible. Second, this study is based off of prior work showing correlations between MDSCs and bone volumes. A prospective study to validate that MDSCs can predict bone regeneration outcomes should be completed in order to further confirm the relationship between circulating MDSCs and regenerative outcomes. This information would help improve experimental design by allowing individualized and targeted treatment of only those exhibiting high levels of MDSCs, for example.

7.5 Conclusions

In this study, we investigated the role of a systemic immunomodulatory therapeutic targeting MDSCs on systemic immune function and local bone regeneration in conjunction with a local treatment strategy (BMP-2). While SNAbs were able to deplete all MDSCs in a pre-clinical rat infected trauma model, SNAbs only depleted one subset of MDSCs, the

high side scatter MDSCs, in a pre-clinical rat composite trauma model. Despite a decrease in high side scatter MDSCs, there was a large significant increase in low side scatter MDSCs in these animals. Likely due to this explosion in low side scatter MDSCs, SNAb-treated rats exhibited decreased bone regeneration at 6 weeks post-treatment (5 weeks post-SNAb delivery) compared to untreated rats. Investigations into the differences in MDSC depletion in infected trauma versus composite trauma rats revealed differing S100A8/A9 expression, the target molecule of the SNAbs. S100A8/A9 had similar expression across MDSC and neutrophil clusters in the infection model, whereas in the composite trauma model, S100A8/A9 expression was highest in neutrophil clusters, suggesting flawed MDSC targeting using SNAbs in the composite trauma model. This study highlighted the complexities of targeting MDSC populations that can change phenotypes depending on the disease or injury model, and it re-confirmed the relationship between higher levels of MDSCs and poor healing. Further work will be essential to better understand key markers of MDSCs in different models and species and how improved and specific targeting of MDSCs in these models impacts treatment outcomes.

CHAPTER 8. CONCLUSIONS AND FUTURE DIRECTIONS

8.1 Conclusions

Overall, this thesis has investigated post-traumatic systemic immune dysregulation and immunosuppression in multiple different trauma models, developed and characterized a novel nanoparticle-based method to target and deplete aberrant immunosuppressive myeloid-derived suppressor cells (MDSCs), and increased the fundamental knowledge about the role of MDSCs on systemic immune function and healing following trauma. These results can be leveraged to more effectively treat challenging bone injuries by identifying patients at higher risk for complications and utilizing targeted and individualized treatment strategies that not only focus on local tissue engineering strategies but also on systemic immunomodulation strategies.

8.1.1 Specific Aim 1: Characterize the development of systemic immune dysregulation and immunosuppression in pre-clinical animal models of delayed non-union, bone infection, and composite trauma and identify immunological markers predictive of poor healing.

In Chapter 3, Chapter 4, and Chapter 5, we explored systemic immune dysregulation and immunosuppression in multiple different trauma models exhibiting challenging bone healing scenarios, including chronic non-union, infection, and concomitant muscle injury.

In Chapter 3, we characterized systemic immune dysregulation in a rat model of chronic non-union and explored the role of immune dysregulation on healing. Our results

showed that delayed treatment of an established nonunion resulted in impaired bone healing compared to acute treatment. Although average levels of circulating immune cells and cytokines were not different between acute and delayed treatment groups overall, univariate and multivariate regression modeling revealed significant correlations between early cell and cytokine biomarkers and functional bone regeneration. Elevated circulating levels of MDSCs, IP-10, and IL-10 were all inversely correlated with healing whereas B cells, T helper cells, IL-6, and IL-13 were positively correlated. Some of these correlations, MDSCs and IL-10, were significant as early as 1-week post-treatment as determined through univariate and multivariate analyses. Taken together, these results suggest that MDSCs and long-term immune dysregulation play a key role in impaired healing after nonunion and could potentially serve as novel therapeutic targets to enhance bone repair[2].

In Chapter 4, we investigated the systemic immune response and immune dysregulation resulting from trauma-associated orthopedic biomaterial infections. The presence of a local, indolent *S. aureus* bacterial infection resulted in widespread systemic effects, including an uncoordinated and dysregulated systemic immune response with systemic increases in immunosuppressive MDSCs and decreases in immune effector cells, including T cells. This systemic immune dysregulation and immunosuppression in combination with the local *S. aureus* infection could contribute significantly to the clinical challenges associated with infected trauma, in particular, chronic and recurring infections and poor bone regeneration. An improved understanding of the systemic immune response and its relationship with the local environment, including bacterial clearance and bone healing, that resulted from this work could provide promising early diagnostic markers and

systemic immunomodulatory targets to improve the ability to fight orthopedic biomaterial-associated infections and improve patient outcomes[3].

In Chapter 5, we further investigated the relationship between local tissue engineering treatment strategies and the systemic immune response in both the chronic nonunion model and in the composite trauma model. The results obtained in this study indicate that if appropriately delivered spatiotemporally, a high dose of BMP-2 may be able to overcome the additional challenges associated with systemic immune dysregulation. Evaluation of the HMP delivery system showed improved bone regeneration and decreased side effects compared to the collagen sponge, and the HMP delivery system was associated with systemic immune effector cells. In contrast, the collagen sponge treatment had decreased bone regeneration and was associated with high levels of systemic MDSCs. This study highlighted the two-way relationship between the systemic immune environment and the local healing environment as an avenue to alter and improve bone regeneration outcomes. Further work will be essential to better understand biological mechanisms of nonunions with and without associated muscle damage, and in particular, how systemic and local immunological changes affect treatment outcomes.

8.1.2 Specific Aim 2: Fabricate and optimize an immunomodulatory therapeutic that targets and depletes MDSCs.

In Chapter 6, we designed, fabricated, and characterized Janus synthetic nanoparticle antibodies (SNAbs) that can target and deplete myeloid-derived suppressor cells (MDSCs), similar to monoclonal antibodies (mAbs). Unlike mAbs, SNAbs use nanoparticles as scaffolds which have a high surface-area-to-volume ratio for the presentation of high

density of ligands, leading to high binding efficiency and increased targeting specificity. As shown by the PA images, *in vitro* killing assays, and single cell RNA sequencing, SNAbs possess strong binding capability to both target (MDSCs) and effector cells, such as macrophages. We also showed that SNAbs were able to induce specific killing of MDSCs derived from two disease-relevant animal models: the murine 4T1 breast cancer model and the rat infected-trauma model, exhibiting the usefulness of SNAbs to alter aberrant immune environments across multiple disease models and species. As a synthetic, functional alternative to mAbs, the potential of SNAbs is not limited to MDSC depletion., The flexibility of SNAbs lies in the tailorability of physical and chemical properties and the plug-and-play facile conjugation of ligands that would allow rapid development of a wide variety of specific cell-depleting nanotherapeutics. Overall, these results demonstrated the synthesis and characterization of a novel class of immunomodulatory nanotherapeutics, and they offer a promising platform tool for treating malignancies, infectious diseases, and other immune disorders[6].

8.1.3 Specific Aim 3: Evaluate the effect of systemic immunomodulation on the immune system status and bone regeneration in vivo following trauma.

In Chapter 7, we investigated the role of a systemic immunomodulatory therapeutic targeting MDSCs on systemic immune function and local bone regeneration in conjunction with a local treatment strategy (BMP-2). While SNAbs were able to deplete all MDSCs in a pre-clinical rat infected trauma model, SNAbs only depleted granulocytic MDSCs (G-MDSCs) in a pre-clinical rat composite trauma model. Despite a decrease in G-MDSCs, there was a large significant increase in monocytic MDSCs (M-MDSCs) in these animals. Likely due to this explosion in M-MDSCs, SNAb-treated rats exhibited decreased bone

regeneration at 6 weeks post-treatment compared to untreated rats. Investigations into the differences in MDSC depletion in infected trauma versus composite trauma rats revealed differing S100A8/A9 expression, the target molecule of the SNAbs. S100A8/A9 had similar expression across MDSC and neutrophil clusters in the infection model, whereas in the composite trauma model, S100A8/A9 expression was highest in neutrophil clusters, suggesting flawed MDSC targeting using SNAbs in the composite trauma model. This study highlighted the complexities of targeting MDSC populations that can exhibit different phenotypes depending on the disease or injury model, and it re-confirmed the relationship between higher levels of MDSCs and poor healing. Further work will be essential to better understand key markers of MDSCs in different models and species and how improved and specific targeting of MDSCs in these models impacts treatment outcomes.

8.2 Future Directions

8.2.1 MDSC Depletion in Mycobacterium Tuberculosis *Infections*

Perhaps not surprisingly, myeloid-derived suppressor cells (MDSCs) are a common feature of aberrant immune responses in multiple other diseases and immune disorders in addition to the role they play in post-traumatic systemic immune dysregulation and immunosuppression. In particular, MDSCs have become a recent area of interest in *Mycobacterium tuberculosis* (Mtb) infections where they contribute to the immunosuppressive environment, hindering T-cell mediated adaptive immune responses and contributing to tuberculosis (TB) progression (316,376). MDSCs have been identified at the site of infection, and MDSC accumulation within the lung has been correlated with

heightened TB lethality and increases in immunosuppressive markers (377,378). Synthetic nanoparticle antibodies (SNAbs) could be particularly useful for targeting MDSCs, reversing the immunosuppressive environment and facilitating adaptive immune responses to improve clearance of the TB infection.

While previous work in this thesis has delivered SNAbs systemically, a more targeted delivery of SNAbs within the lung could be more efficacious to specifically disrupt the immunosuppressive environment at the site of TB infection. Therefore, we conducted *in vivo* imaging of particles delivered intratracheally in mice to confirm that SNAbs can be delivered locally to the lung. Streptavidin coated gold nanoparticles (non-Janus) were incubated with 100x molar excess of Biotin-Cy5.5 overnight at 4C. Particles were then washed via centrifugation and resuspended in 1X sterile PBS. SNAbs were then delivered intratracheally to C57Bl/6 mice and images were taken at 6 hours, 24 hours, and 48 hours. There was evidence of SNAbs in the lungs at all timepoints, although by 48 hours, SNAbs were only present in 2 out of 3 mice (Figure 8.1). Following intratracheal delivery, SNAbs were not present in the spleen, liver, or kidney, and minimal particles were visualized in the stomach at 6 hours which were then cleared by 24 hours (Figure 8.2).

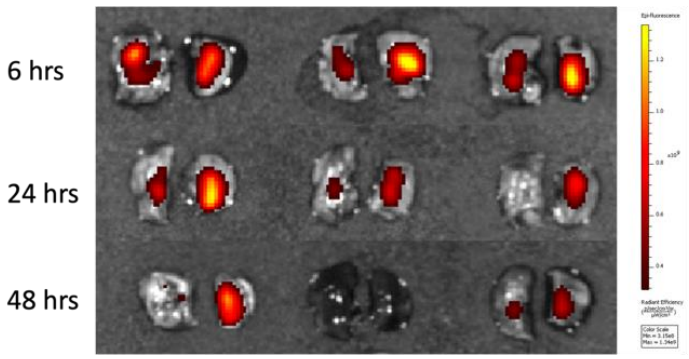

Figure 8.1. Preliminary Intratracheal Delivery of Gold Nanoparticles (AuNPs) to the Lungs.

Cy5 functionalized gold nanoparticles (AuNPs) were delivered intratracheally to the lung of C57Bl/6 mice. IVIS imaging of excised lungs was conducted at 6 hours, 24 hours, and 48 hours post-delivery (n=3 mice per timepoint).

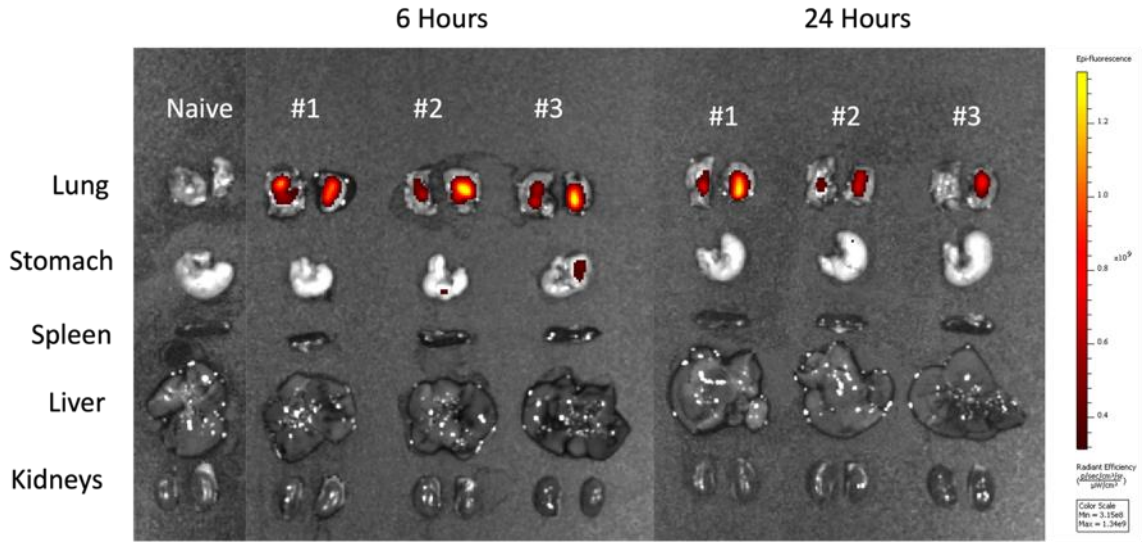

Figure 8.2. Preliminary Intratracheal Delivery of Gold Nanoparticles (AuNPs) to Various Organs.
Cy5 functionalized gold nanoparticles (AuNPs) were delivered intratracheally to C57Bl/6 mice. IVIS imaging of excised organs, including the lung, stomach, spleen, liver, and kidneys, was conducted at 6 hours and 24 hours post-delivery (n=3 mice per timepoint).

After confirming that we could successfully deliver SNAbs intratracheally to the lung, we next wanted to confirm that SNAbs could target TB-derived MDSCs. Murine bone-marrow derived TB MDSCs were stimulated by incubating bone-marrow derived cells with 10ug/mL of Mtb cell wall for 4 days. The cell wall components stimulate proliferation of immunosuppressive MDSCs in an *in vitro* environment. Macrophages and bone-marrow derived TB MDSCs were then co-cultured for 24 hours with or without SNAbs. Preliminary results show that SNAbs can successfully deplete both granulocytic (Ly6G) and monocytic (Ly6Chi) MDSCs, in particular the CD115+ subsets (Figure 8.3).

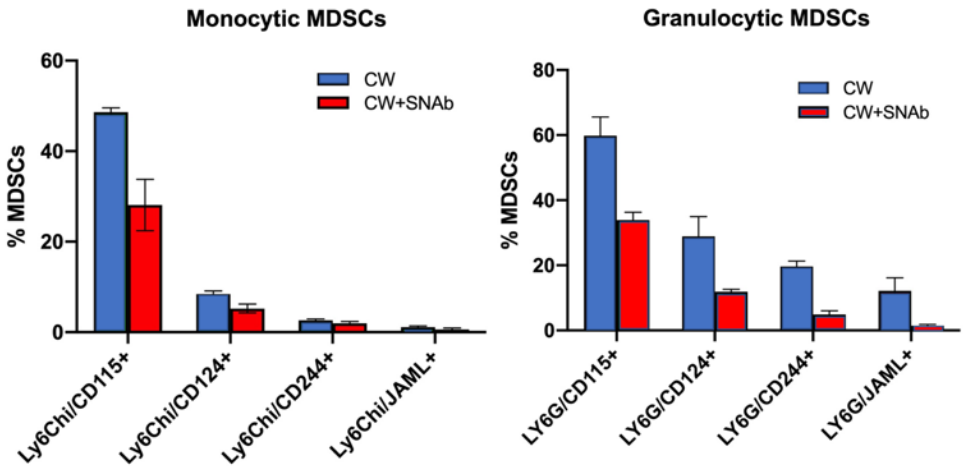

Figure 8.3. Preliminary *In Vitro* Depletion of Tuberculosis (TB) MDSCs.
Bone marrow-derived MDSCs were cultured with 10ug/mL of *Mycobacterium tuberculosis* cell wall (CW) for 4 days. These TB MDSCs were then incubated for 24 hours with macrophages and with or without synthetic nanoparticle antibodies (SNAbs). SNAb treatment resulted in decreased monocytic and granulocytic MDSCs. Data collected in collaboration with Hedwin Kitdorlang Dkhar in Dr. Jyothi Rengarajan's lab at Emory University.

Lastly, we conducted a preliminary *in vivo* experiment to determine the ability of SNAbs to deplete MDSCs in a mouse Mtb infection model. C57Bl/6 mice were treated with 4 doses of SNAbs at Days 15, 17, 19, and 21 following Mtb infection and compared to treatment with anti-Ly6G antibody. SNAbs were successfully able to deplete monocytic MDSCs (Figure 8.4); however, granulocytic MDSCs actually increased following SNAb treatment. In contrast, the anti-Ly6G antibody was able to deplete only the granulocytic SNAbs and not the monocytic MDSCs. Treatment with either the SNAbs or the anti-Ly6G antibody did not result in decreased bacterial load in the lung (Figure 8.5A). Despite no difference in bacterial load, SNAbs still show promise as an immunomodulatory treatment strategy for TB with increases in interstitial macrophages following SNAb treatment (Figure 8.5B). Better targeting of both granulocytic and monocytic MDSCs by SNAbs could potentially lead to improved outcomes and lower disease burden. Another interesting

option could be to use a combination treatment with both SNAbs and anti-Ly6G antibody to try and achieve synergistic depletion that may also improve outcomes and lower disease burden.

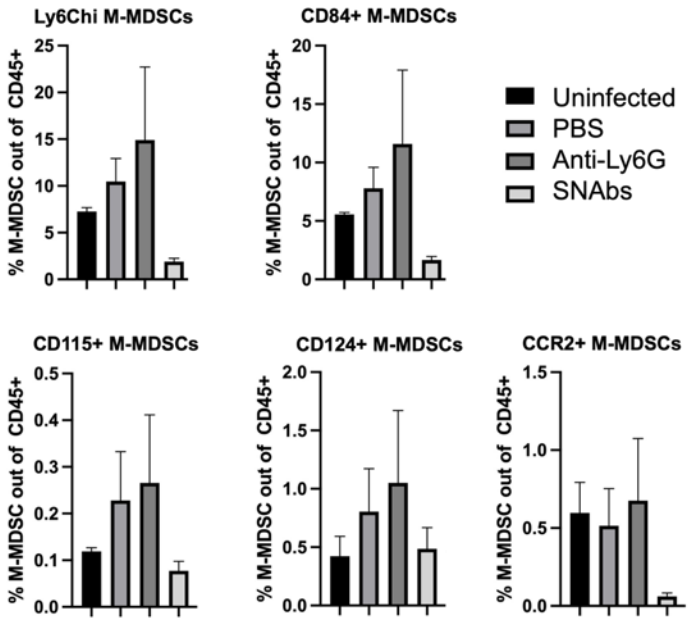

Figure 8.4. Preliminary *In Vivo* Monocytic MDSC (M-MDSC) Depletion in a Tuberculosis Mouse Model.
PBS, anti-Ly6G antibody, or SNAbs were delivered to C57Bl/6 *Mycobacterium tuberculosis* (Mtb) infected mice at days 15, 17, 19, and 21 post-infection. MDSCs in the lung were assessed using flow cytometry, including all monocytic MDSCs (M-MDSCs, Ly6Chi) and CD84, CD115, CD124, and CCR2 M-MDSC subsets. Lungs from uninfected naïve mice were used as a control (n=4 mice per group). Data collected in collaboration with Hedwin Kitdorlang Dkhar in Dr. Jyothi Rengarajan's lab at Emory University.

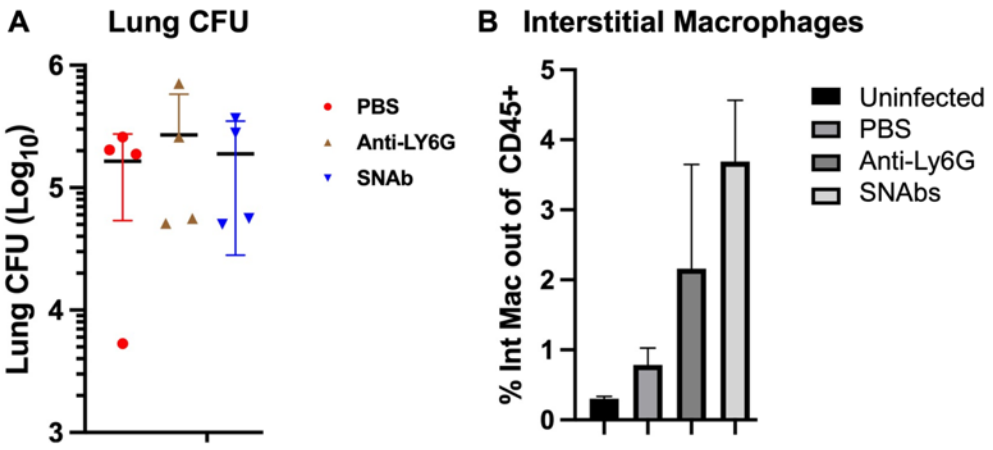

Figure 8.5. Preliminary *In Vivo* Changes to the Lung Environment Following Immunomodulatory Treatment in the Tuberculosis (TB) Model.
A) Lung CFU of TB C57Bl/6 mice following PBS, anti-Ly6G, or SNAb treatment at days 15, 17, 19, and 21 post-infection. B) Percentage of interstitial macrophages out of the CD45+ population in the lungs following PBS, anti-Ly6G, or SNAb treatment at days 15, 17, 19, and 21 post-infection. Lungs from uninfected naïve mice were used as a control (n=4 mice per group). Data collected in collaboration with Hedwin Kitdorlang Dkhar in Dr. Jyothi Rengarajan's lab at Emory University.

Overall, SNAbs could be useful in targeting aberrant myeloid immune populations following Mtb infection. Because of the expansive and complex role played by the immune system, SNAbs have endless applications as an immunomodulatory therapeutic. Appropriate targeting will need to be evaluated with each disease and model.

8.2.2 Improved Understanding of MDSC Markers in Different Models and Diseases

As exemplified in Chapter 7, MDSC populations between different trauma models experience nuanced phenotypic differences based on the expression levels of various immunosuppressive genes, in particular S100A8/A9. While subtle, these changes seem significant enough that SNAb treatment resulted in two drastically different responses between the infected trauma model and the composite trauma model. An improved understanding of MDSC markers across different models and diseases could be essential

for a robust and uniform MDSC depletion response. This could be accomplished by identifying a) MDSC markers that are applicable across multiple different models and diseases, or b) disease specific MDSC markers that result in enhanced MDSC depletion within a specific model. Based on data from this thesis, scenario b seems the most likely way to accomplish robust MDSC depletion.

Targeted MDSC markers in different models and species can be found similar to the way the G3 and cp33 peptides were discovered: phage display screening (341,379). This method allows for identification of a peptide sequence that can specifically bind to the target cells of interest with minimal binding to other cell types without needing to identify specific surface markers. The SNAb platform design facilitates easy substitution of any targeting peptides as long as they can be functionalized to bind to the free streptavidin or the available thiol groups on the surface of the nanoparticles.

In addition, to successfully target both monocytic and granulocytic MDSCs, it may be useful to co-deliver multiple SNAbs with different targeting peptides to ensure complete depletion of both subsets of immunosuppressive MDSCs. As exhibited in Chapter 7, depletion of only the granulocytic MDSCs did not result in any benefit to healing and the associated increase in monocytic MDSCs actually resulted in decreased bone regeneration compared to the untreated group.

Overall, while SNAbs offer significant improvements to target and deplete MDSCs, there is still further work that could be done to enhance specificity. A better understanding of the development of the immunosuppressive MDSC phenotype in response to different diseases is needed, including in response to trauma, burn, sepsis, infection, cancer, and

tuberculosis. This information is essential to attempt to treat the aberrant myeloid immune responses and restore immune homeostasis, ultimately decreasing disease burden and improving patient healing.

8.2.3 Co-Delivery of T Cell-Stimulating Therapeutics

MDSCs are known to contribute to immune dysregulation and immunosuppression by potently inhibiting normal T cell function, hindering the pro-healing response after injury and preventing clearance of infection and tumor cells. T cells utilize the amino acids L-arginine and cysteine to promote their activation, proliferation, and survival during an immune response. However, MDSC expression of arginase-1 results in depletion of L-arginine and high rates of cysteine consumption suppress T cell function (173,174,380). In Chapter 3, this work has shown that SNAbs are able to successfully target and deplete MDSCs and that this in turn enhances T cell proliferation in response to stimulation *in vitro*. However, SNAb treatment *in vivo* did not result in an increase in systemic levels of T cells, even when systemic MDSC levels were decreased. Further work is required to better understand the T cell response to *in vivo* MDSC depletion, and based on current results, an additional T cell-stimulating therapeutic may be required to increase T cell number and function. In order to restore immune homeostasis, it is important that both MDSC and T cell levels are restored to normal levels.

Preliminary work has investigated the co-delivery of the amino acids L-arginine and N-acetylcysteine with SNAbs. It is hypothesized that the combined intervention will result in synergistic therapeutic effects and improve healing following severe musculoskeletal trauma. A T cell proliferation assay was used to assess successful delivery

of SNAbs, amino acids, or the co-delivery of SNAbs + amino acids. PBMCs were isolated from infected trauma rats and a fraction enhanced for MDSCs was further isolated using magnetic activated cell sorting for the His48 marker. PBMCs were then co-cultured with the MDSC enhanced fraction at a 1:1 ratio and co-cultures were treated with SNAbs, amino acids, or SNAbs with amino acids. All cultures were also treated with anti-CD3 and anti-CD28 to stimulate T cell proliferation, and bromodeoxyuridine (BrdU) was added to track proliferating cells. After 48 hours, cells were collected and stained for CD3 and anti-BrdU. PBMCs cultured with MDSCs exhibited the lowest proliferation as expected, and PBMCs cultured without MDSCs showed higher proliferation (Figure 8.6). SNAbs, amino acids, and co-delivery of SNAbs and amino acids all increased T cell proliferation in the presence of MDSCs, but surprisingly did not enhance proliferation in the absence of MDSCs.

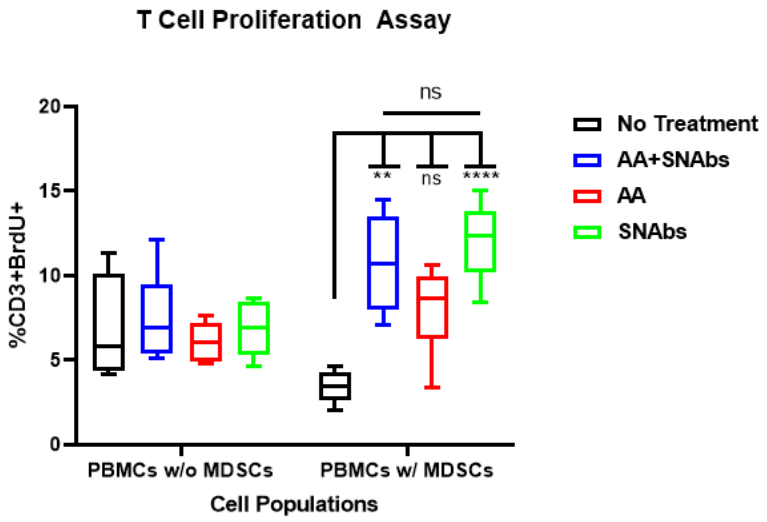

Figure 8.6. Preliminary Data on T Cell Function Following Treatment with SNAbs and Amino Acids.
T cell proliferation assay of PBMCs cultured with and without MDSCs as well as with amino acids (AA), SNAbs, or co-delivery of AAs + SNAbs. Statistical significance determined using ANOVA where $p<0.01$(**), $p<0.0001$(****), or no significance (ns); n=6 replicates. Data collected in collaboration with Clinton Smith.

This preliminary data shows promise that amino acids and SNAbs could potentially work together to deplete MDSCs and enhance T cell function although extensive further work is needed to optimize dosages, delivery methods, and timing of treatment.

REFERENCES

1. Dougherty AL, Mohrle CR, Galarneau MR, Woodruff SI, Dye JL, Quinn KH. Battlefield extremity injuries in Operation Iraqi Freedom. Injury. 2009 Jul 1;40(7):772–7.

2. Banerjee M, Bouillon B, Shafizadeh S, Paffrath T, Lefering R, Wafaisade A. Epidemiology of extremity injuries in multiple trauma patients. Injury. 2013 Aug 1;44(8):1015–21.

3. Binkowska AM, Michalak G, Slotwiński R. Current views on the mechanisms of immune responses to trauma and infection. Cent Eur J Immunol. 2015;40(2):206–16.

4. Harris AM, Althausen PL, Kellam J, Bosse MJ, Castillo R. Complications following limb-threatening lower extremity trauma. J Orthop Trauma. 2009 Jan;23(1):1–6.

5. Gentile LF, Cuenca AG, Efron P a, Ang D. Persistent inflammation and immunosuppression: A common syndrome and new horizon for surgical intensive care. J Trauma Acute Care Surg. 2012;72(6):1491–501.

6. Kimura F, Shimizu H, Yoshidome H, Ohtsuka M, Miyazaki M. Immunosuppression following surgical and traumatic injury. Surg Today. 2010;40(9):793–808.

7. Cuenca AG, Delano MJ, Kelly-Scumpia KM, Moreno C, Scumpia PO, Laface DM, et al. A paradoxical role for myeloid-derived suppressor cells in sepsis and trauma. Mol Med. 2011;17(3–4):281–92.

8. Tschoeke SK, Ertel W. Immunoparalysis after multiple trauma. Injury. 2007;38(12):1346–57.

9. O'Brien EM, Risser GE, Spiller KL. Sequential drug delivery to modulate macrophage behavior and enhance implant integration. Adv Drug Deliv Rev. 2019 May 16;

10. Stahel PF, Smith WR, Moore EE. Role of biological modifiers regulating the immune response after trauma. Injury. 2007;38(12):1409–22.

11. Sadtler K, Estrellas K, Allen BW, Wolf MT, Fan H, Tam AJ, et al. Developing a pro-regenerative biomaterial scaffold microenvironment requires T helper 2 cells. Science (80-). 2016 Apr 15;352(6283):366–70.

12. Spitzer MH, Carmi Y, Reticker-Flynn NE, Kwek SS, Madhireddy D, Martins MM, et al. Systemic Immunity Is Required for Effective Cancer Immunotherapy. Cell. 2017 Jan 26;168(3):487-502.e15.

13. Nahm NJ, Vallier HA. Timing of definitive treatment of femoral shaft fractures in patients with multiple injuries. J Trauma Acute Care Surg. 2012 Nov;73(5):1046–63.

14. Andruszkow H, Probst C, Grü O, Krettek C, Hildebrand F. Does Additional Head Trauma Affect the Long-term Outcome After Upper Extremity Trauma in Multiple Traumatized Patients: Is There an Additional Effect of Traumatic Brain Injury? 2013;

15. Forghani P, Khorramizadeh MR, Waller EK. Silibinin inhibits accumulation of myeloid-derived suppressor cells and tumor growth of murine breast cancer. Cancer Med. 2014 Apr;3(2):215–24.

16. Samaranayake H, Wirth T, Schenkwein D, Räty JK, Ylä-Herttuala S. Challenges in monoclonal antibody-based therapies. Ann Med. 2009 Jan 8;41(5):322–31.

17. Shaughnessy AF. Monoclonal antibodies: magic bullets with a hefty price tag. BMJ. 2012 Dec 12;345:e8346.

18. Smith WR, Stahel PF, Suzuki T, Gabrielle P. Chapter 2. Musculoskeletal Trauma Surgery. In: Skinner HB, McMahon PJ, editors. Current Diagnosis & Treatment in Orthopedics, 5e. New York, NY: The McGraw-Hill Companies; 2014.

19. Dharap SB, Ekhande SV. An observational study of incidence, risk factors & outcome of systemic inflammatory response & organ dysfunction following major trauma. Indian J Med Res. 2017;146(3):346–53.

20. Islam MN, Bradley BA, Ceredig R. Sterile post-traumatic immunosuppression. Clin Transl Immunol. 2016 Apr 29;5(4):e77.

21. Vantucci CE, Roy K, Guldberg RE. Immunomodulatory strategies for immune

dysregulation following severe musculoskeletal trauma. J Immunol Regen Med. 2018 Sep 1;2:21–35.

22. Giannoudis P V., Faour O, Goff T, Kanakaris N, Dimitriou R. Masquelet technique for the treatment of bone defects: Tips-tricks and future directions. Vol. 42, Injury. Elsevier; 2011. p. 591–8.

23. Wang W, Yeung KWK. Bone grafts and biomaterials substitutes for bone defect repair: A review. Bioact Mater. 2017 Dec 1;2(4):224–47.

24. Balogh ZJ, Reumann MK, Gruen RL, Mayer-Kuckuk P, Schuetz MA, Harris IA, et al. Advances and future directions for management of trauma patients with musculoskeletal injuries. Lancet. 2012;380(9847):1109–19.

25. J. C.-L. CL, H. C. C, J.E. F. F. Osteoimmunology - The hidden immune regulation of bone. Autoimmun Rev. 2009;8(3):250–5.

26. Hirsiger S, Simmen HP, Werner CML, Wanner GA, Rittirsch D. Danger signals activating the immune response after trauma. Mediators Inflamm. 2012;2012.

27. Xiao W, Mindrinos MN, Seok J, Cuschieri J, Cuenca AG, Gao H, et al. A genomic storm in critically injured humans. J Exp Med. 2011 Dec 19;208(13):2581–90.

28. Vanzant EL, Lopez CM, Ozrazgat-Baslanti T, Ungaro R, Davis R, Cuenca AG, et al. Persistent Inflammation, Immunosuppression and Catabolism Syndrome after Severe Blunt Trauma. J Trauma Acute Care Surg. 2014;76(1):21–30.

29. Livingston DH, Appel SH, Wellhausen SR, Sonnenfeld G, Polk HC. Depressed Interferon Gamma Production and Monocyte HLA-DR Expression After Severe Injury. Arch Surg. 1988;123(11):1309–12.

30. Delano MJ, Scumpia PO, Weinstein JS, Coco D, Nagaraj S, Kelly-Scumpia KM, et al. MyD88-dependent expansion of an immature GR-1(+)CD11b(+) population induces T cell suppression and Th2 polarization in sepsis. J Exp Med. 2007;204(6):1463–74.

31. Henrich D, Maier M, Relja B, Trendafilov P, Schiessling S, Wirth M, et al. Significant decline of peripheral myeloid dendritic cells following multiple trauma. J Surg Res. 2009;154(2):239–45.

32. Hotchkiss RS, Monneret G, Payen D. Sepsis-induced immunosuppression: from cellular dysfunctions to immunotherapy. Nat Rev Immunol. 2013;13(12):862–74.

33. Takayanagi H. Osteoimmunology and the effects of the immune system on bone. Nat Rev Rheumatol. 2009;5(12):667–76.

34. Li Y, Toraldo G, Li A, Yang X, Zhang H, Qian W-P, et al. B cells and T cells are critical for the preservation of bone homeostasis and attainment of peak bone mass in vivo. Blood. 2007 May 1;109(9):3839–48.

35. Khassawna T El, Serra A, Bucher CH, Petersen A, Schlundt C, Könnecke I, et al. T lymphocytes influence the mineralization process of bone. Front Immunol. 2017 May 24;8(MAY):562.

36. Makarenkova VP, Bansal V, Matta BM, Perez LA, Ochoa JB. CD11b+/Gr-1+ Myeloid Suppressor Cells Cause T Cell Dysfunction after Traumatic Stress. J Immunol. 2006 Feb 15;176(4):2085–94.

37. Albertsmeier M, Quaiser D, von Dossow-Hanfstingl V, Winter H, Faist E, Angele MK. Major surgical trauma differentially affects T-cells and APC. Innate Immun. 2014;

38. Dziedzic T, Slowik A, Szczudlik A. Nosocomial infections and immunity: lesson from brain-injured patients. Crit Care. 2004;8(4):266–70.

39. Scumpia PO, Kelly-Scumpia KM, Delano MJ, Weinstein JS, Cuenca AG, Al-Quran S, et al. Cutting Edge: Bacterial Infection Induces Hematopoietic Stem and Progenitor Cell Expansion in the Absence of TLR Signaling. J Immunol. 2010;184(5):2247–51.

40. Ueda Y, Kondo M, Kelsoe G. Inflammation and the reciprocal production of granulocytes and lymphocytes in bone marrow. J Exp Med. 2005;201(11):1771–80.

41. Visnjic D, Kalajzic I, Gronowicz G, Aguila HL, Clark SH, Lichtler AC, et al. Conditional Ablation of the Osteoblast Lineage in Col2.3Δtk Transgenic Mice. J Bone Miner Res. 2001 Dec 1;16(12):2222–31.

42. Mathias B, Delmas AL, Ozrazgat-Baslanti T, Vanzant EL, Szpila BE, Mohr AM, et al. Human myeloid-derived suppressor cells are associated with chronic immune

suppression after severe sepsis/septic shock. Ann Surg. 2017 Apr;265(4):827–34.

43. Lai D, Qin C, Shu Q. Myeloid-derived suppressor cells in sepsis. Biomed Res Int. 2014;2014.

44. Zhu X, Pribis JP, Rodriguez PC, Morris SM, Vodovotz Y, Billiar TR, et al. The Central Role of Arginine Catabolism in T-Cell Dysfunction and Increased Susceptibility to Infection After Physical Injury. Ann Surg. 2014 Jan;259(1):171–8.

45. Condamine T, Gabrilovich DI. Molecular mechanisms regulating myeloid-derived suppressor cell differentiation and function. Trends Immunol. 2011 Jan 1;32(1):19–25.

46. Tanaka A, Sakaguchi S. Regulatory T cells in cancer immunotherapy. Cell Res. 2017 Jan 20;27(1):109–18.

47. Kumar V, Patel S, Tcyganov E, Gabrilovich DI. The Nature of Myeloid-Derived Suppressor Cells in the Tumor Microenvironment. Trends Immunol. 2016 Mar 1;37(3):208–20.

48. Nakashima T, Takayanagi H. Osteoimmunology: Crosstalk between the immune and bone systems. J Clin Immunol. 2009;29(5):555–67.

49. Yates D, Farrell B, Teasdale G, Sandercock P, Roberts I. Corticosteroids in head injury-the CRASH trial. I'Accid Emerg Med. 1999;16:83–90.

50. Buchman AL. Side Effects of Corticosteroid Therapy. J Clin Gastroenterol. 2001 Oct 1;33(4):289–94.

51. Cui R, Rekasi H, Hepner-Schefczyk M, Fessmann K, Petri RM, Bruderek K, et al. Human mesenchymal stromal/stem cells acquire immunostimulatory capacity upon cross-talk with natural killer cells and might improve the NK cell function of immunocompromised patients. Stem Cell Res Ther. 2016 Jul 7;7(1):88.

52. Lendemans S, Kreuzfelder E, Waydhas C, Schade FU, Flohé S. Infl ammation Research Differential immunostimulating effect of Granulocyte- macrophage colony-stimulating factor (GM-CSF), Granulocyte colony-stimulating factor (G-CSF) and Interferon g (IFNg) after severe trauma. Infl amm res. 2007;5607:38–44.

53. de Metz J, Sauerwein HP, Gouma DJ, Out TA, Reijneke RM, Hack CE, et al. Interferon-gamma administration to patients after major surgery influences cellular immunity without pro-inflammatory response. Eur J Clin Invest. 2002;32(10):787–9.

54. Flohé S, Börgermann J, Lim L, Schade F-U. Interferon-γ counteracts reduced endotoxin responsiveness of whole blood following trauma and cardiopulmonary bypass. J Endotoxin Res. 2000 Dec 3;6(6):431–6.

55. Longbottom ER, Torrance HDT, Owen HC, Fragkou PC, Hinds CJ, Pearse RM, et al. Features of Postoperative Immune Suppression Are Reversible With Interferon Gamma and Independent of Interleukin-6 Pathways. Ann Surg. 2016;264(2):370–7.

56. Perry SE, Mostafa SM, Wenstone R, Shenkin A, McLaughlin PJ. Is low monocyte HLA-DR expression helpful to predict outcome in severe sepsis? Intensive Care Med. 2003 Aug 1;29(8):1245–52.

57. Nierhaus A, Montag B, Timmler N, Frings DP, Gutensohn K, Jung R, et al. Reversal of immunoparalysis by recombinant human granulocyte-macrophage colony-stimulating factor in patients with severe sepsis. Intensive Care Med. 2003;29(4):646–51.

58. Flohé S, Lendemans S, Selbach C, Waydhas C, Ackermann M, Schade FU, et al. Effect of granulocyte-macrophage colony-stimulating factor on the immune response of circulating monocytes after severe trauma. Crit Care Med. 2003 Oct;31(10):2462–9.

59. M.K. S, S.K. B, S. M, D.N. R, A. S. To evaluate the effect of growth factors (EPO, IL3,GM-CSF) on in-vitro hematopoietic stem cell growth/differentiation following trauma hemorrhagic shock. Cytotherapy. 2014 Apr 1;16(4):S54.

60. Mensah KA, Li J, Schwarz EM. The emerging field of osteoimmunology. Immunol Res. 2009;45(2–3):100–13.

61. Meisel C, Schefold JC, Pschowski R, Baumann T, Hetzger K, Gregor J, et al. Granulocyte–Macrophage Colony-stimulating Factor to Reverse Sepsis-associated Immunosuppression. Am J Respir Crit Care Med. 2009 Oct 20;180(7):640–8.

62. Qin H, Lerman B, Sakamaki I, Wei G, Cha SC, Rao SS, et al. Generation of a new therapeutic peptide that depletes myeloid-derived suppressor cells in tumor-bearing

mice. Nat Med. 2014;20(6):676–81.

63. Gao F, Chiu SM, Motan DAL, Zhang Z, Chen L, Ji H-L, et al. Mesenchymal stem cells and immunomodulation: current status and future prospects. Cell Death Dis. 2016 Jan 21;7(1):e2062.

64. Polo-Corrales L, Latorre-Esteves M, Ramirez-Vick JE. Scaffold Design for Bone Regeneration.

65. Brown BN, Badylak SF. Expanded applications, shifting paradigms and an improved understanding of host–biomaterial interactions. Acta Biomater. 2013 Feb 1;9(2):4948–55.

66. Nair A, Tang L. Influence of scaffold design on host immune and stem cell responses. Semin Immunol. 2017 Feb 1;29:62–71.

67. Chen Z, Klein T, Murray RZ, Crawford R, Chang J, Wu C, et al. Osteoimmunomodulation for the development of advanced bone biomaterials. Mater Today. 2016;19(6):304–21.

68. Chen Z, Bachhuka A, Han S, Wei F, Lu S, Visalakshan RM, et al. Tuning Chemistry and Topography of Nanoengineered Surfaces to Manipulate Immune Response for Bone Regeneration Applications. ACS Nano. 2017 May 23;11(5):4494–506.

69. Vasconcelos DM, Gonçalves RM, Almeida CR, Pereira IO, Oliveira MI, Neves N, et al. Fibrinogen scaffolds with immunomodulatory properties promote in vivo bone regeneration. Biomaterials. 2016 Dec 1;111:163–78.

70. Chen Z, Bachhuka A, Wei F, Wang X, Liu G, Vasilev K, et al. Nanotopography-based strategy for the precise manipulation of osteoimmunomodulation in bone regeneration. Nanoscale. 2017 Nov 30;9(46):18129–52.

71. Boehler RM, Graham JG, Shea LD. Tissue engineering tools for modulation of the immune response. Biotechniques. 2011 Oct;51(4):239–40, 242, 244 passim.

72. Yun JK, DeFife K, Colton E, Stack S, Azeez A, Cahalan L, et al. Human monocyte/macrophage adhesion and cytokine production on surface-modified poly(tetrafluoroethylene/hexafluoropropylene) polymers with and without protein preadsorption. J Biomed Mater Res. 1995 Feb;29(2):257–68.

73. Dobrovolskaia MA, McNeil SE. Immunological properties of engineered nanomaterials. Nat Nanotechnol. 2007 Aug 29;2(8):469–78.

74. Garg K, Pullen NA, Oskeritzian CA, Ryan JJ, Bowlin GL. Macrophage functional polarization (M1/M2) in response to varying fiber and pore dimensions of electrospun scaffolds. Biomaterials. 2013 Jun;34(18):4439–51.

75. Galbraith N, Walker S, Carter J, Polk HC. Past, Present, and Future of Augmentation of Monocyte Function in the Surgical Patient. Surg Infect (Larchmt). 2016 Oct 1;17(5):563–9.

76. Becelli R, Renzi G, Perugini M, Iannetti G. Craniofacial traumas: Immediate and delayed treatment. Vol. 11, Journal of Craniofacial Surgery. 2000. p. 265–9.

77. Carr RM, Mathog RH. Early and delayed repair of orbitozygomatic complex fractures. J Oral Maxillofac Surg. 1997 Mar;55(3):253–9.

78. Dosier CR, Uhrig BA, Willett NJ, Krishnan L, Li M-TA, Stevens HY, et al. Effect of Cell Origin and Timing of Delivery for Stem Cell-Based Bone Tissue Engineering Using Biologically Functionalized Hydrogels. Tissue Eng Part A. 2015 Jan;21(1–2):156–65.

79. Galatz LM, Rothermich SY, Zaegel M, Silva MJ, Havlioglu N, Thomopoulos S. Delayed repair of tendon to bone injuries leads to decreased biomechanical properties and bone loss. J Orthop Res. 2005 Nov;23(6):1441–7.

80. Fullarton AC, Glasby MA, Lawson GM. Immediate and delayed nerve repair using freeze-thawed muscle allografts: Associated long-bone fracture. J Hand Surg Eur Vol. 1998 Jun 29;23(3):360–4.

81. Gruber R, Koch H, Doll BA, Tegtmeier F, Einhorn TA, Hollinger JO. Fracture healing in the elderly patient. Exp Gerontol. 2006 Nov 1;41(11):1080–93.

82. Peterson BE, Jiwanlal A, Della Rocca GJ, Crist BD. Orthopedic Trauma and Aging: It Isn’t Just About Mortality.

83. Vester H, Huber-Lang MS, Kida Q, Scola A, van Griensven M, Gebhard F, et al. The immune response after fracture trauma is different in old compared to young patients. Immun Ageing. 2014 Dec 11;11(1):20.

84. Zhang H, Sun T, Liu Z, Zhang J, Wang X, Liu J. Systemic inflammatory responses and lung injury following hip fracture surgery increases susceptibility to infection in aged rats. Mediators Inflamm. 2013 Sep 12;2013:536435.

85. Lammens J, Maréchal M, Geris L, Van der Aa J, Van Hauwermeiren H, Luyten FP, et al. Warning About the Use of Critical-Size Defects for the Translational Study of Bone Repair: Analysis of a Sheep Tibial Model. Tissue Eng Part C Methods. 2017 Nov 1;23(11):ten.tec.2017.0147.

86. Aalami OO, Nacamuli RP, Lenton KA, Cowan CM, Fang TD, Fong KD, et al. Applications of a mouse model of calvarial healing: Differences in regenerative abilities of juveniles and adults. Plast Reconstr Surg. 2004 Sep;114(3):713–20.

87. Lopas LA, Belkin NS, Mutyaba Bs PL, Gray F, Hankenson Dvm KD, Ahn J. Fractures in Geriatric Mice Show Decreased Callus Expansion and Bone Volume. 2014;

88. Dodson SA, Bernard GW, Kenney EB, Carranza FA. In Vitro Comparison of Aged and Young Osteogenic and Hemopoietic Bone Marrow Stem Cells and Their Derivative Colonies. J Periodontol. 1996 Mar;67(3):184–96.

89. Mehta M, Strube P, Peters A, Perka C, Hutmacher D, Fratzl P, et al. Influences of age and mechanical stability on volume, microstructure, and mineralization of the fracture callus during bone healing: Is osteoclast activity the key to age-related impaired healing? Bone. 2010 Aug;47(2):219–28.

90. Meyer MH, Meyer RA. Altered expression of mitochondrial genes in response to fracture in old rats. Acta Orthop. 2006;77(6):944–51.

91. Meyer MH, Meyer RA. Genes with Greater up-regulation in the fracture callus of older rats with delayed healing. J Orthop Res. 2007;25(4):488–94.

92. Meyer MH, Etienne W, Meyer RA. Altered mRNA expression of genes related to nerve cell activity in the fracture callus of older rats: A randomized, controlled, microarray study. BMC Musculoskelet Disord. 2004 Dec 3;5(1):24.

93. Meyer RA, Desai BR, Heiner DE, Fiechtl J, Porter S, Meyer MH. Young, adult, and old rats have similar changes in mRNA expression of many skeletal genes after fracture despite delayed healing with age. J Orthop Res. 2006;24(10):1933–44.

94. Meyer R a, Meyer MH, Tenholder M, Wondracek S, Wasserman R, Garges P. Gene expression in older rats with delayed union of femoral fractures. J Bone Joint Surg Am. 2003;85-A:1243–54.

95. Ode A, Duda GN, Geissler S, Pauly S, Ode J-E, Perka C, et al. Interaction of age and mechanical stability on bone defect healing: an early transcriptional analysis of fracture hematoma in rat. PLoS One. 2014;9(9):e106462.

96. Wang J, Geiger H, Rudolph KL. Immunoaging induced by hematopoietic stem cell aging. Curr Opin Immunol. 2011 Aug 1;23(4):532–6.

97. Gibon E, Loi F, Córdova LA, Pajarinen J, Lin T, Lu L, et al. Aging Affects Bone Marrow Macrophage Polarization: Relevance to Bone Healing HHS Public Access. 2016;2(2):98–104.

98. Schmidt-Bleek K, Marcucio R, Duda G. Future Treatment Strategies for Delayed Bone Healing. J Am Acad Orthop Surg. 2016;24(10):e134–5.

99. Brattström O, Larsson E, Granath F, Riddez L, Bell M, Oldner A. Time dependent influence of host factors on outcome after trauma. Eur J Epidemiol. 2012 Mar 26;27(3):233–41.

100. Rettew JA, Marriott I, Huet YM. Sex differences in innate immune responses to bacterial pathogens. In: Sex Hormones and Immunity to Infection. Berlin, Heidelberg: Springer Berlin Heidelberg; 2010. p. 123–46.

101. Crisostomo PR, Wang M, Herring CM, Markel TA, Meldrum KK, Lillemoe KD, et al. GENDER DIFFERENCES IN INJURY INDUCED MESENCHYMAL STEM CELL APOPTOSIS, EXPRESSION OF VEGF, TNF, AND IL-6 AND ABROGATION VIA TNFR1 ABLATION.

102. Kovats S, Carreras E. Regulation of dendritic cell differentiation and function by estrogen receptor ligands. Vol. 252, Cellular Immunology. Academic Press; 2008. p. 81–90.

103. Frink M, Pape HC, Van Griensven M, Krettek C, Chaudry IH, Hildebrand F. Influence of sex and age on mods and cytokines after multiple injuries. Shock. 2007 Feb;27(2):151–6.

104. Oberholzer A, Keel M, Zellweger R, Steckholzer U, Trentz O, Ertel W. Incidence of Septic Complications and Multiple Organ Failure in Severely Injured Patients Is Sex Specific. J Trauma Inj Infect Crit Care. 2000 May;48(5):932–7.

105. Wohltmann, Christopher D. MD; Spain, David A. MD; Carrillo, Eddy H. MD; Boaz, Phillip W. RN; ALuchette, Fred MD; Kearney PAM. DOES GENDER EFFECT OUTCOME IN TRAUMA PATIENTS? Crit Care Med. 1999;27(1).

106. Gregory MS, Faunce DE, Duffner LA, Kovacs EJ. Gender difference in cell-mediated immunity after thermal injury is mediated , in part , by elevated levels of interleukin-6. 2000;67(March):319–26.

107. Mehta M, Strube P, Perka C, Duda GN. Influence of gender and mechanical stability on bone defect healing: Males show a stronger biological response than females. Bone. 2009 Jun 1;44(Supplement 2):S264–S264.

108. Meszaros LB, Usas A, Cooper GM, Huard J. Effect of Host Sex and Sex Hormones on Muscle-Derived Stem Cell-Mediated Bone Formation and Defect Healing.

109. Mehta M, Duda GN, Perka C, Strube P. Influence of Gender and Fixation Stability on Bone Defect Healing in Middle-aged Rats: A Pilot Study. 2011;

110. Yao W, Lay Y-AE, Kot A, Liu R, Zhang H, Chen H, et al. Improved Mobilization of Exogenous Mesenchymal Stem Cells to Bone for Fracture Healing and Sex Difference. Stem Cells. 2016 Oct 1;34(10):2587–600.

111. Strube P, Mehta M, Baerenwaldt A, Trippens J, Wilson CJ, Ode A, et al. Sex-specific compromised bone healing in female rats might be associated with a decrease in mesenchymal stem cell quantity. Bone. 2009 Dec 1;45(6):1065–72.

112. Tebby J, Lecky F, Edwards A, Jenks T, Bouamra O, Dimitriou R, et al. Outcomes of polytrauma patients with diabetes mellitus.

113. Khalil H, Cullen M, Chambers H, Carroll M, Walker J. Elements affecting wound healing time: An evidence based analysis. Wound Repair Regen. 2015 Jul 1;23(4):550–6.

114. Zura R, Mehta S, Della Rocca GJ, Jones J, Steen RG. A cohort study of 4,190 patients treated with low-intensity pulsed ultrasound (LIPUS): findings in the

elderly versus all patients. BMC Musculoskelet Disord. 2015;16:45.

115. Campos JM de, Prati AJ, Cirano FR, Pimentel SP, Pastore GP, Pecorari VG, et al. Smoking Modulates Gene Expression of Type I Collagen, Bone Sialoprotein, and Osteocalcin in Human Alveolar Bone. J Oral Maxillofac Surg. 2015 Nov 1;73(11):2123–31.

116. Desai KH, Tan CS, Leek JT, Maier R V, Tompkins RG, Storey JD. Dissecting inflammatory complications in critically injured patients by within-patient gene expression changes: A longitudinal clinical genomics study. PLoS Med. 2011;8(9).

117. Fern KT, Smith JT, Zee B, Lee A, Borschneck D, Pichora DR. Trauma patients with multiple extremity injuries: resource utilization and long-term outcome in relation to injury severity scores. J Trauma. 1998 Sep;45(3):489–94.

118. Kapur MM, Jain P, Gidh M. The effect of trauma on serum C3 activation and its correlation with injury severity score in man. J Trauma. 1986;26(5):464–6.

119. Hurtgen BJ, Ward CL, Garg K, Pollot BE, Goldman SM, McKinley TO, et al. Severe muscle trauma triggers heightened and prolonged local musculoskeletal inflammation and impairs adjacent tibia fracture healing. J Musculoskelet Neuronal Interact. 2016 Jun 1;16(2):122–34.

120. Garg K, Ward CL, Hurtgen BJ, Wilken JM, Stinner DJ, Wenke JC, et al. Volumetric muscle loss: Persistent functional deficits beyond frank loss of tissue. J Orthop Res. 2015 Jan 1;33(1):40–6.

121. Willett NJ, Li M-TA, Uhrig BA, Boerckel JD, Huebsch N, Lundgren TS, et al. Attenuated Human Bone Morphogenetic Protein-2–Mediated Bone Regeneration in a Rat Model of Composite Bone and Muscle Injury. Tissue Eng Part C Methods. 2013;19(4):316–25.

122. Utvåg SE, Grundnes O, Rindal DB, Reikerås O. Influence of extensive muscle injury on fracture healing in rat tibia. J Orthop Trauma. 2003 Jul;17(6):430–5.

123. Uhrig BA, Clements IP, Boerckel JD, Huebsch N, Bellamkonda R V., Guldberg RE. Characterization of a composite injury model of severe lower limb bone and nerve trauma. J Tissue Eng Regen Med. 2014 Jun;8(6):432–41.

124. Cheng L, Xu J, Chai Y, Wang C, Han P. Dynamic changes in trauma-induced myeloid-derived suppressor cells after polytrauma are associated with an increased susceptibility to infection. Int J Clin Exp Pathol. 2017;10(11):11063–8.

125. Keel M, Ecknauer E, Stocker R, Ungethüm U, Steckholzer U, Kenney J, et al. Different pattern of local and systemic release of proinflammatory and anti-inflammatory mediators in severely injured patients with chest trauma. J Trauma. 1996;40(6):907–12; discussion 912-4.

126. Kristiansson M, Soop M, Sundqvist KG, Soop A, Suontaka AM, Blombäck M. Local vs. systemic immune and haemostatic response to hip arthroplasty. Eur J Anaesthesiol. 1998 May;15(3):260–70.

127. Hauser CJ, Zhou X, Joshi P, Cuchens MA, Kregor P, Devidas M, et al. The Immune Microenvironment of Human Fracture/Soft-tissue Hematomas and its Relationship to Systemic Immunity. J Trauma Inj Infect Crit Care. 1997 May;42(5):895–904.

128. Horst K, Eschbach D, Pfeifer R, Relja B, Sassen M, Steinfeldt T, et al. Long-Term Effects of Induced Hypothermia on Local and Systemic Inflammation - Results from a Porcine Long-Term Trauma Model. Raju R, editor. PLoS One. 2016 May 4;11(5):e0154788.

129. Decker D, Tolba R, Springer W, Lauschke H, Hirner A, von Ruecker A. Abdominal Surgical Interventions: Local and Systemic Consequences for the Immune System—a Prospective Study on Elective Gastrointestinal Surgery1. J Surg Res. 2005 Jun;126(1):12–8.

130. Tsukamoto T, Pape HC. Animal models for trauma research: What are the options? Vol. 31, Shock. 2009. p. 3–10.

131. Abdullahi A, Amini-Nik S, Jeschke MG. Animal models in burn research. Cell Mol Life Sci. 2014 Sep;71(17):3241–55.

132. Efron PA, Mohr AM, Moore FA, Moldawer LL. The future of murine sepsis and trauma research models. J Leukoc Biol. 2015 Dec;98(6):945–52.

133. Xiong Y, Mahmood A, Chopp M. Animal models of traumatic brain injury. Nat Rev Neurosci. 2013 Feb;14(2):128–42.

134. Reichert JC, Saifzadeh S, Wullschleger ME, Epari DR, Schütz MA, Duda GN, et al. The challenge of establishing preclinical models for segmental bone defect research. Biomaterials. 2009 Apr 1;30(12):2149–63.

135. Frink M, Andruszkow H, Zeckey C, Krettek C, Hildebrand F. Experimental trauma models: An update. Vol. 2011, Journal of Biomedicine and Biotechnology. Hindawi; 2011. p. 797383.

136. Xie H, Yang F, Deng L, Luo J, Qin T, Li X, et al. The performance of a bone-derived scaffold material in the repair of critical bone defects in a rhesus monkey model. Biomaterials. 2007 Aug 1;28(22):3314–24.

137. Li Y, Chen SK, Li L, Qin L, Wang XL, Lai YX. Bone defect animal models for testing efficacy of bone substitute biomaterials. Vol. 3, Journal of Orthopaedic Translation. Elsevier; 2015. p. 95–104.

138. Oortgiesen DAW, Meijer GJ, de Vries RBM, Walboomers XF, Jansen JA. Animal Models for the Evaluation of Tissue Engineering Constructs. In: Tissue Engineering. Berlin, Heidelberg: Springer Berlin Heidelberg; 2011. p. 131–54.

139. Liu F, Chen K, Hou L, Li K, Wang D, Zhang B, et al. Determining the critical size of a rabbit rib segmental bone defect model. Regen Biomater. 2016;3(5):323–8.

140. Zhao MD, Huang JS, Zhang XC, Gui KK, Xiong M, Yin WP, et al. Construction of radial defect models in rabbits to determine the critical size defects. PLoS One. 2016;11(1).

141. Darwiche SS, Kobbe P, Pfeifer R, Kohut L, Pape H-C, Billiar T. Pseudofracture: An Acute Peripheral Tissue Trauma Model. JoVE. 2011;50.

142. Zwingenberger S, Niederlohmann E, Vater C, Rammelt S, Matthys R, Bernhardt R, et al. Establishment of a femoral critical-size bone defect model in immunodeficient mice. J Surg Res. 2013;181(1).

143. Clough BH, McCarley MR, Gregory CA. A Simple Critical-sized Femoral Defect Model in Mice. J Vis Exp. 2015;(97).

144. Manassero M, Viateau V, Matthys R, Deschepper M, Vallefuoco R, Bensidhoum M, et al. A Novel Murine Femoral Segmental Critical-Sized Defect Model

Stabilized by Plate Osteosynthesis for Bone Tissue Engineering Purposes. Tissue Eng Part C Methods. 2013;19(4):271–80.

145. Manassero M, Decambron A, Truong B, Thong H, Viateau V, Bensidhoum M, et al. Establishment of a Segmental Femoral Critical-size Defect Model in Mice Stabilized by Plate Osteosynthesis Establishment of a Segmental Femoral Critical-size Defect Model in Mice Stabilized by Plate Video Link. J Vis Exp. 2016;(11610).

146. Xing J, Jin H, Hou T, Chang Z, Luo F, Wang P, et al. Establishment of a bilateral femoral large segmental bone defect mouse model potentially applicable to basic research in bone tissue engineering. J Surg Res. 2014 Dec 1;192(2):454–63.

147. Menzel CL, Pfeifer R, Darwiche SS, Kobbe P, Gill R, Shapiro RA, et al. Models of lower extremity damage in mice: Time course of organ damage and immune response. J Surg Res. 2011;166(2):149–56.

148. Seok J, Warren HS, Cuenca AG, Mindrinos MN, Baker H V, Xu W, et al. Genomic responses in mouse models poorly mimic human inflammatory diseases. Proc Natl Acad Sci. 2013 Feb 26;110(9):3507–12.

149. Takao K, Miyakawa T. Genomic responses in mouse models greatly mimic human inflammatory diseases. Proc Natl Acad Sci. 2015 Jan 27;112(4):1167–72.

150. Yue F, Cheng Y, Breschi A, Vierstra J, Wu W, Ryba T, et al. A comparative encyclopedia of DNA elements in the mouse genome. Nature. 2014;515(7527):355–64.

151. Bosch C, Melsen B, Vargervik K. Importance of the critical-size bone defect in testing bone-regenerating materials. Vol. 9, The Journal of craniofacial surgery. 1998. p. 310–6.

152. Renaud M, Farkasdi S, Pons C, Panayotov I, Collart-Dutilleul P-Y, Taillades H, et al. A New Rat Model for Translational Research in Bone Regeneration. Tissue Eng Part C Methods. 2015;22(2):ten.tec.2015.0187.

153. Li MTA, Willett NJ, Uhrig BA, Guldberg RE, Warren GL. Functional analysis of limb recovery following autograft treatment of volumetric muscle loss in the quadriceps femoris. J Biomech. 2014;47(9):2013–21.

154. Dobek GL, Fulkerson ND, Nicholas J, Schneider BSP. Mouse model of muscle crush injury of the legs. Comp Med. 2013 Jun;63(3):227–32.

155. Matziolis G, Winkler T, Schaser K, Wiemann M, Krocker D, Tuischer J, et al. Autologous Bone Marrow-Derived Cells Enhance Muscle Strength Following Skeletal Muscle Crush Injury in Rats. Tissue Eng. 2006 Feb;12(2):361–7.

156. Turner NJ, Badylak JS, Weber DJ, Badylak SF. Biologic scaffold remodeling in a dog model of complex musculoskeletal injury. J Surg Res. 2012 Aug;176(2):490–502.

157. Winkler T, von Roth P, Radojewski P, Urbanski A, Hahn S, Preininger B, et al. Immediate and delayed transplantation of mesenchymal stem cells improve muscle force after skeletal muscle injury in rats. J Tissue Eng Regen Med. 2012 Dec 1;6(SUPPL. 3):s60–7.

158. Bates B. Delayed Endothelial Progenitor Cell Therapy Promotes Bone Defect Repair in a Pre-Clinical Rat Model. 2016;2017.

159. An Y, Arciola CR. Animal models of osteomyelitis. Int J Artif Organs. 2009;29(4):407–20.

160. Rink A, Santschi EM, Beattie CW. Normalized cDNA libraries from a porcine model of orthopedic implant-associated infection. Mamm Genome. 2002;13(4):198–205.

161. Kälicke T, Schlegel U, Printzen G, Schneider E, Muhr G, Arens S. Influence of a standardized closed soft tissue trauma on resistance to local infection. An experimental study in rats. J Orthop Res. 2003 Mar 1;21(2):373–8.

162. Gilbert SR, Camara J, Camara R, Duffy L, Waites K, Kim H, et al. Contaminated open fracture and crush injury: a murine model. Bone Res. 2015;3:14050.

163. Eardley WGP, Martin KR, Taylor C, Kirkman E, Clasper JC, Watts SA. The Development of an Experimental Model of Contaminated Muscle Injury in Rabbits. Int J Low Extrem Wounds. 2012 Dec 30;11(4):254–63.

164. Hill PF, Clasper JC, Parker ' SJ, Watkins PE. Early intramedullary nailing in an animal model of a heavily contaminated fracture of the tibia. J Orthop Res.

2002;20:648–53.

165. Li J, Topaz M, Xun W, Li W, Wang X, Liu H, et al. New swine model of infected soft tissue blast injury. J Trauma Acute Care Surg. 2012 Oct;73(4):908–13.

166. Penn-Barwell JG, Rand BCC, Brown K V, Wenke JC. A versatile model of open-fracture infection : a contaminated segmental rat femur defect. Bone Joint Res. 2014 Jun;3(6):187–92.

167. Flohe S, Flohe SB, Schade FU, Waydhas C. Immune response of severely injured patients - Influence of surgical intervention and therapeutic impact. Langenbeck's Arch Surg. 2007;392(5):639–48.

168. Lord JM, Midwinter MJ, Chen YF, Belli A, Brohi K, Kovacs EJ, et al. The systemic immune response to trauma: an overview of pathophysiology and treatment. Lancet. 2014 Oct 18;384(9952):1455–65.

169. Rosenthal MD, Moore FA. Persistent Inflammation, Immunosuppression, and Catabolism: Evolution of Multiple Organ Dysfunction. Surg Infect (Larchmt). 2016 Apr 1;17(2):167.

170. Gabrilovich DI, Nagaraj S. Myeloid-derived suppressor cells as regulators of the immune system. Nat Rev Immunol 2009 93. 2009 Mar;9(3):162–74.

171. Jia W, Jackson-Cook C, Graf MR. Tumor-infiltrating, myeloid-derived suppressor cells inhibit T cell activity by nitric oxide production in an intracranial rat glioma + vaccination model. J Neuroimmunol. 2010 Jun;223(1–2):20–30.

172. Zhang C, Lei GS, Shao S, Jung HW, Durant PJ, Lee CH. Accumulation of myeloid-derived suppressor cells in the lungs during Pneumocystis pneumonia. Infect Immun. 2012;80(10):3634–41.

173. P R, AC O, PC R. Metabolism of L-arginine by myeloid-derived suppressor cells in cancer: mechanisms of T cell suppression and therapeutic perspectives. Immunol Invest. 2012 Aug;41(6–7):614–34.

174. R G, JC R, T W, C B, Y F, T F, et al. L-Arginine Modulates T Cell Metabolism and Enhances Survival and Anti-tumor Activity. Cell. 2016 Oct 20;167(3):829-842.e13.

175. Park M-J, Lee S-H, Kim E-K, Lee E-J, Baek J-A, Park S-H, et al. Interleukin-10 produced by myeloid-derived suppressor cells is critical for the induction of Tregs and attenuation of rheumatoid inflammation in mice. Sci Reports 2018 81. 2018 Feb 28;8(1):1–10.

176. Cheng A, Krishnan L, Pradhan P, Weinstock LD, Wood LB, Roy K, et al. Impaired bone healing following treatment of established nonunion correlates with serum cytokine expression. J Orthop Res. 2019 Jan 3;

177. S M. Current Options for Determining Fracture Union. Adv Med. 2014;2014:1–12.

178. Kolambkar YM, Dupont KM, Boerckel JD, Huebsch N, Mooney DJ, Hutmacher DW, et al. An alginate-based hybrid system for growth factor delivery in the functional repair of large bone defects. Biomaterials. 2011;32(1):65–74.

179. Vantucci CE, Ahn H, Fulton T, Schenker ML, Pradhan P, Wood LB, et al. Development of systemic immune dysregulation in a rat trauma model of biomaterial-associated infection. Biomaterials. 2021 Jan 1;264:120405.

180. Wherry EJ, Kurachi M. Molecular and cellular insights into T cell exhaustion. Nat Rev Immunol 2015 158. 2015 Jul 24;15(8):486–99.

181. R M, TA E. The biology of fracture healing. Injury. 2011;42(6):551–5.

182. X Y, BF R, A H-S, Y S, N PC, MP B. Callus mineralization and maturation are delayed during fracture healing in interleukin-6 knockout mice. Bone. 2007 Dec;41(6):928–36.

183. Frost A, Jonsson KB, BrändstrÖm H, Ljunghall S, Nilsson O, Ljunggren O. Interleukin (IL)-13 and IL-4 inhibit proliferation and stimulate IL-6 formation in human osteoblasts: evidence for involvement of receptor subunits IL-13R, IL-13Rα, and IL-4Rα. Bone. 2001 Mar 1;28(3):268–74.

184. Onoe Y, Miyaura C, Kaminakayashiki T, Nagai Y, Noguchi K, Chen QR, et al. IL-13 and IL-4 inhibit bone resorption by suppressing cyclooxygenase-2-dependent prostaglandin synthesis in osteoblasts. J Immunol. 1996;156(2).

185. Lee EY, Lee ZH, Song YW. CXCL10 and autoimmune diseases. Autoimmun Rev. 2009 Mar 1;8(5):379–83.

186. Angiolillo AL, Sgadari C, Taub DD, Liao F, Farber JM, Maheshwari S, et al. Human interferon-inducible protein 10 is a potent inhibitor of angiogenesis in vivo. J Exp Med. 1995 Jul 1;182(1):155.

187. N U, M S, T S, Y K, J B, K N, et al. Tumor-infiltrating myeloid-derived suppressor cells are pleiotropic-inflamed monocytes/macrophages that bear M1- and M2-type characteristics. J Leukoc Biol. 2008 May;83(5):1136–44.

188. Dross SE, Munson P V, Kim SE, Bratt DL, Tunggal HC, Gervassi AL, et al. Kinetics of myeloid derived suppressor cell frequency and function during SIV infection, combination antiretroviral therapy and treatment interruption. J Immunol. 2017 Jan 15;198(2):757.

189. Hart KM, Byrne KT, Molloy MJ, Usherwood EM, Berwin B. IL-10 Immunomodulation of Myeloid Cells Regulates a Murine Model of Ovarian Cancer. Front Immunol. 2011;2(JUL).

190. Ibrahim ML, Klement JD, Lu C, Redd PS, Xiao W, Yang D, et al. Myeloid-Derived Suppressor Cells Produce IL-10 to Elicit DNMT3b-Dependent IRF8 Silencing to Promote Colitis-Associated Colon Tumorigenesis. Cell Rep. 2018 Dec 11;25(11):3036-3046.e6.

191. Brudecki L, Ferguson DA, McCall CE, Gazzar M El. Myeloid-Derived Suppressor Cells Evolve during Sepsis and Can Enhance or Attenuate the Systemic Inflammatory Response. Infect Immun. 2012;80(6):2026.

192. Bah I, Kumbhare A, Nguyen L, McCall CE, Gazzar M El. IL-10 induces an immune repressor pathway in sepsis by promoting S100A9 nuclear localization and MDSC development. Cell Immunol. 2018 Oct 1;332:32.

193. Könnecke I, Serra A, El Khassawna T, Schlundt C, Schell H, Hauser A, et al. T and B cells participate in bone repair by infiltrating the fracture callus in a two-wave fashion. Bone. 2014;64:155–65.

194. J J, FJN L, AC T, K F, N R, D H, et al. Human monocytic myeloid-derived suppressor cells impair B-cell phenotype and function in vitro. Eur J Immunol. 2020 Jan 1;50(1):33–47.

195. Knier B, Hiltensperger M, Sie C, Aly L, Lepennetier G, Engleitner T, et al. Myeloid-derived suppressor cells control B cell accumulation in the CNS during

autoimmunity. Nat Immunol. 2018 Dec 1;19(12):1341.

196. Wang Y, Schafer CC, Hough KP, Tousif S, Duncan SR, Kearney JF, et al. Myeloid-derived suppressor cells impair B cell responses in lung cancer through IL-7 and STAT5. J Immunol. 2018 Jul 1;201(1):278.

197. Spiller KL, Nassiri S, Witherel CE, Anfang RR, Ng J, Nakazawa KR, et al. Sequential delivery of immunomodulatory cytokines to facilitate the M1-to-M2 transition of macrophages and enhance vascularization of bone scaffolds. Biomaterials. 2015 Jan 1;37:194.

198. S R, S G, WR T, K S-B, K J, V S, et al. Terminally differentiated $CD8^+$ T cells negatively affect bone regeneration in humans. Sci Transl Med. 2013 Mar 20;5(177).

199. Liu Y, Wang L, Kikuiri T, Akiyama K, Chen C, Xu X, et al. Mesenchymal stem cell–based tissue regeneration is governed by recipient T lymphocytes via IFN-γ and TNF-α. Nat Med 2011 1712. 2011 Nov 20;17(12):1594–601.

200. K D, E M-R, RA S. The ageing immune system: is it ever too old to become young again? Nat Rev Immunol. 2009 Jan;9(1):57–62.

201. Montecino-Rodriguez E, Berent-Maoz B, Dorshkind K. Causes, consequences, and reversal of immune system aging. J Clin Invest. 2013 Mar 1;123(3):958.

202. PJ L, K D. Age-related changes in lymphocyte development and function. Nat Immunol. 2004 Feb;5(2):133–9.

203. Shaw AC, Joshi S, Greenwood H, Panda A, Lord JM. Aging of the Innate Immune System. Curr Opin Immunol. 2010 Aug;22(4):507.

204. Agoston D V. How to Translate Time? The Temporal Aspect of Human and Rodent Biology. Front Neurol. 2017 Mar 17;8(MAR):92.

205. NA A, EF S, MR A, LR L. Rat's age versus human's age: what is the relationship? Arq Bras Cir Dig. 2012;25(1):49–51.

206. Braunstein M, Kusmenkov T, Mutschler W, Kammerlander C, Böcker W, Bogner-

Flatz V. Polytrauma in Older Adults Leads to Significantly Increased TIMP-1 Levels in the Early Posttraumatic Period. J Immunol Res. 2020;2020.

207. GE G, C M, T M, R W, J A, A C, et al. Early Immunologic Response in Multiply Injured Patients With Orthopaedic Injuries Is Associated With Organ Dysfunction. J Orthop Trauma. 2019 May 1;33(5):220–8.

208. Schwarz EM, Parvizi J, Gehrke T, Aiyer A, Battenberg A, Brown SA, et al. 2018 International Consensus Meeting on Musculoskeletal Infection: Research Priorities from the General Assembly Questions. J Orthop Res. 2019 May;37(5):997–1006.

209. ter Boo GJA, Grijpma DW, Moriarty TF, Richards RG, Eglin D. Antimicrobial delivery systems for local infection prophylaxis in orthopedic- and trauma surgery. Vol. 52, Biomaterials. Elsevier Ltd; 2015. p. 113–25.

210. Bongers J, Jacobs AME, Smulders K, van Hellemondt GG, Goosen JHM. Reinfection and re-revision rates of 113 two-stage revisions in infected TKA. J Bone Jt Infect. 2020 May 3;5(3):137–44.

211. Australian Orthopaedic Association National Joint Replacement Registry. 2019.

212. Guerra MTE, Gregio FM, Bernardi A, Castro CC de. Infection rate in adult patients with open fractures treated at the emergency hospital and at the ULBRA university hospital in Canoas, Rio Grande do Sul, Brazil. Rev Bras Ortop (English Ed. 2017 Sep;52(5):544–8.

213. Kaufman MG, Meaike JD, Izaddoost SA. Orthopedic Prosthetic Infections: Diagnosis and Orthopedic Salvage. Semin Plast Surg. 2016 May 1;30(2):66–72.

214. Moriarty TF, Kuehl R, Coenye T, Metsemakers W-J, Morgenstern M, Schwarz EM, et al. Orthopaedic device-related infection: current and future interventions for improved prevention and treatment. EFORT open Rev. 2016 Apr;1(4):89–99.

215. Bernard L, Lübbeke A, Stern R, Bru JP, Feron JM, Peyramond D, et al. Value of preoperative investigations in diagnosing prosthetic joint infection: retrospective cohort study and literature review. Scand J Infect Dis. 2004;36(6–7):410–6.

216. Bjarnsholt T. Introduction to biofilms. Biofilm Infections. 2011;1–9.

217. Ricciardi BF, Muthukrishnan G, Masters E, Ninomiya M, Lee CC, Schwarz EM. Staphylococcus aureus Evasion of Host Immunity in the Setting of Prosthetic Joint Infection: Biofilm and Beyond. Vol. 11, Current Reviews in Musculoskeletal Medicine. Humana Press Inc.; 2018. p. 389–400.

218. de Mesy Bentley KL, MacDonald A, Schwarz EM, Oh I. Chronic Osteomyelitis with Staphylococcus aureus Deformation in Submicron Canaliculi of Osteocytes: A Case Report. JBJS case Connect. 2018 Jan 1;8(1):e8.

219. Sanchez CJ, Ward CL, Romano DR, Hurtgen BJ, Hardy SK, Woodbury RL, et al. Staphylococcus aureus biofilms decrease osteoblast viability, inhibits osteogenic differentiation, and increases bone resorption in vitro. BMC Musculoskelet Disord. 2013;14.

220. Seebach E, Kubatzky KF. Chronic Implant-Related Bone Infections-Can Immune Modulation be a Therapeutic Strategy? Vol. 10, Frontiers in immunology. NLM (Medline); 2019. p. 1724.

221. Masters EA, Trombetta RP, de Mesy Bentley KL, Boyce BF, Gill AL, Gill SR, et al. Evolving concepts in bone infection: redefining “biofilm”, “acute vs. chronic osteomyelitis”, “the immune proteome” and “local antibiotic therapy.” Bone Res. 2019 Dec;7(1).

222. Chapter 7. Orthopedic Infections: Basic Principles of Pathogenesis, Diagnosis, and Treatment | Current Diagnosis & Treatment in Orthopedics, 5e | AccessMedicine | McGraw-Hill Medical [Internet]. [cited 2020 Mar 17]. Available from: https://accessmedicine-mhmedical-com.proxy.library.emory.edu/content.aspx?bookid=675&sectionid=45451713#57816196

223. Kavanagh N, Ryan EJ, Widaa A, Sexton G, Fennell J, O’Rourke S, et al. Staphylococcal osteomyelitis: Disease progression, treatment challenges, and future directions. Vol. 31, Clinical Microbiology Reviews. American Society for Microbiology; 2018.

224. Lin X, Yang S, Lai K, Yang H, Webster TJ, Yang L. Orthopedic implant biomaterials with both osteogenic and anti-infection capacities and associated in vivo evaluation methods. Vol. 13, Nanomedicine: Nanotechnology, Biology, and Medicine. Elsevier Inc.; 2017. p. 123–42.

225. Thammavongsa V, Kim HK, Missiakas D, Schneewind O. Staphylococcal

manipulation of host immune responses. Vol. 13, Nature Reviews Microbiology. Nature Publishing Group; 2015. p. 529–43.

226. Heim CE, Vidlak D, Scherr TD, Kozel JA, Holzapfel M, Muirhead DE, et al. Myeloid-Derived Suppressor Cells Contribute to Staphylococcus aureus Orthopedic Biofilm Infection . J Immunol. 2014 Apr 15;192(8):3778–92.

227. Willett NJ, Li M-TA, Uhrig BA, Boerckel JD, Huebsch N, Lundgren TL, et al. Attenuated human bone morphogenetic protein-2-mediated bone regeneration in a rat model of composite bone and muscle injury. Tissue Eng Part C Methods. 2013 Apr;19(4):316–25.

228. Gans I, Jain A, Sirisreetreerux N, Haut ER, Hasenboehler EA. Current practice of antibiotic prophylaxis for surgical fixation of closed long bone fractures: A survey of 297 members of the Orthopaedic Trauma Association. Patient Saf Surg. 2017 Jan 16;11(1):2.

229. Schulte W, Bernhagen J, Bucala R. Cytokines in Sepsis: Potent Immunoregulators and Potential Therapeutic Targets-An Updated View. Mediators Inflamm. 2013;2013:16.

230. Reikerås O. Immune depression in musculoskeletal trauma. Vol. 59, Inflammation Research. 2010. p. 409–14.

231. Muthukrishnan G, Masters EA, Daiss JL, Schwarz EM. Mechanisms of Immune Evasion and Bone Tissue Colonization That Make Staphylococcus aureus the Primary Pathogen in Osteomyelitis. Curr Osteoporos Rep. 2019;

232. Govaert GAM, Kuehl R, Atkins BL, Trampuz A, Morgenstern M, Obremskey WT, et al. Diagnosing Fracture-Related Infection. J Orthop Trauma. 2019 Aug;1.

233. Ost M, Singh A, Peschel A, Mehling R, Rieber N, Hartl D. Myeloid-derived suppressor cells in bacterial infections. Vol. 6, Frontiers in Cellular and Infection Microbiology. Frontiers Media S.A.; 2016.

234. Schrijver IT, Théroude C, Roger T. Myeloid derived suppressor cells sepsis. Vol. 10, Frontiers in Immunology. Frontiers Media S.A.; 2019.

235. Srivastava MK, Zhu L, Harris-White M, Kar U, Huang M, Johnson MF, et al.

Myeloid Suppressor Cell Depletion Augments Antitumor Activity in Lung Cancer. Sarkar D, editor. PLoS One. 2012 Jul 16;7(7):e40677.

236. Pauli NT, Kim HK, Falugi F, Huang M, Dulac J, Dunand CH, et al. Staphylococcus aureus infection induces protein A-mediated immune evasion in humans. J Exp Med. 2014;211(12):2331–9.

237. Goodyear CS, Silverman GJ. Death by a B cell superantigen: In vivo VH-targeted apoptotic supraclonal B cell deletion by a staphylococcal toxin. J Exp Med. 2003 May 5;197(9):1125–39.

238. Parcina M, Miranda-Garcia MA, Durlanik S, Ziegler S, Over B, Georg P, et al. Pathogen-Triggered Activation of Plasmacytoid Dendritic Cells Induces IL-10–Producing B Cells in Response to Staphylococcus aureus . J Immunol. 2013 Feb 15;190(4):1591–602.

239. Keener AB, Thurlow LT, Kang S, Spidale NA, Clarke SH, Cunnion KM, et al. Staphylococcus aureus Protein A Disrupts Immunity Mediated by Long-Lived Plasma Cells . J Immunol. 2017 Feb 1;198(3):1263–73.

240. Basal O, Atay T, Ciris İM, Baykal YB. Epidermal growth factor (EGF) promotes bone healing in surgically induced osteonecrosis of the femoral head (ONFH). Bosn J Basic Med Sci. 2018;18(4):352–60.

241. Edderkaoui B. Potential role of chemokines in fracture repair. Vol. 8, Frontiers in Endocrinology. Frontiers Research Foundation; 2017.

242. Bischoff DS, Zhu J-H, Makhijani NS, Yamaguchi DT. Induction of CXC chemokines in human mesenchymal stem cells by stimulation with secreted frizzled-related proteins through non-canonical Wnt signaling. World J Stem Cells. 2015;7(11):1262–12673.

243. Liu YC, Kao YT, Huang WK, Lin KY, Wu SC, Hsu SC, et al. CCL5/RANTES is important for inducing osteogenesis of human mesenchymal stem cells and is regulated by dexamethasone. Biosci Trends. 2014;8(3):138–43.

244. Miller AC, Rashid RM, Elamin EM. The "T" in Trauma: the Helper T-cell Response and the Role of Immunomodulation in Trauma and Burn Patients. Vol. 63, Journal of Trauma. 2007. p. 1407–17.

245. Flohe SB, Flohe S, Schade FU. Deterioration of the immune system after trauma: signals and cellular mechanisms. Innate Immun. 2008;

246. Drewry AM, Samra N, Skrupky LP, Fuller BM, Compton SM, Hotchkiss RS. Persistent lymphopenia after diagnosis of sepsis predicts mortality. Shock. 2014 Nov;42(5):383–91.

247. Hawkins RB, Raymond SL, Stortz JA, Horiguchi H, Brakenridge SC, Gardner A, et al. Chronic Critical Illness and the Persistent Inflammation, Immunosuppression, and Catabolism Syndrome. Front Immunol. 2018 Jul 2;9.

248. Lewis K. Persister Cells. Annu Rev Microbiol. 2010 Oct 13;64(1):357–72.

249. Lister JL, Horswill AR. Staphylococcus aureus biofilms: Recent developments in biofilm dispersal. Front Cell Infect Microbiol. 2014;4(DEC).

250. Singh R, Ray P, Das A, Sharma M. Role of persisters and small-colony variants in antibiotic resistance of planktonic and biofilm-associated Staphylococcus aureus: An in vitro study. J Med Microbiol. 2009 Aug;58(8):1067–73.

251. Li D, Gromov K, Søballe K, Puzas JE, O'Keefe RJ, Awad H, et al. Quantitative mouse model of implant-associated osteomyelitis and the kinetics of microbial growth, osteolysis, and humoral immunity. J Orthop Res. 2008 Jan;26(1):96–105.

252. Jørgensen NP, Meyer R, Dagnæs-Hansen F, Fuursted K. Correction: A Modified Chronic Infection Model for Testing Treatment of Staphylococcus aureus Biofilms on Implants. Vol. 10, PLoS ONE. Public Library of Science; 2015.

253. Funao H, Ishii K, Nagai S, Sasaki A, Hoshikawa T, Aizawa M, et al. Establishment of a real-time, quantitative, and reproducible mouse model of staphylococcus osteomyelitis using bioluminescence imaging. Bäumler AJ, editor. Infect Immun. 2012 Feb 1;80(2):733–41.

254. Ferreira AM, Gentile P, Chiono V, Ciardelli G. Collagen for bone tissue regeneration. Vol. 8, Acta Biomaterialia. 2012. p. 3191–200.

255. Zhang D, Wu X, Chen J, Lin K. The development of collagen based composite scaffolds for bone regeneration. Vol. 3, Bioactive Materials. KeAi Communications Co.; 2018. p. 129–38.

256. Lang A, Kirchner M, Stefanowski J, Durst M, Weber MC, Pfeiffenberger M, et al. Collagen I-based scaffolds negatively impact fracture healing in a mouse-osteotomy-model although used routinely in research and clinical application. Acta Biomater. 2019 Mar 1;86:171–84.

257. Pollack AN, Watkins-Castiollo SI. Fracture Trends [Internet]. The Burden of Musculoskeletal Diseases in the United States. 2014 [cited 2018 Dec 12]. Available from: http://www.boneandjointburden.org/

258. Garcia P. Rodent non-union models. Eur Cells Mater. 2013;26:1–14.

259. Zura R, Xiong Z, Einhorn T, Watson JT, Ostrum RF, Prayson MJ, et al. Epidemiology of Fracture Nonunion in 18 Human Bones. JAMA Surg. 2016 Nov 16;151(11):e162775.

260. Low EE, Inkellis E, Morshed S. Complications and revision amputation following trauma-related lower limb loss. Injury. 2017 Feb 1;48(2):364–70.

261. MacKenzie EJ, Bosse MJ, Pollak AN, Webb LX, Swiontkowski MF, Kellam JF, et al. Long-Term Persistence of Disability Following Severe Lower-Limb Trauma<sbt aid="1025711">Results of a Seven-Year Follow-up</sbt> J Bone Jt Surg. 2005 Aug 1;87(8):1801.

262. Panteli M, Pountos I, Jones E, Giannoudis P V. Biological and molecular profile of fracture non-union tissue: Current insights. J Cell Mol Med. 2015 Apr 1;19(4):685–713.

263. Zura R, Della Rocca GJ, Mehta S, Harrison A, Brodie C, Jones J, et al. Treatment of chronic (>1 year) fracture nonunion: Heal rate in a cohort of 767 patients treated with low-intensity pulsed ultrasound (LIPUS). Injury. 2015 Oct 1;46(10):2036–41.

264. Casey E. Vantucci, Hyunhee Ahn MLS, Pradhan P, , Levi B. Wood, Guldberg RE, Roy K, Willett NJ. Development of Systemic Immune Dysregulation in a Rat Trauma Model with Biomaterial-Associated Infection. bioRxiv. 2020 Jan 11;1–36.

265. Cheng A, Krishnan L, Pradhan P, Weinstock LD, Wood LB, Roy K, et al. Impaired bone healing following treatment of established nonunion correlates with serum cytokine expression. J Orthop Res. 2018 Nov 27;

266. Walsh MC, Takegahara N, Kim H, Choi Y. Updating osteoimmunology: regulation of bone cells by innate and adaptive immunity. Nat Rev Rheumatol. 2018 Mar 11;14(3):146–56.

267. Kolambkar YM, Boerckel JD, Dupont KM, Bajin M, Huebsch N, Mooney DJ, et al. Spatiotemporal delivery of bone morphogenetic protein enhances functional repair of segmental bone defects. Bone. 2011;49(3):485–92.

268. Krishnan L, Priddy LB, Esancy C, Klosterhoff BS, Stevens HY, Tran L, et al. Delivery vehicle effects on bone regeneration and heterotopic ossification induced by high dose BMP-2. Acta Biomater. 2017;49:101–12.

269. Krishnan L, Priddy LB, Esancy C, Li M-TA, Stevens HY, Jiang X, et al. Hydrogel-based Delivery of rhBMP-2 Improves Healing of Large Bone Defects Compared With Autograft. Clin Orthop Relat Res. 2015 Sep 28;473(9):2885–97.

270. Lykissas M, Gkiatas I. Use of recombinant human bone morphogenetic protein-2 in spine surgery. World J Orthop. 2017 Jul 18;8(7):531–5.

271. Conway JD, Shabtai L, Bauernschub A, Specht SC. BMP-7 Versus BMP-2 for the Treatment of Long Bone Nonunion. Orthopedics. 2014 Dec 1;37(12):e1049–57.

272. Wei F, Zhou Y, Wang J, Liu C, Xiao Y. The Immunomodulatory Role of BMP-2 on Macrophages to Accelerate Osteogenesis. Tissue Eng Part A. 2018 Apr 1;24(7–8):584–94.

273. Boerckel JD, Kolambkar YM, Dupont KM, Uhrig BA, Phelps EA, Stevens HY, et al. Effects of protein dose and delivery system on BMP-mediated bone regeneration. Biomaterials. 2011 Aug;32(22):5241–51.

274. Uludag H, Gao T, Porter TJ, Friess W, Wozney JM. Delivery systems for BMPs: factors contributing to protein retention at an application site. J Bone Joint Surg Am. 2001;83-A Suppl 1(Pt 2):S128-35.

275. Tannoury CA, An HS. Complications with the use of bone morphogenetic protein 2 (BMP-2) in spine surgery. Spine J. 2014;14(3):552–9.

276. Shields LBE, Raque GH, Glassman SD, Campbell M, Vitaz T, Harpring J, et al. Adverse Effects Associated With High-Dose Recombinant Human Bone

Morphogenetic Protein-2 Use in Anterior Cervical Spine Fusion. Spine (Phila Pa 1976). 2006 Mar 1;31(5):542–7.

277. Lee K-B, Taghavi CE, Song K-J, Sintuu C, Yoo JH, Keorochana G, et al. Inflammatory Characteristics of rhBMP-2 In Vitro and in an In Vivo Rodent Model. Spine (Phila Pa 1976). 2011 Feb 1;36(3):E149–54.

278. Zara JN, Siu RK, Zhang X, Shen J, Ngo R, Lee M, et al. High doses of bone morphogenetic protein 2 induce structurally abnormal bone and inflammation in vivo. Tissue Eng Part A. 2011 May;17(9–10):1389–99.

279. Ruehle MA, Krishnan L, Vantucci CE, Wang Y, Stevens HY, Roy K, et al. Effects of BMP-2 dose and delivery of microvascular fragments on healing of bone defects with concomitant volumetric muscle loss. J Orthop Res. 2019 Jan 16;

280. Cowan CM, Aghaloo T, Chou Y-F, Walder B, Zhang X, Soo C, et al. MicroCT Evaluation of Three-Dimensional Mineralization in Response to BMP-2 Doses *In Vitro* and in Critical Sized Rat Calvarial Defects. Tissue Eng. 2007 Mar;13(3):501–12.

281. Sandhu HS, Kanim LE, Kabo JM, Toth JM, Zeegen EN, Liu D, et al. Effective doses of recombinant human bone morphogenetic protein-2 in experimental spinal fusion. Spine (Phila Pa 1976). 1996 Sep 15;21(18):2115–22.

282. Agrawal V, Sinha M. A review on carrier systems for bone morphogenetic protein-2. J Biomed Mater Res Part B Appl Biomater. 2017 May 1;105(4):904–25.

283. Begam H, Nandi SK, Kundu B, Chanda A. Strategies for delivering bone morphogenetic protein for bone healing. Mater Sci Eng C. 2017 Jan 1;70:856–69.

284. Agarwal R, García AJ. Biomaterial strategies for engineering implants for enhanced osseointegration and bone repair. Adv Drug Deliv Rev. 2015 Nov 1;94:53–62.

285. Pakulska MM, Miersch S, Shoichet MS. Designer protein delivery: From natural to engineered affinity-controlled release systems. Science (80-). 2016 Mar 18;351(6279):aac4750–aac4750.

286. Miller T, Goude MC, McDevitt TC, Temenoff JS. Molecular engineering of glycosaminoglycan chemistry for biomolecule delivery. Acta Biomater. 2014

Apr;10(4):1705–19.

287. Hettiaratchi MH, Miller T, Temenoff JS, Guldberg RE, McDevitt TC. Heparin microparticle effects on presentation and bioactivity of bone morphogenetic protein-2. Biomaterials. 2014;35(25):7228–38.

288. Hettiaratchi MH, Rouse T, Chou C, Krishnan L, Stevens HY, Li M-TA, et al. Enhanced in vivo retention of low dose BMP-2 via heparin microparticle delivery does not accelerate bone healing in a critically sized femoral defect. Acta Biomater. 2017 Sep 1;59:21–32.

289. Hettiaratchi MH, Krishnan L, Rouse T, Chou C, McDevitt TC, Guldberg RE. Heparin-mediated delivery of bone morphogenetic protein-2 improves spatial localization of bone regeneration. Sci Adv. 2020 Jan 3;6(1):eaay1240.

290. Oest ME, Dupont KM, Kong H-J, Mooney DJ, Guldberg RE. Quantitative assessment of scaffold and growth factor-mediated repair of critically sized bone defects. J Orthop Res. 2007 Jul;25(7):941–50.

291. Bouxsein ML, Boyd SK, Christiansen BA, Guldberg RE, Jepsen KJ, Müller R. Guidelines for assessment of bone microstructure in rodents using micro-computed tomography. J Bone Miner Res. 2010 Jun 7;25(7):1468–86.

292. Boerckel JD, Kolambkar YM, Stevens HY, Lin ASP, Dupont KM, Guldberg RE. Effects of in vivo mechanical loading on large bone defect regeneration. J Orthop Res. 2012;30(7):1067–75.

293. Nicola R. Early Total Care versus Damage Control: Current Concepts in the Orthopedic Care of Polytrauma Patients. ISRN Orthop. 2013 Mar 21;2013:329452.

294. Sengupta P. The Laboratory Rat: Relating Its Age With Human's. Int J Prev Med. 2013 Jun;4(6):624–30.

295. Fulop T, Larbi A, Dupuis G, Le Page A, Frost EH, Cohen AA, et al. Immunosenescence and Inflamm-Aging As Two Sides of the Same Coin: Friends or Foes? Front Immunol. 2018 Jan 10;8:1960.

296. Ventura MT, Casciaro M, Gangemi S, Buquicchio R. Immunosenescence in aging: between immune cells depletion and cytokines up-regulation. Clin Mol Allergy.

2017;15:21.

297. Hettiaratchi M, Krishnan L, Li M-TA, Temenoff J. BMP-2-Loaded Heparin Microparticles Facilitate Functional Bone Formation in Large Bone Defects | Request PDF. In: Tissue Engineering and Regenerative Medicine International Society World Congress. Boston; 2015.

298. Capila I, Linhardt RJ. Heparin-Protein Interactions. Angew Chemie Int Ed. 2002 Feb 1;41(3):390–412.

299. Deepa SS, Umehara Y, Higashiyama S, Itoh N, Sugahara K. Specific Molecular Interactions of Oversulfated Chondroitin Sulfate E with Various Heparin-binding Growth Factors. J Biol Chem. 2002 Nov 15;277(46):43707–16.

300. Gandhi NS, Mancera RL. Prediction of heparin binding sites in bone morphogenetic proteins (BMPs). Biochim Biophys Acta - Proteins Proteomics. 2012 Dec;1824(12):1374–81.

301. Damon DH, Lobb RR, D'Amore PA, Wagner JA. Heparin potentiates the action of acidic fibroblast growth factor by prolonging its biological half-life. J Cell Physiol. 1989 Feb;138(2):221–6.

302. Shen X, Fang J, Lv X, Pei Z, Wang Y, Jiang S, et al. Heparin impairs angiogenesis through inhibition of microRNA-10b. J Biol Chem. 2011 Jul 29;286(30):26616–27.

303. Anderson SE, Han WM, Srinivasa V, Mohiuddin M, Ruehle MA, Moon JY, et al. Determination of a critical size threshold for volumetric muscle loss in the mouse quadriceps. Tissue Eng - Part C Methods. 2019 Feb 1;25(2):59–70.

304. Suchacki KJ, Cawthorn WP. Molecular Interaction of Bone Marrow Adipose Tissue with Energy Metabolism. Curr Mol Biol Reports. 2018 Jun 28;4(2):41–9.

305. Ozaki K, Leonard WJ. Cytokine and cytokine receptor pleiotropy and redundancy. J Biol Chem. 2002 Aug 16;277(33):29355–8.

306. Wang L-Y, Tu Y-F, Lin Y-C, Huang C-C. CXCL5 signaling is a shared pathway of neuroinflammation and blood–brain barrier injury contributing to white matter injury in the immature brain. J Neuroinflammation. 2016 Dec 6;13(1):6.

307. Conti P, DiGioacchino M. MCP-1 and RANTES Are Mediators of Acute and Chronic Inflammation. Allergy Asthma Proc. 2001 May 1;22(3):133–7.

308. Yao M, Brummer G, Acevedo D, Cheng N. Cytokine Regulation of Metastasis and Tumorigenicity. Adv Cancer Res. 2016 Jan 1;132:265–367.

309. Turner RT, Kalra SP, Wong CP, Philbrick KA, Lindenmaier LB, Boghossian S, et al. Peripheral leptin regulates bone formation. J Bone Miner Res. 2013 Jan;28(1):22–34.

310. Upadhyay J, Farr OM, Mantzoros CS. The role of leptin in regulating bone metabolism. Metabolism. 2015 Jan;64(1):105–13.

311. Evgeny N. Tsiganov, Verbina EM, Radaeva T V., Sosunov V V., George, Kosmiadi A, et al. Gr-1dimCD11b+ immature myeloid-derived suppressor cells but not neutrophils are markers of lethal tuberculosis infection in mice. J Immunol. 2014;192(10):4718–27.

312. Daker S El, Sacchi A, Tempestilli M, Carducci C, Goletti D, Vanini V, et al. Granulocytic myeloid derived suppressor cells expansion during active pulmonary tuberculosis is associated with high nitric oxide plasma level. PLoS One. 2015;10(4):1–10.

313. Suzanne Ostrand-Rosenberg and Pratima Sinha. Myeloid-Derived Suppressor Cells: Linking Inflammation and Cancer. J Immunol. 2009;182(8):4499–506.

314. Mathias B, Delmas AL, Ozrazgat-Baslanti T, Vanzant EL, Szpila BE, Mohr AM, Moore FA, Brakenridge SC, Brumback BA, Moldawer LL EP. Human myeloid-derived suppressor cells are associated with chronic immune suppression after severe sepsis/septic shock. Ann Surg. 2017;265(4):827–34.

315. Schrijver IT, Théroude C, Roger T. Myeloid derived suppressor cells in sepsis. Front Immunol. 2019;10(FEB):1–10.

316. Magcwebeba T, Dorhoi A, Du Plessis N. The emerging role of myeloid-derived suppressor cells in tuberculosis. Front Immunol. 2019;10(APR):e917.

317. Alizadeh D, Trad M, Hanke NT, Larmonier CB, Janikashvili N, Bonnotte B, et al. Doxorubicin eliminates myeloid-derived suppressor cells and enhances the efficacy

of adoptive T-cell transfer in breast cancer. Cancer Res. 2014;74(1):104–18.

318. Vincent J, Mignot G, Chalmin F, Ladoire S, Bruchard M, Chevriaux A, et al. 5-Fluorouracil Selectively Kills Tumor-Associated Myeloid-Derived Suppressor Cells Resulting in Enhanced T Cell-Dependent Antitumor Immunity. Cancer Res. 2010;70(8):3052–61.

319. Obermajer N, Muthuswamy R, Lesnock J, Edwards RP, Kalinski P. Positive feedback between PGE2 and COX2 redirects the differentiation of human dendritic cells toward stable myeloid-derived suppressor cells. Blood. 2011;118(20):5498–506.

320. Ma C, Kapanadze T, Gamrekelashvili J, Manns MP, Korangy F, Greten TF. Anti-Gr-1 antibody depletion fails to eliminate hepatic myeloid-derived suppressor cells in tumor-bearing mice. J Leukoc Biol. 2012 Dec;92(6):1199–206.

321. Xing Y-F, Zhou Y-Q, Ma G-W, Feng D-Y, Cai X-R, Li X. Issues with anti-Gr1 antibody-mediated myeloid-derived suppressor cell depletion. Ann Rheum Dis. 2016;75(8):e49–e49.

322. Sukhatme, Vikas P.; Husain Z. Cancer Therapy Targeting Tetraspanin 33 (Tspan33) IN Myeloid Derived Suppressor Cells. World Intellectual Property Organization; (43) International Publication Date WO 2016/210241 Al, 2016. p. 93.

323. Luu VP, Hevezi P, Vences-Catalan F, Maravillas-Montero JL, White CA, Casali P, et al. TSPAN33 is a novel marker of activated and malignant B cells. Clin Immunol. 2013 Dec;149(3):388–99.

324. Xenaki KT, Oliveira S, Henegouwen PMP van B en. Antibody or Antibody Fragments: Implications for Molecular Imaging and Targeted Therapy of Solid Tumors. Front Immunol. 2017;8:1287.

325. Bourquin J, Milosevic A, Hauser D, Lehner R, Blank F, Petri-Fink A, et al. Biodistribution, Clearance, and Long-Term Fate of Clinically Relevant Nanomaterials. Adv Mater. 2018 May;30(19):1704307.

326. Dykman LA, Khlebtsov NG. Gold nanoparticles in biology and medicine: recent advances and prospects. Acta Naturae. 2011 Apr;3(2):34–55.

327. Manju S, Sreenivasan K. Functionalised nanoparticles for targeted drug delivery. Biointegration Med Implant Mater. 2010 Jan 1;267–97.

328. Kim, J.; Lee, Y.M.; Kang, Y.; Kim WJ. Tumor-homing, size-tunable clustered nanoparticles for anticancer therapeutics. ACS Nano. 2014;8(9):9358–67.

329. Donnelly EM, Kubelick KP, Dumani DS, Emelianov SY. Photoacoustic Image-Guided Delivery of Plasmonic-Nanoparticle-Labeled Mesenchymal Stem Cells to the Spinal Cord. Nano Lett. 2018;18(10):6625–32.

330. Chen B, Jia Y, Gao Y, Sanchez L, Anthony SM, Yu Y. Janus particles as artificial antigen-presenting cells for T cell activation. ACS Appl Mater Interfaces. 2014;6(21):18435–9.

331. Yi Y, Sanchez L, Gao Y, Lee K, Yu Y. Interrogating Cellular Functions with Designer Janus Particles. Chem Mater. 2017;29(4):1448–60.

332. Fu J, An D, Song Y, Wang C, Qiu M, Zhang H. Janus nanoparticles for cellular delivery chemotherapy: Recent advances and challenges. Coord Chem Rev. 2020;422:213467.

333. Behrad Shaghaghi, Sepideh Khoee SB. Preparation of multifunctional Janus nanoparticles on the basis of SPIONs as targeted drug delivery system. Int J Pharm. 2019;559(25):1–12.

334. Guosheng Song, Min Chen, Yanrong Zhang, Liyang Cui, Haibo Qu, Xianchuang Zheng, Max Wintermark, Zhuang Liu and JR. Janus Iron Oxides @ Semiconducting Polymer Nanoparticle Tracer for Cell Tracking by Magnetic Particle Imaging. Nano Lett. 2018;18(1):182–9.

335. Yi Y, Sanchez L, Gao Y, Yu Y. Janus particles for biological imaging and sensing. Analyst. 2016;141(12):3526–39.

336. Espinosa A, Reguera J, Curcio A, Muñoz-Noval Á, Kuttner C, Van de Walle A, et al. Janus Magnetic-Plasmonic Nanoparticles for Magnetically Guided and Thermally Activated Cancer Therapy. Small. 2020;16(11):1–14.

337. Hu J, Zhou S, Sun Y, Fang X, Wu L. Fabrication, properties and applications of Janus particles. Chem Soc Rev. 2012;41(11):4356–78.

338. Kaewsaneha C, Tangboriboonrat P, Polpanich D, Eissa M, Elaissari A. Janus Colloidal Particles: Preparation, Properties, and Biomedical Applications. ACS Appl Mater Interfaces. 2013 Mar 27;5(6):1857–69.

339. Tang JL, Schoenwald K, Potter D, White D, Sulchek T. Bifunctional janus microparticles with spatially segregated proteins. Langmuir. 2012;28(26):10033–9.

340. Peiris PM, Schmidt E, Calabrese M, Karathanasis E. Assembly of Linear Nano-Chains from Iron Oxide Nanospheres with Asymmetric Surface Chemistry. PLoS One. 2011;6(1):e15927.

341. Qin H, Lerman B, Sakamaki I, Wei G, Cha SC, Rao SS, et al. Generation of a new therapeutic peptide that depletes myeloid-derived suppressor cells in tumor-bearing mice. Nat Med. 2014;20(6):676–81.

342. Anne R. Bresnick, David J. Weber and DBZ. S100 proteins in cancer. Nat Rev Cancer. 2015;15(2):96–109.

343. Bronte V, Brandau S, Chen SH, Colombo MP, Frey AB, Greten TF, et al. Recommendations for myeloid-derived suppressor cell nomenclature and characterization standards. Nat Commun. 2016;7:12150.

344. Sinha P, Okoro C, Foell D, Freeze HH, Ostrand-Rosenberg S, Srikrishna G. Proinflammatory S100 Proteins Regulate the Accumulation of Myeloid-Derived Suppressor Cells. J Immunol. 2008;181(7):4666–75.

345. Zhao F, Hoechst B, Duffy A, Gamrekelashvili J, Fioravanti S, Manns MP, et al. S100A9 a new marker for monocytic human myeloid-derived suppressor cells. Immunology. 2012;136(2):176–83.

346. Stephane Bonetto, Loredana Spadola, Andrew G. Buchanan, Lutz Jermutus and JL. Identification of cyclic peptides able to mimic the functional epitope of IgG1-Fc for human FcγRI. FASEB J. 2009;23(2):575–85.

347. Mcenaney PJ, Fitzgerald KJ, Zhang AX, Douglass EF, Shan W, Balog A, et al. Chemically Synthesized Molecules with the Targeting and Effector Functions of Antibodies. J Am Chem Soc. 2014;136:18034−18043.

348. Kubelick KP, Snider EJ, Ross Ethier C, Emelianov S. Development of a stem cell

tracking platform for ophthalmic applications using ultrasound and photoacoustic imaging. Theranostics. 2019;9(13):3812–24.

349. Luke GP, Yeager D ES. Biomedical applications of photoacoustic imaging with exogenous contrast agents. Annu Biomed Eng. 2012;40(2):422–37.

350. Wang S, Song R, Wang Z, Jing Z, Wang S, Ma J. S100A8/A9 in inflammation. Front Immunol. 2018 Jun 11;9(JUN):1298.

351. Lu RM, Hwang YC, Liu IJ, Lee CC, Tsai HZ, Li HJ, et al. Development of therapeutic antibodies for the treatment of diseases. J Biomed Sci 2020 271. 2020 Jan 2;27(1):1–30.

352. Kimiz-Gebologlu I, Gulce-Iz S, Biray-Avci C. Monoclonal antibodies in cancer immunotherapy. Mol Biol Rep. 2018 Dec 1;45(6):2935–40.

353. Zahavi D, Weiner L. Monoclonal Antibodies in Cancer Therapy. Antibodies. 2020 Jul 20;9(3):34.

354. Lin J, Kurilova S, Scott BL, Bosworth E, Iverson BE, Bailey EM, et al. TIRF imaging of Fc gamma receptor microclusters dynamics and signaling on macrophages during frustrated phagocytosis. BMC Immunol. 2016 Mar 12;17(1):1–9.

355. Safenkova I V., Zherdev A V., Dzantiev BB. Correlation between the composition of multivalent antibody conjugates with colloidal gold nanoparticles and their affinity. J Immunol Methods. 2010 May;357(1–2):17–25.

356. Popov J, Kapanen AI, Turner C, Ng R, Tucker C, Chiu G, et al. Multivalent rituximab lipid nanoparticles as improved lymphoma therapies: indirect mechanisms of action and in vivo activity. Nanomedicine (Lond). 2011 Nov;6(9):1575–91.

357. Montet X, Funovics M, Montet-Abou K, Weissleder R, Josephson L. Multivalent effects of RGD peptides obtained by nanoparticle display. J Med Chem. 2006 Oct 5;49(20):6087–93.

358. Curk T, Dobnikar J, Frenkel D. Optimal multivalent targeting of membranes with many distinct receptors. Proc Natl Acad Sci U S A. 2017 Jul 11;114(28):7210–5.

359. Martinez-Veracoechea FJ, Frenkel D. Designing super selectivity in multivalent nano-particle binding. Proc Natl Acad Sci. 2011;108(27):10963–8.

360. Lee K, Yu Y. Janus nanoparticles for T cell activation: Clustering ligands to enhance stimulation. J Mater Chem B. 2017 Jun 14;5(23):4410–5.

361. Pacheco PM, Le B, White D, Sulcheck T. Tunable Complement Activation By Particles With Variable Size and Fc Density. Nano Life. 2013;03(02):1341001.

362. Pacheco P, White D, Sulchek T. Effects of Microparticle Size and Fc Density on Macrophage Phagocytosis. PLoS One. 2013;8(4):1–9.

363. Cheng P, Eksioglu EA, Chen X, Kandell W, Le Trinh T, Cen L, et al. S100A9-induced overexpression of PD-1/PD-L1 contributes to ineffective hematopoiesis in myelodysplastic syndromes. Leuk 2019 338. 2019 Feb 8;33(8):2034–46.

364. Tu S, Bhagat G, Cui G, Takaishi S, Kurt-Jones EA, Rickman B, et al. Overexpression of Interleukin-1β Induces Gastric Inflammation and Cancer and Mobilizes Myeloid-Derived Suppressor Cells in Mice. Cancer Cell. 2008 Nov 4;14(5):408–19.

365. Elkabets M, Ribeiro VSG, Dinarello CA, Ostrand-Rosenberg S, Di Santo JP, Apte RN, et al. IL-1β regulates a novel myeloid-derived suppressor cell subset that impairs NK cell development and function. Eur J Immunol. 2010 Dec;40(12):3347–57.

366. Cai S, Choi JY, Borges TJ, Zhang H, Miao J, Ichimura T, et al. Donor myeloid derived suppressor cells (MDSCs) prolong allogeneic cardiac graft survival through programming of recipient myeloid cells in vivo. Sci Reports 2020 101. 2020 Aug 28;10(1):1–13.

367. Gazon H, Barbeau B, Mesnard JM, Peloponese JM. Hijacking of the AP-1 signaling pathway during development of ATL. Front Microbiol. 2018 Jan 15;8(JAN):2686.

368. Molek P, Strukelj B, Bratkovic T. Peptide phage display as a tool for drug discovery: Targeting membrane receptors. Molecules. 2011;16(1):857–87.

369. Zhou J, Rossi J. Aptamers as targeted therapeutics: Current potential and challenges. Nat Rev Drug Discov. 2017;16(3):181–202.

370. Nixon AE, Sexton DJ, Ladner RC. Drugs derived from phage display From candidate identification to clinical practice Drugs derived from phage display. MAbs. 2014;6(1):73–85.

371. Cheng A, Vantucci CE, Krishnan L, Ruehle MA, Kotanchek T, Wood LB, et al. Early systemic immune biomarkers predict bone regeneration after trauma. Proc Natl Acad Sci U S A. 2021 Feb 23;118(8).

372. Liu J, Toy R, Vantucci C, Pradhan P, Zhang Z, Kuo KM, et al. Bifunctional Janus Particles as Multivalent Synthetic Nanoparticle Antibodies (SNAbs) for Selective Depletion of Target Cells. Nano Lett. 2021 Jan 13;21(1):875–86.

373. Vantucci CE, Krishan L, Cheng A, Prather A, Roy K, Guldberg RE. BMP-2 delivery strategy modulates local bone regeneration and systemic immune responses to complex extremity trauma. Biomater Sci. 2021 Mar 10;9(5):1668–82.

374. Narumi K, Miyakawa R, Ueda R, Hashimoto H, Yamamoto Y, Yoshida T, et al. Proinflammatory Proteins S100A8/S100A9 Activate NK Cells via Interaction with RAGE. J Immunol. 2015;194(11):5539–48.

375. Silvin A, Chapuis N, Dunsmore G, Goubet AG, Dubuisson A, Derosa L, et al. Elevated Calprotectin and Abnormal Myeloid Cell Subsets Discriminate Severe from Mild COVID-19. Cell. 2020 Sep 17;182(6):1401-1418.e18.

376. Leukes V, Walzl G, du Plessis N. Myeloid-Derived Suppressor Cells as Target of Phosphodiesterase-5 Inhibitors in Host-Directed Therapeutics for Tuberculosis. Front Immunol. 2020 Mar 25;11:451.

377. Knaul JK, Jörg S, Oberbeck-Mueller D, Heinemann E, Scheuermann L, Brinkmann V, et al. Lung-residing myeloid-derived suppressors display dual functionality in murine pulmonary tuberculosis. Am J Respir Crit Care Med. 2014 Nov 1;190(9):1053–66.

378. Parveen S, Lun S, Urbanowski ME, Cardin M, Shen J, Murphy JR, et al. Effective Host-Directed Therapy for Tuberculosis by Depletion of Myeloid-Derived Suppressor Cells and Related Cells Using a Diphtheria Toxin Fusion Protein. J Infect Dis. 2021 May 6;

379. Bonetto S, Spadola L, Buchanan AG, Jermutus L, Lund J. Identification of cyclic peptides able to mimic the functional epitope of IgG1-Fc for human Fc gammaRI.

FASEB J. 2009 Feb;23(2):575–85.

380. Srivastava MK, Sinha P, Clements VK, Rodriguez P, Ostrand-Rosenberg S. Myeloid-derived suppressor cells inhibit T-cell activation by depleting cystine and cysteine. Cancer Res. 2010 Jan 1;70(1):68–77.